MOLECULAR DISSECTION OF THE DENGUE VIRUS NS1 PROTEIN

Thomas Burton

Supervisor: Dr Nicholas Eyre

Co-supervisor: Professor Jill Carr

A thesis submitted for the degree of Doctor of Philosophy

Discipline of Virology

Flinders College of Public Health and Medicine

Flinders University

May 2025

Flinders University

Table of Contents

Presentations, publications and awards arising from this PhD

Presentations:

Flinders University Emerging Leader Showcase

Oral Presentation

2021

Talk title: Dengue virus escape mutants against Wolbachia

Adelaide Protein Group

Poster

2022

Poster title: Identification of sulfone-containing inhibitors of dengue virus

Australasian Virology Society Meeting 11

Poster

2022

Poster title: Identification of sulfone-containing compounds that impair dengue virus infectious particle production

Lorne Infection and Immunity

Poster

2023

Poster title: Identification of sulfone-containing compounds that impair dengue virus infectious particle production

Winner of 'Best poster by a student' award

VIIN Young Investigator Symposium

Poster

2023

Poster title: Identification of sulfone-containing compounds that impair dengue virus infectious particle production

Australasian Virology Society Online Meeting

Oral Presentation

2023

Talk title: *In silico* targeting of dengue virus (DENV) non-structural protein 1

Publications

Publication title: Applications of Deep Mutational Scanning in Virology

Authors: Thomas D. Burton and Nicholas S. Eyre

Journal: *viruses*

DOI: https://doi.org/10.3390/v13061020

Received: 29 March 2021 / Revised: 26 May 2021 / Accepted: 26 May 2021 / Published: 28 May 2021

Abbreviations

ADE - Antibody Dependent Enhancement

ApoA1 – Apolipoprotein A1

BAC – Bacterial Artificial Chromosome

Cessa – Cell Screen South Australia

CRISPR – Clustered Regularly Interspaced Short Palindromic Repeats

Cryo-EM – Cryogenic Electron Microscopy

DAR – Downstream AUG Regions

DENV – Dengue Virus

DHF – Dengue Haemorrhagic Fever

DMS – Deep Mutational Scanning

DNA – Deoxyribonucleic Acid

D2R – Dopamine D2 Receptor

DPM – Dolichol-Phosphate Mannose

DPMS – Dolichol-Phosphate Mannose Synthase

E – Envelope

EDI/II/III – Envelope Domain I/II/III

ER – Endoplasmic Reticulum

FASN – Fatty Acid Synthase

GFP – Green Fluorescent Protein

GPI – Glycosylphosphatidylinositol

GROMACS – Groningen Machine for Chemical Simulations

HCMV – Human Cytomegalovirus

HCV – Hepatitis C Virus

HDL – High Density Lipoproteins

HEK – Human Embryonic Kidney

HTS – High-Throughput Screening

IFN – Interferon

IFNAR – Interferon-A/B Receptor

IVT – *In Vitro* Transcription

JAK/STAT – Janus Kinase/Signal Transducer and Activator Of Transcription Proteins

LDL – Low Density Lipoproteins

MBL – Mannose-Binding Lectin

MOE-PCR – Multiple Overlap Extension PCR

MOI – Multiplicity of Infection

NGS – Next Generation Sequencing

NP – Nucleoprotein

ONT – Oxford Nanopore Technology

ORF – Open Reading Frame

SDS-PAGE – Sodium Dodecyl-Sulfate Polyacrylamide Gel Electrophoresis

PAMP – Pathogen-Associated Molecular Pattern

PCR – Polymerase Chain Reaction

PDB – Protein Data Bank

RIG-I – Retinoic Acid-Inducible Gene I

RMSD – Root Mean Square Deviation

RNA – Ribonucleic Acid

RT-PCR – Reverse Transcription Polymerase Chain Reaction

SARS-Cov-2 – Severe Acute Respiratory Syndrome Coronavirus 2

SMRT – Single Molecule Real Time

TM1/2 – Transmembrane Domain 1/2

TSA – Thermal Shift Assay

UAR – Upstream AUG Regions

UTR – Untranslated Region

VTR – Vertical Transmission

WNV – West Nile Virus

ZIKV – Zika Virus

List of Figures

Introduction:

Chapter 3:

List of Tables

Chapter 3:

Chapter 4:

Declaration

I certify that this thesis does not incorporate without acknowledgment any material previously submitted for a degree or diploma in any university and the research within will not be submitted for any other future degree or diploma without the permission of Flinders University; and to the best of my knowledge and belief, does not contain any material previously published or written by another person except where due reference is made in the text.

I acknowledge the contribution of an Australian Government Research Training Program Scholarship to this thesis.

Thomas Darcy Burton

6/04/25

Acknowledgments

Firstly, thank you to my supervisors who have guided me through my PhD. To Nick, for bringing me into the Molecular Virology Lab, providing guidance over the years, sharing your expertise and enabling me to grow into a better scientist. To Jill and Michael, your invaluable contributions as co-supervisors at Flinders Uni and Adelaide Uni were greatly appreciated.

To my lab mates-Brandon, Siena, Steve, Rosa, Roman, Marie, and Laurelle-thank you for the moral support over the PhD, whether over failed experiments or the transition to life at Flinders. To Kylie, Byron, Chuan, Emily and Brooke from the Viral Pathogenesis Lab, and my friends from the MLS, especially Steph, Jia, Ornella and Sandra, thank you for creating such a wonderful work environment. There's no better way to do a PhD than with early knockoff drinks every Friday. And to Josh, Evie, Hawraa, Tim, Luke, Amy and Val, thank you for making the transition to Flinders much easier.

To my collaborators-Dan, Steph and Tom from the MLS, Gustavo and Amanda from Cell Screen SA, Rowena and Chaturaka from UNSW, and Johanna, Robson, and Kathryn from Monash-thank you for your support and for allowing me to contribute to your projects.

To Jase, I appreciate the opportunity to complete this thesis during my employment in the Mackenzie Lab; your support has been invaluable. Apologies for taking so long… And thank you to my wonderful lab members and the amazing people at the Doherty for providing such an amazing place to work while finishing my PhD.

To my friends, thank you for the countless hours of DOTA with the Nuketowners, the Tuesday night basketball, the MTG openings, the holidays to Bali with the KI Crew, the New Year celebrations at Beachport, the Christmases at Minh's and everything else that kept me away from the lab bench late at night or on weekends.

To my family, thank you for supporting me through this journey. Mum and dad, thank you for housing me, feeding me and taking care of me during my PhD. Apologies for haggling my board down.

Abstract

Dengue is the most common mosquito-borne viral disease and is responsible for a major public health burden in tropical and subtropical regions around the world. The dengue virus (DENV) non-structural protein 1 (NS1) has been shown to play roles in pathogenicity, immune system evasion, viral RNA replication and virus production. To date, no antiviral therapeutic for dengue-related illness has been approved for use. Current research on therapeutic candidates that target of NS1 is limited to antibodies, peptides and a heparan sulfate mimetic, with no small molecule inhibitors described. We performed two *in vitro* high-throughput screening approaches to identify antiviral compounds that target NS1: a protein complementation assay to identify inhibitors of NS1 dimerisation/hexamerisation and; a Nanoluciferase-based thermal shift assay to identify NS1-binding compounds. We also performed an *in silico* high-throughput drug-like compound screen to identify potential ligands of NS1, focussing on ligands which may bind at the dimerisation interface of NS1.

While we are yet to unambiguously identified direct inhibitors of NS1 function(s), the thermal shift assay screen revealed a group of structurally related analogues with antiviral properties. A Nanoluciferase-based thermal shift assay in conjunction with a Nanoluciferase-tagged dengue reporter virus (DENV2-NS1-NLuc) was used in a high-throughput compound screen of 3,378 drug-like compounds. Validation studies revealed a collection of structurally related compounds which inhibit DENV infection in a hepatoma cell culture model. Following testing of 37 structurally related analogues, we identified a lead compound (PubChem CID: 50839998) which had minimal impact on viral RNA replication and cell viability but inhibited infectious particle production at low micromolar concentrations. Examination of the impact of this compound on viral protein localization by confocal microscopy revealed dose-dependent reductions in the detection of mature Envelope (E) protein, consistent with the observed inhibition of infectious virus production. Further investigation into the mechanism of action of this compound is warranted to determine its exact molecular target(s), while testing of a wider range of structural analogues may enable identification of related compounds with greater efficacy and lower cytotoxicity.

To identify inhibitors of NS1 dimerisation, the NanoBiT® Protein:Protein Interaction System was used. This NanoBiT or 'split Nanoluciferase' system involves the NanoLuc subunits SmBiT and LgBiT. Each subunit was fused individually to NS1 in mammalian expression vectors, and

in a high-throughput screen, 3,378 drug-like compounds were screened, with luminescence as a readout for NS1 dimerisation levels. While the screen identified three hits, subsequent experiments showed no clear antiviral effects, and the reduction of NS1 dimerisation upon treatment with these compounds could not be verified.

An *in silico* high-throughput drug-like compound screen revealed two binding pockets at the dimerisation interface of NS1. Approximately 7.8 million compounds from the ZINC20 chemical database were tested computationally for binding at these sites and 24 of the top 60 hits were analysed for antiviral efficacy and cytotoxicity via live cell imaging using an mScarlet-tagged dengue reporter virus. The top hit, Compound V2.3, was further analysed. This compound showed high nanomolar inhibition of infectious particle production, with minimal impact on viral RNA replication and low cytotoxicity. Despite being predicted to bind at the dimerisation interface of NS1, Compound V2.3 treatment did not appear to affect NS1 dimerisation, and the binding of Compound V2.3 to NS1 has not yet been confirmed.

Previous studies have identified several key residues of NS1 that are required for its roles in RNA replication and virus production, through analysis of specific hydrophobic regions, conserved residues across multiple orthoflavivirus species and cysteine residues suspected to enable disulphide bonding. We created a DENV mutant library featuring mutants across the envelope (E), precursor Membrane (prM) and NS1 genes. We applied specific selective pressures to the library, including passaging through Huh7.5 cells (human cell line) and C6/36 cells (mosquito cell lines), and preparations are being made for the passaging of the library through *Aedes* mosquitoes, both infected and uninfected with the intracellular bacterium *Wolbachia*. This will allow for identification of DENV mutants which confer resistance to *Wolbachia*-based suppression of DENV, while also identifying E, prM and NS1 residues that are critical to various DENV lifecycle stages and tropism factors. Additionally, we have prepared a library of DENV mutants featuring mutants across NS1 only, as well as a library of mutants covering NS1 in the DENV subgenomic replicon, which will allow for demarcation of residues required for viral RNA replication from those required for infectious particle production.

Chapter 1 – Introduction: Dengue Virus, Deep Mutational Scanning and Antiviral Research

1.1 *Flaviviridae* and dengue virus

DENV is a member of the *Flaviviridae* family of positive-sense single stranded RNA viruses(1). Spread by two species of *Aedes* mosquitoes, *Aedes aegypti* and *Aedes albopictus*, up to 390 million dengue infections occur worldwide per year(2). A patient with dengue infection may present with a fever, accompanied by symptoms including vomiting, headaches and abdominal pain. Progression to severe dengue fever can result in severe plasma leakage, severe bleeding and severe organ involvement(3). While infections are mainly limited to tropical and subtropical areas (Figure 1.1), climate change models predict that the *Aedes* vectors could spread to parts of Europe and Korea in the future(4).

'Dengvaxia' is a live attenuated DENV vaccine that contains DENV structural genes as well as non-structural genes from a yellow fever vaccine strain(5). While moderately effective, there remains serious concern that in certain seronegative recipients, the vaccine could exacerbate pathogenesis of subsequent infections, due to antibody dependent enhancement (ADE) of infection(6). These safety issues have resulted in poor uptake of the vaccine in the 20 countries in which it is licensed(7). QDENGA, a live attenuated tetravalent dengue vaccine candidate, has been reported as efficacious in the prevention of symptomatic dengue, with no evidence of safety risks(8). This vaccine has recently been approved for use in Indonesia, the EU and the UK(9). Currently, the recommended treatment for dengue infection is supportive therapy (fluid therapy and paracetamol)(2), demonstrating a need for further research and development of safer prophylactics and antivirals against DENV.

Four serotypes of DENV exist; DENV1, DENV2, DENV3 and DENV4, with some evidence for the existence of DENV5(10). Virus particles are comprised of a lipid bilayer studded with the glycoproteins E and prM, and an inner icosahedral nucleocapsid comprised of a lattice of capsid (C) proteins. The nucleocapsid encases a single copy of the ~10,700 bp RNA genome that features a large single open reading frame (ORF) that encodes the structural proteins prM, E and C and the non-structural proteins NS1, NS2A, NS2B, NS3, NS4A, NS4B and NS5(11, 12).

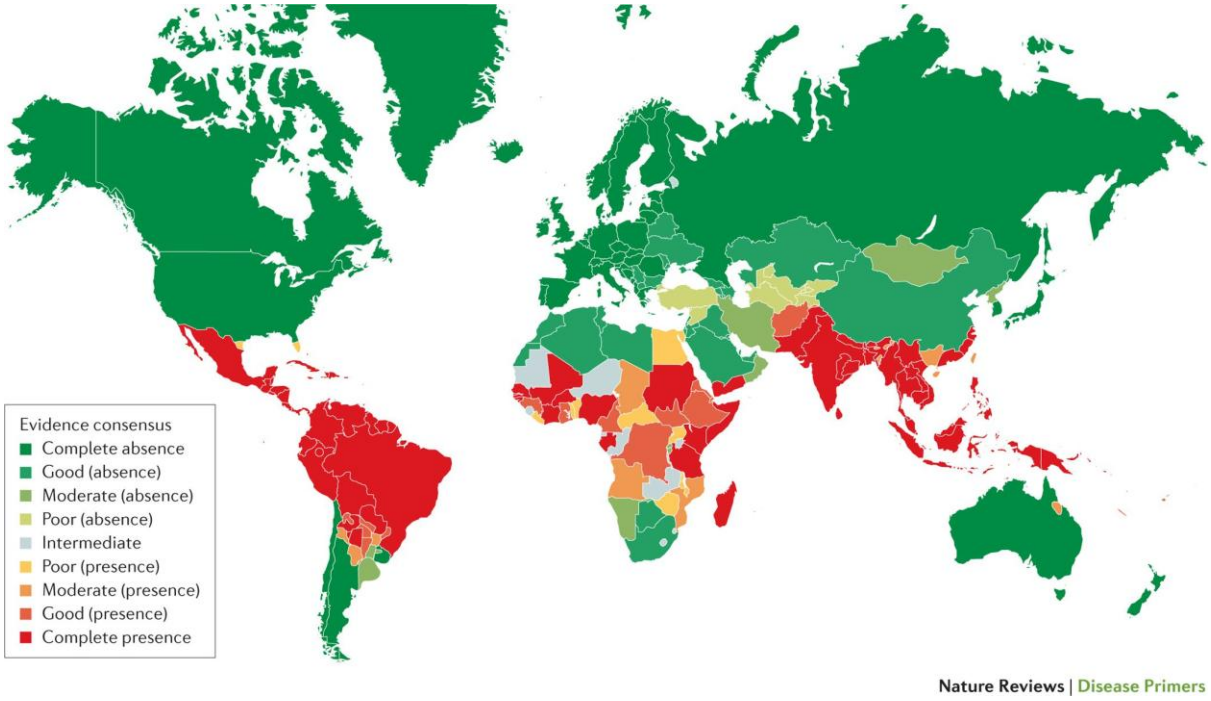

Figure 1.1: Dengue virus national and subnational evidence consensus for complete absence of dengue (dark green) to complete presence of dengue (dark red). Source: (13). Reprinted with permission from Nature Reviews Disease Primers.

NS1 has been identified as a key cause of the symptoms of dengue fever, as well as a contributing factor for evasion of the human immune system(14). As such, NS1 is the overall focus of the projects outlined in this thesis. The creation of a mutant library for *in vitro* and *in vivo* viral fitness analysis via deep sequencing was aimed to elucidate the importance of each nucleotide of DENV NS1 in viral RNA replication and infectious particle production and help to analyse the potential for the emergence of *Wolbachia*-resistant DENV mutants. Three unique drug screens were designed to probe for inhibitors of NS1, using a protein:protein interaction system and an *in silico* docking screen to identify inhibitors of NS1 dimerisation, and a Nanoluciferase-based thermal shift assay to identify NS1-interacting compounds.

1.2 Transmission of dengue virus

As stated, DENV is spread to humans by *Aedes aegypti* and *Aedes albopictus* mosquitoes. The virus exists in two overlapping transmission cycles; the human cycle and the sylvatic cycle (Figure 1.2)(15). In the sylvatic cycle, DENV cycles between non-human primates and mosquitoes. In the human cycle, DENV cycles between humans and mosquitoes(16). The sylvatic cycle maintains an animal reservoir for DENV and can lead to spillovers in rural areas that are inhabited by primates and humans, which can then lead to outbreaks in urban

areas(15). Additionally, DENV can be maintained in mosquito populations vertically via transovarial transmission, in which DENV is transmitted from a female mosquito to its offspring(17, 18). This has been hypothesised to allow persistence of arboviruses during unfavourable periods for mosquito vectors. However, many field studies have attempted to quantify vertical transmission (VTR) and found no evidence for its occurrence(19, 20). As sample sizes typically required to identify vertical transmission of dengue are often impractical, it is commonly thought that VTR is irrelevant in the context of dengue persistence(21).

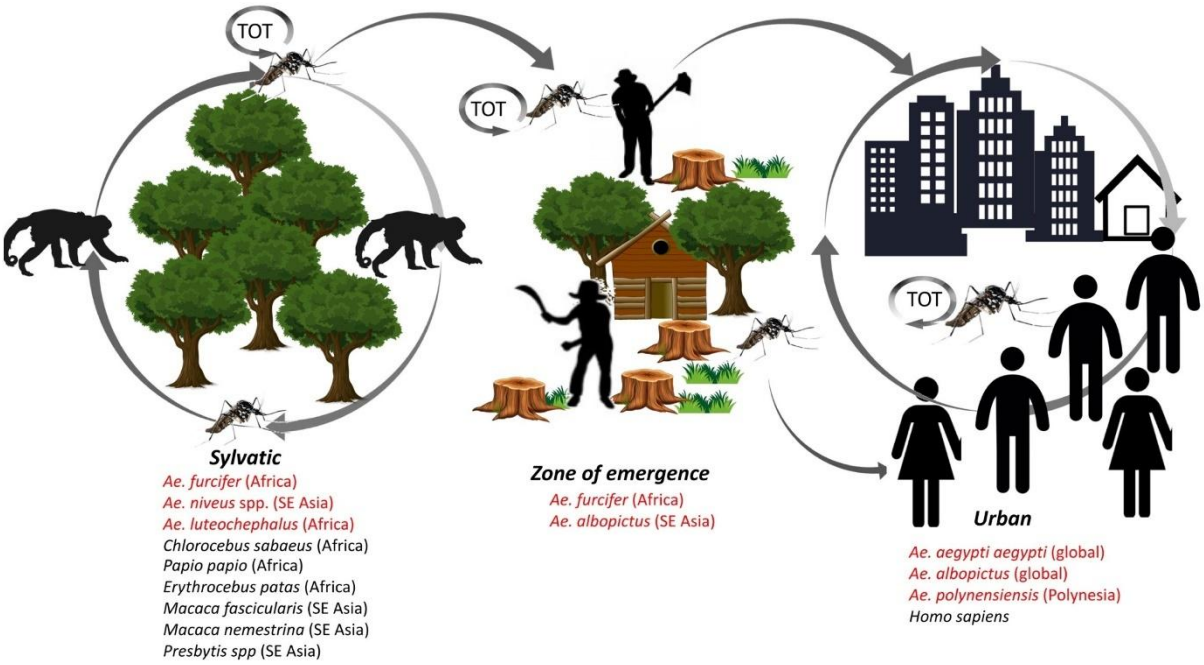

Figure 1.2: The sylvatic (affecting wild animals) and urban transmission cycles of dengue virus. TOT indicates trans-ovarian transmission by *Aedes* mosquitoes. Source: (22). Reprinted with permission from Acta Tropica.

1.3 Clinical manifestations and pathogenesis of dengue virus infection

While it is estimated that 390 million dengue infections occur each year, only a quarter of these cases are symptomatic(23). Typically, symptomatic patients will present with a short-lived febrile illness with rash, severe aches and leukopenia(24). Severe forms of dengue illness are characterised by severe bleeding, plasma leakage severe organ involvement(3). Symptoms are related to the induction of a 'cytokine storm', in which proinflammatory cytokines which enhance vascular permeability are produced in excess(25). During early disease, higher levels of cytokines including IL-6, IL-10 and MIP3α indicate a greater chance of progression to more

severe dengue illness(26). Dengue severity is greatly increased in infants and children(27), with children aged 3 – 4 undergoing a secondary dengue infection having a 15-fold higher mortality rate than children aged 10 - 14(28). Figure 1.3 outlines the symptoms of DENV infection.

Dengue is not typically reported as a disease with neurological manifestations, unlike orthoflaviviruses including Zika virus (ZIKV), which led to an epidemic of microcephaly during the recent ZIKV outbreak in Brazil(29). However, neurological complications including encephalitis and intracranial haemorrhage have been reported to arise from dengue infection, though this is uncommon(30).

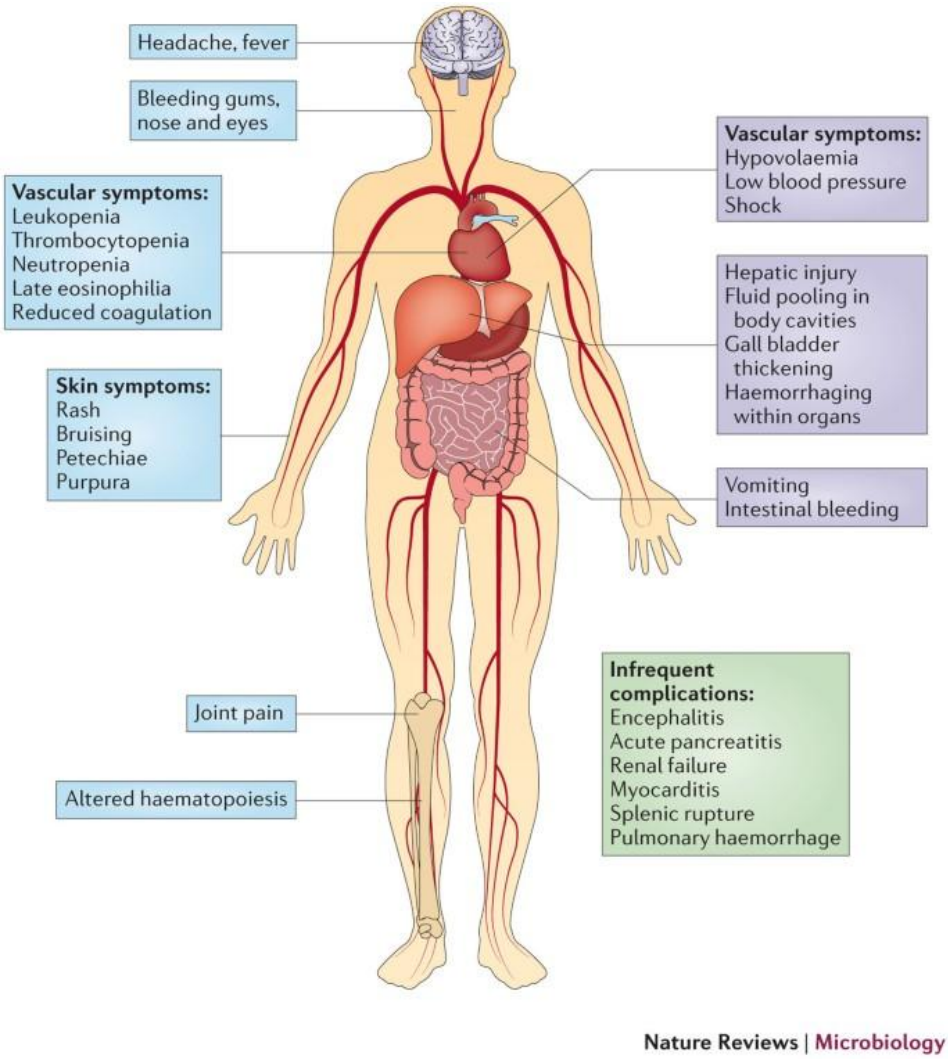

Figure 1.3: Clinical manifestations of dengue infection, including symptoms associated with mild to severe disease. Symptoms associated with severe dengue fever are listed in the three purple boxes. Source: (31). Reprinted with permission from Nature Reviews Microbiology

1.4 The viral genome

The DENV genome exists as a single molecule ~10,700 bp positive sense single-stranded RNA genome (Figure 1.4)(12). Each dengue virion is thought to contain a single copy of this genome, which features a 5' untranslated region (UTR), a single open reading frame (ORF) and a 3' UTR(32). A typical orthoflavivirus 3' UTR features 3 sub-domains; the highly variable region, which facilitates host adaptation(33), a moderately conserved region and a highly conserved region(32). A 5' cap structure (m^7GpppAm) is recognised by the host ribosome machinery to enable viral polyprotein translation(34). Despite not having a poly-A tail, which typically allows interaction between cellular mRNAs and the poly-A-binding protein, the 3' UTR still binds poly-A-binding protein, allowing for translation of the viral protein(35). The orthoflavivirus genome features cyclisation sequences, which form a variety of stem loops structures, allowing for long range RNA-RNA interactions resulting in the cyclisation of the genome. Both the circular and linear conformations of the genome are required for viral replication(36). During infection, by-products of the viral genome, which do not encode viral proteins, are produced. This subgenomic orthoflavivirus RNA (sfRNA) is a result of incomplete degradation of the genome by the host exonuclease XRN1(37). This sfRNA sequesters XRN1, while also interfering with innate immune responses(38, 39). The ORF encodes for a large polyprotein that is cleaved co- and post-translationally by viral and host proteases, releasing the structural and non-structural proteins described below.

Figure removed as permission to reprint was not available.

Figure 1.4: DENV positive-sense single stranded RNA genome schematic diagram. This diagram illustrates DENV 5' and 3' untranslated regions, open reading frame, 5' and 3' cyclisation sequences, upstream AUG regions, cap, and secondary structures of the 5'UTR and 3'UTR. Source: (40).

1.5 Orthoflavivirus structural protein functions

Envelope protein, with prM, forms the surface structure of assembled dengue virions(41). Fusion of E protein with a host cell membrane allows entrance of the virus particle into a

cell(42). Due to E protein being a major focus of Chapter 3, the protein will be further described in section 1.12.

The membrane protein is comprised of an N-terminal domain, present in the immature virion, a flexible M-domain, a stem region and two transmembrane helices. With E, precursor membrane (prM) forms the surface structure of assembled immature dengue virions(41). The N-terminal domain, 'pr', covers the fusion loop of E, preventing immature virions from pre-emptively binding the host cell membrane. In the acidic conditions of the trans-Golgi network, conformational change results in exposure of a furin cleavage site, and the pr peptide is removed by a furin protease before release from the infected cell, resulting in complete maturation of the virion(43).

Capsid is the first protein encoded in the genome. It is connected to prM by a peptide which spans the ER membrane, with C present on the cytoplasmic side(44). C is a highly basic protein which forms homodimers in solution, with high affinity for lipid membranes and nucleic acids(45, 46) and with RNA chaperone activity(47). The first step in assembly of a dengue virion is the formation of the nucleocapsid, which features a single copy of the viral RNA genome and multiple C copies(44). C also accumulates on the surface of lipid droplets and the nucleus, however the function of this variable localisation remains unclear(48).

1.6 Orthoflavivirus non-structural protein functions

NS1 is a multifunctional protein required for virus production and viral RNA replication. NS1 is involved in membrane alterations, immune evasion and contributes to pathogenicity of DENV(49). Due to the importance of NS1 to this thesis, NS1 functionality and structure will be expanded upon in later sections.

NS2A is a small, hydrophobic, non-enzymatic transmembrane protein involved in the viral replication lifecycle(50) and an antagonist of the host immune response(51). NS2A protein features 5 integral transmembrane segments allowing association with the lipid bilayer of the endoplasmic reticulum(52). Immunofluorescence and immunoelectron microscopy analysis have shown the colocalisation of Kunjin virus NS2A with dsRNA and NS4A within vesicle packets(53), and colocalisation of NS2B with NS3 in convoluted membranes(54). Kunjin and DENV NS2A have been shown to bind 3' UTR RNA(53, 55), and a single mutant, NS2A G11A,

has been shown to abolish virion assembly, reduce cleavage at the C-prM cleavage site and cause mislocalisation of C, prM and E proteins(55).

DENV is translated as a single polypeptide, which requires proteolytic processing by the NS2B/NS3 serine protease and other proteases to produce individual viral proteins(56). The N-terminal protease chymotrypsin-like domain of NS3 requires NS2B as a cofactor to form a stable complex(57). The protease features a classical catalytic triad (Asp-His-Ser)(58). Additionally, NS3 has helicase activity, allowing for the unwinding of duplex RNA(59). In ZIKV, this has been shown to require interaction with the NS5 RNA polymerase(60). In addition to being a cofactor for protease activity, NS2B contributes to viral RNA replication and particle formation of JEV(61). NS2B also degrades the cytosolic DNA sensor cyclic GMP-AMP synthase, leading to a reduction of the host immune response to viral infection(62).

The non-enzymatic proteins NS4A and NS4B are connected by the transmembrane peptide 2K, forming NS4A-2K-NS4B, which is cleaved during polypeptide maturation(63). Upon cleavage of the 2K sequence from NS4A, NS4B is translocated to the ER lumen(64), while NS4A remains embedded in the ER membrane. NS4A plays vital roles in the assembly of the viral replication complex and membrane remodelling (65-67), in addition to modulation of autophagy, which prevents cell death during infection, enhancing virus replication(68). NS4B interacts with multiple viral proteins including NS1 and NS3 to aid viral replication and helicase activity(69, 70), and antagonises the host immune response by inhibiting IFN-α/β signalling(71). Mutagenesis studies have revealed an interaction between NS4A and NS4B that is required for viral replication(72). Expression of recombinant NS4A induces membrane alterations allowing for the formation of the viral replication complex, however this only occurs when NS4A is expressed with 2K, indicating that the removal of 2K is linked to this activity(73). An interaction between NS1 and the NS4A-2K-4B cleavage intermediate is also required for viral RNA replication(74).

NS5 is a multifunctional enzyme. Methyltransferase activity via the N-terminal region enables 5’-RNA capping, protecting the viral RNA genome from hydrolysing enzymes and facilitating translation(75). Separated from the N-terminal by a linker of five to six amino acids, the C-terminal region features an RNA-dependent RNA polymerase allowing replication of the DENV RNA genome(76). NS5 is also translocated to the nucleus, where it interferes with splicing by binding to spliceosome complexes, resulting in enhancement of DENV replication(77).

1.7 Structure of dengue virus

The structure of DENV has been determined to a resolution of 2.5 Å using cryo-electron microscopy (cryo-EM)(78). To achieve this, the DENV prM and E genes were inserted into the genome of the insect-specific orthoflavivirus Binjari virus, due to its restriction to growth in mosquitoes(79), then transfected into C6/36 mosquito cells. This Binjari-DENV2 (bDENV-2) virus was purified for cryo-EM imaging. The structure of the mature virion is shown in Figure 1.5.

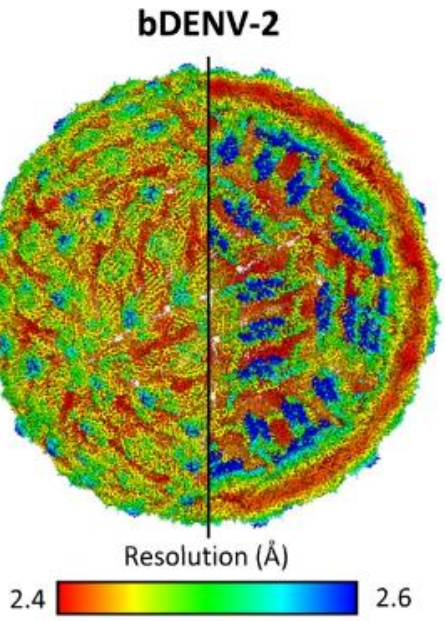

Figure 1.5: 2.5Å Cryo-EM structure of bDENV-2. Source: (78).

1.8 Dengue virus lifecycle

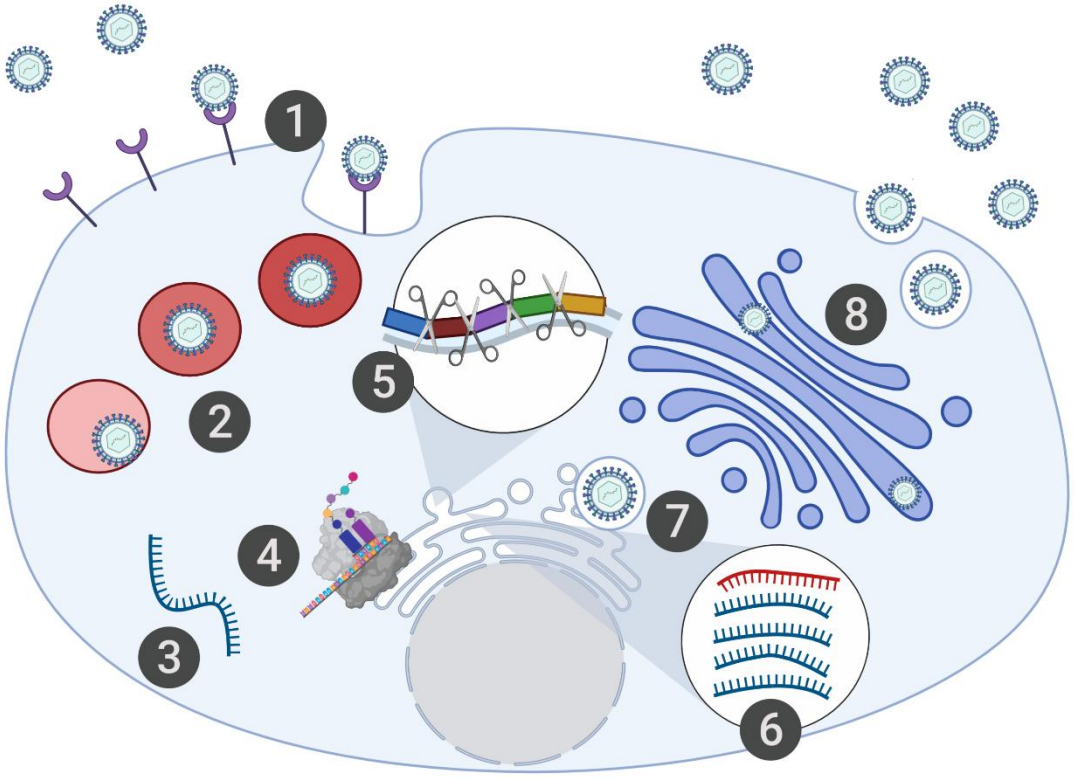

Figure 1.6: DENV life cycle(80). 1) Viral entry. 2) Maturation of virus-containing endosomes. 3) Release of the viral genome into the cytosol. 4) Translation of the RNA genome. 5) Protease-mediated cleavage of the polypeptide. 6) Viral RNA transcription. 7) Viral assembly. 8) Virus trafficking and budding.

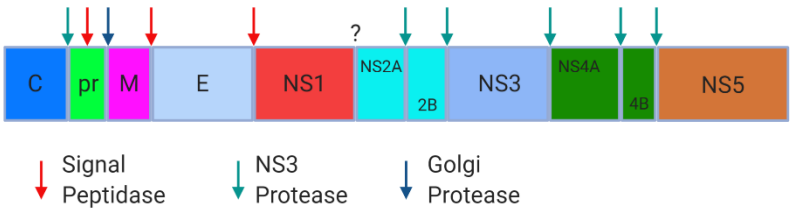

Figure 1.7: Orthoflavivirus polypeptide processing. Arrows illustrate cleavage sites by specific enzymes(49).

Viral Entry:

To enter a cell, DENV particles associate with and diffuse across a cell surface, until receptor engagement and the concentration of DENV particles in a clathrin-coated pit. Particles are internalised via clathrin-mediated endocytosis, with the formation of a clathrin-coated vesicle(81). Alternative pathways have also been reported, but are less well characterised(82).

Infectable cells include endothelial and dendritic cells, hepatocytes, monocytes and macrophages(83). The internalised virus particles are typically trafficked in Rab5-positive early endosomes, which mature into Rab7-positive intermediate endosomes, before the virus particles escape from the endosome via a membrane fusion process, to be released into the cytosol(81). This escape is mediated by the acidic environment in the endosome, which promotes the irreversible trimerization of E, exposing a fusion loop from the virion surface and allowing fusion with host-cell membranes(84). The formation of a fusion pore allows the release of the nucleocapsid into the cytosol(85).

Translation of the RNA genome:

The mechanism for the release of the genomic RNA from the nucleocapsid, and translocation to the ER, is yet to be elucidated. The DENV genome features a 5' type 1 7-methyl guanosine cap structure (m^7GpppAm), 5' untranslated region and a 3' untranslated region lacking a poly(A) tail. The genome contains only one open reading frame, and translation produces a single polypeptide(86). DENV translation relies on the host cell's translational machinery(87).

Initial translation of the positive sense RNA genome after nucleocapsid release is not well understood, due to technical difficulties with investigating the genome while packaged in virions or undergoing translation(88). Translation occurs at the endoplasmic reticulum, with a single polyprotein being produced, to be cleaved by host proteases and the viral protease NS2B/NS3pro to yield 10 viral proteins (Figure 1.7)(89).

The RNA genome displays many features which aid its translation. These features are predominantly present in the 5' and 3' UTRs. NS3 removes a phosphate from the 5' terminus of the vRNA, and NS5 catalyses the addition of a 5' cap structure(88). This 5' cap structure allows for recognition of the vRNA by the eukaryotic initiation factor eIF4G, allowing for scaffolding of several proteins required for interaction with the ribosome and translational initiation factors(90). It is well documented that a 5' cap and a 3' poly(A) tail work synergistically for expression of eukaryotic cellular mRNAs(91). However, DENV does not feature a poly(A) tail, similar to most orthoflaviviruses, and must utilise other 3' features to allow for efficient translation(92). Luciferase experiments have illustrated that the DENV 3' UTR contributes to both translational efficiency and RNA stability of the vRNA, independent of the presence of a 5' cap, compensating for absence of the poly(A) tail(90).

Translation is also regulated by the circularisation of mRNA. For eukaryotic mRNA, this circularisation is a result of communication between the 5' cap and 3' poly(A) tail, caused by interactions of cap and poly(A) binding proteins including eIF4E, eIF4g and Pab1p(93). As DENV vRNA lacks the poly(A) tail, it relies on long range RNA-RNA interactions to circularise. Multiple regions of the DENV genome have been found to contribute to its circularisation, including the 5' and 3' cyclisation sequences (CS)(94), the 5' and 3' upstream AUG regions (UAR)(94), and the 5' and 3' downstream AUG regions (DAR)(95).

Viral RNA transcription:

DENV induces membrane rearrangements in the host cell endoplasmic reticulum. Vesicle packets (VPs), which contain replication complexes, allow for RNA replication via a negative-strand RNA intermediate, protect newly synthesised viral genomes from host nucleases and innate immune effectors, and aid viral RNA release and virion budding(96). The VPs contain NS2B, NS3, NS4A, NS4B, NS5, single stranded vRNA and the replication intermediate, double-stranded RNA, and a 10 nm pore in the membrane allows for the transfer of metabolites and newly created viral RNA in and out of the membrane(97). Convoluted membranes contain the NS2B-NS3 viral protease complex and are hypothesised to be the site of polyprotein processing(97). The induction of these membrane rearrangements requires NS4A. Overexpression of NS4A results in the formation of these virus-induced membrane alterations, although other viral and host factors, including NS1, are hypothesised to contribute(49). These membrane rearrangements do not occur when NS4A is expressed with 2K, the C-terminal linker to NS4B, which permits NS4A translocation to the ER(98).

RNA replication begins with the positive single stranded RNA genome. Upon transcription of a negative strand by the RNA-dependent RNA polymerase NS5, the double-stranded RNA intermediate is formed. The negative strand is then used repeatedly as a template to produce more positive single stranded vRNA, to be packed into the nucleocapsid, serve as a template for translation of the viral polyprotein, or to produce more double-stranded intermediate(99).

Virus assembly:

The first step of DENV assembly involves the formation of a nucleocapsid. This step is not fully understood and is thought to be the result of non-specific electrostatic interactions(100). Other viruses, such as human immunodeficiency virus have been shown to feature a

packaging signal, but a sequence allowing binding of C to DENV vRNA has not yet been identified(101). C proteins have been demonstrated to act as RNA chaperones for the DENV vRNA genome(102), which is common among *Flaviviridae* C proteins, and hypothesised to be important for RNA structural rearrangements in virions(103).

The virus assembly sites are situated near the vesicle pore which is thought to allow for coordinated encapsulation of the newly synthesised positive sense DENV vRNA(97). A recent study has developed a model in which NS2A is heavily involved in virion assembly by binding to the 3' UTR of DENV vRNA as it exits the replication complex. NS2A also recruits C-prM-E and NS2B-NS3, by binding prM and NS3, respectively. After cleavage of the C-prM-E portion of the polyprotein by the NS2B-NS3 protease, the vRNA is bound by the newly formed mature C, forming the nucleocapsid. This leads to the dimerisation of prM and E, which oligomerise and surround the nucleocapsid with a lipid bilayer (Figure 1.8)(55).

Virus trafficking and budding:

After the initial assembly, DENV exists as an immature virion. This virion has a diameter of approximately 60 nm, compared to the ~50 nm mature virion, elongated by prM spikes extending from the virion, with trimeric E surrounding the spike(104). The immature virion is transported to the trans-Golgi network through the secretory pathway before secretion(96). This environment has a pH of approximately 5.5, which results in a conformational change of the prM-E heterodimers, exposing a cleavage site and allowing furin protease to cleave prM to form M proteins(105). The cleaved peptide 'pr' is only released after secretion of the mature virion, to ensure the E protein fusion loop is covered, and to avoid accidental fusion with the cell membrane. The release of pr is mediated by the change in pH in the extracellular space, after the mature virion has been exocytosed from the cell(106).

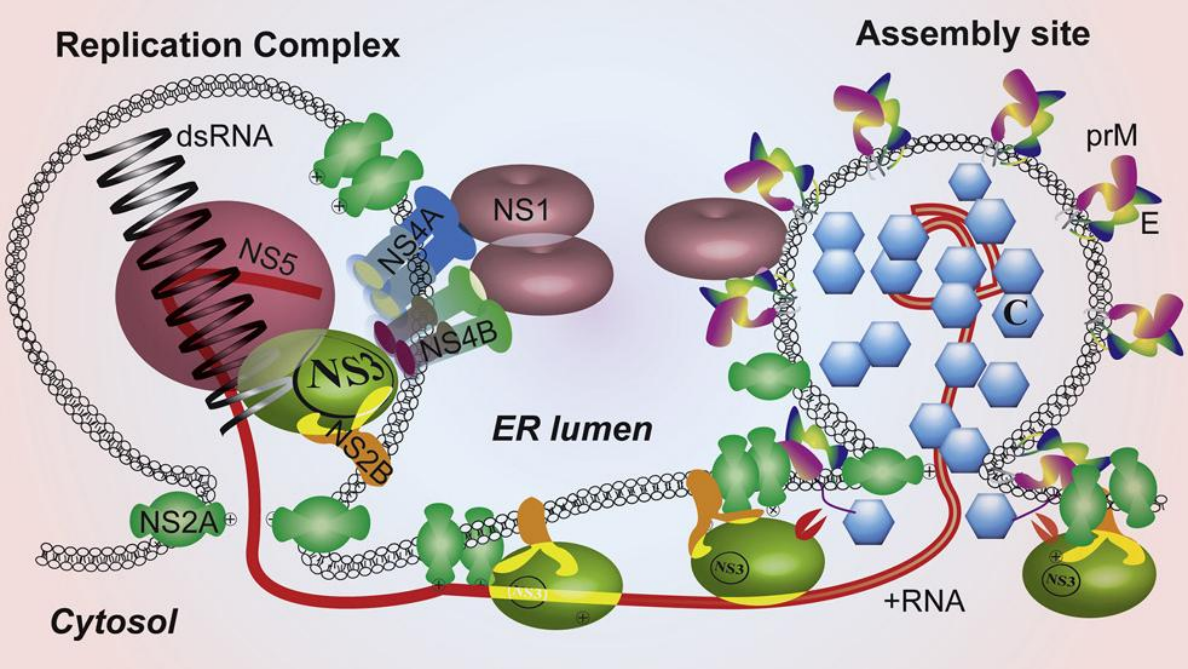

Figure 1.8: Model of DENV RNA replication and virus assembly in virus-induced membrane rearrangements. Source: (50). Figure reprinted with permission from Cell Host & Microbe.

1.9 Host factors

Proviral host factors:

DENV relies on many host cell proteins for all aspects of the viral replication cycle. For entry into mammalian cells, receptors including heparan sulfate, DC-sign and mannose receptor can be utilised, although the entire spectrum of DENV entry factors and their exact roles remains unclear(107). As stated, the main pathway of entry into a mammalian cell is through clathrin-mediated endocytosis, and as such, the factors required for formation of the clathrin lattice are certainly pro-viral proteins and have been identified as targets for potential antivirals. For example, the compound prochlorperazine targets dopamine D2 receptor (D2R), blocking binding of DENV to D2R on the cell surface, and inhibiting clathrin-mediated endocytosis(108).

As another major example of host factors that are co-opted by DENV, NS3 was discovered to directly interact with, activate and recruit fatty acid synthase (FASN) to vesicle packets. This FASN-mediated local fatty acid synthesis is thought to contribute towards the high demand for lipids associated with virus-induced membrane rearrangements and particle synthesis(109). Lipid droplets have been shown to sequester C to the vesicle particle, allowing for formation of a nucleocapsid as NS2A translocates the viral RNA from the vesicle packet(46).

The activation of autophagy by DENV has also been suggested to be proviral due to the increase in production of free fatty acids which enhance dengue replication, as a lipid bilayer is an integral component of a dengue virion(110).

The reliance of dengue on the host endoplasmic reticulum (ER) is illustrated by the requirement of ER-membrane complex subunits 1-7(111). Additionally, proteins required for translation, such as ribosomal stalk proteins RPLP1 and RPLP2, are necessities for production of dengue virions(112).

Antiviral host factors:

Initial infection and replication of DENV in humans occurs in skin cells(113). This is where the immune response begins(114). Pattern recognition receptors recognise a pathogen's protein, nucleocapsid, lipid or carbohydrate structures, or pathogen-associated molecular patterns, triggering intracellular signalling cascades to respond with expression of proinflammatory molecules such as cytokines and chemokines to combat the pathogen(115). Responding to dengue are receptors including cytoplasmic retinoic acid-inducible gene I (RIG-I), melanoma differentiation-associated protein 5 (MDA5) and endosomal Toll-like receptor 3 (TLR3) and 7 (TLR7)(116). RIG-I and MDA5 detect RNA in the cytoplasm, leading to a downstream activation of type I interferons (IFNs)(117). TLR3 and TLR7 recognise dsRNA or ssRNA, respectively, in endosomal compartments. TLR7 leads to activation of nuclear factor-κB (NF-κB)(118), a transcription factor responsible for expression of multiple genes required for defence against a broad range of pathogens(119). The type I IFN response leads to activation of the JAK/STAT pathway, which promotes expression of interferon stimulated genes (ISGs) with antiviral activity(120).

Additionally, DENV infection is known to activate the complement pathway(121). There exist three converging pathways for complement activation, including the classical, lectin and alternative pathways. Each of these pathways converge on the protein C3, which is cleaved to C3b, leading to the formation of a membrane attack complex which lyses pathogens(122). The complement pathway typically acts to limit viral replication, however in some patients results in increased disease severity, contributing towards more severe dengue fever. NS1 is known to be a trigger for complement activation. It enhances production of the terminal complement complex SC5b-9, which may lead to increased vascular leakage common in severe dengue

patients(123). It has also been reported that up-regulation of CD59, an inhibitor of the complement pathway, is stronger in patients with dengue fever in comparison to DHF, suggesting that the complement system may become dysfunctional during DHF and instead increase viral load and tissue damage(124).

The complement protein C1q functions to restrict antibody dependent enhancement (ADE) of infection(125). ADE occurs when antibody concentration is not sufficient to neutralise an infection, but excess cytokine levels and other factors are produced, leading to enhanced disease symptoms, and potentially increasing viral load(126). It has been illustrated that ADE in human macrophages may increase the membrane fusion potential of dengue, enhancing infection and burst size of the virus, while also causing disproportionally strong anti-inflammatory responses(127). By restricting ADE, C1q aids in alleviating symptoms. This effect occurs upon the binding of C1q to E protein of all dengue serotypes causing a reduced inflammatory response through modulation of mRNA expression of immunoregulatory molecules(128). Other components of the complement system have also been shown to reduce viral load and disease symptoms(129).

Emerging tools have paved the way for discovery of proviral and antiviral factors for many viruses. Genome-wide CRISPR/Cas9 gene knockout screens have been used to identify host factors that are important for each stage of the viral lifecycle(130). Additionally, CRISPR activation screens, which utilise a dead Cas9 system to target a gene with transcriptional activators, allow for screening the effects of increased expression of each gene in a culture of cells, facilitating the discovery of antiviral genes which may be specifically downregulated by the virus, or any host gene which alters viral fitness(131, 132). Similarly, genome-wide RNA interference screens are used to investigate host factors, by reducing RNA levels instead of producing a knockout cell line(133). Global proteomic analyses have been performed to identify all interacting proteins with specific dengue proteins. Relevant to this project, the NS1 interactome has been mapped using a functional RNAi screen, revealing both proviral and antiviral host factors(134).

1.10 NS1 structure and functions

NS1 plays multiple roles in the lifecycle of DENV. It exists in multiple oligomeric states. During translation, it is translocated to the ER lumen and cleaved from E protein and NS2A(14). The addition of high-mannose carbohydrate moieties (glycosylation) results in a conformational

change exposing a hydrophobic region, causing NS1 to self-dimerise. This dimerisation event enables the association of NS1 with the ER membrane, and alternately with virus-induced ER-derived vesicle packets and large cytoplasmic vacuoles(135, 136). Upon further glycosylation, NS1 forms a lipid-rich hexamer, which is transported to the Golgi, and secreted from an infected mammalian cell(137, 138).

The structures of the dengue NS1 dimer(139) and hexamer(140) have each been solved, as well as a monomeric C terminal truncation mutant(141). The monomer features 3 domains. This includes a β-roll, Wing and a β-sheet. The first β-roll domain extends from amino acids (AAs) 1-29. It features β hairpins which become intertwined when NS1 dimerises, forming a four-stranded β-sheet. The dimer is stabilised by two disulphide linkages between Cys-4 and Cys-15. The second domain is a Wing structure, formed by amino acids 30-180. This is formed by two subdomains. AAs 38-151 comprise of a four-stranded β-sheet, two α helices and a disordered tip. This is stabilised by an internal disulphide bond between Cys-55 and Cys-143. The wing also contains two glycosylation sites at Asn-130 and Asn-175. Discontinuous connector subdomains from AAs 30-37 and 152-180 links the β-roll and Wing, and the Wing to a central β sheet, respectively, with a disulphide bond between Cys-179 and Cys-223. The third domain, from AAs 181 to 352, is a continuous β-sheet with 9 β-strands, which intertwine with another NS1 monomer to create an antiparallel β-ladder. The hexameric form of NS1 exists as a trimer of dimers, forming a barrel shape with a presumed lipid core(142) (Figure 1.9).

The NS1 dimer predominantly co-localises with dsRNA in replication complexes, which are thought to be contained within ~80 – 100 nm vesicles which are clustered in structures known as vesicle packets(135, 143). It has recently been shown that the NS1 wing domain interacts with NS4A-2K-4B, a cleavage intermediate. This interaction is required for RNA replication, and the authors hypothesised that NS1 may aid NS4A-2K-4B cleavage to NS4A and NS4B(144). NS1 is essential in establishment of vesicle packets, allowing for the successful replication of DENV vRNA(144).

NS1 is also critical for virus production. Specific NS1 mutants have been shown to drastically reduce the production of infectious particles, including S114A, W115A, D180A and T301A(145). Coimmunoprecipitation studies have revealed an interaction of NS1 with C, prM

and E. This is hypothesised to be the result of an interaction between NS1 and assembled virions, suggesting a possible role of NS1 in the formation of virus particles(145).

An immunoprecipitation-based proteomic analysis revealed 64 NS1-interacting proteins in Huh7.5 cells, of which 33 were ribosomal proteins(146). Ribosomal proteins RPL18 and RPL17 were shown to be redistributed during DENV infection to the perinuclear region. Furthermore, silencing of these proteins was shown to significantly reduce viral translation, demonstrating a role of NS1 in translation of the DENV genome(146).

As stated previously, NS1 forms a hexamer, which is secreted from the cell(138). This hexamer contains a lipid-packed core comprised of triglycerides, monoacylglycerol and diacylglycerol, cholesteryl esters and phospholipids, forming a lipoprotein(147). Hexameric NS1 is not required for infectious particle production or viral RNA replication(145), but does serve other purposes, including immune invasion. It has been demonstrated that inoculation of mice with purified secreted NS1 leads to vascular leak syndrome and increased cell permeability when applied to human endothelial cell monolayers(148). Secreted NS1 is a pathogen-associated molecular pattern (PAMP), which activates Toll-like receptor 4 (TLR4), inducing expression of proinflammatory chemokines and cytokines(149). Importantly, blocking TLR4 activity in a mouse model reduces vascular leakage(149).

Hexameric NS1 also binds proteins in the complement pathway, including mannose-binding lectin (MBL). This aids immune evasion by competitively binding MBL, reducing recognition of DENV and suppressing MBL-mediated neutralisation(150). It is known that secondary DENV infections show greater severity in patients(151). In addition to antibody-dependent enhancement (ADE) of infection, this is a result of patients producing anti-NS1 antibodies that cross-react with components of the extracellular matrix, as well as platelets, causing damage and enhancing the disease(152). In line with this, the NS1 antibody generated by patients has been suggested as a method of predicting disease severity(153). Interestingly, levels of secreted NS1 are reportedly decreased, with measured sNS1 levels not correlating with severity, in secondary dengue infection(154). One explanation for this is the sequestering of NS1 in immune complexes in response to high levels of DENV-reactive IgG, blocking NS1 target epitopes from detection via ELISA(155). These immune complexes have been speculated to be involved in pathogenesis(156, 157).

Recently, evidence has challenged the theory that secreted NS1 exists only as a hexamer. Recent mass spectrometry analysis of a 250 kDa native-PAGE band from the supernatant of DENV-infected Vero cells revealed complexes of NS1 protein and apolipoprotein A1 (ApoA1), a component of high-density lipoproteins (HDLs)(158). Utilising plasma from healthy donors spiked with streptavidin-tagged DENV2 NS1, NS1 was also shown to bind Apolipoprotein B, indicating interaction with both high-density lipoproteins and low-density lipoproteins (LDLs). In S2 cells, a Drosophila melanogaster cell line, these NS1-HDL and NS1-LDL complexes were determined to be the predominant NS1 species(159). When a mixture of NS1 and HDL were combined with a molar ratio of 2.5:1, analysis by negative-stain electron microscopy identified three types of NS1-HDL complexes. Approximately 60% of the complexes featured 3 dimers bound to an HDL particle, approximately 25% featured two dimers bound to one HDL particle, while approximately 10% featured four dimers bound to one HDL particle. This demonstrates a dissociation of the NS1 hexamer into dimers upon binding to HDL(159). Cryo-EM analysis of His-tagged NS1 expressed in HEK293-cells displayed high levels of tetramer in supernatants, with a minority (3.1%) hexameric population. The tetrameric population was also shown to exist in stable and loose formations, with stable tetramers forming a β-roll at the N-terminus and loose tetramers forming a β-sheet. Importantly, while the anti-NS1 antibody 5E3 was able to bind NS1 in hexamer and loose tetramer formation, the tetrameric structure was resistant to 5E3 binding, introducing a previously unknown hurdle in producing therapeutics against NS1-induced pathogenesis(160).

Lipid rafts are regions of the plasma membrane with increased cholesterol, glycosphingolipids and outward-looking protein molecules, enabling interactions between the cell and extracellular molecules(161). Treatment of murine macrophage RAW 264.7 cells with purified NS1 protein resulted in the accumulation of these lipid rafts on the cell membrane, facilitating DENV attachment(162). ApoA1 from human serum was shown to interact with both glycosylated hexameric NS1 and nonglycosylated dimeric NS1, as well as reducing cell-bound NS1 in a concentration-dependent manner. Further investigation demonstrated an ApoA1-mediated depletion of lipid rafts, showing a protective effect. However, this protective effect is inhibited by high concentrations of NS1 protein(162). Further studies have demonstrated that the formation of these NS1-ApoA1 complexes convey pro-inflammatory signals(163). The

properties of secreted NS1, as well as interactions between NS1 and ApoA1, require more investigation to reveal the complicated nature of the protein.

1.11 Dengue NS1 mutants and effects

Multiple studies have identified critical residues of NS1 in the viral replication lifecycle. Early studies demonstrated that NS1 does not dimerise after removal of the 79 amino acids at the C-terminus(164). Upon further investigation the three most C-terminal cysteine residues were found to be responsible, while mutating the three most N-terminal cysteine residues of NS1 to alanine caused instability of the dimer(165). The highly hydrophobic region at Trp-330 and Tyr-331, when mutated to alanine, completely prevents dimer formation(165).

Mutation of glycosylated sites Asn-130 and Asn-207 to alanine results in diminished, but not complete elimination of dimerisation and secretion(166). This experimental finding is supported by a study which illustrated that glycosylation is not required for NS1 dimerisation by use of a glycosylation inhibitor(136).

A recent study analysed the importance of 46 conserved DENV residues via site-directed mutagenesis(145). This revealed 18 residues that are required for viral RNA replication or efficient infectious particle production(145). It is likely that additional critical determinants of NS1 functions remain to be characterised and that a larger-scale approach would facilitate identification of a greater number of additional residues that are critical to NS1 function, furthering our understanding of DENV.

A 2021 study on DENV evolution utilised next-generation sequencing (NGS) to identify DENV mutants after long-term passage in both Huh-7 and C6/36 cells(167). Over the course of the experiment, repeated passage of virus in one cell line resulted in increased fitness, accompanied by a decrease in fitness when used to infect the alternate cell line, as expected. After 9 passages, multiple mutations reached ~80% frequency in a cell line. In the mosquito cell line, it was observed that high frequency mutants commonly occurred in E, NS3 and the 3’UTR, while in the human-derived cell line, NS2A and NS4B mutants were more common. However, none of these mutants were reintroduced into the DENV genome and verified for changes to fitness. While no mutants of similar significance were identified from either cell line for NS1, it is important to note that this experiment did not involve a comprehensive mutagenesis approach such as deep mutational scanning(168) to create a library with high or

complete mutational coverage and study the effects of introduced mutations in a comprehensive manner. Over 9 passages, while reasonable coverage across the entire genome was ensured, certainly not all nucleotide changes within NS1 would have occurred and been given sufficient opportunity to outcompete wild-type NS1 and register as a mutant of importance according to the study's criteria.

To identify molecular determinants of orthoflavivirus NS1 which confer binding to endothelial cells, *Lo et al.* created multiple chimeric NS1 proteins containing exchanged β-roll, Wing and β-ladder domains from DENV, West Nile Virus (WNV) and ZIKV(169). The DENV NS1 Wing domain was determined to be responsible for tissue-specific binding to endothelial cells, while both the Wing and β-ladder domains were required for induction of endothelial permeability. Examining conservation of the Wing domain across the orthoflavivirus genus, combined with experiments with NS1 mutants, residues 91-93 of DENV and WNV NS1 were identified as determinants of endothelial permeability *in vitro*.

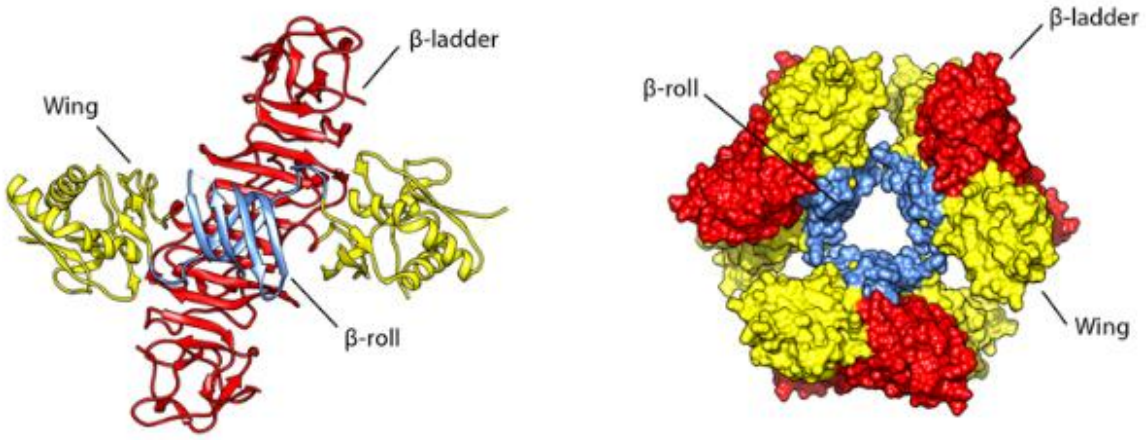

Figure 1.9: 3D structure of the DENV NS1 dimer and hexamer, obtained via x-ray crystallography and cryo-EM, respectively(145).

1.12 Envelope structure and function

Mature dengue virions display 180 copies of the E glycoprotein, present as 90 dimers forming a smooth shell on the virus surface(170). Each E monomer consists of three domains, EDI, EDII and EDIII, joined by flexible hinges which permit irreversible conformational changes during the lifecycle of DENV(171). Additionally, the protein features a fusion loop which allows fusion with target membranes(172), two antiparallel transmembrane domains (TM1 and TM2) which

are also required for membrane fusion(173), and a stem region connecting TM1 to EDIII (Figure 1.10 F).

E undergoes three conformational changes during infection. At neutral pH conditions, E protein is present as a dimer, anchored to the lipid bilayer by the transmembrane domains(173). In the low pH extracellular environment, E protein forms a hairpin-like structure, exposing the fusion loop and allowing for entry into the cell via contact with specific cell surface receptors and receptor-mediated endocytosis(174, 175). In the low pH environment of the endosome, a ring of five E trimers forms, which destabilise the host membrane, allowing fusion of the endosomal membrane and viral membrane, resulting in the opening of a fusion pore(171, 176) (Figure 1.10 A-E).

While EDI is located at the N-terminus of the protein, structurally it is flanked by EDII and EDIII, allowing for stabilisation of the protein(41). For DENV, N-glycosylation occurs at N67 (EDII) and N153 (EDI)(177). N67, which is not a common glycosylation site among orthoflaviviruses, has been demonstrated to interact with the host-cell receptor DC-SIGN via cryo-EM(178). N153 mutants have been shown to alter the pH threshold for fusion with the cell membrane, potentially due to decreased stability of E dimers(179). EDI and EDII are both discontinuous peptides, linked by the EDI/EDII hinge which features four peptide linkers. This hinge region is a major target of neutralising antibodies(180). EDII features the dimerisation domain as well as the fusion loop, therefore playing a major role in the formation of the fusion pore(181). EDIII folds independently from EDI and EDII(182). It is thought to be responsible for receptor binding via interactions with receptors including heparan sulfate(183, 184), and is considered a primary target for blocking virus entry by monoclonal antibodies(185).

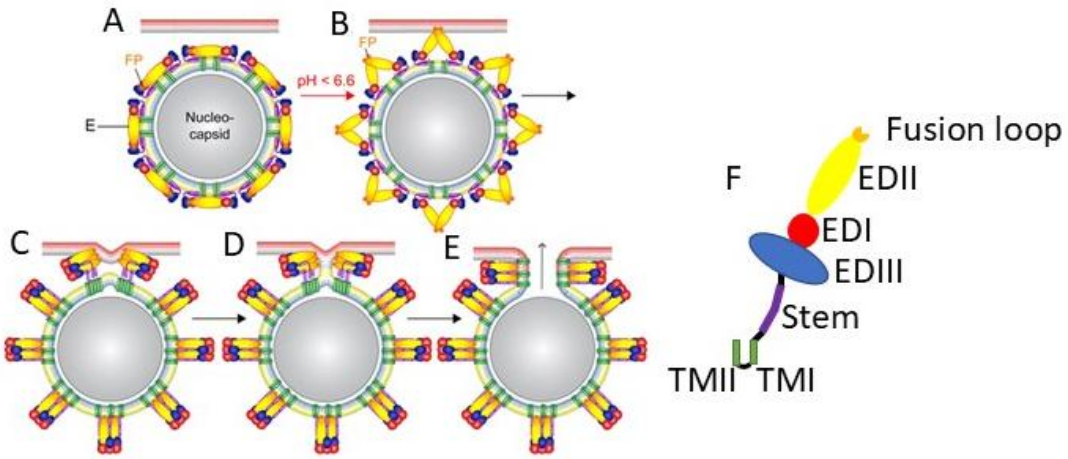

Figure 1.10: Steps of the orthoflavivirus membrane fusion process. A) E protein exists on the surface of the membrane as a dimer, due to the neutral pH of the extracellular environment and early endosomal conditions. Fusion loops are buried within dimer contacts. B) Due to decreased pH within the endosome, E protein assumes a hairpin-like structure, exposing the fusion loop and resulting in binding of E protein to the endosomal membrane. C) Formation of rings of five E trimers. D) The viral lipid bilayer begins to fuse with the endosomal membrane, forming a hemifusion. E) The fusion pore is opened allowing for exit of genetic material into the cytoplasm. E protein exists in its final post-fusion trimer (186). F) Schematic diagram of E, adapted from (41). Colour code: Fusion loop = orange, EDI = red, EDII = yellow, EDIII = blue, stem = purple, TM1/2 = green.

1.13 Current antivirals against dengue virus

While no antiviral therapeutics against DENV are currently approved, several publications have reported small molecule compounds which target viral or host proteins that are vital to the lifecycle of the virus. Multiple stages of the lifecycle have been identified as promising targets of small molecule inhibitors. These stages have been categorised as follows:

1. Virus entry;
2. Endocytosis;
3. Membrane fusion and the release of viral RNA;
4. Transcription of negative and positive strand RNA;
5. Translation, cleavage and post-translational processing of the viral polyprotein;
6. Formation of the replication complex and events within the complex;
7. Virus assembly;
8. Secretion of infectious particles;

We will briefly review small molecule inhibitors that have been determined to specifically inhibit these lifecycle stages, with a focus on E protein and NS1 due to their significance to this thesis.

1.14 Structural proteins as targets

Multiple stages of the viral replication cycle could potentially be disrupted by small molecule inhibitors that target the viral structural proteins C, prM or E. E protein in particular has been the focus of many antiviral development efforts. A common E protein target site is the conserved binding pocket in the hinge region between EDI and EDII, which binds the small detergent molecule N-octyl-β-D-glucoside (βOG)(187). Interaction with this binding pocket by small molecules has been demonstrated to inhibit membrane fusion by inhibiting a 'zipping' of the stem of E protein, which allows formation of the hemifusion membrane by bringing the fusion loop and transmembrane anchor together(188, 189). Multiple small compounds have been shown to inhibit virus entry through this mechanism, including 1662G07 (IC_{90}: 16.9 µM)(188), doxycycline and rolitetracycline (IC_{50}: 55.6 and 67.1 µM, respectively)(190),

NITD448 (IC_{50}: 6.8 µM)(191), Compounds 3e and 3h (IC_{50}: 1.19 and 0.66 µM, respectively)(192) and P02 (IC_{50}: 13 µM)(193).

EDIII is important for virus entry, as the domain recognises host cell receptors. EDIII is therefore a common target for antiviral therapy(194). Multiple receptors involved in virus entry have been identified, including glycosaminoglycans such as heparan sulfate(183). The heparan binding motif, a positively charged region of EDIII, has since been successfully targeted with multiple negatively charged compounds, such as glycosaminoglycans(195). Heparin, a mimetic of heparan sulfate, was shown to inhibit DENV (IC_{50}: 0.3 µg/mL for DENV2 PL0146, 3 µg/mL for DENV2 New Guinea C strain)(196). Many further mimetics have been identified which inhibit DENV *in vitro*, but due to low bioavailability, are ineffective *in vivo*(197). An exception to this is the mimetic PI-88 (IC_{50}: 200 µg/mL)(198).

ST-148 (IC_{50}: 16 nM) is a compound which directly interacts with C protein and was suggested to inhibit uncoating and potentially other later stages of the DENV lifecycle(199). Follow up studies demonstrated the compound stabilises C protein self-interaction, interfering with uncoating by inducing structural rigidity of the nucleocapsid(200).

No antivirals specifically targeting prM have been reported.

1.15 Non-structural proteins as targets

Targeting of viral non-structural proteins has the potential to disrupt viral RNA replication, viral replication, organelle formation, viral protein translation, viral polyprotein cleavage events, virus particle assembly and/or aspects of viral immune evasion. While no small molecule drug-like compounds have been shown to have NS1-specific antiviral activity, disease neutralising NS1 antibodies and the heparan sulfate mimetic PG545 have shown promise as active therapeutics. Both E protein and NS1 are glycosaminoglycan-binding proteins, and PG545 binds each of these proteins(201). The interaction of PG545 with E protein is hypothesised to result in virion lysis, while the interaction of PG545 with NS1 appears to abolish NS1-mediated endothelial disruption, without a specific NS1-based antiviral effect(201). Monoclonal anti-NS1 antibodies 1G5.3 and 2B7 have been identified as broadly protective orthoflavivirus inhibitors(202, 203). Each of these antibodies were determined by x-ray crystallography to bind the NS1 β-ladder domain, and both prevent NS1 from disrupting endothelial integrity. The α-glucosidase inhibitor, celgosivir, has been demonstrated to cause misfolding of NS1,

resulting in its accumulation in the endoplasmic reticulum(204). However, clinical trials have shown no effect in reducing viral load or fever in dengue patients(205).

The NS3 protease is a serine protease which requires NS2B as a cofactor and is responsible for cleavage of the viral polypeptide at 8 of the 13 cleavage sites(206, 207). Multiple drug-like small molecules have been identified which inhibit NS2B/3-mediated proteolysis. One such example is BP2109, which was shown to inhibit viral RNA replication as determined using a reporter-encoding DENV2 replicon with an IC_{50} of 0.17 μM(208). In addition to its protease activity, which resides within its N-terminus, NS3 also functions as a helicase via its C-terminal ATPase/helicase domain. An interaction between NS3 and NS4B causes the dissociation of NS3 with single stranded RNA, enhancing helicase activity(209, 210). In addition to its essential roles in membrane rearrangements that support viral replication and mitochondrial elongation(211), NS4B also plays roles in countering innate immune responses including type I interferon (IFN) signalling, RNA interference, the unfolded protein response and stress granule formation(212). Multiple inhibitors of NS4B function have been identified(197), with the most promising being analogues JNJ-A07 and JNJ-1802 which are both inhibitors of the NS3-NS4B interaction(213, 214). JNJ-A07 directly targets the NS4B protein, and disrupts NS3-NS4B complex formation, but does not disrupt pre-formed complexes. DENV mutants identified via repeated passage in Vero cells showed minimal growth in C6/36 cells, indicating that spread of JNJ-A07 resistant DENV is unlikely. The reported IC_{50} in Vero cells was ~778 pM, and JNJ-A07 has shown strong potency in AG129 mice even when treatment commenced at the peak of viremia (5-6 days post-infection). The analogue JNJ-1802 has been shown to have similar activity and resistance to mutations to that of JNJ-A07 and has also successfully completed a phase 1 clinical study(215).

NS5 is a multi-functional protein, with N-terminal methyltransferase and C-terminal RNA dependent RNA polymerase enzymatic activities. The NS5 crystal structure revealed two cavities suitable for inhibitor binding, one of which contained multiple amino acids critical for viral replication, inspiring development of nucleoside inhibitors and non-nucleoside inhibitors targeting the conserved cavity(216). Research into targeting the NS5 methyltransferase has also identified inhibitors, including methyltransferase competitive inhibitors(217, 218) and compounds which bind a conserved cavity near the S-adenosyl-methionine binding site(219).

Targeting of nucleocytoplasmic trafficking of NS5 has also been explored as a therapeutic strategy(220). While replication of the RNA genome occurs in the cytoplasm, NS5 is predominantly located in the nucleus during infection(221), although the ratio of nuclear to cytoplasmic NS5 is dependent on the strain of DENV(222). Cytoplasmic NS5 is thought to aid immune suppression and contribute to pathogenesis(223, 224). Ivermectin has been shown to prevent binding of NS5 to importin β1(225), which recognises nuclear localisation sequences within NS5(221). This resulted in inhibition of DENV with an IC_{50} of 1.2 - 1.6 µM.

In addition to common preferences for an orally bioavailable drug that is safe and effective, there are additional safety considerations and requirements for DENV antivirals. Disease burden is skewed towards the paediatric population(226). Furthermore, the antiviral must quickly cease progression from mild illness to more severe dengue fever, and must be active against all four DENV serotypes(227).

1.16 Dengue control measures and *Wolbachia*

Due to the lack of approved antiviral therapeutics and effective vaccines, research has also focussed on management of the DENV vectors, *Aedes albopictus* and *Aedes aegypti*. For individuals, preventative strategies against dengue infection involve reducing risk of mosquito bites, using mosquito repellent, mosquito nets, clothing that covers arms and legs and reducing the number of mosquitoes by removing still water from household objects such as buckets(228). At a larger scale, efforts involving insecticide/larvicide usage have been met with operational challenges due to the emergence of resistant populations against all major classes of neurotoxic insecticides, including pyrethroids, organophosphates, carbamates, and organochlorines(229).

In 2011, a successful strategy for the reduction of dengue transmission from *Aedes* mosquitoes was described(230). When *Aedes aegypti* mosquitoes infected with the intracellular bacterium *Wolbachia pipientis* are released into an area, the bacterium rapidly spreads into uninfected *Aedes* populations. Embryonic mortality occurs upon mating between a *Wolbachia*-infected male and a *Wolbachia*-free female, while larvae produced from mating of two *Wolbachia*-infected mosquitoes, two Wolbachia-free mosquitoes, or a *Wolbachia*-infected female and a *Wolbachia*-free male are unaffected, allowing rapid, and potentially permanent introduction of the bacterium into a population of mosquitoes (Figure 1.11)(231). A *Wolbachia*-infected mosquito is less likely to transmit DENV, due to a number of reasons,

including shortened of the mosquito lifespan, decreased reproductive fitness, and decreased egg viability(231, 232). Mosquitoes infected with *w*Mel, *w*MelCS and *w*AlbB *Wolbachia* strains are all, in comparison to uninfected mosquitoes, less susceptible to intrathoracic DENV challenge, more resistant to DENV replication, and show decreased DENV transmission potential based on infectious virus present in the saliva(233). The *w*Mel or *w*AlbB strains have now been used in countries including Australia(234), Malaysia(235) and Indonesia(236) to successfully reduce levels of DENV infection in communities where these programs have been undertaken.

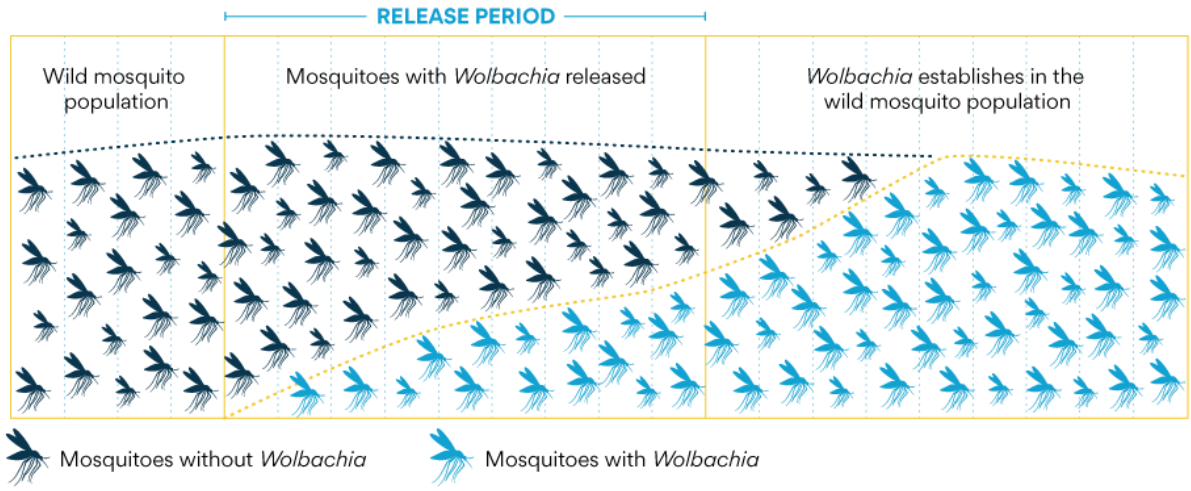

Figure 1.11: Theoretical establishment of released *Wolbachia*-infected mosquitoes in a wild mosquito population(237).

While successful so far, the possibility exists that evolution of *Aedes* mosquitoes, DENV or *Wolbachia pipientis* may reduce the effectiveness of this strategy. An Australian study into a released *w*Mel-infected *Aedes aegypti* colony found few differences in the *Wolbachia* genome post-release, compared to 8 years later(238). Additionally, stability of *Wolbachia* infection in mosquitoes has been shown to remain stable for at least 2 years, despite causing deleterious fitness effects and a small subpopulation of uninfected mosquitoes persisting(239). While *Aedes aegypti* genetics have been shown to impact on the level of DENV 'blocking', mosquitoes that have reduced viral infection, or greater blocking, were also shown to have reduced fitness and will therefore be unlikely to be selected in the field(240).

To characterise the frequency at which DENV may evolve to overcome suppression by *Wolbachia*, it is important to understand how DENV is suppressed. In a study on *Wolbachia*-

mediated blocking of DENV in *Aedes aegypti*, 50% of *w*Mel-infected mosquitoes which fed on viremic dengue patients displayed infectious virus in saliva after 15.8 and 19 days for DENV-1 and DENV-4, respectively, while for *Wolbachia*-free mosquitoes, these values were 9.3 and 14.9 days, respectively(241). This, and similar studies(233) demonstrate that inhibition of DENV replication is incomplete, and that the success of the *Wolbachia* strategy is a result of a reduction of transmission through decreasing the proportion of mosquitoes that are capable of transmitting DENV, and by minimising the time period in which a DENV-infected mosquito remains infectious. However, the cohabitation of DENV and *Wolbachia* in *Aedes* mosquitoes means that resistance to *Wolbachia* may arise over time(242).

The complete mechanism behind *Wolbachia*'s blocking of DENV replication is not fully understood. Numerous studies have identified multiple mechanisms by which *Wolbachia* exerts an antiviral effect. Perturbation of intracellular cholesterol trafficking by *Wolbachia* has been shown to result in DENV inhibition through localised cholesterol accumulation(243). Furthermore, release of reactive oxygen species upon infection of a *Wolbachia*-infected mosquito leads to the activation of immune pathways, resulting in the production of antimicrobial peptides(244). Interestingly, *Wolbachia* has been shown to induce expression of the RNA methyltransferase Dnmt2, and this has been implicated in the control of RNA viruses(245). While more research is required, the impact of *Wolbachia* on DENV replication in mosquitoes appears to be multi-factorial and broad.

Cell culture models have demonstrated that *Wolbachia* and DENV do not generally cohabitate within a single cell, although this is dependent on the density of the *Wolbachia* infection(246). This is supported by research that demonstrates that the antiviral protection of *Wolbachia* is cell-autonomous, and cells uninfected by *Wolbachia* have no increased resistance to arboviruses(247). Within a mosquito, pools of DENV mutants may spawn from *Wolbachia*-free cells, before selection in nearby *Wolbachia*-infected cells.

It is known that DENV exists as a viral quasispecies, due to the error-prone RNA dependent RNA polymerase. The high error rate and number of virus genomes present during a human infection suggests that most single mutants and many double mutants are likely to occur(248). For a variant strain to become widespread, it must replicate efficiently in both humans and mosquitoes. Upon a mosquito taking a blood meal, the mutant DENV must first establish in the midgut. The transferral from human to mosquito is known to be a genetic bottleneck, with

~90% of single nucleotide variants (SNVs) being lost upon transmission(249). The mutant DENV must then disseminate through the mosquito to reach the salivary glands, with a further 90% of SNVs being lost(250). For a *Wolbachia*-resistant strain to become dominant, it must display increased fitness in both *Wolbachia*-infected mosquitoes and humans, or else mutants may dwindle on one side of the transmission cycle and be lost to bottlenecks.

A serial-passage experiment revealed that the DENV1 E mutant E203K displays increased fitness in *w*Mel-infected *Aedes aegypti* mosquitoes, although fitness was decreased when passaged in *w*Mel-free mosquitoes and human cells, with a rapid return to the progenitor sequence observed(251). This highlights the potential for DENV adaption to *Wolbachia*-based suppression. The possibility of rescue mutations which may restore viral fitness, or other *Wolbachia* resistant mutations which may appear, demonstrates the need for further research into how DENV may evolve to overcome specific *Wolbachia* species, which DENV serotypes and isolates are more prone to *Wolbachia* resistance, and how this can be surveyed and combatted.

1.17 Deep mutational scanning (published review)

Note: The following sections are adapted from the review 'Applications of Deep Mutational Scanning in Virology', published in 2021 in *Viruses* by Thomas D Burton and Nicholas S Eyre. The review can be found in full in Appendix V.

Deep sequencing is a method that allows the sequencing of nucleic acid sequences multiple times. Deep mutational scanning (DMS) is a technique that utilises deep sequencing technology in combination with a library of mutant genes or genomes produced by random or directed mutagenesis to probe the functional effects of mutations at many or all nucleotide positions within a gene or genome, linking genotype to phenotype in a single high-throughput experiment. This technique has been applied to various proteins to reveal residue-specific information regarding many aspects of protein biology. For example, under certain conditions replacement of a yeast gene with a mutant library of a human orthologue can allow for determination of mutants which impact growth and may be linked to human disease(252, 253). Unbiased selection and identification of mutants with improved properties or activities for specific requirements, such as increased solubility, have furthered the field of protein engineering(254). Numerous other applications have also been pursued through DMS, including construction of complete functional activity landscapes of genes(255, 256), establishment of quantitative evolutionary models(257, 258), and contributions to structural biology(259, 260).

Before DMS, studies typically utilised alanine substitution to reveal residues or regions of importance in a viral protein. Commonly in targeted mutagenesis studies, residues for mutation are selected by analysis of protein structure, conservation with other orthologous isolates or strains, or amino acid biophysical properties(261, 262). Alternatively, large regions of interest may be interrogated by alanine scanning mutagenesis as a less targeted approach(263, 264). Alanine mutagenesis is commonly employed, as alanine features an inert, non-bulky methyl functional group, and does not alter main-chain conformation(265). In these studies, mutants of interest are typically loss of function mutants, as this is indicative of the absence of a functionally important residue. In the context of virology, experiments attempting to generate adaptive, or gain of function mutations often rely on serial passages of a virus in cell culture or animal models(167, 266, 267), relying on an error-prone viral

polymerase to generate mutants. A limiting factor is that combinations of mutations that may be required to enhance viral fitness in a given host may not be realised within the system. This method can also be time consuming as multiple rounds of infection are required. In regards to analysis of the impact of amino acid substitutions on viral protein function or viral replicative fitness, DMS can allow the substitution of a given residue with all possible amino acids, increasing the probability of identifying gain of function mutations that otherwise require more than one nucleotide substitution.

DMS studies in virology are generally performed using a three-step approach. First, a mutant library of a gene or genome of interest is prepared, ideally with genetic variants encoding every single possible residue change within the sequence of interest, or insertions introduced at every possible site. Second, a selective pressure is applied to the library, enabling the enrichment of mutations that encode a selective advantage and the removal of deleterious mutations. Finally, the frequency of mutations within the library is quantified via next generation sequencing (NGS) and compared before and after the application of the selective pressure. In studies of viral replicative fitness, a mutant with a cost to fitness will be selected against, while an enhancing mutant, such as an antiviral escape mutant, will become enriched. Selective pressures, such as drug/antibody presence, stimulation of antiviral innate immunity, growth in cell types of different species, and binding potential to a host receptor have been applied to studies of many viral genes.

1.18 Reverse genetics systems to study RNA viruses

Due to the absence of DNA in the lifecycle of RNA viruses, the construction of cDNA clones of infectious RNA viruses has become a vital tool in studying their lifecycle. Generally, a reverse genetics system is comprised of genomic viral RNA that is reverse transcribed into cDNA and then cloned into a plasmid, allowing for stable propagation of a virus genome within bacteria or yeast. The plasmid can then be manipulated by standard molecular methods, with the introduction of mutations and tags, or the removal of segments of the genome(268).

There are multiple key requirements for an infectious positive sense RNA virus cDNA clone. A common approach involves incorporation of a DNA dependent RNA polymerase promoter at the 5’ end of a cloned viral genome to enable *in vitro* transcription of infectious viral RNA via a corresponding RNA polymerase, with or without a type I 5’ cap structure, if required(269). This is commonly achieved using bacteriophage promoters/polymerases such as those of SP6

and T7. Produced RNA can then be purified and transfected into cells to initiate the viral replication cycle. A constitutive promoter such as a human cytomegalovirus (HCMV) promoter can also be utilised, with viral RNA produced by host Polymerase II after direct transfection of a full-length cDNA clone into cells. As it is necessary to produce viral RNA with precise ends, a self-cleaving hepatitis delta or hammerhead ribozyme or a T7 terminator sequence may be added to the 3' end of the viral genome to enable generation of authentic 3' ends (270, 271). Alternatively, for *in vitro* transcription (IVT) systems, a unique restriction endonuclease site can be inserted at the 3' end of the virus genome to allow for plasmid linearization, such as with the DENV infectious clone, pFK-DVs, commonly used for experiments within this thesis(272). Some of the limitations of these plasmid systems are instability in bacteria, due to the presence of cryptic bacterial promoters and other factors leading to recombination during growth, and poor plasmid yields(273). As the preparation of mutant libraries involving plasmid clones of viral cDNA often requires the pooling of a large number of bacterial colonies, it is important in DMS studies to have a plasmid with both minimal recombination, to ensure that recombination of the plasmid in bacteria does not affect cell culture experiments/analysis, as well as high transformation efficiency to ensure that a library of sufficient mutational diversity can be prepared. For these reasons, several bacterium-free approaches such as circular polymerase extension reaction (CPER)(274) and yeast artificial chromosome approaches, including transformation-associated recombination cloning in *Saccharomyces cerevisiae*(275), have also been employed to enable efficient propagation and manipulation of (+)RNA virus cDNA clones. Similarly, bacterial artificial chromosome (BAC) systems and modified plasmid DNA clones with features designed to minimise viral cDNA recombination and toxicity in bacteria have also been applied to various reverse genetics systems for (+)RNA viruses(271). The reliability and ease of manipulation of viral cDNA using these systems is an important determinant of the success of DMS experiments.

Reverse genetics systems exist for many *Flaviviridae* species. Construction of these systems is often considered to be relatively straightforward, although as detailed above, challenges in genome construction due to repetitive elements, toxicity in *E. coli* and associated instability and recombination in *E. coli* are well-documented. Reverse genetics systems have traditionally been used in low-throughput mutational studies, to analyse the effect of single point mutations. Coupling reverse genetics with deep sequencing and random mutagenesis has

allowed for high-throughput mutational studies, with analysis of hundreds of thousands of mutants being made possible in a single experiment.

1.19 Next generation sequencing

Advances in Next Generation Sequencing (NGS) have been crucial to the development of DMS as a tool in the field of molecular virology. The first generation of sequencing consisted mainly of Sanger sequencing and the Maxam and Gilbert technique. The second generation of sequencing introduced mass parallelisation of reactions. The current generation of sequencers enable real-time, single molecule sequencing(276). We will discuss three commonly used platforms in DMS studies; Pacific Biosciences (PacBio) Single Molecule Real Time (SMRT) sequencing, Oxford Nanopore Technologies (ONT) real time sequencing, and the Illumina short read sequencing-by-synthesis technology, which is part of the second generation of sequencing.(277).

1.20 Single-molecule long-read sequencing

Produced by Pacific Biosciences, PacBio SMRT technology (henceforth referred to as SMRT) utilises a sequencing by synthesis approach. Initially, the DNA is fragmented into pieces several kilobases in length and the addition of hairpin adaptors to the DNA results in the formation of a circular SMRTbell DNA conformation. Next, the circular DNA is introduced to a flow cell lined with picolitre wells with a transparent bottom (a zero-mode waveguide) and a DNA polymerase enzyme fixed to the bottom of the well. The polymerase then incorporates a fluorescently tagged nucleotide into the elongating DNA strand, and the fluorescent signal emitted by the individual nucleotide being incorporated is recorded by a camera. Finally, each fluorophore is cleaved by the polymerase and diffuses before the next read occurs. A major advantage of this technology is that the circular SMRTbell DNA conformation allows for many rounds of sequencing of a single DNA fragment, producing an accurate circular consensus sequence(278) (Figure 1.12).

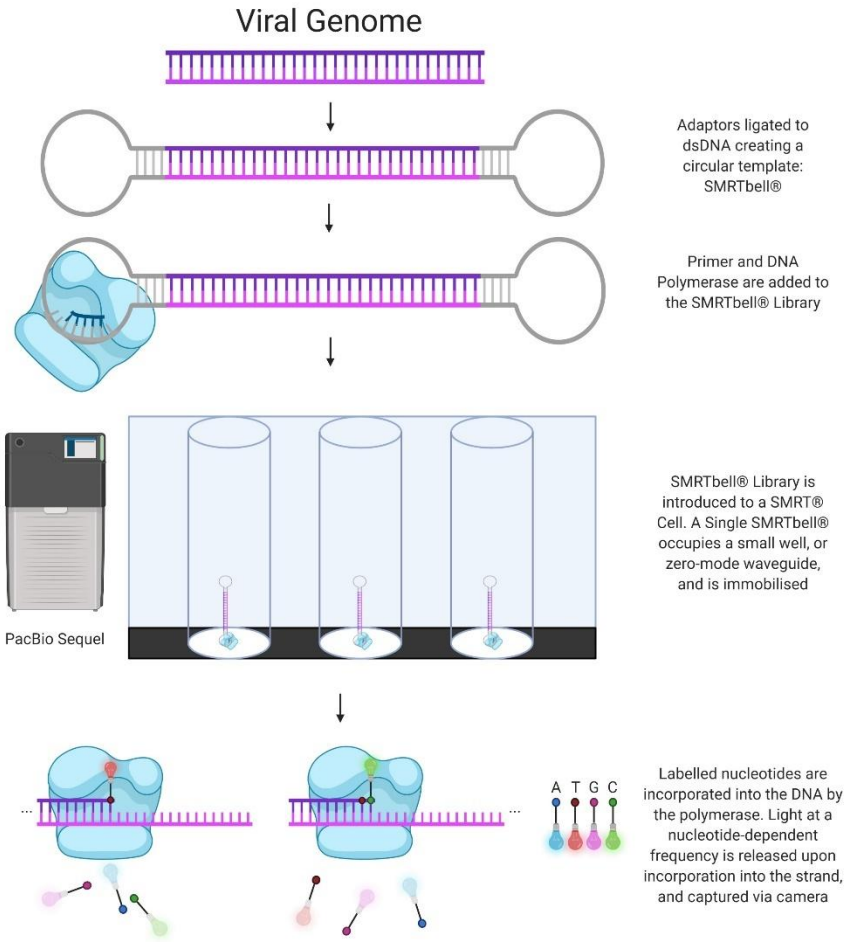

Figure 1.12: Next Generation Sequencing: PacBio SMRT Technology

The Oxford Nanopore system (henceforth referred to as ONT) sequences DNA in a unique manner. DNA is fragmented into pieces of several kilobases in length, then a motor protein and a hairpin adaptor are added to either side of the DNA. A leader sequence directs the DNA to a pore embedded in an electrically resistant membrane, and the motor protein allows ssDNA to be pulled through the aperture of the pore. Simultaneously, an electric current passes through the pore protein. As the ssDNA passes through the pore, a characteristic disruption of the electrical current occurs, dependent on the multiple bases present in the pore. By analysis of this disruption, a DNA sequence can be identified by its unique 'k-mer', which can be translated into a sequence (for example, AAGT will have a distinct disruption compared to AGAT). The hairpin adaptor allows for bidirectional sequencing of the DNA fragment, and the read from the forward and reverse strands can be used to generate a consensus sequence(279) (Figure 1.13).

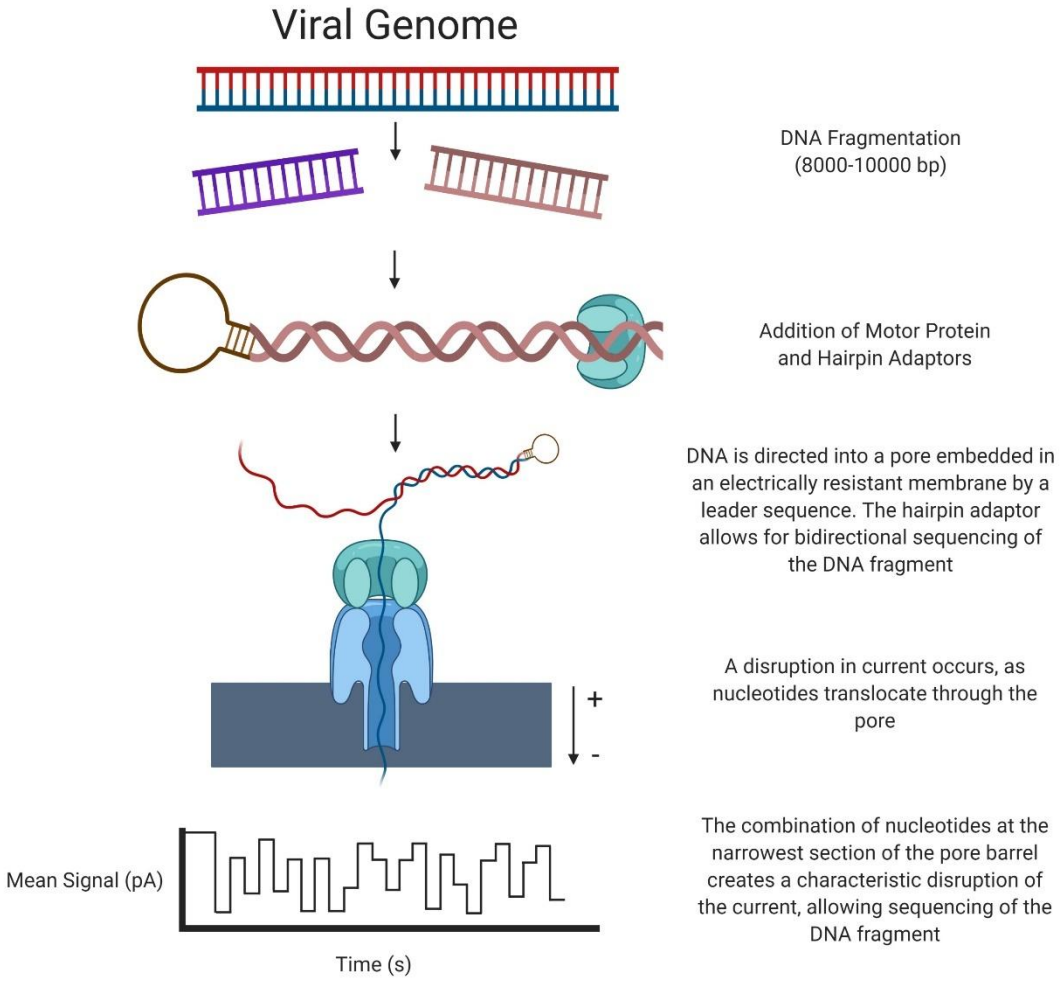

Figure 1.13: Next Generation Sequencing: Oxford Nanopore Technology

1.21 Sequencing by synthesis

Used in Illumina sequencing instruments, DNA molecules are sheared to ≤ 300 base pair fragments then ligated to adapter sequences which allow for hybridisation to complementary oligonucleotides present in nanowells across a patterned flow cell. The DNA fragments are amplified via bridge amplification, resulting in clonal clusters of DNA. Subsequent addition and imaging of fluorophore-labelled terminator nucleotides allows for highly parallel sequencing(280) (Figure 1.14).

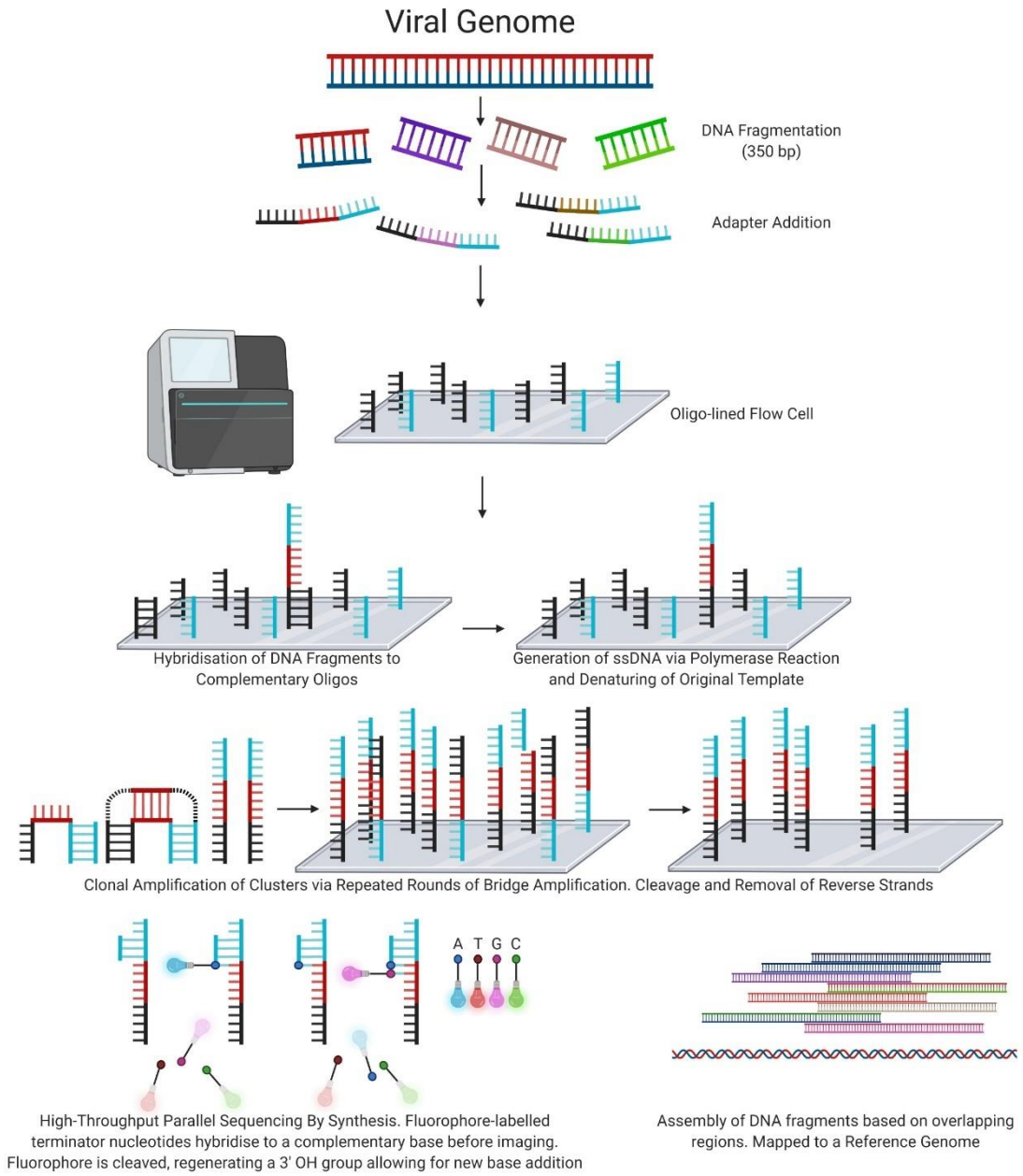

Figure 1.14: Next Generation Sequencing: Illumina short read technology

1.22 Next generation sequencing technologies: A comparison

The main limitation of Illumina short read technology in DMS studies is the short read length. Viral segments for analysis are often much longer than the read length of the instrument. If two distant mutants are present in a single viral genome, and a specific phenotype is observed, it is difficult to determine without further experimentation if they are acting in a pairwise manner or if a single mutation is wholly responsible for the phenotype. Thus, pairwise epistatic mutations are not always resolvable using short read technology. A partial solution to this problem is to create multiple adjacent mutant libraries of short lengths, 'tiling' across a gene, to restrict epistatic mutations to within a readable window(281). Alternatively, subassembly can be utilised. In this approach, tagging each template molecule with a unique DNA barcode or 'unique molecular identifier' (UMI) allows for the grouping and analysis of multiple short reads on the basis of their original template molecule(282). Resolution of distant mutants is only possible using third generation long-read sequencing strategies, offered by both SMRT and ONT.

Of the long read sequencing platforms, SMRT is far more common than ONT in DMS studies, likely attributed to its higher accuracy. The circular SMRTbell DNA conformation allows for increased sequencing depth, or how often a base is sequenced on average, to form a consensus sequence, as the SMRTbell can be repeatedly sequenced. Errors in PacBio sequencing are distributed randomly, and therefore the accuracy increases with increased reads of a single SMRTbell molecule(283). Oxford Nanopore sequencing utilises dsDNA fragments, but does not allow continuous sequencing. A consensus sequence can be formed by sequencing one strand of dsDNA, followed immediately by the complementary strand, referred to as $1D^2$ sequencing, though the accuracy is somewhat limited compared to PacBio and Illumina strategies(283). Interestingly, a recent study has reported a high-throughput amplicon sequencing approach that combines UMIs with PacBio or ONT to enable generation of high-accuracy single-molecule consensus sequences for large DNA regions(284). This and similar approaches will help to overcome compromises in accuracy that have previously been associated with the above long-read sequencing strategies. To date, however, Illumina sequencing remains the most commonly used platform in DMS studies due to its cost-effectiveness and high levels of accuracy.

1.23 Deep mutational scanning: Library construction

As mentioned previously, the first step in a DMS experiment is the construction of a mutant library. Multiple approaches have been developed and applied to mutant library generation, which are briefly described below.

The simplest and most cost-effective method to generate a genetic library bearing random point mutations involves error-prone PCR. In this method, one or more polymerases are employed to exponentially amplify a region of DNA, with initial template amount and cycle number varied to optimise mutation rate(285). *Taq* DNA polymerase, a popular error-prone polymerase, has a reaction-buffer dependent mutation rate of approximately 8 x 10^{-6} errors/nucleotide(286). However, the use of Taq polymerase alone in library construction is limited as AT → GC transitions and AT → TA transversions at a frequency that is approximately 2-4-fold the mutation rate of G and C residues. In contrast, a polymerase named Mutazyme DNA polymerase has a 2-4-fold stronger preference for GC → AT transitions and GC → TA transversions(287). In combination, these enzymes can be used to produce a relatively unbiased mutant library with a somewhat controllable mutation rate. A major drawback of this method is that not all amino acid residues are accessible with single nucleotide polymorphisms(288). Additionally, this technique can often result in multiple mutations present in a single DNA fragment that can confound results, especially when using short read sequencing strategies to quantify mutation frequency, as mentioned earlier.

First described in virology studies by the Bloom laboratory in an Influenza nucleoprotein (NP) study, synthetic oligonucleotides were designed to contain a randomised triplet for each codon present in the gene, with 16 leading and lagging nucleotides that anneal specifically to the NP gene, as well as the reverse complement of these oligonucleotides. Using a series of joining PCR steps and restriction enzyme cloning, a product pool containing all possible amino acid mutations of NP was cloned into an Influenza reverse genetics system(257). When designing oligonucleotides with randomised triplets, codon usage should be considered. NNK degeneracy (N: Ade/Cyt/Gua/Thy, K: Gua/Thy) encodes all amino acids, while NDT (N: Ade/Cyt/Gua/Thy, D: Ade/Gua/Thy, T: Thy) and DBK (D: Ade/Gua/Thy, B: Cyt/Gua/Thy, K: Gua/Thy) each encode 12 amino acids, feature no stop codons and exhibit all major biophysical types, while potentially decreasing workload. However, with decreased coverage, the amount of interesting variants will also be reduced(289). This method is more costly

compared to the error-prone PCR method, but can be used to generate libraries with complete mutational coverage.

A synthetic approach to mutant library generation is also available. Gene synthesis begins with oligonucleotide construction. These are designed such that adjacent oligonucleotides in the final product contain overlapping sequences. The overlap results in a DNA duplex which, through an assembly reaction with DNA polymerase, results in the construction of the gene of interest(290). Multiple methods allow for controlled or randomized insertion of mutations into a target DNA sequence. For example, the “Spiked Genes” method uses oligonucleotides spiked, or interspersed, with mutants to create a pooled mutant fragment(291). Synthetic construction of multiple types of mutant libraries is possible through commercially available gene synthesis services. Available mutant library types include controlled randomised libraries, scanning alanine mutagenesis libraries and scanning codon mutagenesis libraries.

An additional type of mutant library discussed briefly within this thesis is the transposon insertion library. This is facilitated by a transposase protein, such as Tn5, Tn7 or MuA that recognizes the ends of a transposon, or a mobile DNA element, and forms a protein-DNA complex termed the ‘transpososome’. This complex catalyses cleavage of target DNA at a random site, although evidence of insertion bias exists(292), and joining reactions allow for the introduction of the transposon into a DNA template. For many applications, the transposon is engineered to feature an antibiotic resistance gene, allowing for selection of genetic elements with successful transposon integration. In these systems the transposon also features two identical restriction enzyme sites on each end of the DNA elements. Upon purification, the resulting unique plasmids are digested with the corresponding restriction enzyme. Gel electrophoresis allows for the removal of the majority of the introduced DNA element by size separation, with a small insertion remaining after ligation of the plasmid backbone(293, 294). High-throughput random mutagenesis of a cloned viral genome paired with deep scanning allows for powerful studies which can probe regions of genomic flexibility and functionality.

1.24 Standard deep mutational scanning experiment methodology

DMS experiments often follow a similar methodology. Using a reverse genetics system, a mutant virus library is generated via a method such as randomised mutagenesis, controlled site-saturation mutagenesis, or transposon mutagenesis. This library is often initially amplified

using bacteria, with a higher number of uniquely transformed plasmids resulting in increased mutational diversity. This library, or derivative IVT RNA, is transfected into cells, allowing for the propagation of RNA replication-competent viral genomes, as well as production of viral particles. Infection of naïve cells with virus-containing cell culture supernatants allows for propagation of genomes which are capable of both RNA replication and infectious particle production. Variant analysis by NGS is then employed to identify specific variants which are present at higher or lower levels at certain stages of the viral lifecycle in comparison to the initial input (Figure 1.15).

While not a major focus in this thesis, it is important to note that DMS studies of individually expressed proteins have been highly informative, particularly in the context of the interactions of viral glycoproteins with host receptors or neutralizing antibodies. For example, angiotensin-converting enzyme 2 (ACE2), the host receptor for SARS-CoV-2(295), has been analysed for mutants which enhance binding to the spike glycoprotein, to explore the use of an engineered soluble ACE2 as a potential therapeutic(296, 297). The binding of computer-generated miniprotein inhibitors and ACE2 decoys to the spike glycoprotein has also been effectively optimised using DMS(298, 299). A similar strategy was used to enhance the affinity and specificity of a computationally designed protein that targets H1N1 Influenza haemagglutinin(300, 301).

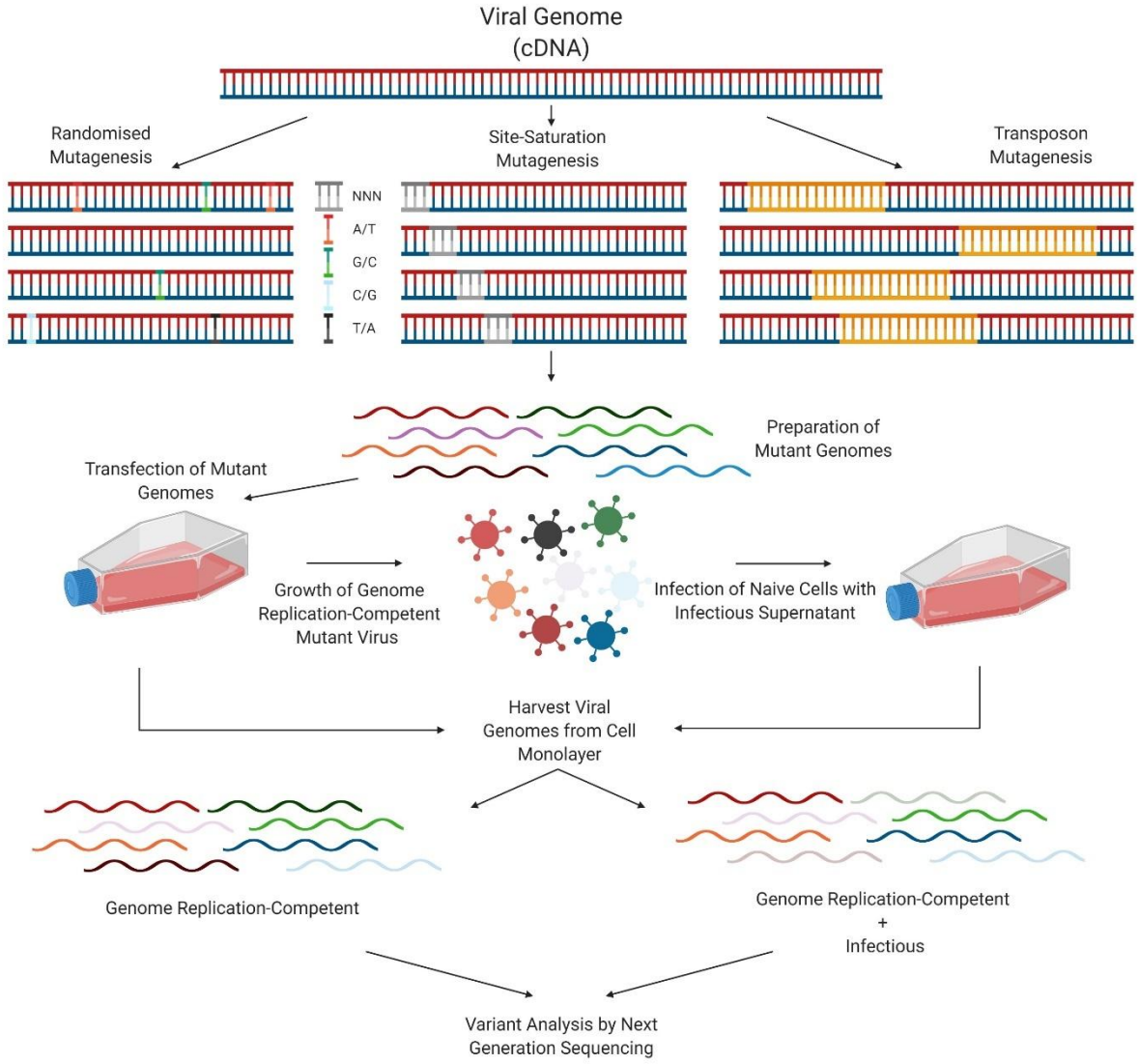

Figure 1.15: Standard methodology of a DMS experiment.

1.25 Bioinformatic Tools for Deep Mutational Scanning Data Analysis and Visualisation

Multiple software packages are available which facilitate variant analysis. Software packages such as 'dms_tools' and 'Enrich2'calculate amino acid preferences under a selective pressure(302, 303). Furthermore, 'dms-view' allows straightforward visualisation of DMS data in the context of a protein structure(304). 'MaveDB' (multiplex assays of variant effect database) provides a tool for sharing DMS data analyses.

1.26 Deep mutational scanning experiments

In this section we will briefly describe several past applications of DMS in virology, focussing on the *Flaviviridae* family of viruses. Transposon mutagenesis has been applied to several viruses to identify genomic regions that are tolerant to small insertions. An insertion with

minimal impact on fitness indicates genomic flexibility, or high mutability, at a specific area, which may allow for adaptation of the virus to a new environment. Disruption of function from an insertion may also reveal a region of functionality within a gene or protein. The identification of a region of insertional tolerance can be exploited by incorporation of epitope tags or reporter genes for further research. DMS projects focussing on single nucleotide polymorphisms and codon mutagenesis have focussed on several biological aspects, including identifying determinants of viral tropism, epistatic interactions, drug and antibody escape mutants, and residues that are critical to several biological functions. Here, we focus mainly on studies of viral replicative fitness and immune evasion.

Hepatitis C virus (HCV)

Transposon analysis

In a comprehensive early study by Remenyi *et* al, the Mu-transposon system was used to insert 15 nucleotide (nt) sequences (of which 10 nt are transposon-derived and 5 nt are duplicated target sites) into an HCV plasmid based on the chimeric sequence of genotype 2a J6 and JFH1 viruses(305). This mutant library was propagated in human hepatoma Huh-7.5.1 cells, then passaged onto naïve Huh-7.5.1 cells to separately analyse genomes capable of viral RNA replication and infectious particle production. Regions tolerant to an insertion illustrate flexibility at the genomic level, and potentially highlight a region that is non-essential for *in vitro* growth. P7 and non-structural protein 2 (NS2), each coordinators of virus assembly(306), and envelope protein 2 (E2) were identified as potential areas for insertion of a tag or small peptide with minimal costs to replicative fitness due to the regions of high genomic flexibility uncovered. The impact of NS4B transposon insertions on infectious particle production helped to reveal a previously unknown functional region of NS4B which was suggested to play a role in viral assembly.

In a subsequent study by the same group, a similar methodology was used to assess insertions that confer sensitivity to the antiviral cytokine Interferon alpha (IFN-α)(307)**.** After two rounds of passage in Huh-7.5.1 cells in the presence or absence of IFN-α, it was observed that mutants conferring sensitivity to IFN-α were clustered in p7, the 3' untranslated region (UTR) and non-structural protein 5A (NS5A), which is important for viral replication, infectious virus particle production and modulation of host cell signalling(308). Eight IFN-α sensitive p7 insertion mutants were constructed for validation and revealed the role of p7 in immune evasion. An

interferon stimulated gene (ISG) cDNA expression library screen demonstrated that 13 of these ISGs were particularly antiviral against viruses with mutant p7 in comparison to wild-type p7. Amongst these ISGs, IFI6-16 was identified as a major target of p7-mediated immune evasion. Coimmunoprecipitation was then used to show a direct interaction between p7 and IFI6-16, which was previously unknown. Each of these DMS studies furthered understanding of the roles of HCV proteins in infection.

Variant analysis

In an important application of DMS towards understanding emergence of viral resistance to antiviral drugs, Qi et al applied high-throughput variant analysis towards understanding resistance to Daclatasvir(309); a potent inhibitor of NS5A(310). An NS5A mutant library of the J6/JFH1 strain (genotype 2a) was prepared and passaged twice in Huh7.5.1 cells in the presence or absence of daclatasvir, before analysis of viral sequences by NGS. Drug selection resulted in selection of drug-resistant mutations at NS5A residues 28, 31, 38, 92 and 93, and increased drug resistance of other mutations. These escape mutants can be used to identify daclatasvir-resistant strains of HCV(311). In support of this methodology, many of these resistance mutations have also been identified in numerous *in vitro* and clinical studies of HCV resistance to Daclatasvir and related inhibitors(312).

Zika virus (ZIKV)

Transposon analysis

In the first published study involving high-throughput mutational analysis of ZIKV a transposon insertion mutant library was generated for the ZIKV MR-766 strain(313). Human embryonic kidney 293T (HEK 293T) cells were used to propagate the virus, then naïve African green monkey kidney Vero cells were infected with viral supernatants over two rounds. The first pool of selected viral RNA, reflecting viral RNA replication requirements in HEK 293T cells, showed high levels of flexibility in the structural proteins Envelope (E), precursor membrane (prM) and capsid (C), and also non-structural protein 1 (NS1), which is essential for ER remodelling and viral RNA replication(314). The third pool, consisting of infectious particle production-competent genomes, displayed most flexibility in the structural proteins. Some insertions present in NS1 rendered the virus incapable of infectious particle production while enhancing viral RNA replication capacity. In this context, an insertion after amino acid 174 resulted in

>650-fold enrichment in the initial HEK 293T cell viral RNA population compared to the input RNA library, yet was not present in the Vero cell populations. Together, this study revealed regions of genetic rigidity in the ZIKV genome across multiple lifecycle stages.

Variant analysis

Envelope:

Several mutational analyses of the ZIKV Envelope (E) protein have been performed. An envelope mutant library for the MR766 ZIKV strain was constructed by Sourisseau *et al*. to examine how mutants affect viral neutralisation by monoclonal antibodies(315). The MR-766 strain was first tested for the effects of mutations on viral fitness, with a focus on infectious particle production in Vero cells. After validation, mutational antigenic profiling was performed, whereby the selective pressure of a neutralising antibody results in the enrichment of escape mutants present in the mutant library. Two antibodies were used in this screen; ZKA64, which binds domain III of recombinant E protein, and ZKA185, for which the mechanism of neutralisation was not known(316). Domain III of E protein is responsible for binding an undetermined host cell receptor, and is a common target of potent ZIKV neutralising antibodies(317). The mutant ZIKV library was subjected to these antibodies individually. ZKA64 and ZKA185 treatment resulted in strong selection of several mutations that corresponded to sites within E, with mutants selected by ZKA64 present in envelope domain III, and mutants selected by ZKA185 present on envelope domain II. Antibody escape resistance mutations A333T and T335E for ZKA64, and D67A and K118R for ZKA185, were confirmed in follow-up neutralisation assays, illustrating the utility and accuracy of mutational antigenic profiling for escape mutant predictions, and demonstrating that antibody escape mutants can appear outside the receptor binding domain.

The impact of Envelope on tropism using ZIKV strain PRVABC59 has also been examined(318). This study analysed mutant library growth in three cell types: C6/36 cells, derived from *Aedes albopictus* larvae, A549 adenocarcinomic human epithelial cells and hCMEC/D3 cells, a human blood-brain barrier endothelial cell line. NGS analysis revealed that a mutation at N154, an N-linked glycosylation site on the ZIKV envelope protein, resulted in a significantly higher fitness of ZIKV in mosquito cells, but not in human cells. Additionally, ablation of glycosylation through mutations surrounding the N154 position enhanced viral entry into C6/36 cells,

resulting in increased levels of viral replication. DC-SIGN is a known viral entry factor for ZIKV that is not expressed in 293T cells such that overexpression of DC-SIGN in 293T cells enhances ZIKV infection(319). A comparison between wild-type ZIKV and ZIKV glycosylation mutants showed that, with overexpression of DC-SIGN, infection of 293T cells by the glycosylation mutant ZIKV was significantly diminished compared to wild-type ZIKV, demonstrating the requirement of N-linked glycosylation of E protein in viral entry into mammalian cells, despite the resultant loss of fitness in mosquito cells.

In a similar study into cell tropism, a mutant library for the C-terminal region of the E protein of ZIKV (PRVABC59) was prepared and grown in Vero and C6/36 cells for 8 and 13 days, respectively, to identify host-adaptive substitutions(320)**.** In C6/36 cells, mutants K316Q and S461G were preferentially selected. The K316Q/S461G virus replicated less efficiently in a selection of human cell lines, with lower levels of cytotoxicity compared to wild-type, while no change was seen in C6/36 and Aag2 mosquito cell lines. This combinatorial mutant was determined to decrease the thermal stability of E, and as mosquito cell lines are typically grown at a lower temperature (28° C) than human cell lines, the effect was not observed in the mosquito cell line. ZIKV infection can result in severe developmental defects in the brain(321). The K316Q/S461G virus was used to infect induced-pluripotent stem cell-derived human brain organoids. Development of these organoids infected with the K316Q/S461G virus greatly decreased growth retardation in comparison to wild-type ZIKV. Importantly, infection of interferon alpha receptor knockout mice showed attenuated infection by the K316Q/S461G virus, and protection against a later wild-type ZIKV infection, indicating its potential as an attenuated vaccine candidate.

Dengue virus (DENV)

Transposon analysis

To identify regions of genetic flexibility in DENV, our group applied the Mu transposase system to generate a library of mutants containing single random 15 nt insertions in a serotype 2 Dengue virus (DENV-2) genome (strain 16681)(143). Analysing both viral RNA replication and infectious particle production in Huh-7.5 hepatoma cells, non-structural protein NS1, required for RNA replication(322) and virus assembly(261), as well as structural protein capsid (C), demonstrated highest tolerance to the insertions. Lowest tolerance of insertions was seen in

structural protein prM and non-structural protein 2A (NS2A), which is essential for virus assembly(55). Across the genome, flexibility peaked at the C termini for C, E, NS1, NS2B and NS4B, and at the N termini of NS3 and NS4B. These experiments allowed for the tagging of NS1 with epitope tags and reporter proteins including FLAG, APEX2 and NLuc, with minimal loss of viral fitness in Huh7.5 cells. Since publication, we have produced a Huh7.5-adapted DENV-NS1-mScarlet reporter virus, which features unpublished mutations which greatly increase viral fitness (Centofanti S, Johnson SM et al; unpublished).

A similar transposon mutagenesis study of DENV-2 (16681) was performed by Perry et al(323)**.** This study identified regions of genetic flexibility and enabled identification of well-tolerated insertion sites within non-structural protein 4B (NS4B), which is involved in membrane rearrangements(324), and C, which were utilized to create a DENV-2 clone expressing HA-tagged capsid, incapable of infectious particle production, and a replication competent infectious DENV-2 clone expressing HA-tagged NS4B. Together, these studies identified regions of genetic flexibility within DENV-2 and exploited this information to generate infectious reporter virus tools.

1.27 Experimental rationale, hypotheses and aims

Hypothesis 1: The DENV NS1 dimer is indispensable for viral RNA replication and infectious particle production. Inhibitors of NS1 and inhibitors of NS1 dimerisation may be suitable as therapeutics against dengue fever.

Aim 1: Identify NS1 targeting DENV antivirals

1.1 - Screen compounds which have been identified as ligands of NS1 in a high-throughput Nanoluciferase-based thermal shift assay for antiviral and cytotoxic properties and determine their mechanism of action

1.2 - Establish an assay for detection of NS1 dimerisation with high-throughput capacity and screen a library of drug-like compounds to identify inhibitors of NS1 dimerisation

1.3 - Perform an *in silico* screen for potential inhibitors of NS1 dimerisation and determine antiviral and cytotoxic properties of top hits, then explore their mechanism of action

Hypothesis 2: The potential for resistance against *Wolbachia*-based suppression by DENV is not fully understood. Application of deep mutational scanning to unveil *Wolbachia*-resistant mutants in DENV will help to inform the presence and emergence of *Wolbachia*-resistant DENV mutants in the field. Additionally, deep mutational scanning will allow for identification of E, prM and NS1 residues that are critical to various aspects of the DENV lifecycle and tropism.

Aim 2: Identify dengue virus E, prM and NS1 residues of functional importance using deep mutational scanning

2.1 - Generate mutant libraries of E, prM and NS1 for the full-length DENV-2 clone (16681)

2.2 - Transfect viral RNA libraries into Huh7.5 and C6/36 cells to identify host-specific NS1 residues that are of importance in the DENV lifecycle

2.3 - Infect mosquitoes carrying multiple strains of *Wolbachia* with these mutant libraries to identify residues which may allow DENV to escape *Wolbachia* mediated repression

Chapter 2: Materials and Methods

2.1 Cell Culture

Mammalian cell lines were maintained in Dulbecco's Modified Eagle Medium (DMEM; ThermoFisher Scientific) supplemented with 10% (v/v) heat-inactivated Foetal Bovine Serum (FBS; ThermoFisher Scientific) and penicillin (100 U/ml)/streptomycin (100 µg/ml) (Sigma-Aldrich) and incubated in a humidified incubator at 37 °C and 5% CO_2. Huh-7.5 hepatoma cells were generously provided by Charles Rice (Rockefeller University, New York, USA). HEK293FT cells, a clonal isolate of HEK293 embryonic kidney epithelial cells, were purchased from ThermoFisher Scientific. The sgDVs-GFP subgenomic replicon, developed by C. Ansarah-Sobrinho et al. was introduced to the Vero cell line by Jillian M. Carr (Flinders University).

C6/36 cells were maintained in Basal Medium Eagle (BME; ThermoFisher Scientific) supplemented with 10% FBS, penicillin/streptomycin, MEM non-essential amino acids (ThermoFisher Scientific), 2mM GlutaMAX Supplement (ThermoFisher Scientific) and 1 mM sodium pyruvate (ThermoFisher Scientific) and cultured in a humidified incubator at 28 °C and 5% CO_2. C6/36 cells were generously provided by Jillian M. Carr (Flinders University).

Anti-E hybridoma cells (D1-4G2-4-15) were purchased from ATCC, and anti-capsid hybridoma cells (6F3.1) were generously provided by John Aaskov (Queensland University of Technology). These were maintained in Hybri-Care medium (ATCC) supplemented with 10% FBS and sodium bicarbonate and cultured in a humidified incubator at 37 °C and 5% CO_2.

Cells were maintained in vent-capped tissue culture flasks. At 90 - 100% confluency, cells were passaged by aspirating media, washing with 6 mL of Phosphate-Buffered Saline (PBS), and incubating with 1-2 mL of Trypsin-EDTA solution (Sigma-Aldrich) at 29 °C (C6/36 cells) or 37 °C (mammalian cell lines) in a humidified 5% CO_2 incubator for approximately 5 minutes, before resuspension in complete cell culture medium and sub-culturing into new flasks at a 1:5 split ratio.

Upon harvesting of cells for experimentation, the concentration of cells in a resulting suspension was calculated using an improved Neubauer haemocytometer and 0.4% (w/v) Trypan Blue solution (Sigma-Aldrich). Briefly, 50 µL of inactivated trypsinised cells was transferred to a microcentrifuge tube containing 50 µL of Trypan Blue solution and mixed by pipetting. 10 µL of this solution was loaded onto a chamber of a haemocytometer and, using

an inverted IX70 cell culture microscope with a 10× objective (Olympus), the number of live cells present in the central (0.1 mm^3) gridded square were counted. These counts were performed at least twice and values were averaged to improve accuracy. The concentration of cells in the original cell suspension in cells/mL was determined by multiplying the average number of cells in the central grid by the dilution factor (2) and 10^4.

2.2 Polymerase Chain Reaction (PCR)

PCR was performed according to the manufacturer's instructions with annealing temperatures calculated using the NEB Tm Calculator online tool.

25 µL Q5® High-Fidelity DNA Polymerase (New England Biolabs) reactions were prepared with 1X Q5 reaction buffer, 200 µM dNTPs, 0.5 µM Forward primer (IDT), 0.5 µM Reverse primer (IDT), 1 - 10 ng template DNA and 0.02 Units/µl Q5 High-Fidelity DNA Polymerase, in nuclease-free H_2O. Reactions were performed at 98 °C for 30 seconds, 25 - 35 cycles of 98 °C for 10 seconds, 50 – 72 °C for 30 seconds (primer-dependent) and 72 °C for 30 seconds/kb, followed by a final extension step of 72 °C for 2 - 5 minutes. Samples were then stored at 4 °C (short-term) or -20 °C (long-term), as appropriate.

25 µL Mutazyme II DNA polymerase (Agilent) reactions were prepared with 1X Mutazyme II reaction buffer, 200 µM dNTPs, 0.5 µM Forward primer (IDT), 0.5 µM Reverse primer (IDT)and 2.5 Units/µl Mutazyme II DNA Polymerase, in H_2O. The concentration of DNA template was optimised per reaction. Reactions were performed at 95°C for 2 minutes, 19 cycles of 95 °C for 30 seconds, 50 - 72°C for 30 seconds (primer-dependent), 72°C for 60 seconds/kb, followed by a final extension step of 72 °C for 10 minutes. Samples were then stored at 4 °C (short-term) or -20 °C (long-term), as appropriate.

Primer design was generally performed using SnapGene® software. PCR was performed using an S1000™ Thermal Cycler (Bio-Rad). All primers were purchased from IDT and sequence details are provided in Appendix X.

2.3 Agarose Gel Electrophoresis

DNA samples were separated by agarose gel electrophoresis using 1 - 2% (w/v) agarose gels (Bioline) containing 3 µL RedSafe™ Nucleic Acid Staining Solution (iNtRON Biotechnology) per 100 mL molten agarose, in 1X Tris-acetate-EDTA (TAE) buffer. DNA samples were first mixed with an appropriate volume of Gel Loading Dye, Purple (6X) (New England Biolabs) and loaded

into the wells of agarose gels that were submersed in TAE buffer in a Mini-Sub Cell GT Cell tank (Bio-Rad). To determine the size of DNA fragments, 0.5 µg of 100 bp DNA Ladder or 1 kb DNA Ladder (New England Biolabs; pre-diluted to 0.1 µg/µl in water containing Gel Loading Dye, Purple) was run on an adjacent lane to samples. Samples were separated by electrophoresis at 80 – 120V for 40 minutes to 1 hour. Gels were then visualised using the GelDoc Go Imaging System (Bio-Rad) and analysed using Image Lab 6.1 software (Bio-Rad).

2.4 Restriction Enzyme Digest

To perform a restriction enzyme digest, 20 µL reactions were prepared with 1X NEB CutSmart Buffer, ≤5 µg of purified PCR product or plasmid, and 0.5 - 2 units of restriction enzyme(s) (New England Biolabs) in nuclease-free H_2O. These reactions were incubated for 4 hours or overnight at the recommended temperature in a S1000™ Thermal Cycler (Bio-Rad).

2.5 Gel Extraction and DNA Clean-up

Gel-electrophoresed DNA fragments were visualised using a UV transilluminator and excised from the agarose gel for transferral to a microcentrifuge tube. Samples were purified using a NucleoSpin® Gel and PCR Clean-up kit (Macherey-Nagel), as per manufacturer's instructions. Briefly, 200 µL of Buffer NT1 per 100 mg of gel was added, then the samples were dissolved by heating for 10 minutes at 60 °C with intermittent vortexing. If gel extraction was not required, PCR or restriction enzyme digest samples were diluted in nuclease-free H_2O to 100 µL, before addition of 200 µL of Buffer NT1 and mixing.

The sample was then transferred to a NucleoSpin® Gel and PCR Clean-up Column and centrifuged at 11,000 x *g* for 30 seconds to bind the DNA. Flow-through was discarded. 700 µL of buffer NT3 was added, and the column was centrifuged at 11,000 x *g* for 30 seconds. Flow-through was discarded. The column was dried by centrifugation at 11,000 x *g* for 60 seconds. The column was placed into a clean microcentrifuge tube, and 10-30 µl of H_2O or TE buffer was added to the tube, and incubated for 1 minute, before centrifugation at 11,000 x *g* for 30 seconds. Purified DNA samples were then analysed for DNA concentration and purity using a NanoDrop 2000 spectrophotometer (ThermoFisher Scientific).

2.6 DNA Assembly

DNA assembly was performed using the NEBuilder® HiFi DNA Assembly kit (New England Biolabs). Reactions were prepared with 1X NEBuilder HiFi DNA Assembly Master Mix, 50 ng of vector DNA, insert DNA (with a 1:3 vector:insert molar ratio), and H_2O. Samples were then

incubated at 50 °C for 15 minutes in an S1000™ Thermal Cycler (Bio-Rad) and stored at 4 °C (short-term) or -20 °C (long-term), as appropriate, prior to transformation.

2.7 DNA Ligation

DNA ligation reactions were performed with T4 DNA Ligase (NEB). 21 µ Reactions were prepared with 1X T4 DNA Ligase buffer, 50 ng vector DNA, insert DNA (typically with a 1:3 vector:insert ratio), 1 µL T4 DNA ligase and H_2O. Samples were then incubated at 16 °C overnight, and heat inactivated at 65 °C for 10 minutes in an S1000™ Thermal Cycler (Bio-Rad) and stored at 4 °C (short-term) or -20 °C (long-term), as appropriate, prior to transformation.

2.8 Bacterial Transformation (chemically competent cells)

For DNA transformations, 10 ng of intact plasmid, or 1 µL of NEBuilder HiFi DNA Assembly product or T4 DNA ligase reaction product were transferred to a microcentrifuge tube containing 50 µL of NEB 5-alpha Competent E.coli (High Efficiency) competent cells (NEB) or NEB Stable Competent E.coli (High Efficiency) competent cells (NEB) on ice and mixed gently. After 20 minutes, samples were heat-shocked at 42 °C for 30 seconds, then returned to ice for 2 minutes. 150 µL of super optimal broth with catabolite repression (SOC; NEB) was transferred to each sample and mixed in by gentle flicking. Samples were incubated at 37 °C for 1 hour, then added to an LB agar plate containing 100 µg/mL ampicillin (Sigma-Aldrich) and incubated at 37 °C for approximately 16 hours, or until colonies were of sufficient size for selection. To further grow cultures, individual colonies were picked using a sterile pipette tip and placed into a flask or tube containing Luria Broth (LB) Medium and 100 µg/mL ampicillin and grown for approximately 16 hours at 37 °C with shaking. For small scale plasmid DNA extractions, LB volumes of 5 - 10 mL in 15 mL centrifuge tubes were used, while for large scale plasmid DNA extractions LB volumes of 200 mL or 500 mL were used in 1 L or 2 L conical flasks, respectively.

2.9 Bacterial Transformation (electrocompetent cells)

Electroporation cuvettes (1 mm gap; Bio-Rad) were pre-chilled on ice. In a sterile environment, 10 ng of intact plasmid, or 1 µL of NEBuilder HiFi DNA Assembly reaction product was transferred to 50 µL of electrocompetent NEB Stable cells in the cuvette and mixed by pipetting. Electroporation was performed with the following settings: 1.2 kV, 25 µF, 200 Ω using a Gene Pulser Xcell Total electroporation system (Bio-Rad). 950 µL of room-temperature SOC media was then immediately added and samples were transferred to microcentrifuge tubes and incubated at 37 °C, with shaking, for 1 hour before plating onto LB agar plates

containing 100 µg/mL of ampicillin. Plates were incubated at 37 °C for approximately 16 hours, or until colonies were of sufficient size for selection.

2.10 Plasmid Purification: Mini

Small scale preparation of plasmid DNA was performed using a NucleoSpin® Plasmid kit (Macherey-Nagel), as per manufacturer's instructions. Briefly, 5 mL of bacterial culture was pelleted by centrifugation for 1 minute at 4000 x *g*, and the supernatant was discarded. The cell pellet was resuspended in 250 µL Buffer A1 by vortexing and transferred to a microcentrifuge tube, then lysed for 5 minutes with the addition of 250 µL Buffer A2, with gentle inversion 6 times. The reaction was neutralised with the addition of 300 µL Buffer A3 and repeated gentle inversions until no blue colour remained. The sample was then centrifuged for 5 minutes at 11,000 x *g*, and the supernatant was transferred to a NucleoSpin® Plasmid Column and centrifuged for 1 minute at 11,000 x *g*. The flow-through was discarded, and 700 µL Buffer A4 was added to wash the spin columns, which were centrifuged again for 1 minute at 11,000 x *g*. The supernatant was discarded, and the spin column was dried by centrifugation for 2 minutes at 11,000 x *g*. DNA was then eluted by transfer of the spin column to a new microcentrifuge tube, addition of 50 µL of nuclease-free H_2O or Elution Buffer AE, incubation for 1 minute and centrifugation for 1 minute at 11,000 x *g*. DNA concentrations and 260/280 and 260/230 absorbance values were measured using a NanoDrop 2000 spectrophotometer (ThermoFisher Scientific). A 260/280 ratio of ~1.8 was expected for 'pure' DNA.

2.11 Plasmid Purification: Midi

Where appropriate, plasmids were purified using a NucleoBond® Xtra Midi kit (Macherey-Nagel), according to manufacturer's instructions. Briefly, 100 mL bacterial cultures were pelleted by centrifugation at 4,000 x *g* for 15 minutes at 4 °C and the supernatant was discarded. Cells were resuspended in 8 mL of Resuspension Buffer RES (containing RNAse A) by vortexing. Cells were lysed by the addition of 8 mL of Lysis Buffer LYS, mixing by inversion 4-6 times and incubation for 5 minutes at room temperature. Then the reaction was quenched by the addition of 8 mL of Neutralisation Buffer NEU and mixing by gentle inversion until the blue colour indicator turned clear. The mixture was inverted 3 times to ensure a homogeneous precipitate suspension, then added to a Nucleobond® Xtra Column Filter, pre-equilibrated with 12 mL Equilibration Buffer EQU, and allowed to empty by gravity flow. The column filter

was washed with 5 mL of Equilibration Buffer EQU, then the filter was removed, and the silica membrane washed with 8 mL of Wash Buffer WASH. The plasmid DNA was then eluted into a new 50 mL centrifuge tube using 5 mL of elution buffer ELU. The DNA was precipitated with the addition of 3.5 mL of isopropanol followed by centrifugation at 10,000 x *g* for 30 minutes at 4 °C. The supernatant was discarded, then 1 mL of 70% (v/v) ethanol was added to the pellet, which was centrifuged at 5,200 x *g* for 5 minutes at room temperature. The ethanol was discarded, and the plasmid DNA was dried at room temperature for 2 - 5 minutes. The plasmid DNA pellet was dissolved in 100 µL nuclease-free H_2O and DNA concentration and 260/280 and 260/230 absorbance values were determined using a NanoDrop 2000 spectrophotometer (ThermoFisher Scientific). A 260/280 ratio of ~1.8 was expected for 'pure' DNA.

For plasmid purification: Maxi, a similar protocol was followed using the NucleoBond® Xtra Maxi kit (Macherey-Nagel), with larger volumes, as appropriate and recommended by the manufacturers.

2.12 Sanger Sequencing

DNA samples were sequenced by the Australian Genome Research Facility (AGRF). Each sample was prepared with 600 - 1500 ng of plasmid DNA, 1 µL of 10 µM primer and nuclease-free H_2O in a 12 µL volume in a microcentrifuge tube and submitted to AGRF for sequencing. Alignment of the FASTA format file to a reference gene/genome was performed using SnapGene software.

2.13 Immunofluorescent Staining

Cell monolayers were washed with PBS, then fixed by incubation with ice-cold acetone:methanol (1:1) for 5 minutes at 4 °C. Cells were then washed with PBS and incubated with 5% (w/v) Bovine Serum Albumin (BSA; Sigma-Aldrich) in PBS for 30 minutes at room temperature. The BSA solution was removed and replaced with primary antibody diluted appropriately in 1% (w/v) BSA in PBS. Samples were then incubated for 1 hour at room temperature. Cells were then washed with PBS, and incubated for 1 hour in the dark at 4 °C with Alexa Fluor-488, -555 or -647 conjugated secondary antibody (ThermoFisher Scientific) diluted to between 1 in 200 and 1 in 500 in 1% (w/v) BSA in PBS. Cells were then washed with PBS. Where appropriate, cells were incubated for 10 minutes in 1 µg/mL DAPI (Sigma-Aldrich) in PBS at 4 °C or for 15 minutes in 50 µM DRAQ5 (ThermoFisher Scientific) in PBS at room

temperature to stain the nuclei. To stain the endoplasmic reticulum, cells were incubated for 30 minutes in 25 nM IraZolve-ER Blue™ in PBS at room temperature. Cells were then washed with PBS and imaged immediately or stored at 4 °C in the dark prior to imaging. Antibody and fluorescent stain details are provided in Appendix III.

2.14 Automated Cell Counting and Calculation of Infection Percentage by Immunofluorescence Microscopy

Cells were cultured in 96-well black wall imaging plates (Pheno-Plate-96, PerkinElmer), infected and/or treated as appropriate, cultured, fixed and stained by indirect immunofluorescence. Samples were imaged using a Cytation 5 Cell Imaging Multimode Reader (BioTek) using a 10× or 4× objective and appropriate fluorescent filters and settings. Infection levels were calculated from stitched images using the Gen5 Software, as follows. Total cell numbers were enumerated based on nuclei that were DAPI-stained to define the 'primary mask', while infected cells were identified by using anti-Capsid immunofluorescent staining within a 'secondary mask' that included and expanded upon the primary mask and thresholding of associated fluorescence levels such that <1% of uninfected cells were positively identified by anti-Capsid immunofluorescence. The percentage of infected cells was determined for each well and expressed as a percentage of average values for those of DMSO-treated controls.

2.15 Live Cell Imaging

Live cell imaging was performed using the Incucyte® SX5 Live-Cell Analysis Instrument (Sartorius). Cells were seeded into black-walled 96-well imaging plates (Pheno-Plate-96, PerkinElmer) at 2 x 10^4 cells/well, and after 24 hours, infected with DENV2-NS1-mScarlet with or without treatment, as indicated. Plates were transferred to the Incucyte®, which is contained within a humidified 37 °C and 5% CO_2 incubator for the length of the experiment. Images were acquired (4 fields per well) using Phase Contrast and Red Fluorescence channels and a 10x objective at specified intervals over 72 hours. Analysis was performed using the Incucyte® 2021C Basic Analyzer tool.

2.16 Confocal Microscopy

8-well #1.5H glass-bottom chamber slides (µ-Slide; Ibidi) were coated with 0.2% (w/v) gelatin in PBS for 1 hour, before washing with PBS and seeding with cells at 2 × 10^4 cells/well. After culture and treatments, cells were fixed and stained as described in section 2.13. Imaging was

performed using a ZEISS LSM880 Fast Airyscan confocal microscope system using a 63× (N.A. 1.4) Plan-Apochromat oil immersion objective. Appropriate laser lines (405, 488, 561 and 633 nm) were used at 2% of maximal power, with master gain settings adjusted to enable signal visualisation with minimal saturation. Pinhole size was set to 1.0 Airy units for the longest-wavelength fluorophore and matched for all tracks. Images were primarily captured using Z-stack or tile scan options in ZEN (black edition) system 2.3 software (ZEISS). Images were analysed and processed using the ZEISS Zen Blue version 3.2 software. For colocalisation analysis, Bezier regions of interest were drawn around fluorescently labelled cells and Pearson's correlation coefficients were determined for each cell.

2.17 Western Blotting and Sample Preparation

Cell monolayers were washed with ice-cold PBS before lysis with RIPA buffer (see Appendix II) containing mammalian protease inhibitor cocktail (Sigma-Aldrich). Cells were lysed for 30 minutes at 4 °C, then transferred to microcentrifuge tubes and frozen at -20 °C. Samples were thawed and centrifuged at 15,000 x *g* for 15 minutes, and supernatants were then transferred to new tubes, with the cell debris discarded. When probing for NS1, non-reducing sample buffer (see Appendix II) was added, while other primary antibodies required reducing sample buffer (see Appendix II). Samples were heated at 95 °C for 5 minutes, before separation by SDS-PAGE using 4 - 20% Tris-HCl pre-cast gels (Bio-Rad). Proteins were transferred to nitrocellulose membranes using a Trans-Blot® Turbo™ Transfer System (Bio-Rad).

Membranes were washed in PBS containing 0.1% [v/v] Tween-20 (PBS-T), then blocked for approximately 60 minutes in 5% (w/v) skim milk in PBS-T at room temperature (RT). Membranes were then incubated overnight with primary antibody diluted in 5% skim milk in PBS-T at 4 °C. Membranes were washed in PBS-T for 3 × 5 minutes at room temperature, incubated with IRDye®-800CW-conjugated secondary antibody (LI-COR Biosciences) (1:20,000) in PBS-T for one hour at room temperature, then washed 3 × 5 minutes in PBS-T. The LI-COR Odyssey® Imaging System (LI-COR Biosciences) was used to image the membranes. Fluorescence was recorded at 700 and 800 nm. Image Studio Lite was used for quantification purposes.

2.18 *In vitro* RNA Transcription

RNA transcription was performed using an mMESSAGE mMACHINE® SP6 Transcription Kit (ThermoFisher Scientific), according to manufacturer's instructions. Briefly, for each reaction,

10 µL of 2X NTP/CAP solution (comprised of 10 mM ATP, 10 mM CTP, 10 mM UTP, 2 mM GTP and 8 mM cap analog [m7G(5')ppp(5')G]), 4.5 µL of 10X Reaction Buffer, 1.5 µL of 20 mM GTP, 2 µL SP6 RNA polymerase enzyme mix and 4.5 µL (0.5 – 1.0 µL) of digested, purified DNA were added to a nuclease-free 0.2 mL PCR tube. After mixing by pipetting, the reaction was incubated at 37 °C for 3 hours, before adding 1 µL of TURBO DNase, mixing and incubation for 15 minutes. RNA was then extracted using the method outlined in section 2.18.

2.19 RNA Extraction

Total RNA was extracted from cells or *in vitro* transcription (IVT) reaction products using TriSURE™ (Bioline), according to manufacturer's instructions. Briefly, near-confluent cells in a 6-well plate were washed with PBS, then 1 mL of TriSURE™ was added, and shaken for 15 minutes at room temperature, before transferral to nuclease-free microcentrifuge tubes. Alternatively, IVT reaction products were transferred to a nuclease-free tube and 1 mL of TriSURE was added and samples were mixed by pipetting. To each sample, 200 µL of chloroform was added, before mixing by shaking. Samples were centrifuged at 12,500 x *g* for 15 minutes at 4 °C. The aqueous layer was then isolated and transferred to a new nuclease-free microcentrifuge tube. To each sample, 500 µL of isopropanol was then added, and samples were mixed and incubated for 15 minutes at room temperature. Samples were then centrifuged at 12,500 x *g* for 15 minutes at 4 °C to pellet the RNA. After removal of liquid, the RNA pellet was washed with 1 mL of 75% ethanol, and centrifuged at 7,500 x *g* for 5 minutes at 4 °C. The ethanol was removed, and the pellet was dissolved in 50 – 100 µL of RNAse free H_2O, and stored at -80 °C. RNA concentrations and 260/280 and 260/230 absorbance values were measured using a NanoDrop 2000 spectrophotometer (ThermoFisher Scientific). A 260/280 ratio of ~2.0 was expected for 'pure' RNA.

2.20 DNA Transfections

DNA transfections were performed using Lipofectamine™ 2000 Transfection Reagent (Thermo Fisher Scientific), according to manufacturer's instructions. Briefly, cells were seeded one day prior to the transfection, at a seeding density allowing for 80 - 90% confluency by the time of transfection. In a standard 6-well plate transfection (with smaller sized wells scaled down according to the surface areas of wells), two tubes were prepared. Tube A contained 100 µL OptiMEM (Thermo Fisher Scientific) and 3 µL of Lipofectamine 2000 reagent, while tube B contained 100 µL of OptiMEM and 2 µg of plasmid DNA. Each tube was gently vortexed and

briefly centrifuged in a benchtop microcentrifuge, then the tubes' contents were combined and mixed by pipetting. The solution was incubated at room temperature for 15 minutes, before being applied dropwise to a well containing cells with complete cell culture medium. After 4 hours, the cells were washed with PBS, replenished with cell culture medium and returned to culture conditions.

2.21 RNA Transfections

RNA transfections were performed using DMRIE-C Transfection Reagent (Thermo Fisher Scientific). Cells were seeded one day prior to the transfection, at a seeding density allowing 80 - 90% confluency by the time of transfection. In a standard 6-well plate transfection (with smaller sized wells scaled down according to the surface areas of wells), 1 mL of OptiMEM (Thermo Fisher Scientific) and 6 µL of DMRIE-C were mixed gently by vortexing. Cell culture medium was removed, and cells were washed in PBS, which was then removed. To the OptiMEM/DMRIE-C solution 5 µg RNA was added and mixed gently by flicking. The solution was added to the cells, which were then returned to cell culture conditions. After 4 hours, the cells were washed with PBS, replenished with cell culture medium and returned to culture conditions.

2.22 Thermal Shift Assay (Preparation of Lysate)

Cells were seeded at 2 x 10^5 cells/well in a 6-well tray. After culture for 24 hours, DENV2-NS1-NLuc RNA was transfected into cells using DMRIE-C (Thermo Fisher Scientific) as per protocol 2.20. After 3 hours, the media was replaced with DMEM containing 10% FCS and Penicillin/Streptomycin. After culture for 72 hours, all cells were reseeded into 75 cm^2 flasks (1 flask per 3 wells) and grown until confluent at 6 days post-transfection. Supernatants were removed and cells washed once with PBS. To prepare lysates, PBS was removed and ice-cold NP-40 lysis buffer (1% NP-40, 150 mM NaCl, 50 mM Tris [pH 8.0]) containing 1:100 protease inhibitor cocktail (Sigma-Aldrich) was added to the cell monolayer at 5 mL/flask, then flasks were incubated for 5 minutes at 4 °C. The lysate was collected and homogenised by repeatedly passing the mixture through a 25-gauge syringe, approximately 25 times. The debris was then removed by centrifugation at 10,000 x *g* for 5 minutes at 4 °C. Clarified lysates were then aliquoted and stored at -80 °C. Control samples were prepared in a similar manner, except that Huh-7.5 cells were transfected with an expression plasmid encoding unfused NLuc, and lysates were prepared at 24 hours post-transfection.

To perform the assay, DENV2-NS1-NLuc lysate was thawed on ice, then diluted 1 in 10 in OptiMEM (Thermo Fisher Scientific). For each compound for testing, 45 µL of lysate/OptiMEM and 5 µL of a compound in DMSO was added to each tube in PCR tube 8-cap strips. The entire strip was incubated at room temperature for 2 hours while rocking. The tube strips were transferred to a gradient PCR machine (gradient-enabled S1000 Thermal Cycler; Bio-Rad) and incubated at 40 - 54 °C or 56 - 70 °C for 3 minutes, before immediately being removed and returned to room temperature. 25 µL was then transferred to a white walled 96-well plate. A 25 µL solution of OptiMEM with 1:100 NanoLuc substrate (Promega) was added and samples were mixed, then incubated at room temperature for 10 minutes. Luminescence was then measured using a Cytation 5 Imaging Multimode Reader (Agilent) or SpectraMax iD5 Multi-Mode Microplate Reader (Molecular Devices), with results expressed as a percentage of those of the samples treated at 40 °C.

2.23 NaLTSA High-Throughput Screening

For high throughput screening, 40 nL of each compound from the Open Scaffold collection from Compounds Australia (Griffith University, Australia) at 5 mM (in DMSO) was dispensed into each well of 384-well PCR plates (Bio-Rad) in triplicate. For negative controls, 40 nL of DMSO was plated for 40 wells/plate (columns 1, 24 and half of 23), while methyl-beta-cyclodextrin (MβCD, Sigma-Aldrich) served as a technical positive control and for this 530 nL of MβCD at 50 mM (in DMSO) was plated into 8 wells/plate (second half of column 23). Lysates were diluted 1 in 10 in OptiMEM (Thermo Fisher Scientific), as above, and to each well 20 µl of diluted lysate was added before mixing by agitation and incubation at room temperature for 2 hours. Plates were subjected to heat denaturation in a Bio-Rad S1000 thermal cycler by incubating at 54 °C for 5 mins, then 24 °C for 2 mins. During this time, 9 µl of NanoLuc substrate (Nanoluciferase Assay, Promega), pre-diluted 1 in 100 in OptiMEM, was added to each well of a 384-well opaque assay plate (OptiPlate, PerkinElmer) and then 9 µl of heat-denatured lysate was added to each well. Plates were then shaken, incubated for 18 mins and luminescence was measured using an EnSight Multimode Plate Reader (PerkinElmer). Data was analysed using TIBCO Spotfire software (PerkinElmer) on a per plate basis. In most instances the Z-prime value was approximately 0.85, the MβCD:DMSO signal was approximately 2.1 and the %CV values were 5 - 10%.

2.24 NanoBiT Protein:Protein Interaction Assay

Cells were cultured in 96-well white walled plates (Sigma-Aldrich). At 70 - 80% confluency, these cells were transfected with SmBiT and/or LgBiT expression plasmids, for both NS1-LgBiT and NS1-SmBiT constructs and the control dimerisation pair, SmBiT-PRKACA and LgBiT-PRKAR2A (Promega). After culture for 48 hours, cells were washed once with PBS, then lysed with 40 µL 1X Passive Lysis Buffer (Promega) in H_2O for 10 minutes. A 40 µL solution of NanoLuc substrate (Nanoluciferase Assay, Promega), pre-diluted 1 in 100 in OptiMEM (Thermo Fisher Scientific), was then added to each well, and incubated for 5 minutes while shaking the plate. Luminescence signal was then measured using the BioTek Cytation 5 Cell Imaging Multimode Reader (Agilent). Signal from the NS1-SmBiT/NS1-LgBiT constructs were normalised to the control dimerisation pair, SmBiT-PRKACA/LgBiT-PRKAR2A, where required.

2.25 NanoBiT® Protein:Protein Interaction System High-Throughput Screening

For high-throughput screening, HeLa cells were seeded into a 6-well plate at $2x10^5$ cells/well. After culture for 24 hours, each well was transfected with 4 µg of pLenti-NS1-SmBiT and pLenti-NS1-LgBiT plasmids (2 µg each), or the pPRKACA-SmBiT and pPRKAR2A-LgBiT control dimerisation pair, using 6 µL Lipofectamine™ 3000 (ThermoFisher Scientific) and 500 µL OptiMem (Thermo Fisher Scientific) per well. After a 3 hour incubation, cells were washed with PBS and 2 mL of complete DMEM culture media was added. After culture for 24 hours, cells were trypsinised and re-seeded into black-walled 384-well plates (Bio-Rad) at 1700 cells/well in 50 µL of media. These plates were pre-coated with 1 µL of DMSO, or with compound solubilised in DMSO to allow for a final concentration of 10 µM, with compounds from the Open Scaffold collection from Compounds Australia (Griffith University, Australia). After culture for 24 hours, media was aspirated and 20 µL of CellTitre-Blue® (Promega), pre-diluted 1:4 in DMEM, was added to each well, and plates were shaken slowly for 10 seconds. One hour later, fluorescence readings were recorded using an EnSight® Multimode Plate Reader (PerkinElmer). Cells were then washed three times with 50 µL PBS, and 20 µL of NanoLuc substrate (Nano-Glo® Luciferase Assay System), pre-diluted 1:80 in OptiMEM, was added and plates were shaken slowly for 10 seconds. After ten minutes, luminescence readings were recorded with the EnSight® Multimode Plate Reader.

2.26 Virtual Screen for NS1-Interacting Compounds

For targeting of the NS1 monomer and dimerisation interface, separation of a NS1 dimer structure (PDB accession code: 7K93) was performed in PyMOL software (version 2.5.4; Schrodinger). Prediction of binding sites on the surface of the NS1 monomer was performed using QuickVina-W(325), with an exhaustiveness value of 25. Molecular dynamics simulations were performed using GROMACS(326), with a 500 ns simulation. The Gromos algorithm was used for RMSD-based clustering for 50,001 frames with a 0.2 nanometre distance cut-off. An ensemble of 6 structures was selected representing 99% of the simulation. QuickVina-W(327) was used to screen the 7.8 million compound ZINC20 library, filtered for purchasable compounds, against the two identified binding pockets. The top 30 hits at each site were assigned with a weighted score based on interaction with the specific binding pocket.

2.27 Construction of the E, prM and NS1 Mutant Libraries for the Full-Length Dengue Virus Infectious Clone

To prepare libraries of DENV with a mutagenised region spanning E, prM and NS1, three ~2000 base pair regions of the DENV 16681 infectious clone (pFK-DVs) were amplified using Q5® High-Fidelity DNA Polymerase (New England BioLabs), as per Section 2.2, to prepare a template for further amplification of subregions containing the *Sal*I-*Sph*I, *Sph*I-*Mlu*I and *Mlu*I-*Kas*I restriction enzyme digest sites. These 1219, 1218 and 1056 base pair subregions extending from the *Sal*I-*Sph*I, *Sph*I-*Mlu*I and *Mlu*I-*Kas*I restriction enzyme sites, respectively, were then amplified with the error-prone DNA polymerase Mutazyme II (Agilent) as per Section 2.2, using primers with 40 nucleotide overhangs allowing for insertion into a pUC57 (GenScript) shuttle vector via NEBuilder HiFi DNA Assembly (NEB). The pUC57 shuttle vector was digested using restriction enzyme pairs *Sal*I and *Sph*I, *Sph*I and *Mlu*I, or *Mlu*I and *Kas*I, as per Section 2.4. To generate 0 – 2 mutations per DNA fragment, a 19 cycle PCR with 175 ng of the ~2000 base pair DNA fragment was performed. Using NEBuilder HiFi DNA Assembly, per section 2.6, the Mutazyme II-amplified fragments were cloned into the digested pUC57 shuttle vector. Across multiple samples, 100 µL of the NEBuilder HiFi DNA Assembly mixture was transformed into NEB® Stable Competent *E. coli* (New England BioLabs) and plated onto LB agar plates containing ampicillin, as described in section 2.8, with NEBuilder HiFi DNA Assembly products containing the cloned *Sal*I-*Sph*I, *Sph*I-*Mlu*I and *Mlu*I-*Kas*I regions, respectively, transformed and plated separately. Plates were incubated at 30 °C for 40 hours. Luria Broth was added to each plate, and the plates were shaken for 10 minutes to dislodge

and resuspend bacterial colonies. The Luria Broth was then collected, with each library pooled separately (>1 x 10^6 colonies per subregion). The protocol for maxi-prep plasmid purification was then followed as per section 2.11.

After purification of the pUC57- *Sal*I-*Sph*I, pUC57- *Sph*I-*Mlu*I and pUC57-*Mlu*I-*Kas*I mutant libraries, each of the libraries were digested with their respective restriction enzymes. The desired fragment was isolated using gel electrophoresis and column purification as per Section 2.5. Similarly, pFK-DVs was digested with either *Sal*I-*Sph*I, *Sph*I-*Mlu*I or *Mlu*I-*Kas*I restriction enzymes, and the desired ~13 kb plasmid backbone fragment was isolated. The mutant fragments were then ligated with the pFK-DVs backbone using T4 DNA ligase (New England BioLabs) as per Section 2.7. For each sample, 100 µL of the ligation reaction product was then transformed into NEB® Stable Competent *E. coli* and plated onto LB agar plates containing ampicillin, as described in section 2.8, with the pFK-DVs- *Sal*I-*Sph*I, pFK-DVs- *Sph*I-*Mlu*I and pFK-DVs- *Mlu*I-*Kas*I plasmids transformed and plated separately. LB plates were incubated at 30 °C for 24 hours, at which time all visible colonies were highlighted. The plates were returned to the incubator for a further 16 hours, then the highlighted colonies were removed using a 1 mL pipette tip. Using the same protocol as for the pUC57 libraries, the pFK-DVs libraries were collected and purified. Approximately 200,000 uniquely transformed colonies were collected for each of the pFK-DVs-*Sal*I-*Sph*I, pFK-DVs- *Sph*I-*Mlu*I and pFK-DVs-*Mlu*I-*Kas*I libraries.

2.28 Construction of the NS1 Mutant Libraries for the Full-Length Dengue Virus Infectious Clone

To prepare libraries of DENV with a mutagenised NS1 region, pFK-DVs was digested with restriction enzymes *Bam*HI and *Kas*I, isolating the entire NS1 gene. The 1455 bp DNA fragment was amplified using PCR with Mutazyme II DNA polymerase, which was performed using 250 ng of template DNA and a 30 cycle PCR. Primers were designed with 6 overhanging nucleotides to allow for efficient restriction enzyme digestion of this PCR product. This mutagenised fragment pool was then ligated into a pUC57 shuttle vector, also digested with *Bam*HI and *Kas*I, as per Section 2.7, following agarose gel electrophoresis and gel extraction of the corresponding DNA fragments, as described in Section 2.5. The library was transformed into NEB® Stable Competent *E. coli* cells (New England BioLabs), as per section 2.8. After purification of this library, as per section 2.11, the library was digested with *Bam*HI and *Kas*I,

and the mutated NS1-containing fragment was isolated using gel electrophoresis and column purification as per Section 2.5. Additionally, the 12,378 bp backbone of pFK-DVs was amplified using Q5® High-Fidelity DNA Polymerase, and purified via the same method. NEBuilder HiFi DNA Assembly was used to join the PCR-amplified backbone and the digested NS1-fragment, and transformation and purification of plasmid was performed as per Section 2.27. The NEBuilder HiFi DNA Assembly mixture was transformed into NEB® Stable Competent *E. coli* across three separate batches, and colonies from each transformation were kept separate. Together, the three libraries totalled approximately 2,000,000 uniquely transformed colonies.

2.29 Construction of the NS1 Mutant Libraries for the Subgenomic Dengue Virus Infectious Clone

To prepare libraries of the subgenomic replicon of DENV with a mutagenised NS1 region, the NS1 gene-containing region was first liberated from pFK-sgDVs-R2A by restriction enzyme digestion with *Age*I and *Kas*I and purified by gel extraction (Section 2.5) following agarose gel electrophoresis (Section 2.3). This region was then PCR-amplified using Mutazyme II, as per Section 2.2, using primers designed with sufficient overhanging nucleotides to allow for efficient digestion, 50 ng of template DNA and a 25 cycle PCR. This mutagenised fragment pool was then purified (Section 2.5) and digested using *Age*I and *Kas*I restriction enzymes. Plasmid pFK-sgDVs-R2A was also digested using *Age*I and *Kas*I and, following agarose gel electrophoresis and gel extraction, *Age*I/*Kas*I-digested mutagenized NS1 was cloned into similarly digested pFK-sgDVs-R2A plasmid backbone (11,268 bp) via T4 DNA ligation, as per Section 2.7. Transformation of electrocompetent NEB® Stable E. coli cells was performed as per section 2.9, and purification of plasmid proceeded as per section 2.26. The ligation mixture was transformed into NEB® Stable Competent *E. coli* across three separate batches, and colonies from each transformation were kept separate. Together, the three libraries totalled ~500,000 uniquely transformed colonies.

2.30 Focus Forming Assay

Virus infectivity was determined by focus-forming assays. Huh-7.5 cells were seeded into 96-well plates at 2×10^4 cells/well and cultured overnight. Following preparation of 10-fold serial dilutions of virus-containing supernatants, cells were infected using 40 µL/well of each diluted inoculum. Cells were then cultured for 3 hours, washed once with PBS and returned to culture in normal media for 72 h, prior to fixation and indirect immunofluorescent labelling using anti-

Capsid or anti-Envelope primary antibodies (as per Section 2.13). Infected cell foci were enumerated and virus infectivity was expressed as focus-forming units (FFU) per mL.

2.31 Viral RNA Replication Assay

To determine levels of viral RNA replication within cells, subgenomic replicon-harbouring Vero-sgDVS-GFP cells were used(328). Cells were seeded in 96-well black-walled imaging plates (PhenoPlate-96; PerkinElmer) at 1×10^4 cells/well and cultured overnight. After treatment, cells were stained using Hoechst 33342 dye (Sigma-Aldrich) diluted to 1 µg/ml in PBS for 5 minutes at room temperature, then washed three times with PBS. Total GFP and Hoechst 33342 fluorescence readings for each well were measured immediately using a Cytation 5 Imaging Multimode Reader (Agilent), and GFP-associated fluorescence values were normalised to those of Hoechst 33342. Normalised GFP fluorescence was expressed as a percentage of average (DMSO-treated) control values as a surrogate measure of viral RNA replication.

Chapter 3: Identification of NS1-interacting DENV inhibitors

3.1.1 Introduction

There currently exists no approved antiviral therapeutic against DENV(2). Potent small molecule inhibitors of DENV are in development and many such inhibitors are directed towards targets including the NS3/NS2B protease, the NS3 helicase, Envelope protein and the methyltransferase and RNA dependent RNA polymerase domains of NS5(329). Although promising disease ameliorating monoclonal antibodies against the non-enzymatic NS1 protein have been recently developed(202, 330), small molecule inhibitors that specifically target NS1 remain to be discovered. Given the essential roles of NS1 in viral RNA replication, infectious particle production and disease pathogenesis(145), we propose that NS1 is a promising target for future small molecule therapeutics.

To date the most promising small molecule inhibitor of DENV NS1 is arguably the heparan sulfate mimic PG545(201). This molecule is bifunctional, interacting with Envelope protein to reduce DENV infection, and with NS1 to block NS1-mediated endothelial glycocalyx disruption. A study that employed the lethal dengue mouse model AG129, deficient in the Interferon α/β receptor(331), demonstrated that PG545 increases mouse survival, lowers viraemia and decreases circulating NS1(201). However, the direct acting antiviral effect is hypothesised to be the result of the interaction of PG545 with E protein, while the interaction with NS1 reduces disruption of endothelial integrity, and blocks NS1-induced IL-6 production(332). In another recent study, a phage display library was utilised to identify a series of 12-mer peptides which bind NS1(333). With the attachment of a C-terminal cell penetrating tag, these peptides were shown to have antiviral activity in Huh7 cells for DENV1, DENV2 and DENV4(334). The Ig5.3 mouse monoclonal antibody, isolated from NS1-immunised mice(335), has been shown to inhibit NS1-induced endothelial permeability in multiple cell lines, and decrease viraemia, circulating NS1 levels and increase survival rates in *ifnar*$^{-/-}$ and AG129 mice models(202). This antibody was also shown to bind NS1 protein of a range of clinically relevant orthoflaviviruses, supporting its potential future application in the treatment of multiple different orthoflavivirus infections(202). While not specifically targeting NS1, celgosivir targets the unfolded protein response, resulting in misfolding and accumulation of NS1 in the endoplasmic reticulum(204). Despite this progress, there is a

distinct lack of NS1-targetting small molecules which inhibit the roles of NS1 in viral RNA replication and infectious particle production.

The primary aim of the following research was to identify small molecules inhibitors of NS1 functions that act through a direct interaction with NS1. To identify such inhibitors, we utilised three unique approaches. Firstly, a Nanoluciferase-based thermal shift assay, in conjunction with a Nanoluciferase-tagged DENV clone, was utilised in a high-throughput screen to identify NS1-interacting compounds. While we were unable to unambiguously identify an NS1 interacting compound, we did identify a potent inhibitor of DENV infectious particle production, referred to henceforth as Compound 14. Further research identified a dose-dependent impact on the maturation of Envelope protein, revealed by probing for Envelope protein using both a conformation-specific antibody and a polyclonal antibody.

It is known that the dimerisation of NS1 is required for infectious particle production and viral RNA replication(336), and levels of secreted NS1 correlate with disease severity(337). Accordingly, our next approach to the identification of NS1-specific inhibitors was to identify compounds which decrease dimerisation of NS1. To this end, we developed a system to measure levels of NS1 dimerisation using the NanoBiT® Protein:Protein interaction system(338), aiming to identify inhibitors of NS1 dimerisation through analysis of decreased luminescent signal upon treatment with drug-like compounds. This was applied in a high-throughput screen, however the three hit compounds identified could not be validated as inhibitors of NS1 dimerisation or general inhibitors of the DENV lifecycle.

Finally, we performed a computational drug screen to identify compounds which theoretically bind an NS1 dimer crystal structure, with a focus on the dimerisation interface. We identified a potent inhibitor of infectious particle production with a minor impact on viral RNA replication. This compound is henceforth referred to as Compound V2.3. While the computational studies predicted binding at the dimerisation interface, we did not observe an effect of Compound V2.3 on NS1 dimerisation using the NanoBiT assay and have not yet been able to identify any NS1-specific effects.

3.1.2 Identification of sulfonamide compounds that impair dengue virus infectious particle production

Note: The following section is adapted from a manuscript titled 'Identification of sulfonamide compounds that impair dengue virus infectious particle production', to be published by Thomas D Burton, Gustavo Bracho, Tom Avery, Marie Lowe, Siena Centofanti, Steve Johnson, Amanda L Aloia, Michael R Beard, Jillian M Carr and Nicholas S Eyre. The manuscript is included in Appendix VI.

Thermal shift assays (TSA) exploit the principle that a protein bound to a ligand is likely to be more stable than the same unbound protein, and this will result in increased resistance to denaturation at high temperatures(339). In the NanoLuc luciferase thermal shift assay (NaLTSA), denaturation of a protein is monitored via measurement of coelenterazine-derived luminescence that is generated by a Nanoluciferase (NLuc) reporter protein that is fused to a protein of interest. As the protein of interest denatures upon heat treatment, NLuc, which is intrinsically thermostable, also denatures, resulting in decreased luminescence. If a ligand is bound to the protein of interest, the denaturation profile of the fusion protein is expected to change, observable by a modified luminescence output(340). We recently combined insertional mutagenesis with next-generation sequencing(341), a variation of deep mutational scanning(342), to identify regions of genetic flexibility within the DENV genome that may be exploited in the generation of infectious tagged reporter viruses. This enabled the generation of several DENV derivatives that encode reporter proteins or epitope tags inserted within the NS1 protein, including a variant that featured insertion of NLuc within NS1 with minimal impact on replicative fitness in a cell culture model. Here, we applied this DENV2-NS1-NLuc virus to the development of a NaLTSA that allows for a luminescence-based measurement of NS1 thermal stability and is amenable to high-throughput screening (HTS) for NS1-binding compounds.

Using this assay, we screened 3,378 drug-like compounds from a scaffold-based library for compounds that limited heat-induced reductions in NLuc activity, using lysates prepared from Huh-7.5 cells that were transfected with *in vitro* transcribed RNA for the DENV2-NS1-NLuc

reporter construct. These screens identified 22 hits from 3 different scaffold families as candidate NS1-interacting compounds. While we were unable to verify these hits as NS1-interactors, likely due to their stabilisation of NLuc rather than NS1, hit validation studies nonetheless identified a group of structural analogues with antiviral properties, with the lead candidate displaying low micromolar antiviral activity and minimal cytotoxicity. Here, we describe a sulfonamide family of compounds, specifically Compound 14 (PubChem CID: 50839998), which inhibit DENV2 infectious particle production and perturb the detection and localisation of mature E protein. We propose that derivatives of Compound 14 with improved antiviral potency and safety warrant further investigation, as does the exact mechanisms involved in the effect of these compounds on infectious DENV particle production.

3.1.3 Results

To identify inhibitors of DENV NS1 function, we developed a luminescence-based target engagement assay that is compatible with high-throughput screening. The NanoLuc luciferase thermal shift assay was utilised in conjunction with a previously described DENV2-NS1-NLuc reporter virus(341), allowing for the coupling of a luminescent signal with the folded state of NS1 protein(340) (Figure 3.1.1). A library of 3,378 drug-like compounds was tested for stabilisation of NS1-NLuc, which ultimately led to the identification of a group of candidate DENV inhibitors.

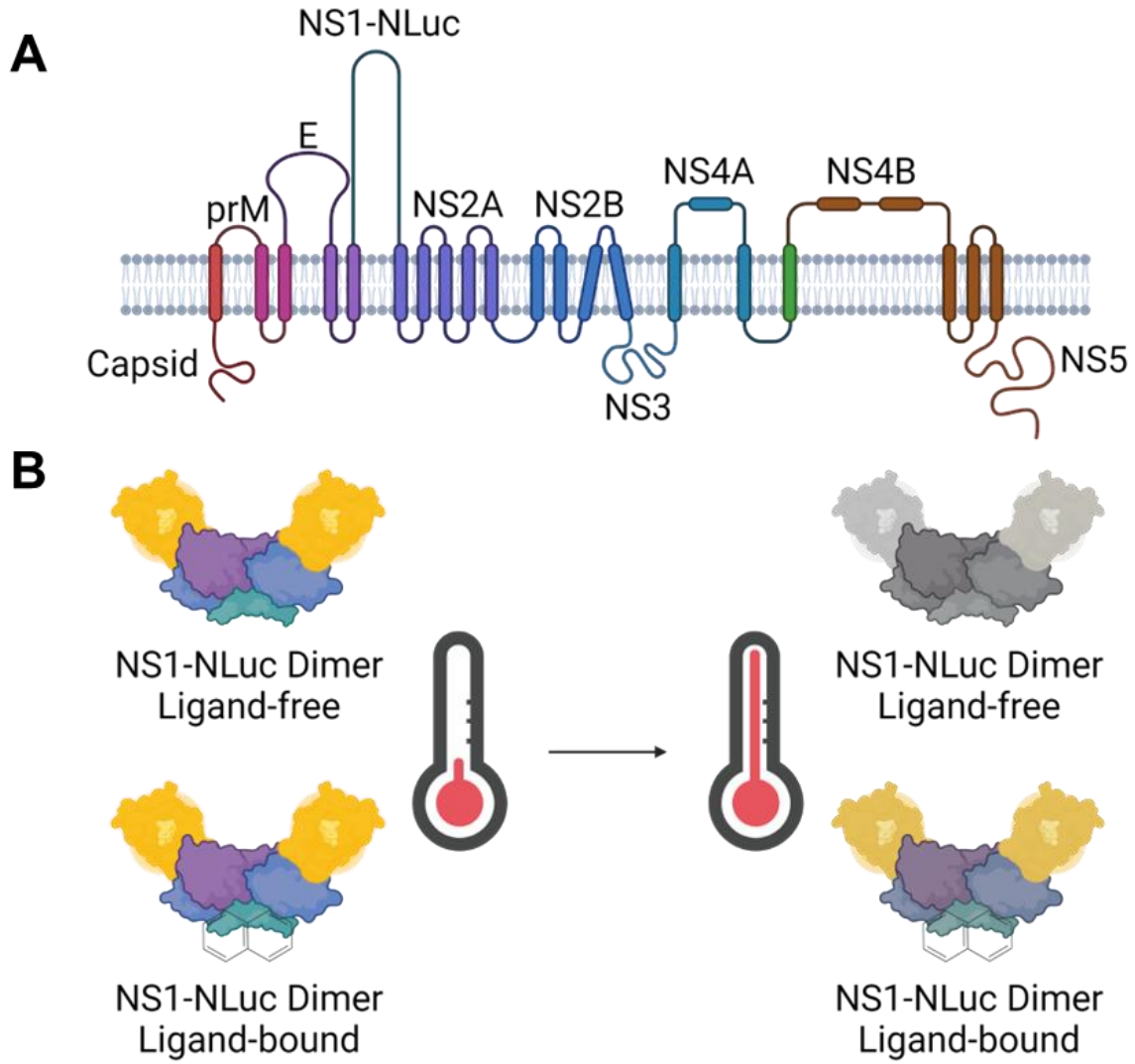

Figure 3.1.1: A) Topology of a single DENV polypeptide chain. The elongated NS1 represents insertion of the Nanoluciferase protein(343). B) Principle of the NaLTSA. A bound ligand modifies the heat-induced denaturation profile of the protein. The coupled Nanoluciferase protein allows a luminescence-based measurement of the folded state of the protein of interest. Decreased colour reflects a theoretical decrease in luminescence.

Detergent lysates of Huh-7.5 hepatoma cells that had been transfected with DENV2-NS1-NLuc reporter virus RNA were applied to 384-well plates that contained compounds from a scaffold-based library. For each of 1,226 distinct drug-like scaffolds, 1 compound was tested at a final concentration of 10 µM, with triplicate data points for each compound and two identical

repeat screens. DMSO (0.2% [v/v]) served as a carrier control for compound effects while methyl-beta cyclodextrin (MβCD, 5 mM final concentration) served as a technical positive control for stabilization of NanoLuc activity. Following incubation at room temperature with compounds, samples were heat-treated at 55 °C for 5 minutes using a thermal cycler. A fraction of each sample was then transferred to a 384-well white-walled plate containing NanoLuc substrate and incubated at room temperature before measurement of luminescence. Hits were defined as compounds which increased relative luminescence levels to >130% of that of the DMSO controls or decreased luminescence by >40%. Overall, these screens were designed to identify compounds which either stabilise or destabilise NS1 upon binding, known as N-ligands, or U-ligands, respectively(344). In total, 15 hits were recorded, with 8 N-ligands and 7 U-ligands (Figure 3.1.2). On average, Z' values were approximately 0.85 and %CV values for controls were generally less than 5%, indicating strong reproducibility of the primary screening data.

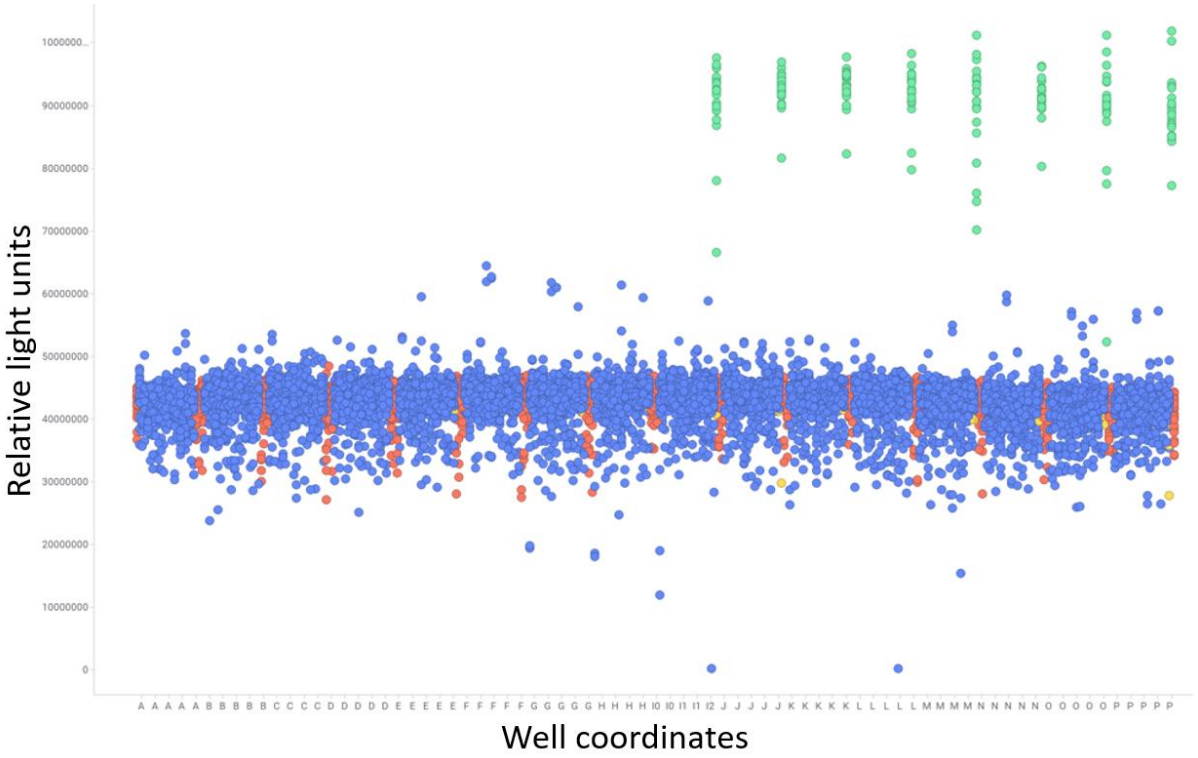

Figure 3.1.2: Identification of compounds which increase/decrease stabilisation of NS1-NLuc in a NaLTSA. Lysate from Huh-7.5 cells infected with the DENV2-NS1-NLuc reporter virus was added to 3,378 pre-dispensed drug-like compounds, with compounds at a final concentration of 10 µM. The positive control, MβCD, was applied at a final concentration of 5 mM. After incubation of each compound with lysate at room temperature for 2 hours, followed by a 5 minute heat treatment at 50 °C, an aliquot was transferred from each well to a white-walled plate with 9 µL of prepared Nano-Glo® assay substrate. After an 18 minute incubation, luminescence was measured for all wells. Blue spheres represent data points for drug-like compounds (n=2 per compound), Orange spheres represent DMSO control wells (n=40 per plate), Yellow spheres represent empty wells and Green spheres represent the MβCD positive control wells.

For each of these hits, 28-30 structural analogues from the relevant scaffolds were tested in a subsequent screen of the same format, such that a total of 427 compounds were analysed. As shown in Table 3.1.1, 21 compounds satisfied N-ligand criteria (>130% of DMSO control), while one compound satisfied U-ligand criteria (<40% of DMSO control). These 22 compounds were then tested for antiviral activity and for a concentration-dependent effect on NS1 thermal stabilisation, with lysates from Huh-7.5 cells transfected with an NLuc expression plasmid used as a control for NS1-independent NLuc stabilisation.

Table 3.1.1: Potential NS1-interacting compounds identified using a high-throughput NaLTSA drug screen. Avg(%DMSO) indicates the increase or decrease in relative luminescence units compared to the DMSO control.

Compound	QCL_SAMPLE_NUMBER	increase/decrease	Avg(%DMSO)	SCAFFOLD_ID	COMPOUND_ID	found_in
1	SN00775760	increase	134.05	SC002718	Z54316000	both replicates validation screen
2	SN00776650	increase	132.7	SC005543	Z57238485	both replicates validation screen
3	SN00776652	increase	137.71	SC005543	Z57238504	both replicates validation screen
4	SN00776653	increase	135.87	SC005543	Z57382940	both replicates validation screen
5	SN00776654	increase	133.86	SC005543	Z57238109	both replicates validation screen
6	SN00776655	increase	141.38	SC005543	Z57238119	both replicates validation screen
7	SN00776667	increase	169.68	SC005543	Z319215790	both replicates validation screen
8	SN00776672	increase	135.86	SC005543	Z335452708	both replicates validation screen
9	SN00784185	increase	144.55	CL1050	C066-4659	both replicates validation screen
10	SN00794051	increase	141.93	CL8321	J023-0485	both replicates validation screen
11	SN00795388	increase	132.71	CL9224	L356-0243	both replicates validation screen
12	SN00797921	increase	141.21	CL7988	M071-0013	both replicates validation screen
13	SN00797922	increase	145.2	CL7988	M071-0019	both replicates validation screen
14	SN00797925	increase	132.05	CL7988	M071-0045	both replicates validation screen
15	SN00797928	increase	142.6	CL7988	M071-0080	both replicates validation screen
16	SN00797930	increase	143.76	CL7988	M071-0086	both replicates validation screen
17	SN00797933	increase	131.07	CL7988	M071-0113	both replicates validation screen
18	SN00797940	increase	133.36	CL7988	M071-0220	both replicates validation screen
19	SN00776666	increase	130.38	SC005543	Z317045570	rep1 validation screen
20	SN00795375	increase	131.6	CL9224	L356-0003	rep2 validation screen
21	SN00795385	increase	131.51	CL9224	L356-0222	rep2 validation screen
22	SN00785809	decrease	43.03	CL7499	D116-0230	both replicates validation screen

To test the antiviral efficacy of the 22 hits, each compound was pre-plated into black walled 96-well plates, and Huh-7.5 cells in a DENV2-containing medium (MOI: ~0.7) were directly seeded onto the compounds to achieve final compound concentrations ranging from 0.5 to 40 µM. After 42 hours, the cells were fixed and labelled by indirect immunofluorescence using an anti-Capsid antibody and counterstained with the nuclear fluorescent dye DAPI. A DAPI-based cell count was used for a measurement of cytotoxicity. The percentage of cells infected with DENV2 was calculated using automated imaging and analysis software, whereby a threshold of fluorescence intensity in an area surrounding each DAPI-identified cell was utilised to differentiate between infected and non-infected cells. This revealed a potential antiviral scaffold (Compounds Australia scaffold CL7988) represented by compounds 12 – 18; all of which displayed comparable levels of antiviral activity and cytotoxicity, relative to DMSO-treated controls (Figure 3.1.3).

The 22 hits were also analysed for thermal stabilisation of the aforementioned DENV2-NS1-NLuc- and NLuc-expressing Huh-7.5 lysates for 7 concentrations ranging from 1 µM to 30 µM. While these results generally supported specific NS1-stabilisation (not shown), subsequent NaLTSA experiments with compounds 12, 14 and 18 that involved a fixed compound

concentration (20 µM) and a gradient of temperatures ranging from 40-70 °C revealed largely indistinguishable NaLTSA profiles of NS1-NLuc and NLuc lysates (Figure 3.1.4 and Table 3.1.2), indicating that these compounds interfere with NanoLuc activity. As such, we cannot conclude that our hits interact with NS1 or modify NS1 stability.

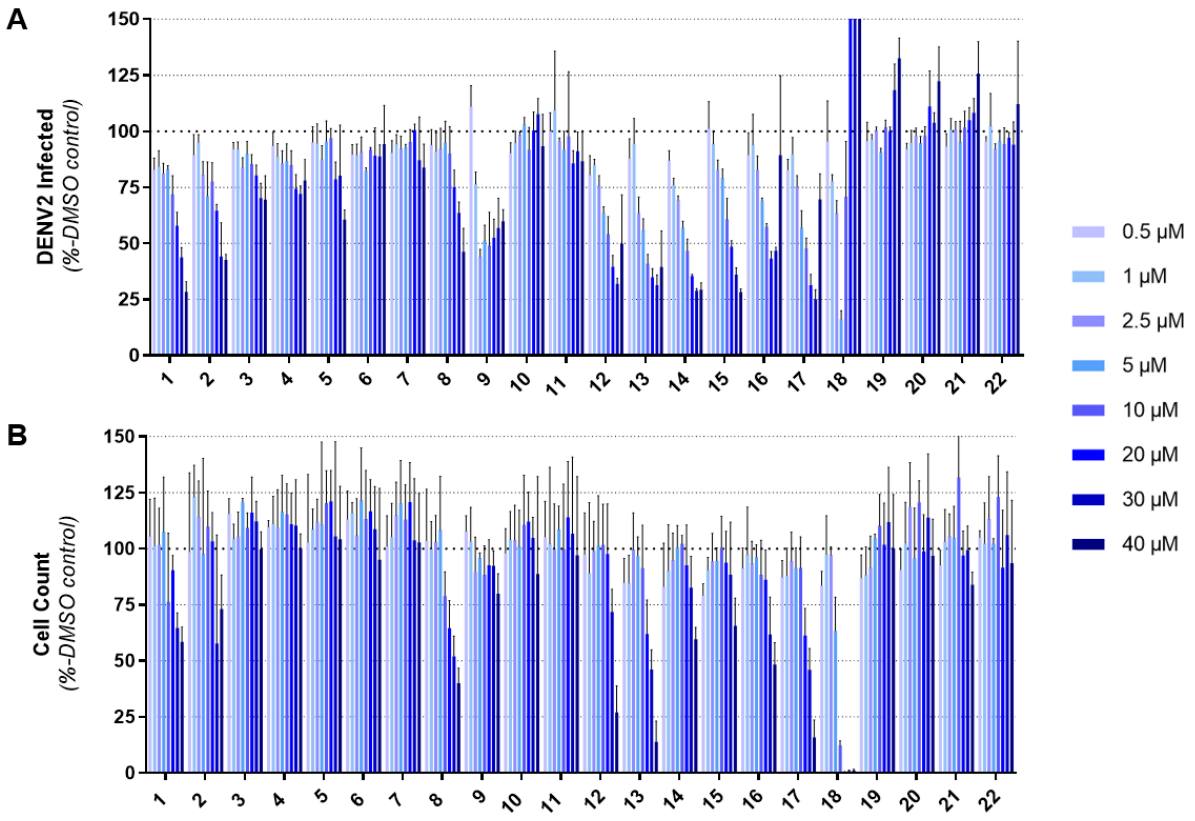

C

12

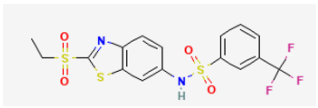

IC50: 19.9 µM
CC50: 32.5 µM
SI: 1.63

13

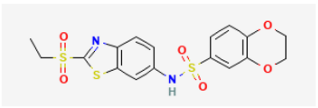

IC50: 15.3 µM
CC50: 24.6 µM
SI: 1.61

14

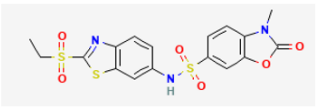

IC50: 22.3 µM
CC50: >40 µM
SI: > 1.79

15

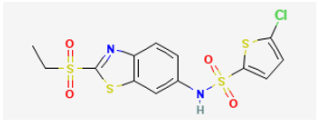

IC50: 23 µM
CC50: >40 µM
SI: > 1.74

16

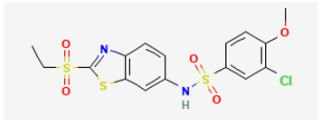

IC50: 23.4 µM
CC50: >40 µM
SI: > 1.71

17

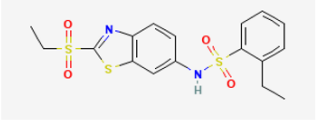

IC50: 16.7 µM
CC50: 27.1 µM
SI: 1.62

18

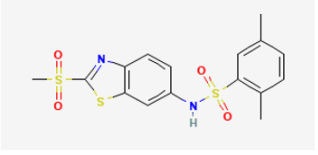

IC50: 7.98 µM
CC50: 11.1 µM
SI: 1.39

Figure 3.1.3: Dose-response analysis of the antiviral effects of the top 22 hits from the NaLTSA screen. Huh-7.5 cells were mixed with DENV2-containing media (MOI: ~0.7) and plated into black-walled 96-well plates containing pre-dispensed compounds or DMSO, such that final compound concentrations ranged from 0 to 40 μM and DMSO was present at a final concentration of 0.8% (v/v). Uninfected cells served as an additional control. Cells were incubated with compound and virus for 42 hours, then fixed, labelled by indirect immunofluorescence using an anti-Capsid antibody and counterstained with DAPI. Percentage of cells that were infected (A) and cell counts (B) were calculated via automated fluorescence microscopy. Data are means ± SD (n=4 per condition). (C) Structures of compounds 12 – 18, with IC50 and CC50 as calculated from the data presented in Figures 3.1.3A-B. All structures belong to the Compounds Australia CL7998 scaffold of structural analogues. Selectivity Index (SI) calculated as CC_{50}/IC_{50}.

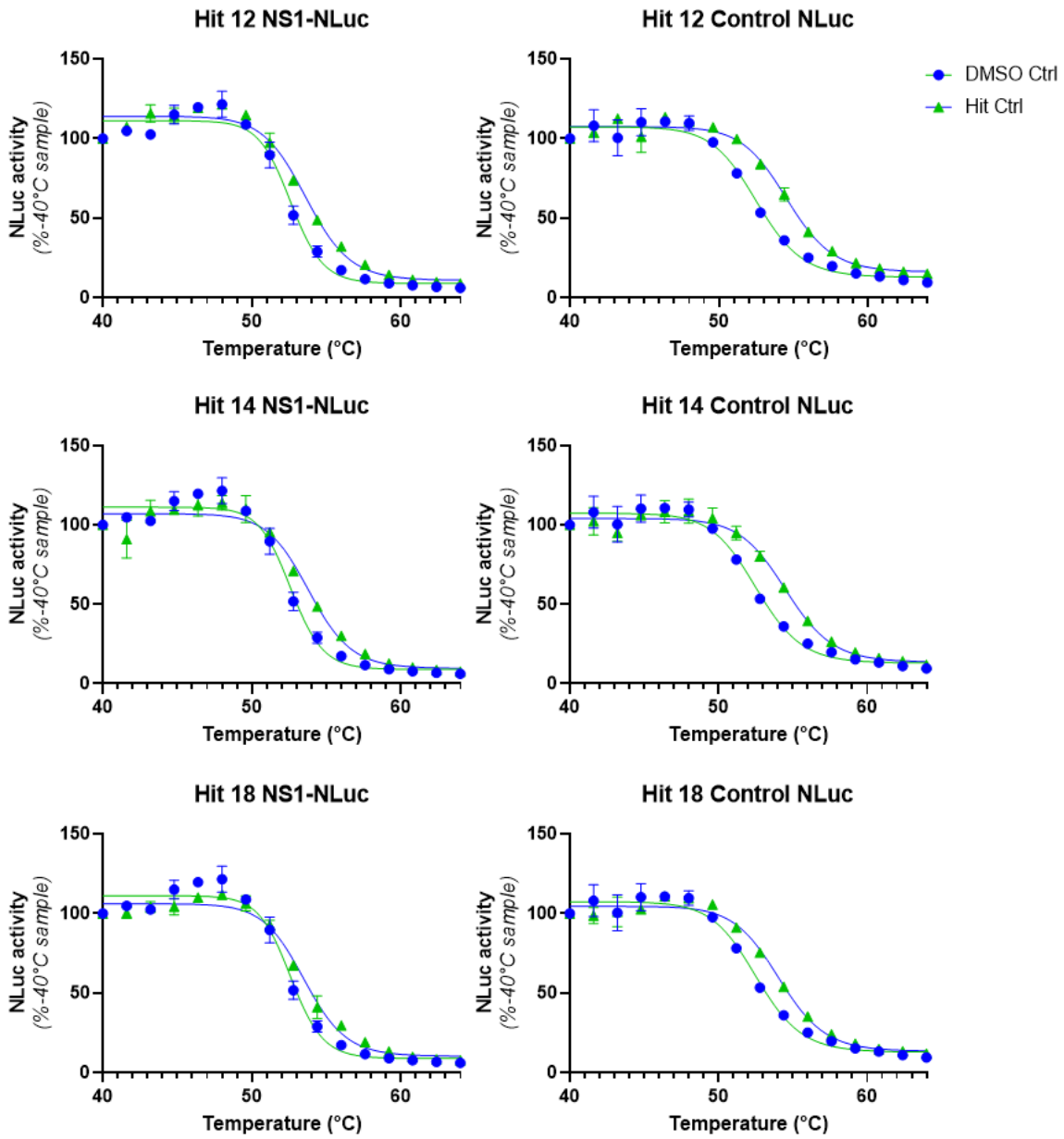

Figure 3.1.4: Determination of NS1 interaction of 3 top hits from the high-throughput NaLTSA screen. Lysate collected from Huh-7.5 cells transfected with DENV2-NS1-NLuc RNA, or an expression plasmid encoding NLuc alone, were treated with carrier (DMSO at 0.8% [v/v]) or the stated compound at a final concentration of 20 µM for 2 hours at room temperature, then heat treated for 3 minutes at the indicated temperatures. After cooling to room temperature, the samples were transferred to a 96-well white-walled plate containing Nano-Glo assay substrate, and luminescence was measured. Measurements are presented as a percentage of the luminescence recorded for the 40 °C treatment. Data are means ± S.D. (n=2) for each temperature point. Four parameter logistic (4PL) regression curves for each dataset are displayed.

Table 3.1.2: Validation of the stabilisation effects of hit compounds (20 µM) from the high-throughput NaLTSA screen. Numbers represent the average temperatures at which luminescence equates to 50% of the average value recorded at 40 °C, as determined using a sigmoidal 4PL regression model.

	NS1-NLuc (°C)		NLuc (°C)		Compound Stabilisation (°C)		NS1 stabilisation net effect (°C)
	DMSO	Compound	DMSO	Compound	ΔNS1-NLuc	ΔNLuc	(ΔNS1-NLuc) – (ΔNLuc)
Hit 12	52.61	53.66	52.55	54.57	1.05	2.02	-0.97
Hit 14	52.61	53.84	52.61	53.53	1.23	0.92	0.31
Hit 18	52.55	54.09	52.55	54.55	1.54	2	-0.46

While this scaffold appeared to possess antiviral properties, the antiviral efficacy of the compounds in this immunofluorescence-based assay was modest. Amongst these compounds, 'Compound 14' was identified to display the best compromise of antiviral activity and toxicity, with a CC_{50} greater than 40 µM and an IC_{50} of 22.3 µM (Figure 3.1.3). Given that the 42 hour immunofluorescence-based assay may favour identification of antiviral compounds that impair early events in the viral replication cycle and viral RNA replication, we reasoned that if Compound 14 and related analogues inhibit infectious particle production or secretion, such an effect may be under-represented in this assay. To address this possibility, Huh-7.5 cells were treated with a 10 µM concentration of Compounds 12 and 14 and infected with DENV2. Supernatants were collected for measurement of viral infectivity. A decrease in infectivity of approximately 80% was seen for Compound 14 compared to the control cells that were treated with carrier alone. Dose-response analysis of Compound 14 using this assay format demonstrated dose-dependent reduction of infectivity, with an IC_{50} value of 1.13 µM (Figure 3.1.5), demonstrating a strong effect of Compound 14 on DENV infectious particle production.

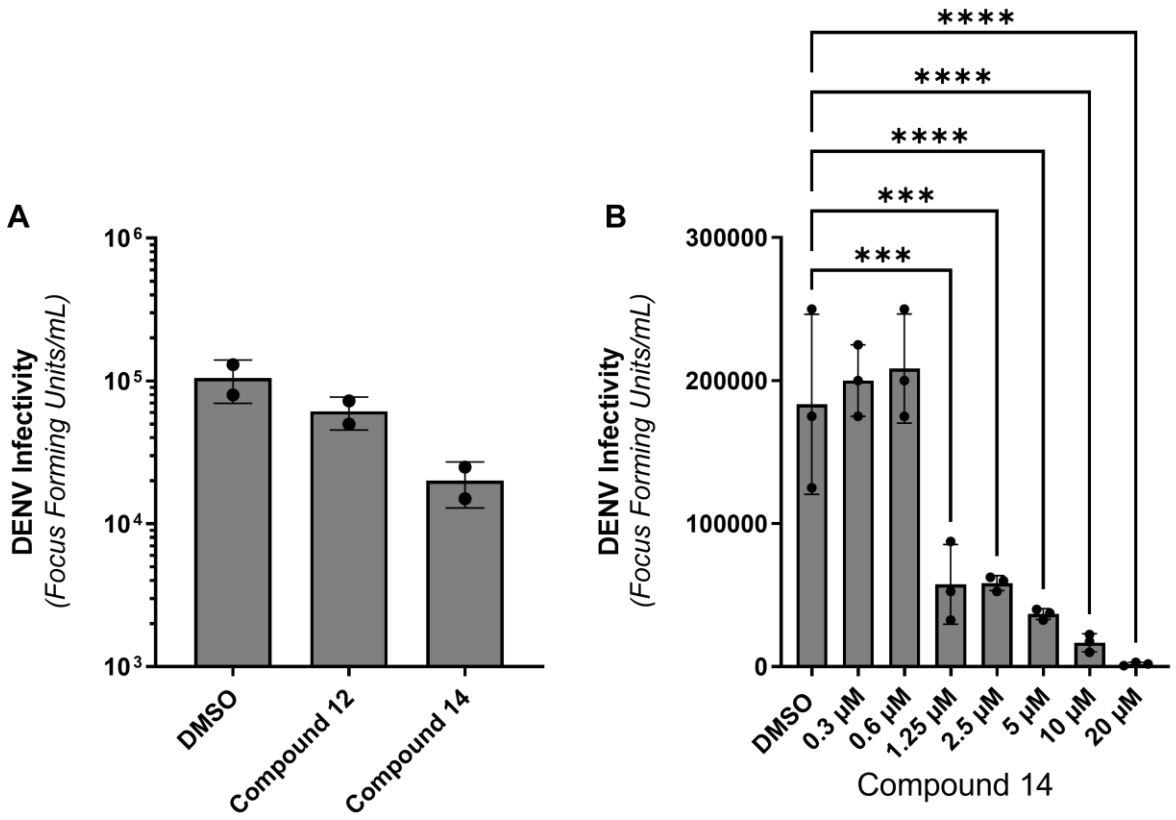

Figure 3.1.5: Analysis of the inhibition of infectious virus particle production by Compounds 12 and 14. Huh-7.5 cells were infected with DENV2 (MOI: ~0.1) and treated with the indicated compound at a final concentration of 10 µM (A) or the indicated concentration of Compound 14 (B). Seventy-two hours later, supernatants were collected and frozen for downstream measurement of infectivity by focus-forming assays. Data are means ± S.D (n= 2-3). In Figure B, *, $P < 0.05$; **, $P < 0.01$; ***, $P < 0.001$; ****, $P < 0.0001$ indicate statistically significant differences compared to DMSO treatment, by one-way ANOVA (multiple comparisons).

Next, we screened 37 commercially available structural analogues of Compound 14, with the aim of exploring varied ring system electronics, general structural changes and structures with reduced logP (a measure of lipophilicity(345)) (Figures 3.1.6, 3.1.7, 3.1.8). While none of these analogues displayed greatly improved antiviral activity or reduced toxicity in comparison to Compound 14, it was noteworthy that changes to the 2-ethylsulfonyl group on the benzothiazole core resulted in increased toxicity or abrogated antiviral activity (Figure 3.1.6).

Ai

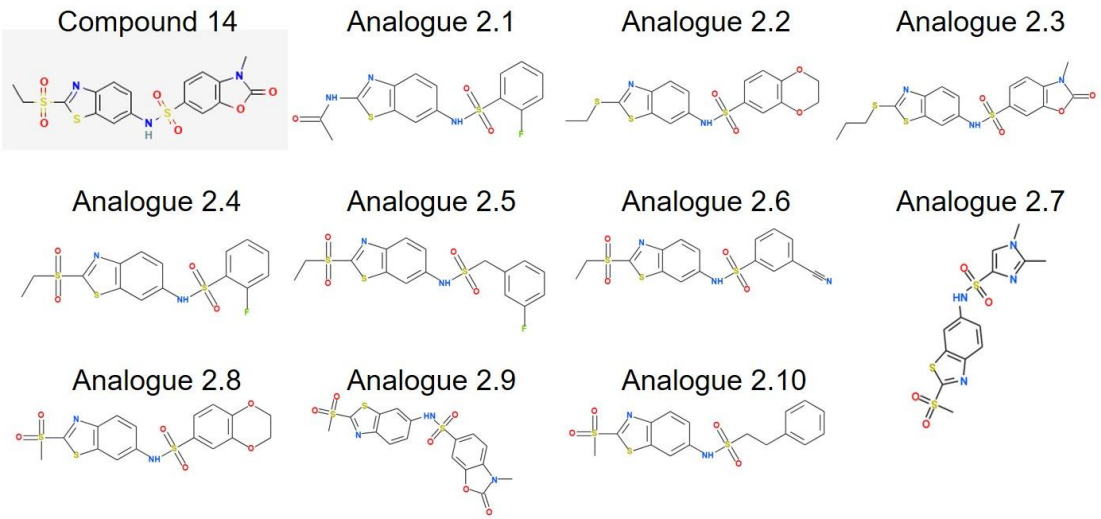
Compound 14
Analogue 2.1
Analogue 2.2
Analogue 2.3
Analogue 2.4
Analogue 2.5
Analogue 2.6
Analogue 2.7
Analogue 2.8
Analogue 2.9
Analogue 2.10

Bi

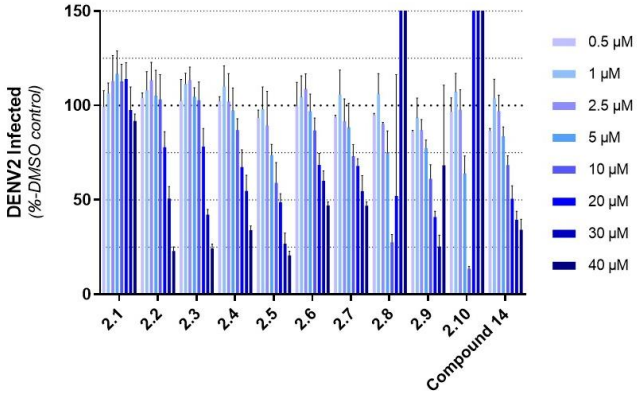
DENV2 Infected
(%-DMSO control)
150
100
50
0
0.5 µM
1 µM
2.5 µM
5 µM
10 µM
20 µM
30 µM
40 µM
2.1
2.2
2.3
2.4
2.5
2.6
2.7
2.8
2.9
2.10
Compound 14

Ci

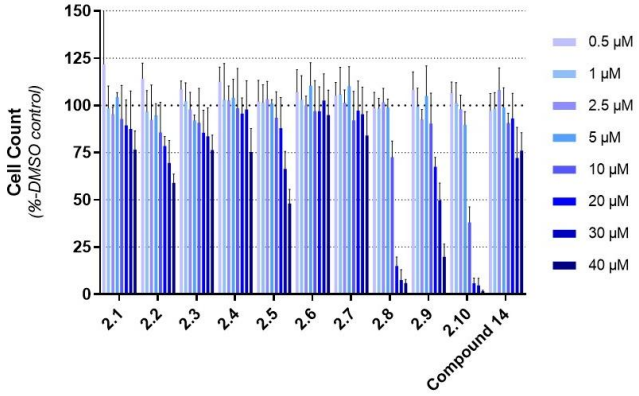
Cell Count
(%-DMSO control)
150
125
100
75
50
25
0
0.5 µM
1 µM
2.5 µM
5 µM
10 µM
20 µM
30 µM
40 µM
2.1
2.2
2.3
2.4
2.5
2.6
2.7
2.8
2.9
2.10
Compound 14

Di

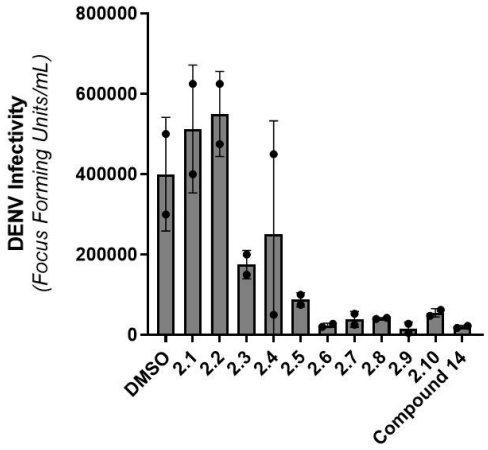
DENV Infectivity
(Focus Forming Units/mL)
800000
600000
400000
200000
0
DMSO
2.1
2.2
2.3
2.4
2.5
2.6
2.7
2.8
2.9
2.10
Compound 14

Figure 3.1.6: Dose-response analysis of the antiviral effects of structural analogues 2.1 – 2.10 via immunofluorescence assays, and analysis of the inhibition of infectious particle production. A) Compound structures. B/C) Immunofluorescence assays. Huh-7.5 cells were simultaneously infected with DENV2 (MOI: ~0.7) and treated with the indicated compounds at concentrations ranging from 0.5 to 40 μM then incubated for 42 hours. Cells were fixed, labelled by indirect immunofluorescence using anti-Capsid antibody and counterstained with DAPI. Cell counts and the percentage of cells infected were calculated via automated fluorescence microscopy. Data are means + S.D. (n=4). D) The impact of compound treatment on infectious virus particle production: Huh-7.5 cells were simultaneously infected with DENV2 (MOI: ~0.1) and treated with the indicated compound at a 10 μM final concentration. Seventy-two hours later, supernatants were collected and frozen, prior to analysis of infectivity via focus forming assays. Data are means ± SD (n=2).

A

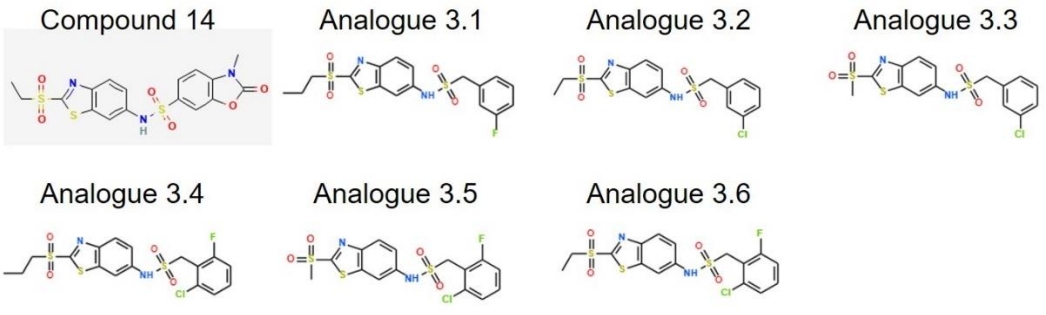
Compound 14
Analogue 3.1
Analogue 3.2
Analogue 3.3
Analogue 3.4
Analogue 3.5
Analogue 3.6

B

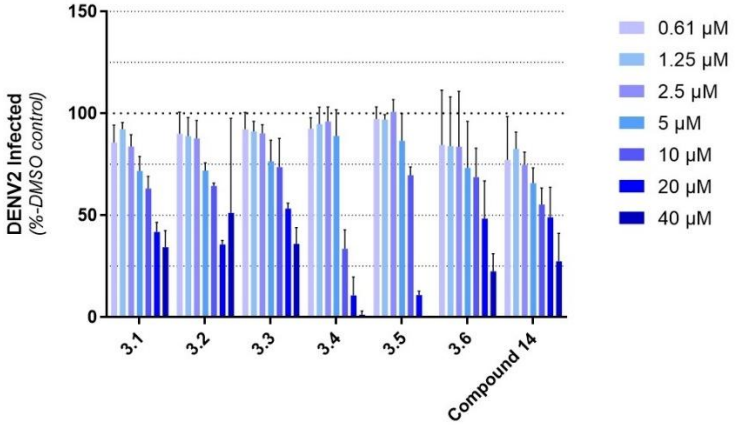
DENV2 Infected
(%-DMSO control)
150
100
50
0
0.61 µM
1.25 µM
2.5 µM
5 µM
10 µM
20 µM
40 µM
3.1
3.2
3.3
3.4
3.5
3.6
Compound 14

C

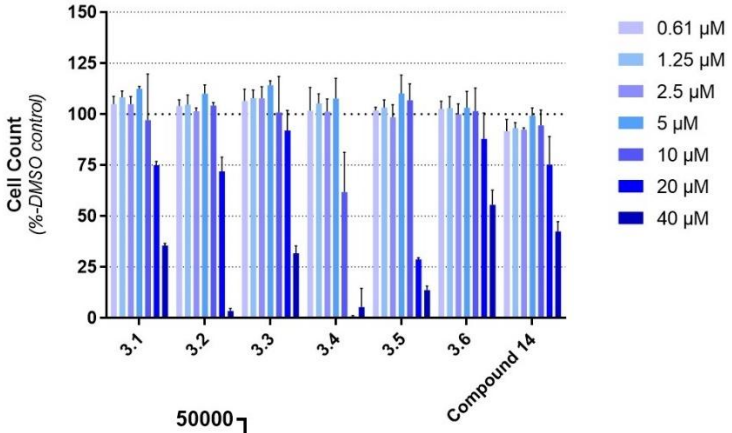
Cell Count
(%-DMSO control)
150
125
100
75
50
25
0
0.61 µM
1.25 µM
2.5 µM
5 µM
10 µM
20 µM
40 µM
3.1
3.2
3.3
3.4
3.5
3.6
Compound 14

D

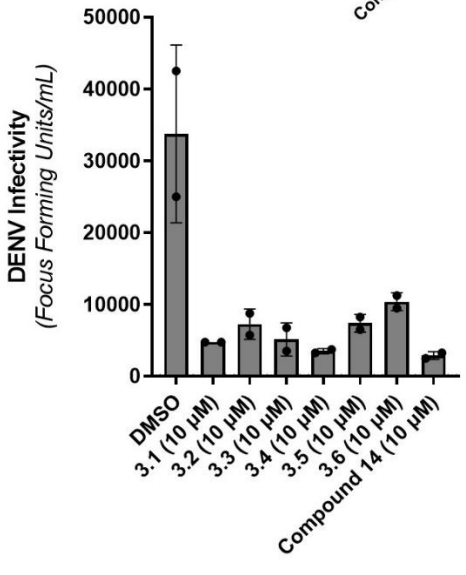
DENV Infectivity
(Focus Forming Units/mL)
50000
40000
30000
20000
10000
0
DMSO
3.1 (10 µM)
3.2 (10 µM)
3.3 (10 µM)
3.4 (10 µM)
3.5 (10 µM)
3.6 (10 µM)
Compound 14 (10 µM)

Figure 3.1.7 Dose-response analysis of the antiviral effects of structural analogues 3.1 – 3.6 via immunofluorescence assays, and analysis of the inhibition of infectious particle production. A) Compound structures. B/C) Immunofluorescence assays. Huh-7.5 cells were simultaneously infected with DENV2 (MOI: ~0.7) and treated with the indicated compounds at concentrations ranging from 0.5 to 40 μM then incubated for 42 hours. Cells were fixed, labelled by indirect immunofluorescence using anti-Capsid antibody and counterstained with DAPI. Cell counts and the percentage of cells infected were calculated via automated fluorescence microscopy. Data are means + S.D. (n=4). D) The impact of compound treatment on infectious virus particle production: Huh-7.5 cells were simultaneously infected with DENV2 (MOI: ~0.1) and treated with the indicated compound at a 10 μM final concentration. Seventy-two hours later, supernatants were collected and frozen, prior to analysis of infectivity via focus forming assays. Data are means ± SD (n=2).

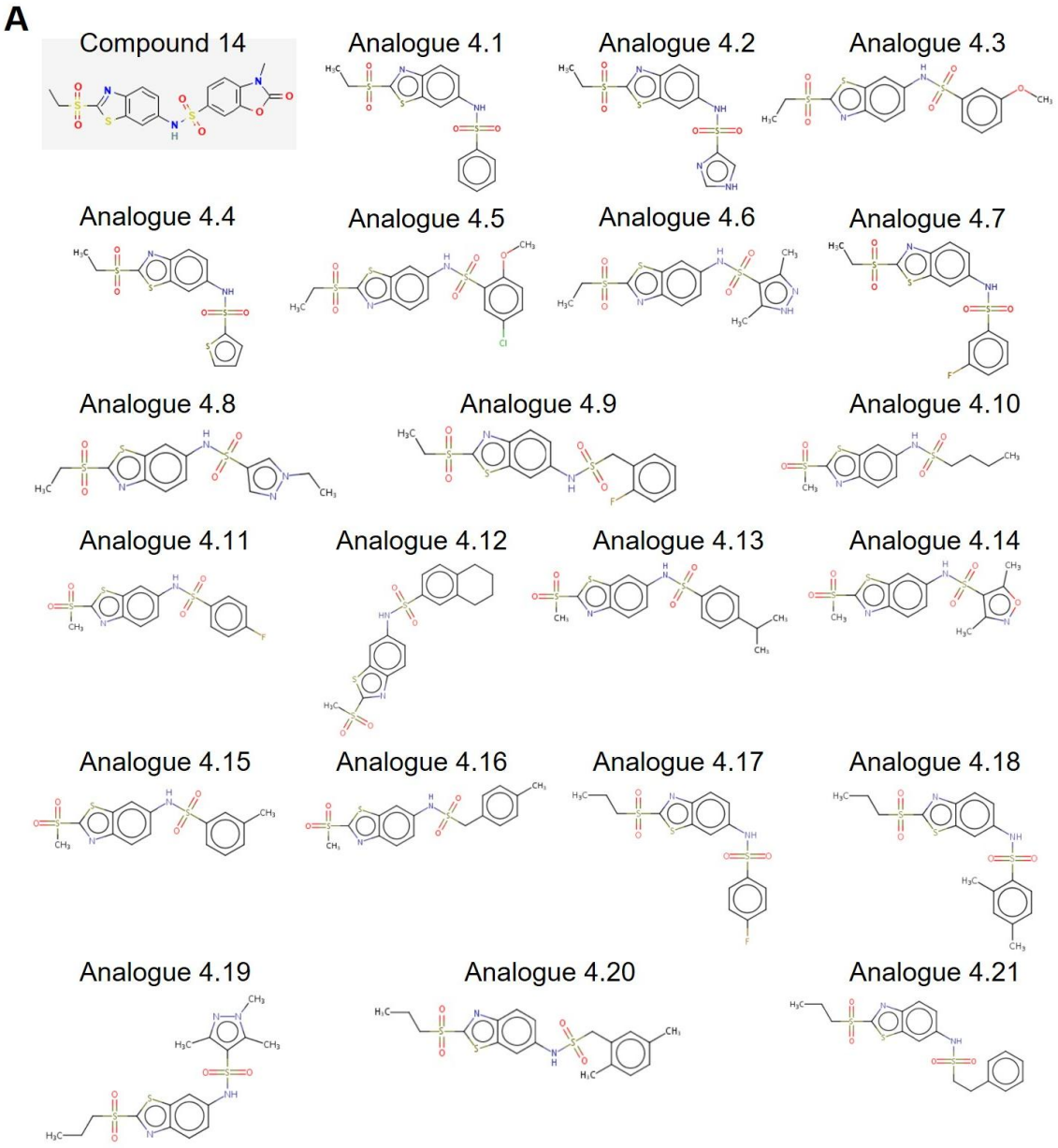
A
Compound 14
Analogue 4.1
Analogue 4.2
Analogue 4.3
Analogue 4.4
Analogue 4.5
Analogue 4.6
Analogue 4.7
Analogue 4.8
Analogue 4.9
Analogue 4.10
Analogue 4.11
Analogue 4.12
Analogue 4.13
Analogue 4.14
Analogue 4.15
Analogue 4.16
Analogue 4.17
Analogue 4.18
Analogue 4.19
Analogue 4.20
Analogue 4.21

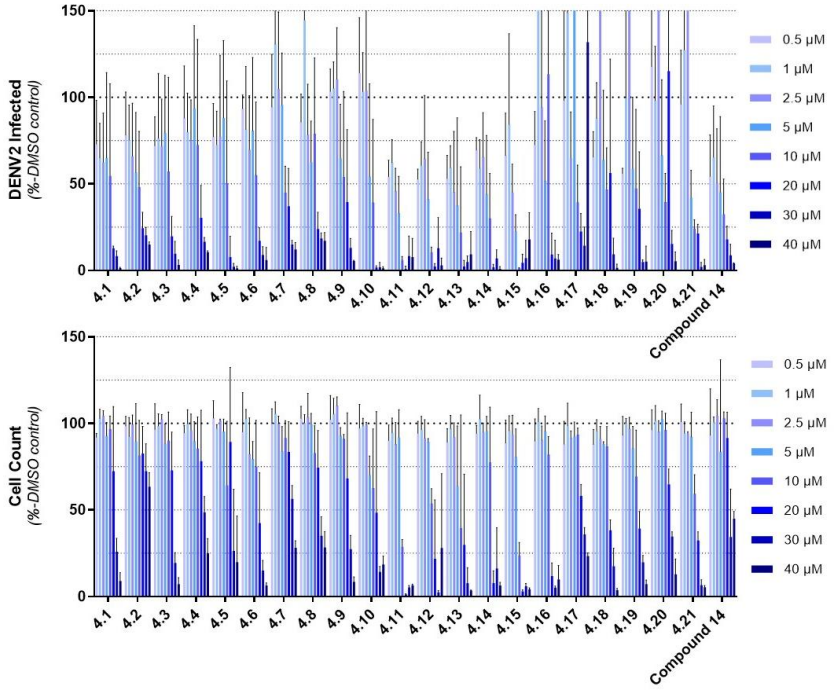
B
DENV2 Infected
(%-DMSO control)
150
100
50
0
0.5 µM
1 µM
2.5 µM
5 µM
10 µM
20 µM
30 µM
40 µM
4.1 4.2 4.3 4.4 4.5 4.6 4.7 4.8 4.9 4.10 4.11 4.12 4.13 4.14 4.15 4.16 4.17 4.18 4.19 4.20 4.21 Compound 14

C
Cell Count
(%-DMSO control)
150
100
50
0
0.5 µM
1 µM
2.5 µM
5 µM
10 µM
20 µM
30 µM
40 µM
4.1 4.2 4.3 4.4 4.5 4.6 4.7 4.8 4.9 4.10 4.11 4.12 4.13 4.14 4.15 4.16 4.17 4.18 4.19 4.20 4.21 Compound 14

Figure 3.1.8: Dose-response analysis of the antiviral effects of structural analogues 4.1 – 4.21 via immunofluorescence assays. A) Compound structures. B/C) Immunofluorescence assays. Huh-7.5 cells were simultaneously infected with DENV2 (MOI: ~0.7) and treated with the indicated compounds at concentrations ranging from 0.5 to 40 µM then incubated for 42 hours. Cells were fixed, labelled by indirect immunofluorescence using anti-Capsid antibody and counterstained with DAPI. Cell counts and the percentage of cells infected were calculated via automated fluorescence microscopy. Data are means + S.D. (n=4).

Due to the significant effect of Compound 14 on infectious virus particle production, we next sought to analyse the impact of the drug on the spread of DENV2 via live cell imaging using a derivative of a DENV2-NS1-mScarlet reporter virus (341), which has been adapted to improve its replicative fitness (Centofanti S, Johnson SM and Eyre NS, unpublished data). Huh-7.5 cells in 96-well imaging plates were infected with the adapted DENV2-NS1-mScarlet reporter virus (MOI: ~0.05) and treated with Compound 14 at concentrations ranging from 0.313 µM to 20 µM, as indicated. Automated imaging every 2 hours for 72 hours was performed, capturing mScarlet fluorescence to monitor DENV2 infection levels and phase contrast images to monitor cell viability and growth (Figure 3.1.9). Quantitative analysis of the mScarlet fluorescence revealed dose-dependent inhibition of viral spread, with an IC_{50} of 8.15 µM at 72 hours post-treatment.

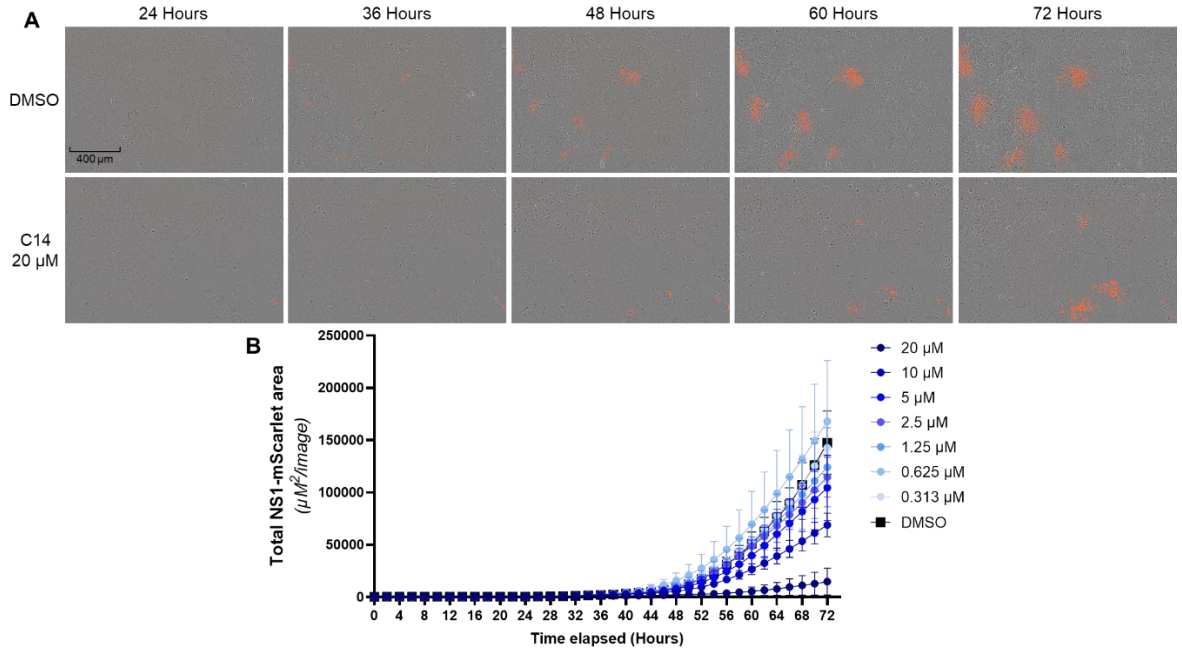

Figure 3.1.9: Dose-response analysis of the inhibition of viral spread by Compound 14. Huh-7.5 cells in a black-walled 96-well plate were treated with DMSO (0.8 % [v/v]) or Compound 14 at concentrations ranging from 0.313 µM to 20 µM and infected with DENV2-NS1-mScarlet (MOI: ~0.05). Cells were immediately imaged using an Incucyte® SX5 Live Cell Analysis System. A) Phase contrast and red fluorescence channel images were acquired every 2 hours for 72 hours. Each image is representative of 5 captured fields of view. Scale bar: 400 µm. B) Images from all wells and all timepoints were analysed for the total area containing red fluorescent signal as a proxy measurement for NS1-mScarlet translation. Data are means ± S.D., with values calculated from all 5 images per well.

To confirm the inhibition of DENV2 by Compound 14 in an orthogonal assay, we pre-treated Huh-7.5 cells for 20 hours with Compound 14 at concentrations ranging from 0.625 µM to 20 µM, then infected the cells with DENV2. Twenty-four hours later, the cells were lysed and analysed by Western Blot for levels of NS3. Quantification of NS3 showed a dose-dependent decrease in protein level, with NS3 protein levels reduced by approximately 80% in cells that were treated with Compound 14 at 20 µM (Figure 3.1.10 A/B). This 24 hour viral growth experiment is consistent with a direct impact of Compound 14 on the first replication lifecycle

of DENV2 in cells, potentially through decreased virus entry, translation or early replication events. Time of addition assays with 30 µM Compound 14 treatments revealed that in a 24 hour infection experiment, a 16 hour pre-treatment reduced the overall percentage of cells infected with DENV as determined by automated fluorescent imaging of anti-capsid antibody and DAPI, while no antiviral effect was observed when Huh-7.5 cells were coinfected/treated for 2 hours, before removal of both virus and drug. Delaying treatment from directly after infection to 2 hours after infection appeared to reduce effectiveness of the drug. While unclear, Figure 3.1.10 C appears to indicate that addition of Compound 14 after viral replication is established limits its antiviral effects. However, due to the weak antiviral efficacy observed by Compound 14 in shorter term experiments, it is difficult to draw conclusions on the precise lifecycle stage being inhibited.

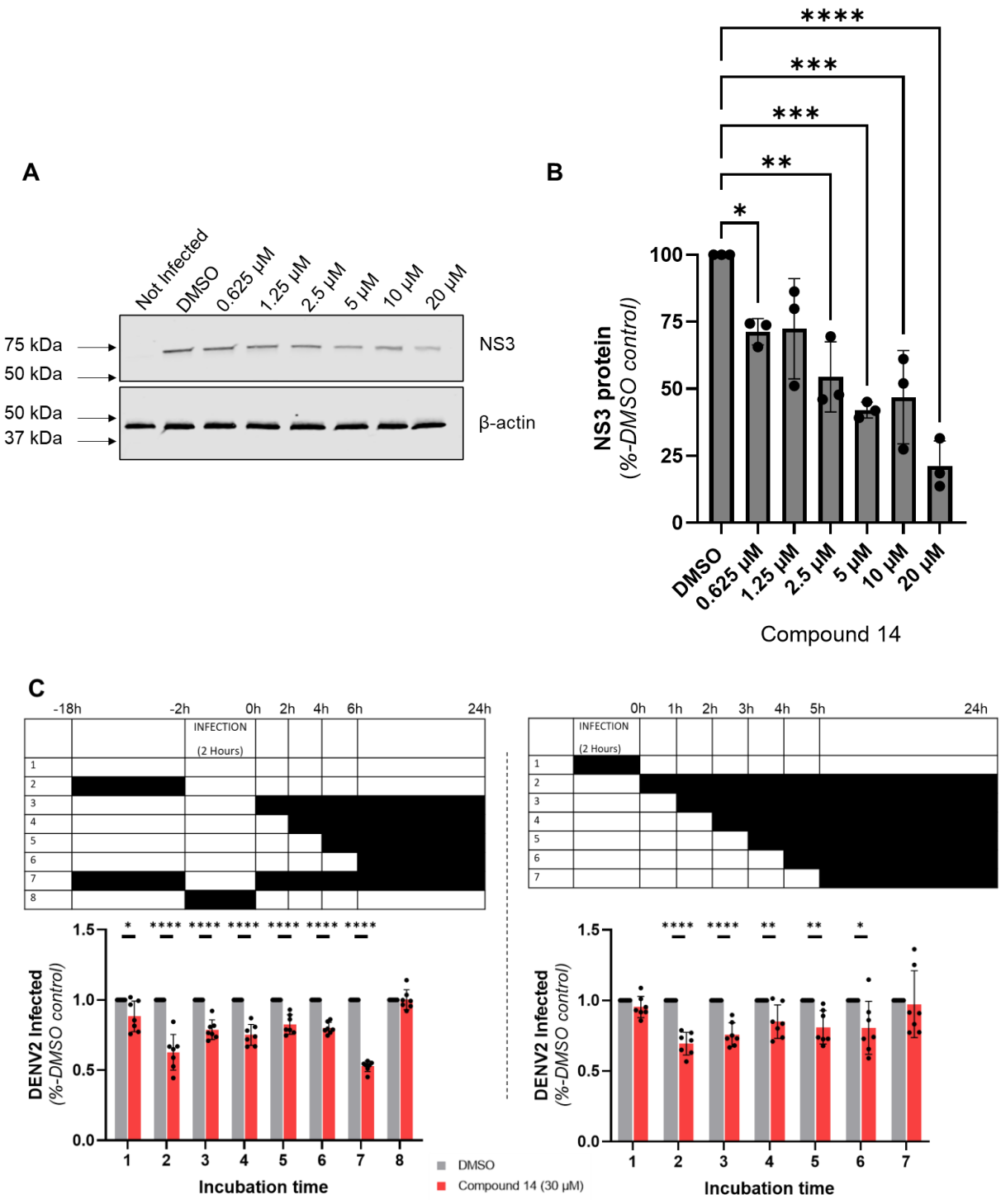

Figure 3.1.10: Dose-response analysis of the effects of Compound 14 on DENV2 NS3 protein levels and time-of-additional analysis of the antiviral effects of Compound 14. A) Huh-7.5 cells were seeded and treated with Compound 14 at the indicated concentrations for 20 hours, then infected with DENV2 (MOI: ~3.6), while maintaining Compound 14 treatment at the same indicated concentrations. After 24 hours, cells were lysed and samples were analysed via immunoblotting with the indicated antibodies B) Quantitative

analysis of NS3 protein levels, normalized to those of the loading control, β-actin. Data are means ± S.D. (n=3). *, P < 0.05; **, P < 0.01; ***, P < 0.001; ****, P < 0.0001 indicate statistically significant differences compared to DMSO treatment, by one-way ANOVA (multiple comparisons). C) Effect of the time of addition of Compound 14 on DENV2 infection levels. Huh-7.5 cells were infected with DENV (MOI: ~1.5) for 2 hours, before removal of the inoculum. Compound 14 was applied at the specified time points at a final concentration of 30 μM. At 24 hours post-infection, cells were fixed, labelled by indirect immunofluorescence using anti-Capsid antibody and counterstained with DAPI. Automated imaging and analysis was performed to determine cell counts and the percentage of cells that were infected. Data are means ± S.D. (n=7). *, P < 0.05; **, P < 0.01; ***, P < 0.001; ****, P < 0.0001 indicate statistical significance by student's t-test.

To explore the effect of Compound 14 on viral RNA replication, we utilised a DENV subgenomic replicon, which allows for the study of autonomous replication of viral RNA and expression of viral non-structural proteins in the absence of the structural proteins and infectious virus production. For these experiments, we utilized Vero cells that harbour autonomous replication of a GFP-tagged DENV2 subgenomic replicon(328). Cells were seeded into 96-well plates and treated with Compound 14 for 24, 48 and 72 hours at concentrations ranging from 0.313 μM to 20 μM. The NS3-NS4B inhibitor JNJ-A07 was used as a positive control for inhibition of viral RNA replication, at a concentration 45 times greater than the reported IC_{50}(213). At 24, 48 and 72 hours, the positive control showed a reduction in fluorescent signal, normalised to cell number, of 30%, 67% and 80% respectively. By comparison, Compound at 20 μM resulted in a decrease of 14%, 22% and 24% at the same respective time points (Figure 3.1.11). While each of these decreases were statistically significant, these modest antiviral effects are not consistent with inhibition of viral RNA replication and translation being the primary mechanism of action of Compound 14.

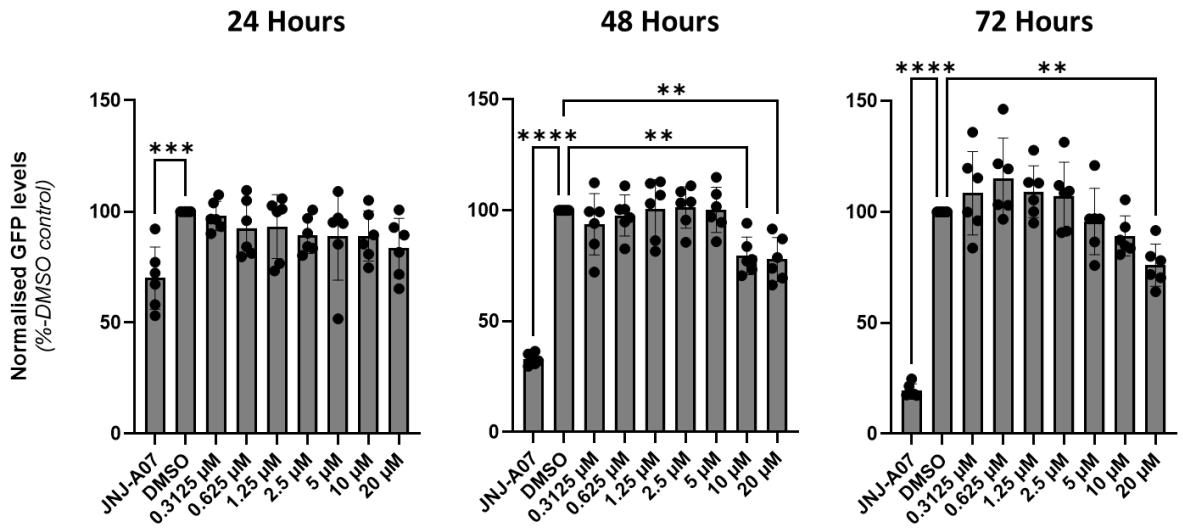

Figure 3.1.11: Temporal and dose-response analysis of Compound 14 on viral RNA replication. Vero cells that stably harbour autonomous replication of a DENV2 subgenomic replicon encoding a GFP reporter were treated with JNJ-A07 at 35 nM or Compound 14 at the specified concentrations for 24, 48 or 72 hours. At the end of each incubation, whole well green fluorescence levels was measured, then cells were fixed and counterstained with DAPI. Whole well blue fluorescence was used as an indirect measurement of cell count/confluency, allowing normalisation of viral RNA replication (GFP signal) to cell count (DAPI signal). Results are representative of two identical plates, prepared at the same time. Data are means ± S.D. (n = 6). *, $P < 0.05$; **, $P < 0.01$; ***, $P < 0.001$; ****, $P < 0.0001$ indicate statistically significant differences compared to DMSO treatment, by one-way ANOVA (multiple comparisons).

To investigate the effects of Compound 14 on the localisation of viral proteins, Huh-7.5 cells were seeded in glass chamber slides, infected with DENV2-NS1-mScarlet (MOI: ~0.3) and treated with Compound 14 at 20 µM, or DMSO carrier alone. At 48 hours post-infection, cells were fixed and labelled by indirect immunofluorescence using an anti-NS4B antibody in combination with either anti-E or anti-Capsid antibodies for analysis via confocal microscopy. No clear differences were seen in the expression and localisation patterns of NS4B, capsid or NS1-mScarlet when comparing the effects of Compound 14 treatment to those of the DMSO carrier control (Figure 3.1.12 A). Unexpectedly, however, analysis of cells stained for E and NS4B revealed a large proportion of cells expressing both NS1-mScarlet and NS4B, but lacking detectable expression of E protein (Figure 3.1.12 B). Colocalisation analysis of large numbers of infected cells revealed a significant decrease in colocalisation of NS1-mScarlet and E protein

in response to the Compound 14 treatment (Figure 3.1.12 C). Of note, these experiments involved the use of a conformation-specific anti-E monoclonal antibody, '4G2', that recognizes the fusion loop of domain II (EDII)(346). Accordingly, it is possible that impaired folding and/or maturation of E protein, rather than loss of E protein expression, in Compound 14 treated cells may explain these observations.

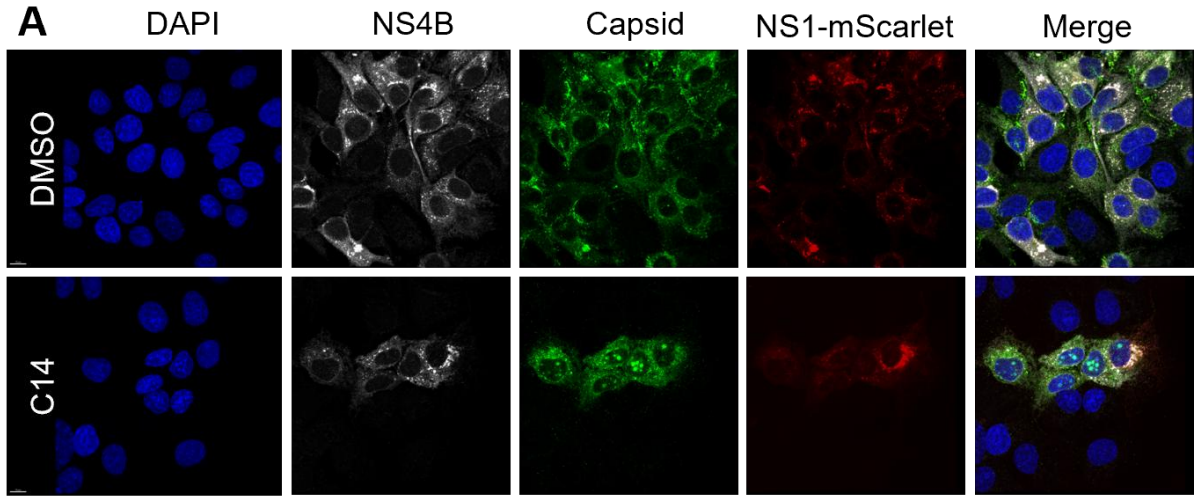
A
DAPI
NS4B
Capsid
NS1-mScarlet
Merge
DMSO
C14

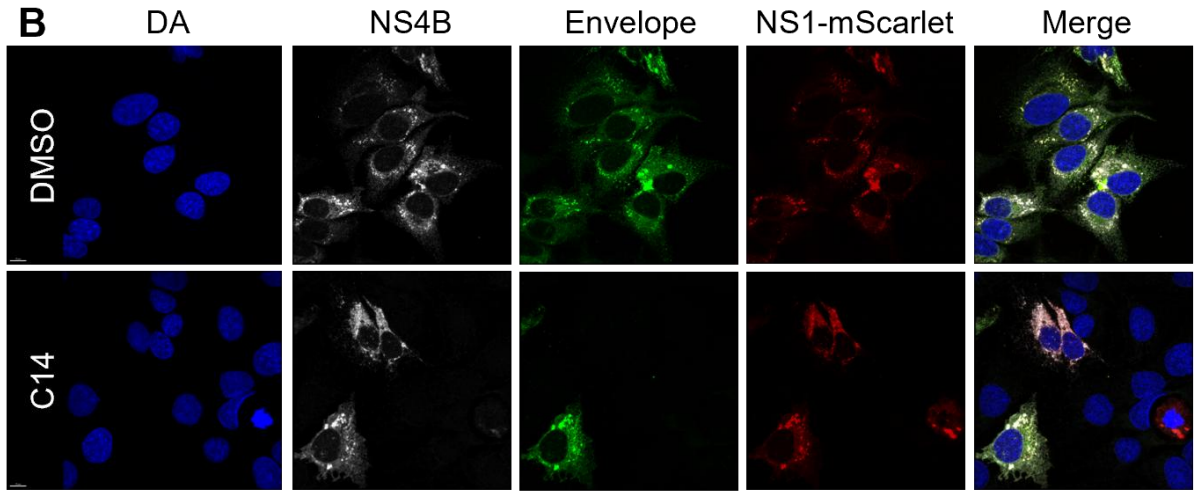
B
DA
NS4B
Envelope
NS1-mScarlet
Merge
DMSO
C14

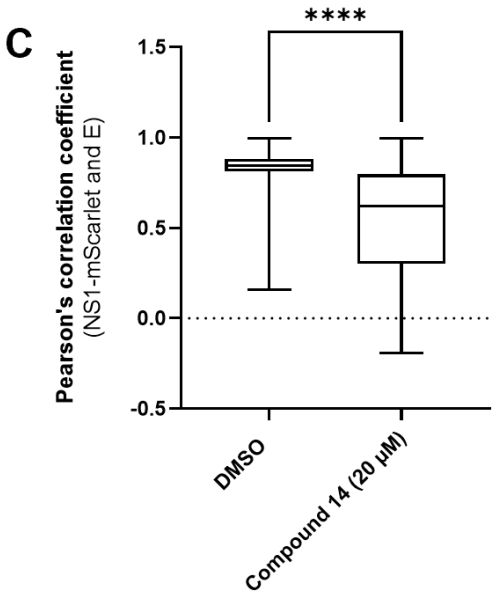
C
****
Pearson's correlation coefficient
(NS1-mScarlet and E)
1.5
1.0
0.5
0.0
-0.5
DMSO
Compound 14 (20 µM)

Figure 3.1.12: The effect of Compound 14 on the colocalisation of viral proteins. Huh-7.5 cells were infected with DENV2-NS1-mScarlet (MOI: ~0.3) and treated with Compound 14 or DMSO carrier alone, then incubated for 48 hours. Cells were fixed, labelled by indirect immunofluorescence using anti-NS4B antibody in combination with anti-Capsid (A) or anti-Envelope (B) antibodies and counterstained with DAPI, then imaged via confocal microscopy. Scale bar, 10 μm. C) Quantitative analysis of NS1-mScarlet and E protein colocalization. Pearson's correlation coefficients were determined for individual NS1-positive cells treated with DMSO (0.1% [v/v]) carrier alone (n = 65 cells) or Compound 14 (20 μM) (n= 119 cells). Box and whisker plots display the 25-75% distribution (boxes) and minimum and maximum values (whiskers), while central bars depict median values. *, $P < 0.05$; **, $P < 0.01$; ***, $P < 0.001$; ****, $P < 0.0001$ indicate statistical significance by student's t-test.

To further quantify the reduced levels of mature, detectable E protein in DENV2-infected cells that have been treated with Compound 14, Huh-7.5 cells were simultaneously infected with DENV2-NS1-mScarlet and treated with a range of concentrations of Compound 14. Forty-eight hours later, cells were fixed and labelled by indirect immunofluorescence with anti-E (4G2) primary antibody and DAPI. Using automated imaging and fluorescence intensity thresholds set for uninfected cells, cells positive for NS1 alone, or NS1 *and* mature E, were counted. To calculate the portion of infected cells with both NS1 and detectable E, the following calculation was performed (Equation 3.1.1):

$$\frac{Cells\ with\ both\ NS1\ AND\ mature\ E}{Cells\ with\ NS1}$$

This analysis revealed that Compound 14 treatment induces a dose-dependent decrease in the proportion of NS1-positive cells that also displayed detectable expression of mature E protein (Figure 3.1.13). Representative images from this experiment are shown in Figure 3.1.14. We hypothesise that this effect may be a result of Compound 14-mediated inhibition of E protein maturation, thereby affecting epitope accessibility to mAb 4G2. Interestingly, similar inhibition of E protein recognition by 4G2 has also been observed in response to knockout of the ER resident dolichol-phosphate mannose synthase (DPMS) complex, which is

required for synthesis of dolichol-phosphate mannose (DPM) which serves *N*-glycosylation, glycosylphosphatidylinositol (GPI) anchor biosynthesis and C- or O-glycosylation of protein in the lumen of the ER (347). It is possible that Compound 14 also affects this pathway to cause E protein misfolding.

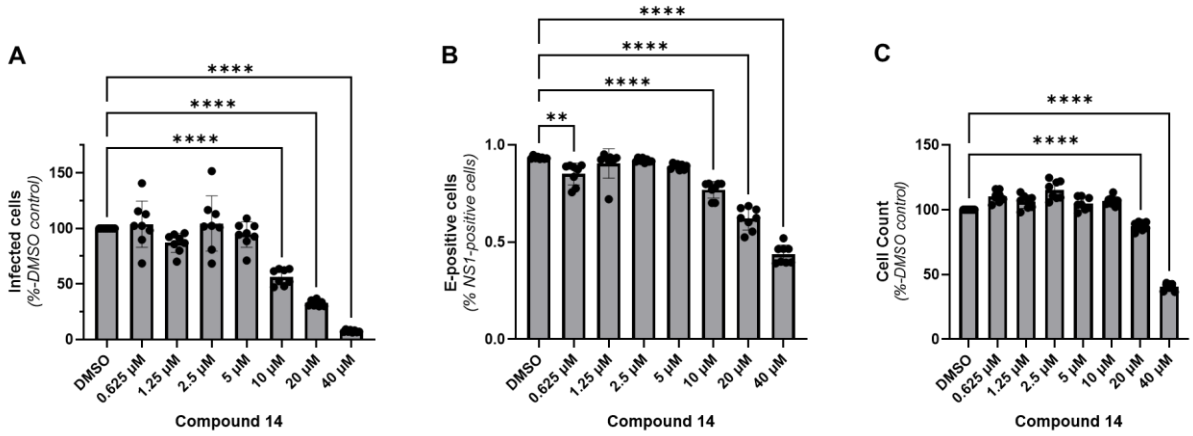

Figure 3.1.13: Dose-response analysis of the impact of Compound 14 treatment on mature E protein detection in NS1-mScarlet-positive infected cells. Huh-7.5 cells were simultaneously infected with DENV2-NS1-mScarlet (MOI: ~0.3) and treated with DMSO carrier alone or Compound 14 at the indicated concentrations. After 48 hours, cells were fixed, labelled by indirect immunofluorescence using anti-E antibody (4G2) and counterstained with DAPI. Automated fluorescent imaging was used to capture whole well images, then identify DAPI-labelled cells which express the relevant viral proteins above a specified fluorescence threshold. A) Quantification of infected cells, as determined by NS1-mScarlet detection, presented as a percentage of those of cells treated with the DMSO carrier alone. B) The portion of NS1-mScarlet-positive cells in which E protein was detected. C) Cell counts as a percentage of the DMSO carrier control. Data are means ± S.D. (n = 6). *, $P < 0.05$; **, $P < 0.01$; ***, $P < 0.001$; ****, $P < 0.0001$ indicate statistically significant differences compared to DMSO treatment, by one-way ANOVA (multiple comparisons). Statistically significant differences not displayed in Figure C for increased cell counts.

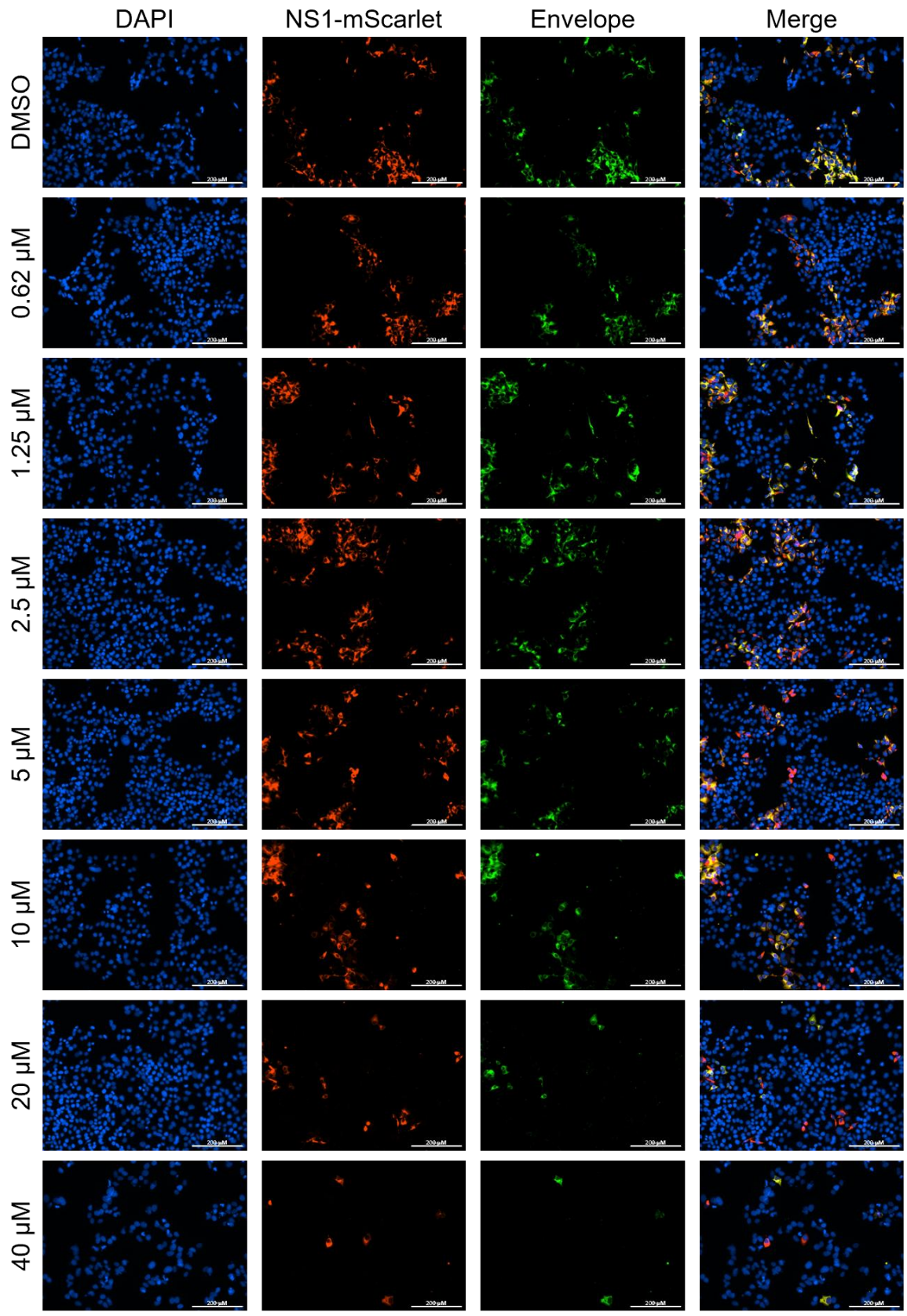

Figure 3.1.14: Representative images from the dose-response analysis of E- and NS1-mScarlet-expressing cells from Figure 3.1.13. Scale bar, 200 µM.

To probe for conformations of E protein which may not be visualised by the conformation-specific monoclonal antibody (4G2), further immunolabelling experiments were performed using a polyclonal anti-E antibody that is expected to recognise both immature and mature forms of E protein. Huh-7.5 cells were simultaneously infected with wild-type DENV2 (MOI: ~0.1) and treated with Compound 14 (20 μM) or DMSO carrier alone. After 48 hours, cells were fixed and labelled by indirect immunofluorescence with both the monoclonal anti-E antibody and the polyclonal anti-E antibody, as well as an endoplasmic reticulum dye and a DNA stain. Confocal analysis revealed distinct subpopulations of infected cells, presumably with mature E protein visualised by both the monoclonal and polyclonal anti-E antibodies, and immature E protein visualised by only the polyclonal anti-E antibody (Figure 3.1.15 A). Infected cells with immature E protein were readily detected in both treatment groups, although the proportion of these cells compared to cells expressing mature E protein appeared higher in Compound 14-treated cells. Additionally, we frequently observed Compound 14-treated cells displaying reticular web-like localisation patterns of both immature E protein and the endoplasmic reticulum, which was not observed in DMSO vehicle-treated control cells (Figure 3.1.15 B).

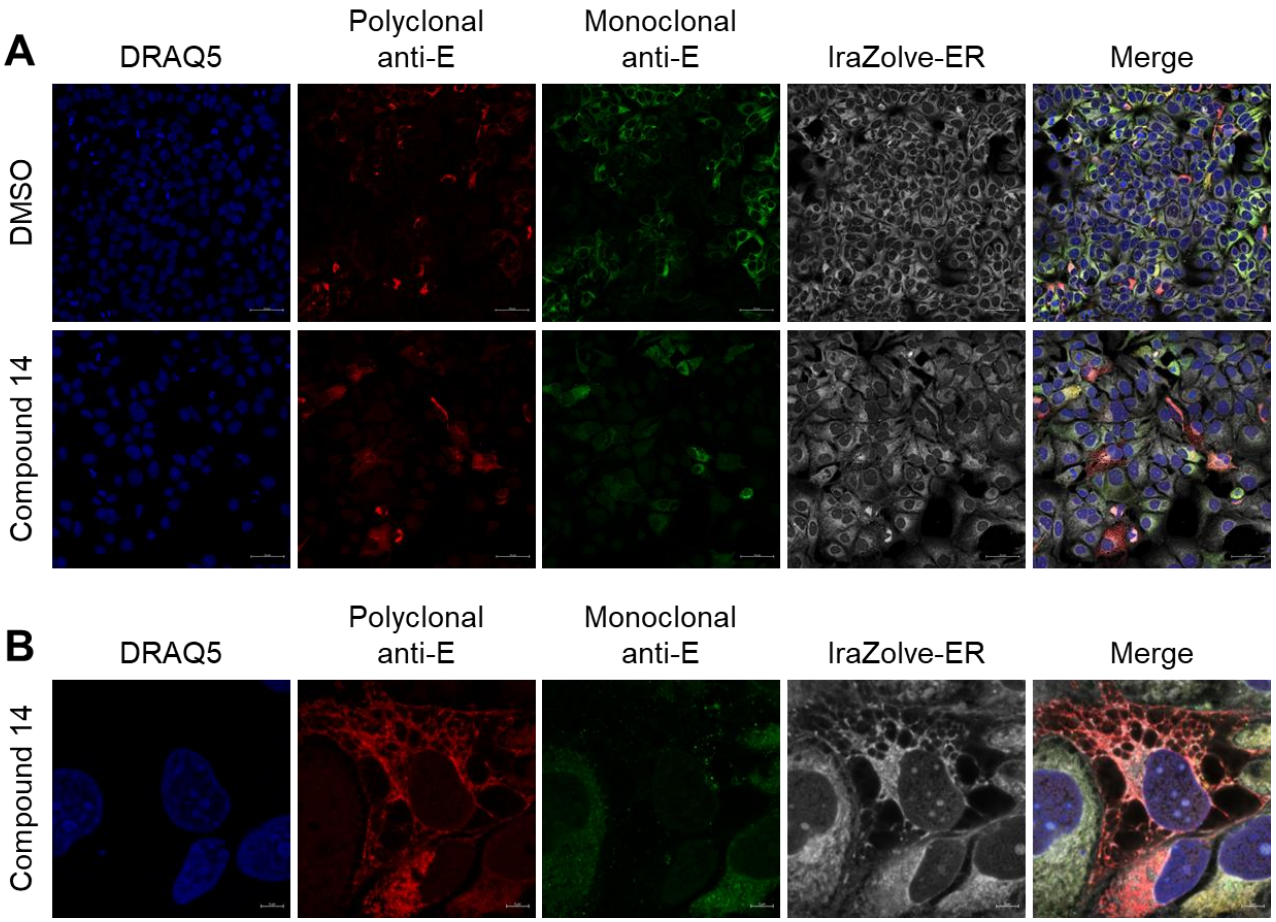

Figure 3.1.15: The effect of Compound 14 on the E protein localization and maturation and endoplasmic reticulum morphology during DENV infection. Huh-7.5 cells were seeded in a glass coverslip bottom chamber slide and simultaneously infected with DENV2 (MOI: ~0.1) and treated with DMSO carrier alone or Compound 14 (20 µM) and incubated for 48 hours. Cells were fixed and stained with the specified antibodies and dyes, then visualised via confocal microscopy. A) 3x3 tile scan (mosaic) images. Scale, 50 µm. B) Zoom image. Scale bar, 5 µm.

To further confirm that the maturation of E protein is altered by Compound 14 treatment, Huh-7.5 cells in a 96-well imaging plate were infected with DENV2 (MOI: ~0.1) and treated with DMSO carrier alone or Compound 14 at concentrations of 5 µM, 10 µM and 20 µM for 48 hours prior to fixation and labelling with the polyclonal and monoclonal anti-E antibodies. Automated imaging and analysis was then used to enumerate immature E and mature E protein expression profiles in infected cells, as determined by co-labelling with the polyclonal and monoclonal anti-E antibodies described above. This revealed a dose-dependent decrease

in the proportion of cells with mature E protein with increasing concentrations of Compound 14 (Figure 3.1.16 D).

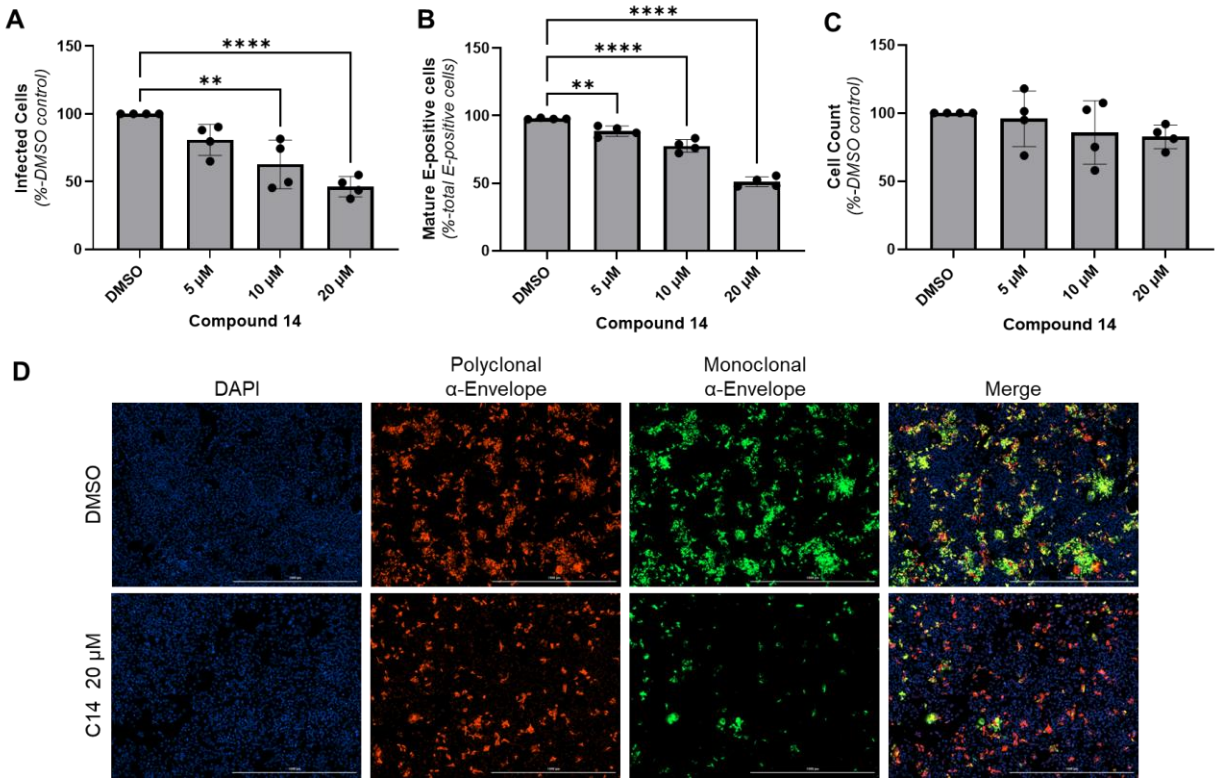

Figure 3.1.16: Dose-response analysis of the impact of Compound 14 on E protein maturation. Huh-7.5 cells were infected with DENV2 (MOI: ~0.1) and treated with DMSO carrier alone or Compound 14 at the indicated concentration. After 48 hours, cells were fixed, labelled with the specified antibodies and counterstained with DAPI. Automated fluorescence imaging and analysis was used to quantify cells above a specified fluorescent threshold for each marker. A) Infected cells as determined by detection with the polyclonal anti-E antibody, presented as a percentage of the DMSO carrier control. B) Infected cells with mature E protein detected by the monoclonal anti-Envelope antibody (4G2), presented as a percentage of the total infect cell population as determined by labelling with the polyclonal anti-E antibody. C) Cell count as a percentage of the DMSO control. Data are means ± SD (n = 4). D) Representative immunofluorescent images of samples of contributing towards graphs A-C are depicted. Scale bars, 1000 µm. *, $P < 0.05$; **, $P < 0.01$; ***, $P < 0.001$; ****, $P < 0.0001$ indicate statistically significant differences compared to DMSO treatment, by one-way ANOVA (multiple comparisons).

3.2 High-throughput compound screening using the NanoBiT® Protein:Protein interaction assay

As another approach to identify inhibitors of essential NS1 properties, we developed an assay to identify inhibitors of NS1 dimerisation using the NanoBiT® Protein:Protein interaction system. Dimerisation of NS1 is indispensable for infectious particle production and viral RNA replication and plays a key role in the pathogenesis of DENV infections (348). The NanoBiT® assay utilises two subunits, SmBiT and LgBiT, which structurally complement to form the bright NanoBiT® enzyme (Figure 3.2.1)(338). Due to the weak binding affinity between these subunits, structural complementation occurs only when these subunits are in close proximity. These subunits were cloned as C-terminal fusions to NS1 in mammalian expression vectors such that the co-expression and dimerisation of NS1 drives the complementation of SmBiT and LgBiT. This system therefore allows for the measurement of NS1 dimerisation with a luminescence readout.

Using this NS1-based dimerisation assay, 3,378 drug-like compounds, from the same scaffold-based library used in the high-throughput NaLTSA screen, were screened to identify compounds which decrease NS1 dimerisation-mediated luminescence in transfected HeLa cells. To control for compounds that alter NanoBiT activity, rather than NS1 dimerisation, these compounds were also screened in parallel for inhibition of an unrelated positive control NanoBiT pair; SmBiT-PRKACA and LgBiT-PRKAR2A. From these screens, three hits were identified (PubChem CIDs: 17494878, 72114204, 53504017) as potential inhibitors of NS1 dimerisation, that displayed minimal cytotoxic effects and minimal effects on the NanoBiT® control dimerisation pair. However, in subsequent validation experiments using these compounds we were unable to confirm inhibition of NS1 dimerisation using the NanoBiT assay. Furthermore, analysis of DENV infection levels following treatment with these compounds at a range of concentrations for 48 hours revealed no significant antiviral effects in the absence of cytotoxic effects.

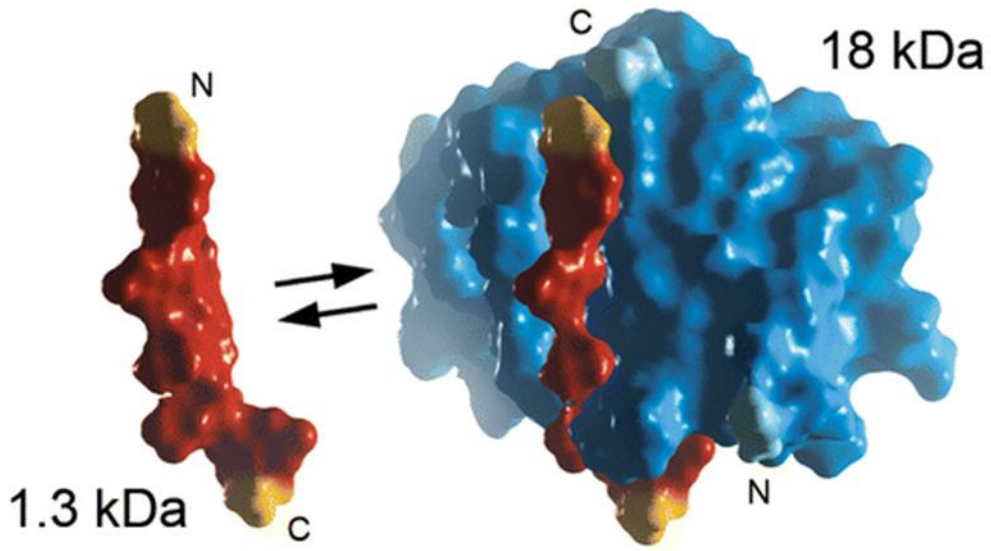

Figure 3.2.1: Structural complementation of SmBiT (yellow and red) and LgBiT (blue), resulting in the formation of the highly luminescent NanoBiT® enzyme. Available at (349).

3.2.1 Results

To identify inhibitors of NS1 dimerisation, we developed NS1 constructs for use with the NanoBiT® Protein:Protein interaction system. To allow for high-throughput screening, lentiviral expression constructs were selected for insertion of the NS1 constructs, as they enable the efficient generation of stable cell lines. Using NEBuilder DNA Assembly, NS1 was fused to SmBiT or LgBiT with a Gly-Ser-Gly oligopeptide linker between them. To allow for proper processing of NS1, the sequence encoding an N-terminal signal peptide of 24 amino acids (72 nucleotides) originating from the 24 amino acids at the C-terminus of Envelope directly upstream of NS1 in the DENV2 polyprotein was included in the DNA fragment(350). The NS1-SmBiT fragment was inserted into a pLenti6/V5-D-TOPO vector harbouring a blasticidin resistance gene, and the NS1-LgBiT fragment was inserted into a pLenti MS2-P65-HSF1 vector harbouring a hygromycin B resistance gene. These vectors contain genetic elements required for expression of the gene of interest, and when transfected into cells with lentiviral packaging plasmids psPAX2 and pMD2.G, an RNA copy of the expression construct is packaged into recombinant pseudoviral particles. These particles allow efficient transduction and integration of the construct into genomic DNA(351).

To validate the dimerisation of these constructs, HEK293FT cells were seeded in white-walled 96 well plates and co-transfected with the NS1-SmBiT and NS1-LgBiT expression vectors or appropriate empty (negative control) plasmid combinations. At 48 hours post-transfection, luminescence was measured in live cells (Figure 3.2.2). When expressed alone, the NS1-LgBiT construct gave rise to ~100x greater luminescence levels compared to cells transfected with empty vector and NS1-SmBiT controls, indicating that expression of the LgBiT subunit alone results in significant background noise. However, co-transfection of NS1-SmBiT and NS1-LgBiT constructs resulted in ~500x greater luminescence compared to NS1-LgBiT alone. This high signal:background ratio demonstrated the suitability of this dimerisation assay for use in high-throughput compound screens.

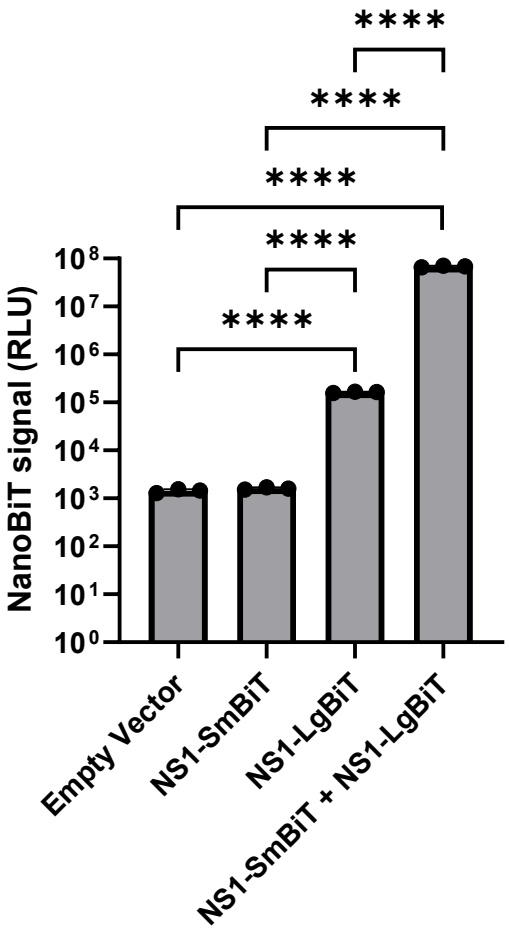

Figure 3.2.2: Validation of the NanoBiT® Protein:Protein complementation assay with NS1-SmBiT and NS1-LgBiT expression constructs. HEK293FT cells were co-transfected with the indicated plasmids and cultured for 48 hours. Cells were washed once with PBS, then lysed and incubated with appropriately diluted NanoLuc substrate. After a 5 minute incubation, luminescence was recorded for each well. The statistical significance of differences between groups was calculated using an unpaired Student's t-tests. Date are means ± S.D. (n = 3).

To identify inhibitors of NS1 dimerisation, a high-throughput drug screen was performed in collaboration with Dr Amanda Aloia and Dr Gustavo Bracho from Cell Screen SA at Flinders University. Factors to be considered and optimised before the initial screen included transfection timing, transfection conditions, cell seeding density in 384-well plates, and multiplexing of the NanoBiT® Protein:Protein interaction assay with a fluorescence-based cell viability assay. The workflow of the screen included a large-scale transfection of HeLa cells, selected for their high transfectability, plating of transfected cells into 384-well plates

containing compounds present at a final concentration of 10 µM, and measurement of luminescence and fluorescence.

To test compound toxicity, the CellTiter-Blue® cell viability assay was used. This assay allows an indirect measurement of the number of viable cells in a well. An indicator dye, resazurin, is reduced to the highly fluorescent resorufin by cells with metabolic capacity. Nonviable cells lack the capacity to reduce resazurin, and therefore do not produce a fluorescent signal(352). By multiplexing the NanoBiT® Protein:Protein interaction assay with the CellTiter-Blue® cell viability assay, luminescent signal, indicative of NS1 dimerisation, can be normalised to cell viability within the same well. Toxic compounds which indirectly reduce total NS1 dimerisation can be identified by a proportional decrease in viability-associated fluorescence. This assay was included in the final compound screen only.

To summarise the optimised conditions, luciferase readings were found to be highest at 48 hours post-transfection with a plating cell density (in 384-well plates) of 1700 cells/well. For optimal signal:background ratio, transfections were performed using semi-confluent HeLa cells in 6-well plates using a Lipofectamine 2000 (µL):DNA (µg) ratio of 3:1. The screen was performed by transfecting HeLa cells with the NS1 constructs or control constructs, allowing a 24 hour incubation, then plating the cells into plates containing pre-dispensed compounds for an additional 24 hour treatment. See Section 2.24 for the complete protocol.

Similar to the NaLTSA high-throughput screen (Section 3.1), the screen was performed using a library of 3,378 drug-like compounds, with 3 representative individual compounds from each of the 1,126 drug-like scaffolds of the Compounds Australia Open Scaffolds library. Compounds found to reduce luminescence by >40% while not causing significant cellular toxicity were to be designated as ‘hits’ for follow up. This was performed two times independently, with n=1 per compound per experiment. Unfortunately, between these two experiments there were large variations, likely due to differences in the efficiency of transfection between the repeat screens, as well as liquid handling errors when using the automated Janus® liquid handler. The first independent screen identified a modest number of hits, while the second independent screen identified far greater effects from a higher number of compounds (Figure 3.2.3). The correlation between replicates for Nanoluciferase activity normalised to the untreated DMSO control was $R^2 = 0.344$, indicating low correlation.

Together, 15 of the 1,126 scaffolds tested were identified as containing ≥2 hits in both screens. We hypothesised that hits from scaffolds that showed consistent activity across each screen would have a higher likelihood of being true hits compared to scaffolds with only a single hit. For these scaffolds, all ~30 compounds were featured in the follow up screen, totalling 450 compounds. In addition to the NS1-SmBiT and NS1-LgBiT transfections, the control dimerisation pair, SmBiT-PRKACA and LgBiT-PRKAR2A, were transfected to test for inhibition of general luminescence, or inhibition of SmBiT/LgBiT structural complementation. For the final screen, each compound was tested in triplicate for both inhibition of NS1 dimerisation and dimerisation of the control pair. The protocol was unchanged, except to account for a changed number of wells.

Unfortunately, none of the hits identified in the two primary screens showed statistically significant inhibition of NS1 dimerisation in the validation screen. As the validation screen had a higher number of technical replicates for each compound (n=3), compared to the two initial screens (n=1, repeated), it was decided to overlook the results of the initial screens in favour of potential hits from the validation screen. For identification of novel hits from this screen, two criteria were set: an average >75.45% reduction in NanoBiT® activity for NS1 transfected cells and a <81.97% reduction in NanoBiT® activity for control plasmid transfected cells, compared to DMSO (carrier)-treated controls. From this, three hits were identified, as displayed in Figure 3.2.3 as green data points, Figure 3.2.4 and Table 3.2.1.

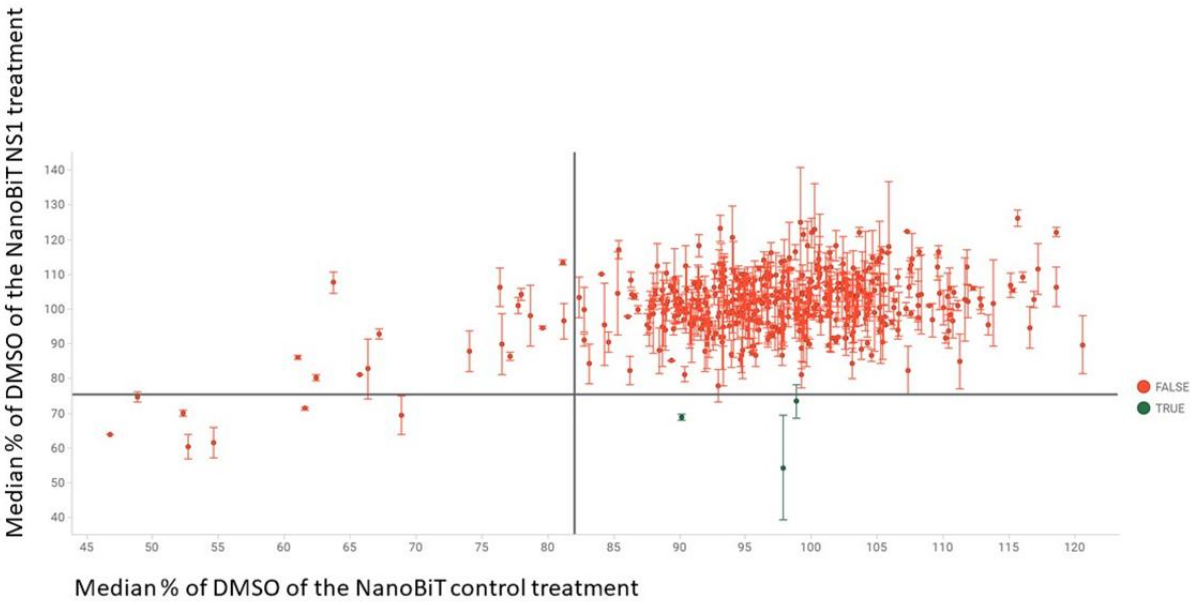

Figure 3.2.3: Results from the high-throughput validation screen for inhibitors of NS1 dimerisation. HeLa cells in a 6-well plate were transfected with NS1-SmBiT and NS1-LgBiT, or with the control SmBiT-PRKACA and LgBiT-PRKAR2A constructs, or with empty vector and single construct controls. After three hours, transfection reagents were removed and replaced with fresh cell culture media. At 24 hours post-transfection, the cells were trypsinised and plated into 384-well plates containing DMSO or one of 450 compounds dissolved in DMSO, to achieve a final concentration of 10 µM. After 24 hours, Nanoluciferase substrate was added and luminescence was recorded. Criteria for a 'hit' were a >25.55% reduction in NS1 dimerisation-associated luminescence, and a <18.03% reduction in control NanoBiT partner (PRKACA/PRKAR2A) dimerisation-associated luminescence. Hits are highlighted green. N=3. Error bars represent ± S.D.

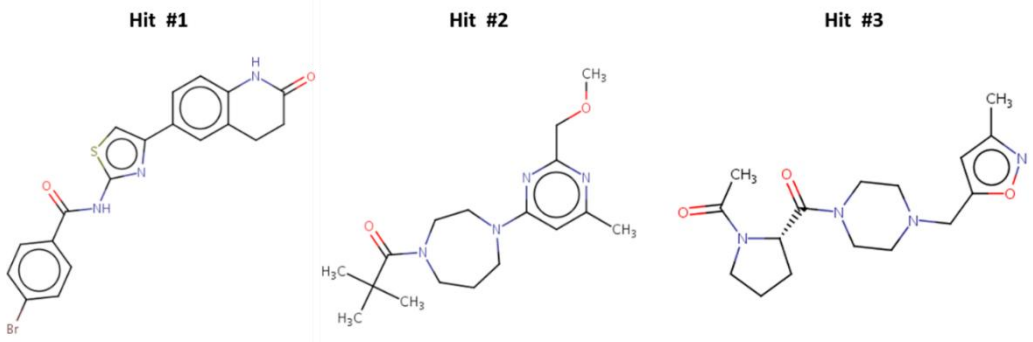

Figure 3.2.4: Three compounds from the final NanoBiT® Protein:Protein interaction system high-throughput compound screen, identified as potential inhibitors of NS1 dimerisation.

Table 3.2.1: Potential inhibitors of NS1 dimerisation identified via high-throughput compound screening.

Compound ID	NS1 % inhibition compared to DMSO	Control % inhibition compared to DMSO	CTB fluorescence % compared to DMSO
SN00776953 CAS#: 949301-66-0	73.16	91.55	85.53
SN00782421 CAS#: 1384654-43-6	55.6	100.88	91.17
SN00782557 CAS#: 1281193-48-3	59.59	101.33	91.02

The three hits were tested for antiviral activity. Huh-7.5 cells were seeded into 96-well plates, cultured overnight then infected with DENV2 (MOI: ~1) and treated with each compound at concentrations ranging from 0.31 µM to 20 µM. After 48 hours, the cells were fixed and labelled by indirect immunofluorescence using an anti-Capsid antibody and counterstained with DAPI. The percentage of cells infected with DENV2 was calculated using automated imaging and analysis software, whereby a threshold of fluorescence intensity in an area surrounding each DAPI-identified nucleus was utilised to differentiate between infected and non-infected cells. Using a similar methodology, the DAPI-based cell count was used for a measurement of cytotoxicity. Hits #2 and #3 did not appear to have antiviral activity or cytotoxicity. Hit #1 showed strong antiviral activity, with an IC_{50} of 6.69 µM. However, a high CC_{50} of 15.7 µM indicated that this antiviral activity may be linked to cytotoxicity (Figure 3.2.5).

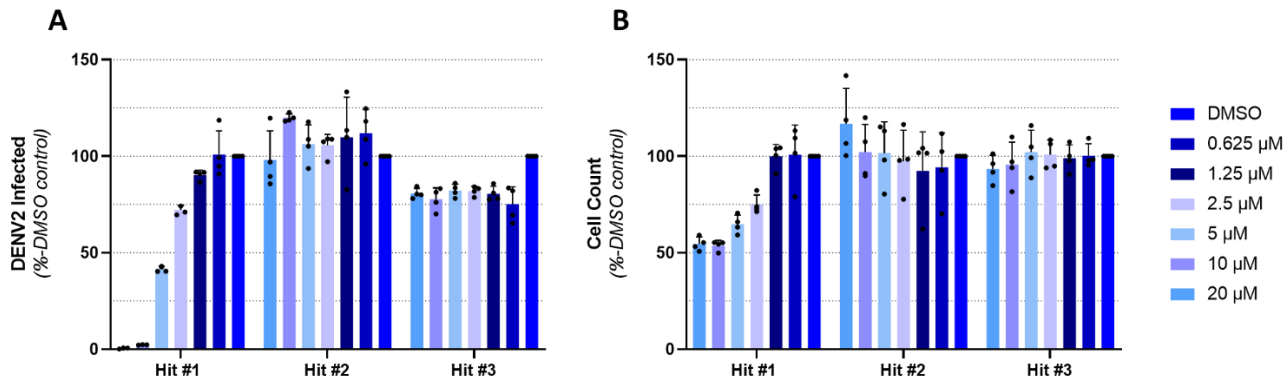

Figure 3.2.5: Dose-response analysis of the antiviral and cytotoxic effects of the top 3 hits from the high-throughput NS1 dimerisation inhibitor screen. Huh-7.5 cells in a 96-well plate were infected with DENV2 (MOI: ~1) and treated with each compound at of the indicated concentrations for 48 hours, then fixed, labelled by indirect immunofluorescence using an anti-Capsid antibody and counterstained with DAPI. The percentage of cells infected with DENV (A) and the cell count (B) were calculated via automated fluorescence microscopy. Data are means ± S.D. (n = 4).

To confirm the inhibition of NS1-dimerisation by each of the three hits from the high-throughput drug screen, we repeated the NanoBiT® dimerisation assay. Huh-7.5 cells were transfected in a 6-well tray with either NS1-SmBiT and NS1-LgBiT, or the SmBiT and LgBiT dimerisation controls, then returned to culture for 24 hours before plating into a 96-well tray with compounds at a final concentration of 20 µM and incubation for an additional 24 hours. These studies indicated hits #2 and #3 have no significant impact on NS1-dimerisation or dimerization of the SmBiT and LgBiT dimerization positive control pair (PRKACA/PRKAR2A). While Hit #1 decreased NS1 dimerization-associated luminescence, it also reduced luminescence associated with PRKACA-PRKAR2A dimerization to similar levels (Figure 3.2.6). As cell viability assays performed using the same compound concentrations and treatment duration demonstrated comparable reductions in cell viability (Figure 3.2.5), the observed Hit #1-mediated decreases in dimerization-associated luminescence are likely a result of cell death, not specific inhibition of the NanoBiT® signal.

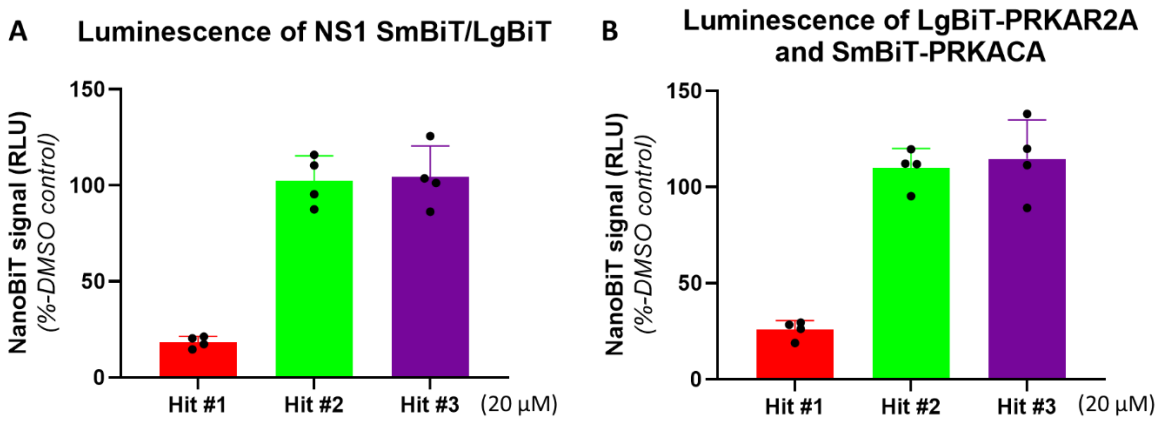

Figure 3.2.6: Effect of hit compounds on NS1 dimerisation. Huh-7.5 cells in 6-well plates were co-transfected with either NS1-SmBiT and NS1-LgBiT (A) or the control dimerisation pair, SmBiT-PRKACA and LgBiT-PRKAR2A (B). 24 hours later, the cells were trypsinised and transferred to 96-well plates, treated with 20 µM compound or 0.1% (v/v) DMSO carrier alone and incubated for a further 24 hours. Cells were lysed with passive lysis buffer and incubated with Nanoluciferase substrate. Luminescence was then recorded for all samples, and signals were normalised to that of the average of the DMSO control values. Data are means ± S.D. (n = 4).

While the NanoBiT® assay and infectivity assays demonstrated a low likelihood of the three hits being NS1-specific interacting compounds, this had not been conclusively shown. To investigate whether any of the three hits interacted with NS1, NaLTSA assays were performed to analyse each hit for stabilisation of the luminescent signal associated with detergent lysates of Huh-7.5 hepatoma cells that had been transfected with DENV2-NS1-NLuc reporter virus RNA. The lysate was incubated with each drug, or a DMSO control, for 2 hours at a final concentration of 20 µM. These lysates were then treated at temperatures ranging from 40 – 70 °C for 3 minutes, before addition of NanoLuc substrate and measurement of luminescence (Figure 3.2.7). The results illustrate that no significant increase in stability occurred for any of the three hits when compared to DMSO carrier controls. Taken together, these results indicated that none of these compounds are likely to interact with NS1, or inhibit NS1 dimerisation.

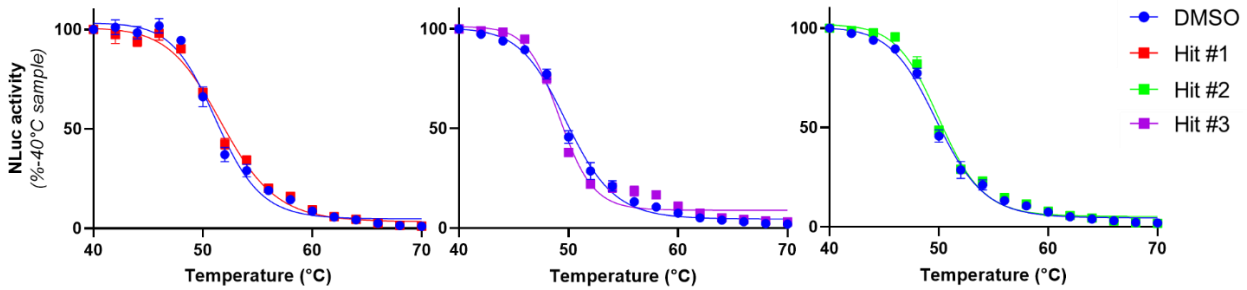

Figure 3.2.7: NanoLuc luciferase thermal shift assay (NaLTSA) to interrogate the interaction of Hits #1-3 with the NS1-NLuc fusion protein. Detergent lysates prepared from Huh-7.5 cells transfected with DENV2-NS1-NLuc RNA (7 days post-transfection) were treated with 0.1% (v/v) DMSO carrier or the stated compound at a final concentration of 20 μM for 2 hours at room temperature, then heat treated for 3 minutes at the indicated temperatures, ranging from 40 °C – 70 °C. After cooling to room temperature, the samples were transferred to a 96-well white-walled plate containing appropriately diluted Nano-Glo assay substrate and luminescence was recorded. Measurements are presented as a percentage of the average luminescence values recorded for the corresponding 40 °C treatment. Data are means ± S.D. (n = 3). Sigmoidal 4PL regression models are displayed.

3.3 Virtual Drug-Like Compound Screen of Potential NS1 inhibitors

As neither the NaLTSA high-throughput screen nor the NanoBiT Protein:Protein interaction high-throughput screen had unambiguously identified an NS1-interacting compound, we next pursued an *in silico* approach, again focussed on the inhibition of NS1 dimerisation. All *in silico* work in this section was performed in collaboration with Daniel McDougal and Dr John Bruning (University of Adelaide), using the open-source pipeline 'warpDOCK'(353).

Computer-aided drug design is an attractive approach to drug screening, as time and cost can be significantly reduced, while the scale of a screen in terms of compound diversity and number can be drastically increased. While this study was performed using a library of millions of purchasable compounds, state-of-the-art technologies have allowed screens of billions of compounds, although greater processing power is required for such screens (354). When screening for ligands of a protein, it is helpful to know the structure of the protein, although other pathways exist(355). The structure of NS1 has been interrogated multiple times using x-ray crystallography and cryo-EM(160, 356, 357). We utilised specific computational tools to identify binding pockets of NS1, then performed molecular dynamics simulations of the NS1 protein to better represent the flexibility of the structure. An ultra large chemical library of 7.8 million compounds was then screened against two binding pockets within the dimerisation interface of NS1.

From the 60 top hits across the two putative compound binding pockets in the NS1 dimer interface, 24 compounds were purchased and tested for antiviral and cytotoxic properties in a medium throughput assay using live cell imaging and infection with the DENV2-NS1-mScarlet reporter virus. Due to its high efficacy and low toxicity, Compound V2.3 (PubChem CID: 92887269) was selected for further investigation. This compound strongly inhibits DENV2 infectious particle production and has a minor effect on viral RNA replication. However, a NanoBiT® Protein:Protein interaction assay revealed no evidence for an impact on NS1 dimerisation, while the NaLTSA did not indicate thermal stabilisation of NS1. The exact antiviral mechanism of action of this compound will be determined in future studies.

3.3.1 Results

To perform the *in silico* screen, we selected a crystal structure of the NS1 dimer in complex with a neutralising single-chain variable fragment (PDB: 7K93) (203), due to the high resolution of the crystal structure and its overlap with unbound NS1 structures (data not shown). For identification of NS1-binding ligands which interrupt dimerisation, we sought to target regions of NS1 near the dimerisation interface. Using PyMol, the NS1 dimer structure was split into monomers, allowing for targeting of this interface (Figure 3.3.1). The monomeric form of NS1 exists briefly, for 20 – 40 minutes post-translation, which we hypothesise would allow sufficient time for binding of ligands before the interface becomes inaccessible (358).

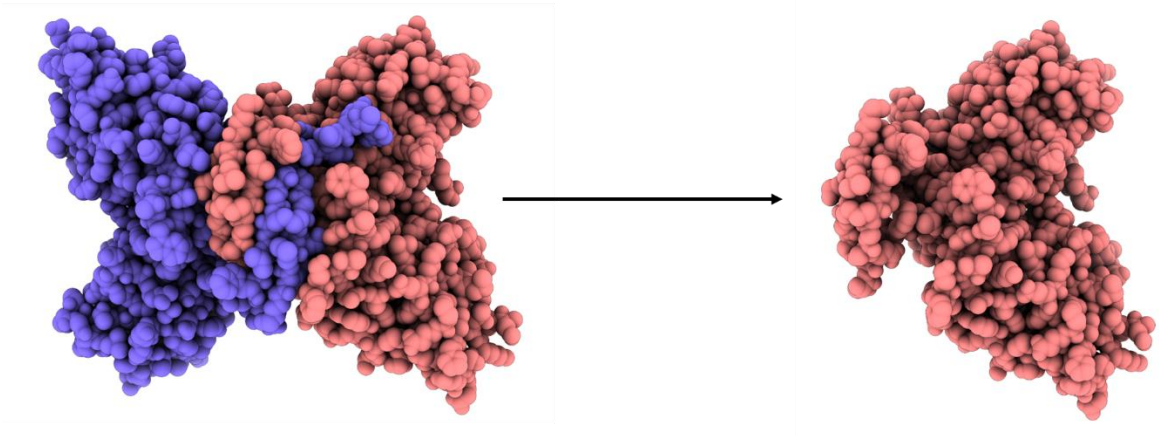

Figure 3.3.1: Structure of dimeric DENV NS1 (left, PDB accession code: 7K93) with monomeric NS1 (right), separated using PyMol, allowing visualisation of the dimerisation interface.

For binding site prediction, QuickVina-W was utilised(325). This is a faster, more accurate version of AutoDock Vina(359), more suitable for wide space search. Identification of potential binding sites through 'blind docking' involves the docking of many ligands across the entire surface of a protein, revealing areas in which ligands are most likely to bind, leading to the modulation of protein activity(360). This typically occurs within small pockets, or concave regions of a protein. Docking algorithms predict the most likely orientation of a ligand in a binding pocket, considering degrees of freedom, rotation and possible flexible bonds within the ligand, as well as identifying van der Waals and electrostatic interactions between ligand and protein, which are scored and weighted by a scoring function to predict binding affinity of a ligand to the protein(361). 4,300 ligands from a library of world-approved drugs were utilised in the blind-docking approach with the NS1 monomer (seen in Figure 3.3.1). Multiple

sites showed enrichment of ligand binding, with high levels of expected binding at the dimerisation interface. We selected two sites within the dimerisation interface for further interrogation, highlighted in Figure 3.3.2. All other identified binding pockets were excluded in further probing for screening efficiency.

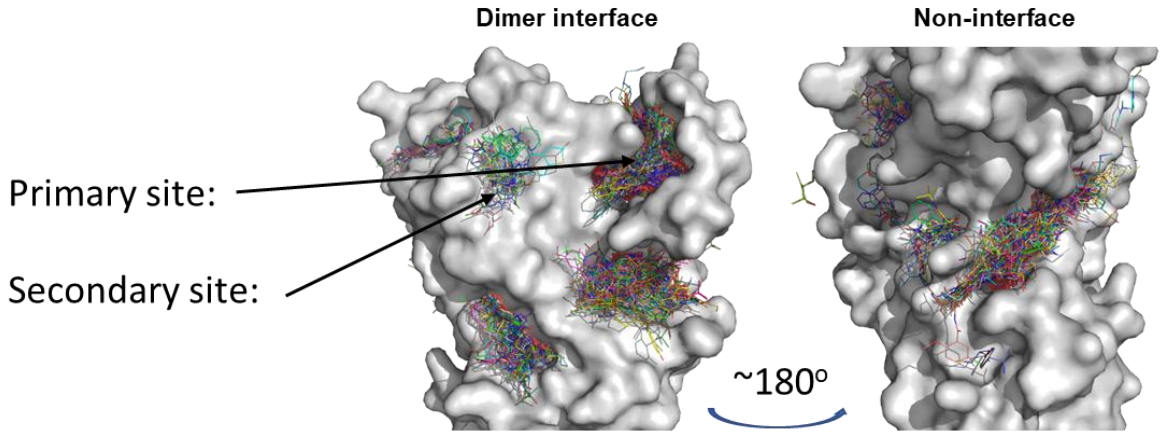

Figure 3.3.2: Identification of binding pockets using QuickVina-W. ~4,300 ligands were screened against monomeric NS1 (PDB accession code: 7K93, split from dimer to monomer to reveal dimerisation interface) with an exhaustiveness value of 25. Binding pockets selected for further interrogation are highlighted with arrows.

A crystal structure is a snapshot of the shape of a protein. However, as protein-ligand recognition and binding is a dynamic process, this is a limiting factor for virtual drug screening(362). To generate a representative set of the possible conformations in which NS1 may exist, we used a molecular dynamics approach, whereby interatomic interactions and motions are calculated using Newtonian equations, to give the expected position of atoms over time. A 500 nanosecond molecular dynamics simulation generated using GROMACS (GROningen Machine for Chemical Simulation)(326) allowed the generation of 6 conformations which best represent the simulation of NS1 (Figure 3.3.3).

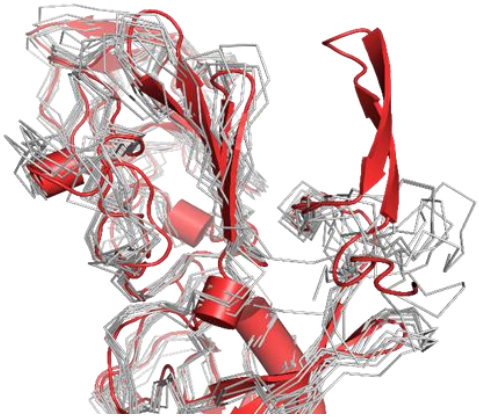

Figure 3.3.3: Generation of a conformational ensemble of monomeric NS1 utilising the molecular dynamics simulator GROMACS with a 500 nanosecond simulation. The Gromos algorithm was used for RMSD-based clustering for 50,001 frames with a 0.2 nanometre distance cut-off. The top 6 clusters, shown in the Figure, represent > 99% of the ensemble.

To perform the final screen, we used QuickVina-2(327) for our docking simulation focussed on the two enriched binding pockets identified with QuickVina-W, with each compound screened against all 6 structures identified with GROMACS during the 500 ns simulation. Compounds were selected from the ZINC20 ultralarge-scale chemical database(363), filtered for 'in-stock' molecules, for a total of ~7.8 million compounds. After screening of all compounds against the 6 generated NS1 structures as well as the original crystal structure, ligands were assigned a weighted score based on interaction with each structure. From the top 30 hits for each site, we attempted to purchase all available compounds. Table 3.3.1 lists the 24 ligands which were available for purchase and were found to be DMSO-soluble.

Table 3.3.1: Selected commercially available and readily dissolvable hit compounds from the NS1 virtual screen.

Primary Site	11 total	Secondary Site	13 total
Code	Zinc number	Code	Zinc Number
V1.4	ZINC000023882398	V2.1	ZINC000010039118
V1.8	ZINC000033300975	V2.2	ZINC000023605987
V1.9*	ZINC000009581101	V2.3	ZINC000033250837
V1.10	ZINC000057503332	V2.4	ZINC000009990415
V1.11	ZINC000009695527	V2.5	ZINC000021867071
V1.12	ZINC000009493835	V2.6	ZINC000253411290
V1.16	ZINC000011835515	V2.7	ZINC000225686677
V1.17	ZINC000008596825	V2.8	ZINC000012628833
V1.21	ZINC000049006563	V2.10	ZINC000103327057
V1.22	ZINC000002433975	V2.11	ZINC000028290028
V1.25	ZINC000012316620	V2.14	ZINC000030658448
		V2.15	ZINC000009453603
		V2.28	ZINC000033250835

To test the properties of the 24 selected hits, we used the previously described Huh-7.5-adapated DENV2-NS1-mScarlet reporter virus to allow for medium-throughput analysis of antiviral and cytotoxic properties without the requirement for fixation and staining. Huh-7.5 cells in 96-well imaging plates were infected with this reporter virus at a low MOI and treated with each compound at concentrations ranging from 0.63 to 40 µM. Automated imaging every hour for 72 hours was performed, capturing mScarlet fluorescence to monitor DENV2 infection levels and phase contrast images to monitor cytotoxicity and any discernible compound precipitation. Quantitative, dose-dependent, temporal analysis of the mScarlet fluorescence upon treatment with each compound is shown in Figure 3.3.4 A. The data revealed that Compound V2.3 displays strong antiviral activity with limited cytotoxicity, with an IC_{50} of 4.72 µM and a CC_{50} of 49.1 µM. Representative images of cells infected with the reporter virus and treated with Compound V2.3 are presented in Figure 3.3.4 B. Figure 3.3.4 C displays the total red area per image at each time point for all concentrations of Compound V2.3. IC_{50}, CC_{50}, selectivity indices and observations of compound precipitation are listed in Table 3.3.2

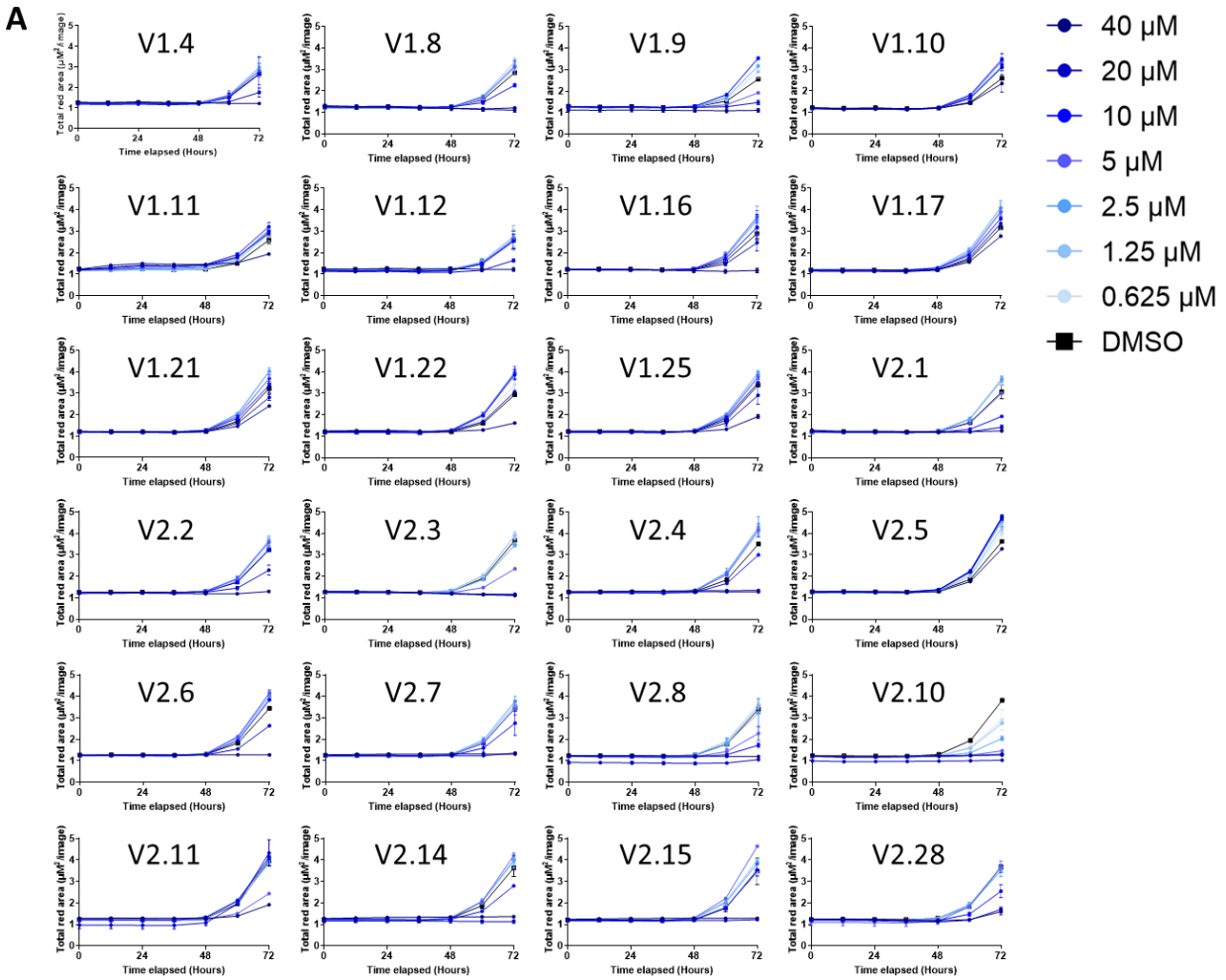
A
V1.4
V1.8
V1.9
V1.10
V1.11
V1.12
V1.16
V1.17
V1.21
V1.22
V1.25
V2.1
V2.2
V2.3
V2.4
V2.5
V2.6
V2.7
V2.8
V2.10
V2.11
V2.14
V2.15
V2.28
Total red area (μM²/image)
Time elapsed (Hours)
40 μM
20 μM
10 μM
5 μM
2.5 μM
1.25 μM
0.625 μM
DMSO

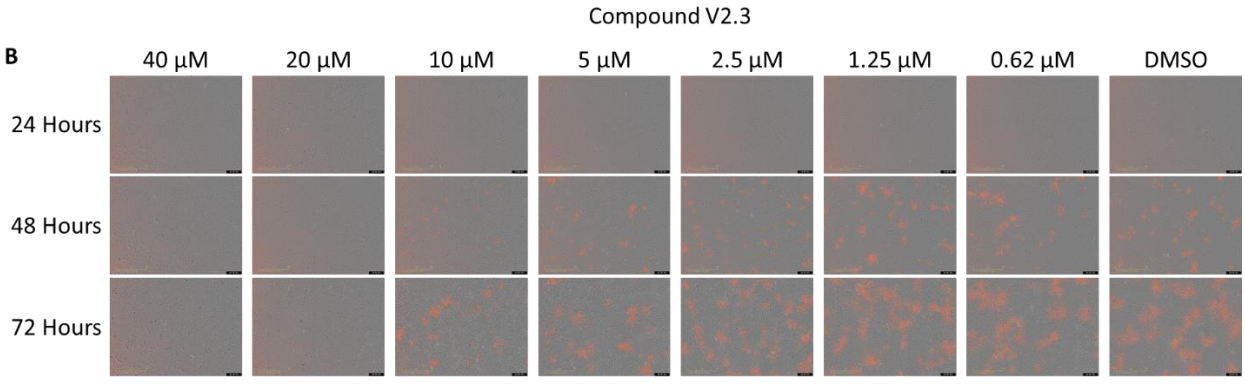
B
Compound V2.3
40 μM
20 μM
10 μM
5 μM
2.5 μM
1.25 μM
0.62 μM
DMSO
24 Hours
48 Hours
72 Hours

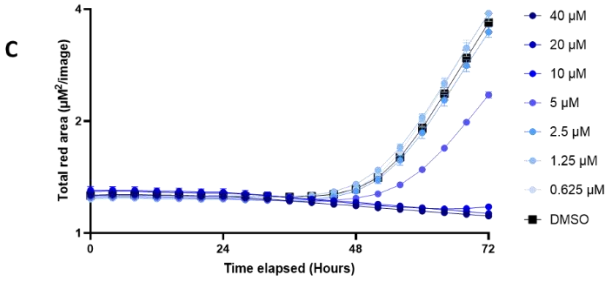
C
Total red area (μM²/image)
Time elapsed (Hours)
40 μM
20 μM
10 μM
5 μM
2.5 μM
1.25 μM
0.625 μM
DMSO

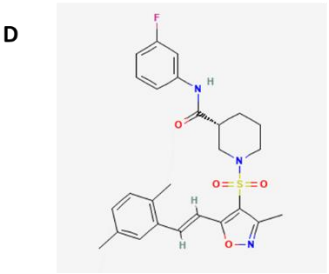
D

Figure 3.3.4: A) Dose-response analysis of the antiviral effects of 26 of the top 60 hits identified in the NS1 virtual ligand screen. Huh-7.5 cells in 96 well plates were treated with 0.1% (v/v) DMSO carrier alone or the stated compound at concentrations ranging from 0.625 µM to 40 µM and infected with DENV2-NS1-mScarlet (MOI: ~0.05) and placed in an Incucyte® SX5 Live-Cell Analysis System. Phase contrast and red fluorescent channel images were acquired every hour for 72 hours. Graphs depict data from each 12 hour time-point. The antiviral effect is inferred by a reduction in the total red area in each image. Data are means ± S.D. (n = 2), calculated from 4 images per well. B) Dose-response analysis of the inhibition of DENV-2-NS1-mScarlet spread by Compound V2.3. Each image is representative of 4 captured fields of view. Scale bars, 400 µm. C) Images captured at 4 hour intervals of Compound V2.3-treated cells were analysed for the total area containing NS1-mScarlet red fluorescent signal as a readout of viral infection and spread. Data are means ± S.D. (n = 4) for replicate wells per data point, calculated from all 4 images taken of each well. D) Structure of Compound V2.3

Table 3.3.2: Antiviral and cytotoxic effects of the NS1 virtual screen hits. Antiviral activity (IC_{50}) was calculated using the reduction in total area containing red fluorescent signal, as displayed in Figure 3.3.4, and CC_{50} was calculated from corresponding brightfield phase contrast images using the Incucyte® AI Confluence Analysis Workflow. Selectivity Index calculated as CC_{50}/IC_{50}. Precipitation indicates the growth of crystal-like structures in drug-treated wells. Selectivity Index calculated as CC_{50}/IC_{50}.

Compound	IC50 (72 hrs)	CC50 (72 hrs)	Selectivity Index	Precipitation	Compound	IC50 (72 hrs)	CC50 (72 hrs)	Selectivity Index	Precipitation
V1.4	17.13	58.5	3.42		V2.1	7.61	>>40		Yes
V1.8	10.62	54.7	5.15		V2.2	19.90	56.4	2.83	
V1.9	18.50	39.0	2.11		V2.3	4.72	49.1	10.4	
V1.10	48.64	>>40			V2.4	10.38	36.8	3.54	
V1.11	47.80	51.4	1.08		V2.5	>>40	>>40		
V1.12	17.03	41.3	2.43		V2.6	20.43	45.5	2.23	Yes
V1.16	23.37	48.7	2.08		V2.7	11.16	38.8	3.48	
V1.17	24.78	>>40			V2.8	5.19	48.7	9.38	Yes
V1.21	15.48	>>40			V2.10	1.52	45.2	29.7	Yes
V1.22	21.71	>>40		Yes	V2.11	>40	>>40		
V1.25	24.53	>>40			V2.14	10.22	35.3	3.45	
					V2.15	11.73	39.1	3.33	
					V2.28	9.89	>>40		

As Compound V2.3 showed the most promise among all inhibitors, based on antiviral efficacy, cytotoxicity and absence of precipitate, we decided to focus on this compound for further experiments. Figure 3.3.5 illustrates the binding site of Compound V2.3 within the NS1 dimerisation interface, and displays the predicted molecular interactions between the ligand and protein. The dimethylphenol group hydrophobically packs against I188 and L231. While weak pi-stacking may occur with W232, further investigation is required to support this possibility. The pentyl ring oxygen is predicted to form a hydrogen bond with N234 and the ligand sulfonyl group is predicted to form a hydrogen bond with S233. The phenol ring is predicted to hydrophobically interact with L231. Another hydrogen bond may form with the backbone of S229, and the fluorophenol group potentially forms weak hydrogen bonding with the A186 and or H229 backbone. The conservation of these amino acids can be seen in Figure 3.3.6 and Table 3.3.3, and across DENV serotypes there is high conservation of these residues and surrounding motifs, supporting the interpretation that such ligand-protein interactions would be conserved for other DENV serotypes and closely related orthoflaviviruses (364).

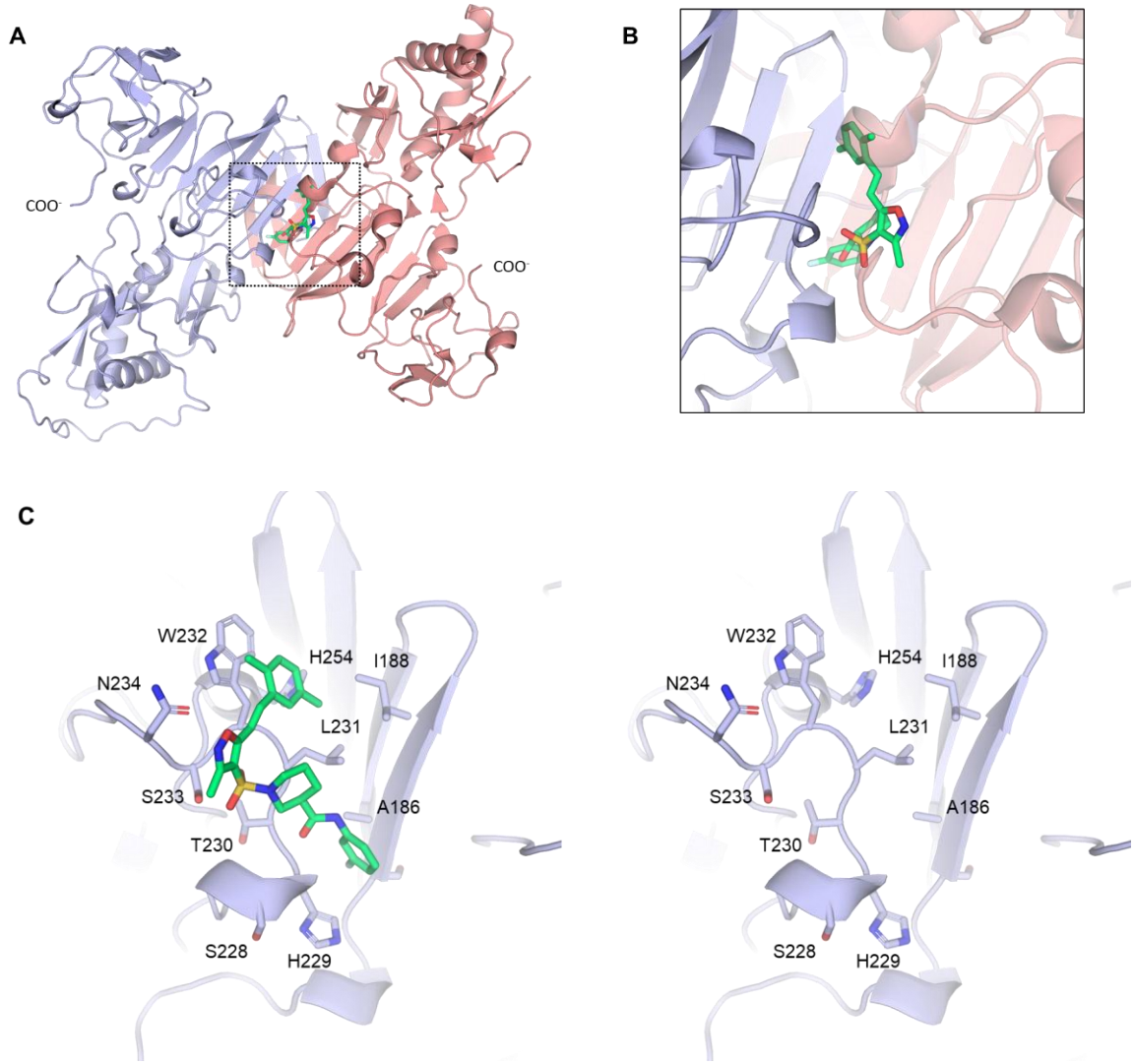

Figure 3.3.5: Predicted binding of Compound V2.3 to the NS1 dimerisation interface (secondary site). Colour scheme of Compound V2.3: F – grey, Green – Carbon, Red – Oxygen, Blue – Nitrogen, Yellow – Sulphur. Hydrogen atoms are not shown.

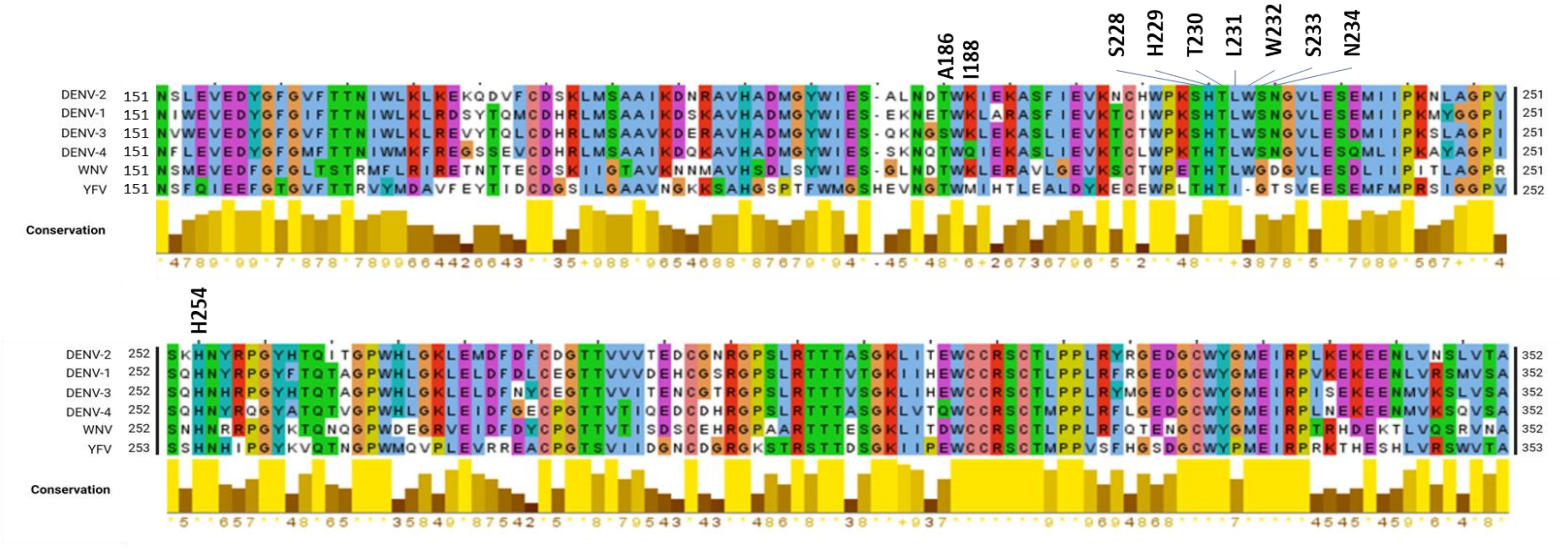

Figure 3.3.6: Conservation of orthoflavivirus NS1 residues as well as potential interacting residues with Compound V2.3.

Table 3.3.3: Conservation of NS1 amino acids predicted to interact with Compound V2.3. DENV conservation indicates the number of DENV serotypes which share a residue at the specified site.

Residue	DENV Conservation
A186	4/4
I188	3/4
S228	3/4
H229	4/4
T230	4/4
L231	4/4
W232	4/4
S233	4/4
N234	4/4
H254	4/4

We next sought to test the antiviral efficacy of Compound V2.3 against wild type DENV2. Huh-7.5 cells were seeded into 96-well plates, then infected with DENV2 at a low MOI (~0.05) for 2 hours and treated with Compound V2.3 at concentrations ranging from 0.625 µM to 40 µM, as indicated. 42 hours later, the cells were fixed and stained using an anti-capsid antibody and counterstained with DAPI. Automated imaging and analysis software was used to determine both a cell count and the percentage of cells infected with DENV2. Compound V2.3 reduced DENV2 infection with an IC_{50} of 7.81 µM and a CC_{50} of 39.0 µM (Figure 3.3.7).

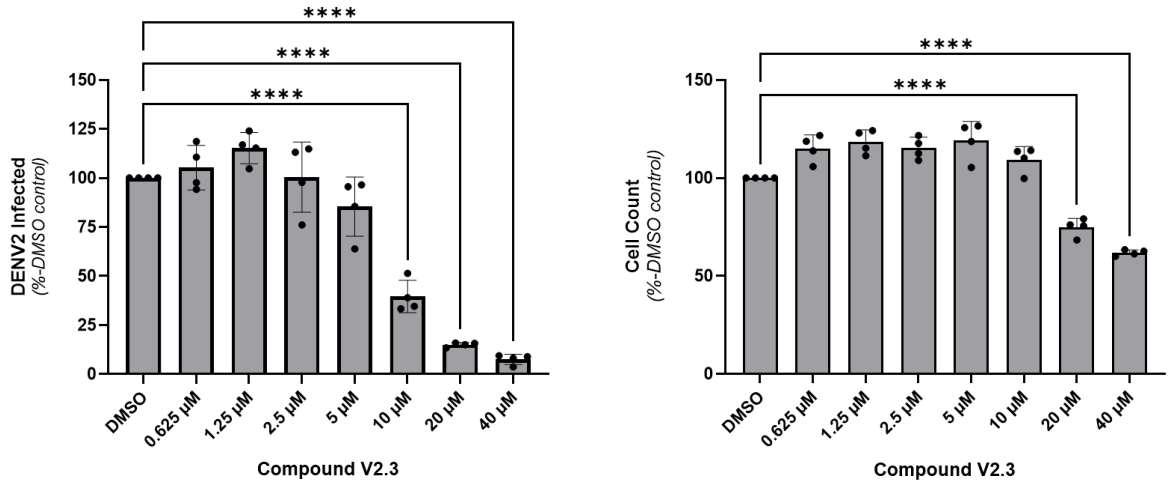

Figure 3.3.7: Dose-response analysis of the antiviral and cytotoxic effects of Compound V2.3. Huh-7.5 cells were infected with DENV2 (MOI: ~0.1) and incubated with a range of concentrations of Compound V2.3, as indicated, for 42 hours. Cells were then fixed, labelled by indirect immunofluorescence using an anti-Capsid antibody and counterstained with DAPI. Cell counts and the percentage of cells infected were calculated via automated fluorescence microscopy using a Cytation 5 Cell Imaging Multi-Mode Reader and associated Gen5 software. Data are means ± S.D. (n = 4). *, $P < 0.05$; **, $P < 0.01$; ***, $P < 0.001$; ****, $P < 0.0001$ indicate statistically significant differences compared to DMSO treatment, by one-way ANOVA (multiple comparisons). Statistical significance not displayed for increases in cell count compared to DMSO treatment.

To investigate the antiviral mechanism of action of Compound V2.3, we sought to delineate the effect of the compound on infectious particle production and viral RNA replication. To analyse the effect of Compound V2.3 on infectious particle production, Huh-7.5 cells were infected with DENV2 (MOI: ~0.1) and treated with Compound V2.3 at concentrations ranging from 0.63 µM to 40 µM for 72 hours. Infectious virus particle production was then assayed via focus forming assays. Compound V2.3 resulted in decreased infectious virus particle production with an IC_{50} of 599 nM (Figure 3.3.8 A). To assess inhibition of viral RNA replication, Vero cells harbouring stable replication of a GFP-tagged DENV2 subgenomic replicon were seeded in 96-well plates and treated with the same range of concentrations of Compound V2.3, as well as with JNJ-A07, a positive control for inhibition of viral RNA replication. 72 hours later, live cells were stained with Hoechst dye, then green and blue fluorescence levels were recorded. Viral RNA replication was inhibited by Compound V2.3 with an IC_{50} of 23.8 µM (Figure 3.3.8 B). As the IC_{50} for reduction of infectious particle production was significantly lower than for reduction of viral RNA replication, we concluded that the high antiviral efficacy of the drug is most strongly related to its inhibition of infectious virus particle production.

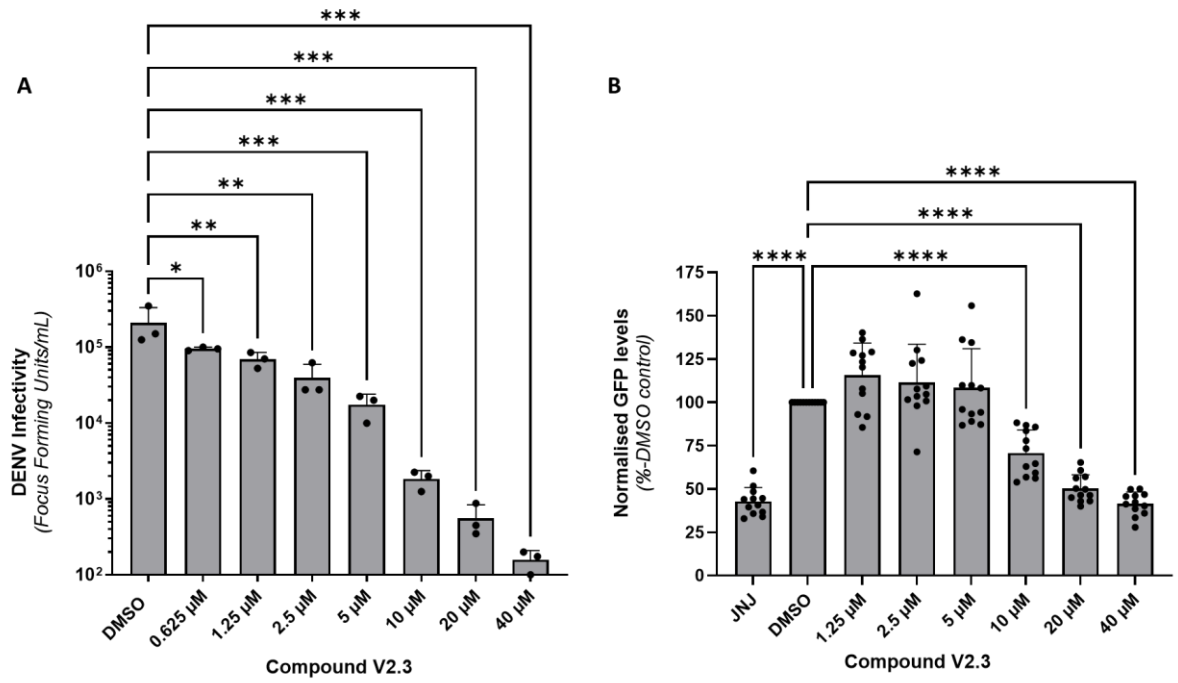

Figure 3.3.8: A) Analysis of the inhibition of infectious virus particle production by Compound V2.3. Huh-7.5 cells were infected with DENV2 (MOI: ~0.1) and treated with the indicated compound. After culture for 72 hours, cell culture supernatants were collected and stored at -80 °C. Infectivity of cell culture supernatants were then determined via Focus Forming Assays. Data are means ± S.D. (n = 3) B) Dose-response analysis of Compound V2.3 on viral RNA replication. Vero cells harbouring stable replication of a DENV subgenomic replicon encoding GFP were treated with JNJ-A07 at 35 nM or Compound V2.3 at the specified concentrations for 72 hours. Live cells were counterstained with Hoechst dye, then washed. Whole well green and blue fluorescence was measured. Whole well blue fluorescence was used as an indirect measurement of cell count/confluency, allowing normalisation of viral RNA replication (GFP signal) to cell count (Hoechst signal). Data are means ± S.D. (n = 12). *, $P < 0.05$; **, $P < 0.01$; ***, $P < 0.001$; ****, $P < 0.0001$ indicate statistically significant differences compared to DMSO treatment, by one-way ANOVA (multiple comparisons).

As Compound V2.3 had been identified computationally as an interactor with NS1, we sought to verify this interaction using the previously described NanoLuc luciferase thermal shift assay (NaLTSA). Detergent lysates from Huh-7.5 cells that had been transfected with the DENV2-NS1-NLuc reporter virus RNA (7 days post-transfection) or transfected with a Nanoluciferase expression plasmid as a control, were incubated with DMSO carrier control or Compound V2.3

(40 µM) for 2 hours, then heat-treated at a range of temperatures. The samples were then cooled to room temperature, and Nanoluciferase substrate was added. After a brief incubation, the luminescence of each sample was recorded (Figure 3.3.9). While there appeared to be stabilisation of NS1-NLuc by the compound, this stabilisation was also seen for the Nanoluciferase control, indicating that Compound V2.3 is either not directly interacting with NS1, or that the effect is masked by an additional interaction with Nanoluciferase.

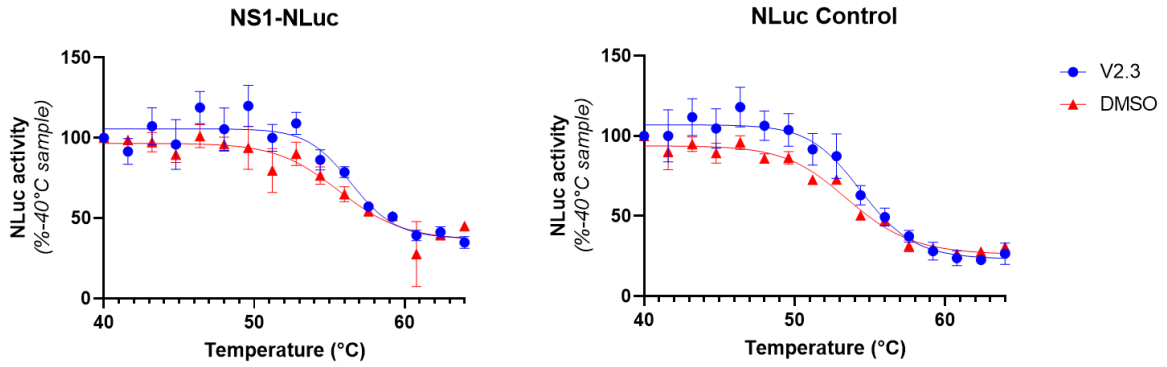

Figure 3.3.9: Determination of an NS1 interaction with Compound V2.3. Lysate collected from Huh-7.5 cells transfected with DENV2-NS1-NLuc RNA (7 days post-transfection), or with an expression plasmid encoding NLuc alone, were treated with DMSO carrier control or Compound V2.3 at a final concentration of 40 µM for 2 hours at room temperature, then heat treated for 3 minutes at varying temperatures, as indicated. After cooling to room temperature, the samples were transferred to a 384-well white-walled plate containing Nano-Glo assay substrate, incubated for 10 minutes, then luminescence was recorded. Measurements are presented as a percentage of the average luminescence recorded for the 40 °C treatment. Data are means ± S.D. (n = 2). Sigmoidal 4PL regression models are displayed.

To investigate the effect of Compound V2.3 on the dimerisation of NS1, we used the previously described NanoBiT® Protein:Protein interaction assay. HeLa cells in a 96-well plate were co-transfected with NS1-SmBiT and NS1-LgBiT or SmBiT-PRKACA and LgBiT-PRKAR2A expression plasmids, as indicated. Following incubation for 16 hours, the cells were treated with Compound V2.3 at concentrations ranging from 1.25 µM to 40 µM. After a further 48 hour incubation, the cells were lysed and Nanoluciferase substrate was added, then luminescence was recorded. At 40 µM concentration of Compound V2.3, there was no appreciable reduction

of NS1 dimerisation-associated luminescence, when normalised to the control dimerisation pair (Figure 3.3.10).

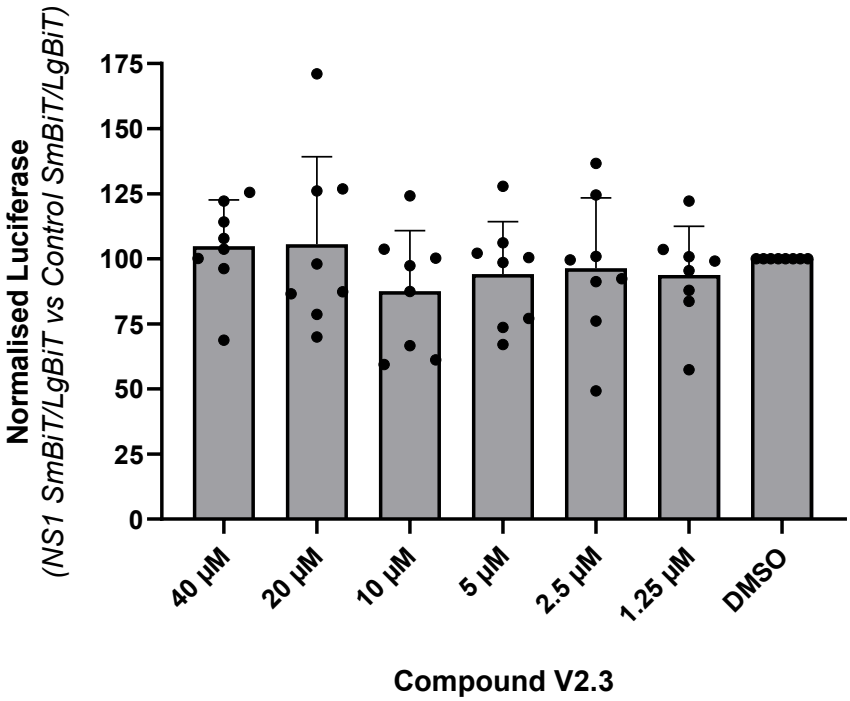

Figure 3.3.10: The effect of Compound V2.3 on the dimerisation of NS1. HeLa cells in white-walled 96-well plates were co-transfected with either NS1-SmBiT and NS1-LgBiT or the control dimerisation pair, SmBiT-PRKACA and LgBiT-PRKAR2A. Sixteen hours later, the cells were treated with DMSO carrier alone or Compound V2.3 at a range of concentrations, as indicated, and incubated for 48 hours. Cells were lysed with passive lysis buffer and incubated with appropriately diluted Nanoluciferase substrate. Luminescence was then recorded for all samples, and NS1 SmBiT/LgBiT signal was normalised to the control dimerisation pair to account for toxicity or non-specific inhibition of the NanoBiT® assay. Data are means ± S.D. (n = 8). *, $P < 0.05$; **, $P < 0.01$; ***, $P < 0.001$; ****, $P < 0.0001$ indicate statistically significant differences compared to DMSO treatment, by one-way ANOVA (multiple comparisons).

3.4 Discussion

3.4.1 Identification of sulfonamide compounds that impair dengue virus infectious particle production

Despite significant advances in the development of promising antiviral drug candidates, there remains no available treatment for patients suffering from dengue fever, besides supportive care. The goal of this study was to identify NS1-specific inhibitors using a Nanoluciferase-based thermal shift assay (NaLTSA). While we were unable to verify an interaction with NS1, we did identify a group of structurally related compounds which inhibit DENV and, to our knowledge, have not been previously studied for their antiviral properties. Compound 14 was identified as the most promising candidate amongst the compounds tested when considering efficacy and cytotoxicity and was shown to reduce infectious particle production with an IC_{50} of 1.1 µM. While multiple structural analogues were also subsequently tested, Compound 14 remained the most effective candidate. While subgenomic replicon experiments indicated a slight impact of Compound 14 on viral RNA replication, the small effect is unlikely to reflect its marked inhibition of infectious particle production. Surprisingly, Western blotting experiments indicated that short-term Compound 14 treatment significantly reduces levels of NS3 protein in DENV-infected cells. It is possible that infectious virus production is more sensitive than viral RNA replication to reduced levels of NS3 protein and/or similarly reduced levels of associated viral factors in an infected cell, such that this compound has a stronger effect on infectious virus production than it does on viral RNA replication. However, more detailed mechanistic studies are required to support this conclusion. As Compound 14 is more effective in long term experiments, it is difficult to identify which DENV lifecycle stage(s) is being inhibited based on our time of addition assay results. If a more potent analogue of Compound 14 were to be identified, this may allow for more definitive interrogation of the specific stage(s) of the viral lifecycle that are being affected.

Confocal microscopy was employed to investigate the impact of Compound 14 treatment on the localisation of viral proteins in cells that were infected with the DENV2-NS1-mScarlet reporter virus. Interestingly, we found that Compound 14 treatment frequently resulted in an inability to detect E protein when visualised with the monoclonal anti-E antibody 4G2 in cells expressing both NS1 and NS4B. This antibody targets domain II of Envelope protein (EDII)(346), which is required for binding to the host cell receptor DC-SIGN(365), and is known to detect a conformational epitope, suggesting that E protein misfolding and/or failure to

mature may be caused by Compound 14 treatment. Using automated fluorescence microscopy, these effects were observed to be dose-dependent, with Compound 14 treatment at 20 µM resulting in an approximately 40% reduction in detection of mature E protein in cells that express NS1-mScarlet, relative to that of vehicle-treated controls. To further investigate this phenomenon, we probed wild-type DENV2-infected cells with both the 4G2 monoclonal anti-E antibody and a polyclonal anti-E antibody that is predicted to recognize multiple forms of E protein. As the concentration of Compound 14 was increased, the proportion of infected cells that were labelled with both the conformation-specific monoclonal anti-E antibody and the conformation-insensitive polyclonal anti-E antibody decreased, indicating a Compound 14-induced impairment of the recognition of mature E protein.

Targeting of specific host proteins has been previously reported to alter envelope epitope accessibility(347). The ER-resident dolichol-phosphate mannose synthase (DMPS) complex is required for protein glycosylation and glycosylphosphatidylinositol anchor biosynthesis in the ER lumen(366). Specifically, knockout of a subunit of this complex, DPM1, was shown to result in abnormal glycosylation of E protein. This was suggested to be the result of decreased epitope accessibility due to protein misfolding. In a similar manner, we hypothesise that Compound 14 may impact upon the folding and/or post-translational modification of E protein, and propose that the impact of Compound 14 on the glycosylation of E protein should be investigated in future studies.

Among the infected Compound 14-treated cells that lack mature E protein, confocal microscopy revealed web-like localisation patterns for E protein and the ER itself. Several proteins that are involved in regulation of ER morphology are known. Amongst these proteins, the Atlastin protein family, including ATL1, which is predominantly localised to the Golgi, and ATL2 and ATL3, which are localised to the ER, are GTPases that are important determinants of ER tubule structure due to their role in the formation of three-way junctions, which connect the ER network of sheets and tubules(367, 368). Triple Atl1/2/3 knockout NIH-3T3 cells have been shown to display this disrupted ER network, or web-like pattern, caused by a reduction in the ER tubule fusion events which are required to generate these three-way junctions(369). Relating to DENV, knockdown of ATL2 in DENV-infected A549 cells results in reduced viral titres and reduced intracellular viral RNA(370). Similar to our observed effects of Compound 14,

knockdown of ATL3 results in reduced viral titres, but not viral RNA replication (370). It is tempting to speculate that ATL2 knockdown and Compound 14 treatment have similar effects on ER morphology. Further mechanistic studies of the impact of Compound 14 on ER architecture are warranted.

E protein has been shown to be the target of many experimental DENV antiviral small molecule drug candidates. The mechanism of action of these compounds includes inhibition of virus binding to cell receptors, cellular entry and fusion of viral envelopes with endosomal membranes to allow for nucleocapsid release(371). A common target site within E protein is the conserved binding pocket in the hinge region between EDI and EDII, which binds to the small detergent molecule N-octyl-β-D-glucoside (βOG)(187). Interaction of this binding pocket with small molecule drug candidates has been demonstrated to inhibit a crucial step in membrane fusion(188, 189), and multiple ligands that bind to this pocket have displayed antiviral activity(188, 190-193). Domain III of E protein is important for virus entry, as this domain recognizes host cell receptors(194). Multiple receptors involved in virus entry have been identified, including glycosaminoglycans such as heparan sulfate(183). The heparan binding motif, a positively charged region of EDIII, has since been successfully targeted with multiple negatively charged compounds, often glycosaminoglycan mimetics(195-198). However, to our knowledge the impact of Compound 14 on the maturation of E protein and ER morphology in infected cells has not been reported for candidate inhibitors of E protein or other anti-DENV drug candidates, suggesting a novel mode of anti-DENV activity for Compound 14.

In summary, Compound 14 shows high efficacy in reducing infectious virus particle production and appears to disrupt post-translational processing/maturation and localisation of E. This study suggests that further investigation into its mechanism of action and exact molecular target(s) of Compound 14 is warranted and, specifically, it will be important to better understand the impact of Compound 14 on the morphology of the endoplasmic reticulum in DENV-infected cells and how this relates to the maturation of E protein. Additionally, we hypothesise that the antiviral efficacy and safety profile of Compound 14 may be improved upon via further rational medicinal chemistry efforts.

3.4.2 High-throughput drug screening using the NanoBiT® Protein:Protein interaction assay

This study attempted to identify inhibitors of NS1 dimerisation, by individually fusing NS1 to SmBiT and LgBiT from the NanoBiT® Protein:Protein interaction system, and performing a high throughput compound screen to identify compounds which decrease complementation of these constructs, measurable by a decrease in luminescence.

Two identical screens were performed initially, with 3,378 compounds assayed once per screen. The screens displayed poor reproducibility (r^2=0.34). During the running of this screen, technical issues resulted in the Janus® liquid handler inaccurately dispensing liquid volumes, resulting in a drift effect across all 384-well plates used. It is likely that this had a large impact on the validity of the results. For the following validation screen, it was decided that compounds which satisfied hit criteria in both screens, which were also structural analogues of other hits, would be tested. In this validation, three compounds fulfilled the pre-determined criteria for a hit. Hits #2 and #3 showed >40% inhibition of NS1 dimerisation, while Hit #1 displayed an approximate ~27% decrease. Each of the hits decreased cell-viability associated fluorescence by <15%, despite Hit #1 showing considerable levels of toxicity in follow-up experiments. None of the hits from the two initial screens satisfied the criteria for a hit in the validation screen, again bringing into question the validity of the primary screens. As the validation screen featured a greater number of technical replicates, this data was considered to be more reliable in the selection of hit compounds for further experimental analysis.

Validation experiments then revealed that none of the three hits from the validation screen were true inhibitors of NS1 dimerisation. Hits #2 and #3 had no effect on NS1 dimerisation and displayed no antiviral activity. While Hit #1 appeared to be potentially antiviral, due to the lack of evidence for an interaction with NS1 and its high cytotoxicity at a low micromolar range, we did not perform further research into its antiviral mechanism of action. In the validation screen, each of the hits decreased cell-viability associated fluorescence by <15%. The high levels of cytotoxicity seen during treatment with Hit #1 indicates that the measurement of toxicity in the screen may have been inaccurate. However, it is important to recognise that HeLa cells were used in the high-throughput screen due to their transfectability,

while Huh-7.5 cells were used in follow-up experiments, which may be more susceptible to the cytotoxic effects of this particular compound.

The requirement for transient co-transfection of NS1-SmBiT and NS1-LgBiT expression constructs for the screens likely introduced high variability of NS1-SmBiT and NS1-LgBiT expression between replicate screens, in addition to the liquid handling technical issues that were observed to result in a 'drift effect' across each of the 384-well plates in the first primary screen replicate. It is unlikely that our failure to identify inhibitors of NS1 dimerisation is due to inappropriateness of the NanoBiT® system used. A previous study identified several inhibitors of HIV replication using a NanoBiT® assay detecting the interaction between HIV-1 reverse transcriptase and cellular eukaryotic translation elongation factor 1A(372). The same Compounds Australia scaffold library was used in that study, with a single compound from each of the 1,126 scaffolds tested initially. Overall, 0.33% of the compounds were determined to inhibit the specified interaction, with an improved 10.66% success rate for structural analogues of the hits. A similar strategy has also been successfully applied to the critical NS2B-NS3 interaction in Zika virus(373). While it is plausible that the hit rate for inhibitors of NS1 dimerisation could be significantly lower due to the biological nature of NS1 dimerisation itself and its potentially inherent resistance to chemical inhibition, it is more likely that screening issues were responsible for the lack of identified NS1 dimerisation inhibitors. Arguably, with the limited number of hits identified in the primary screens (1.3%), the subsequent screen of structural analogues of hits may have been somewhat confounded by the relatively limited chemical diversity of the library that was used in the secondary screen.

To repeat this experiment, it would be preferable to use monoclonal Huh-7.5 cells with stable expression of both NS1-SmBiT and NS1-LgBiT constructs. This cell line was generated (data not shown), however it was not available for use at the time of the screen. A monoclonal cell line would likely have reduced variability between wells and screens, due to the uniform expression of both NS1 constructs in each cell. When optimising the high-throughput screen, a major concern with this stable cell line approach was the relatively low NS1 dimerisation-associated luminescence levels of the stable cell lines that were tested, compared to that of transiently transfected cells, with the monoclonal Huh-7.5 NS1-SmBiT NS1-LgBiT cell line displaying only ~20x greater luminescence compared to non-transduced Huh-7.5 cells. The high cytotoxicity induced by Hit #1 in validation experiments, which was not detected in the

validation screen, also suggests that the CellTiter-Blue® Cell Viability Assay that was used in the screens may not have successfully detected cytotoxic effects throughout the screen. An additional valuable control to include in these assays would be mutant NS1-SmBiT and/or NS1-LgBiT constructs, to allow for a measurable signal of decreased NS1 dimerisation. Alanine mutagenesis of *N*-glycosylation sites Asn-130 and Asn-207 has been previously shown to reduce NS1 dimer stability (374), and similar mutations of these residues may have been helpful to further validate the NS1 NanoBiT dimerization assay and provide a biological comparator for small molecule drug-like compound-mediated inhibition of NS1 dimerization. Unfortunately, no inhibitors of NS1 dimerisation were available for use as a positive control for chemical inhibition of NS1 dimerization, which would have otherwise further validated the NS1 NanoBiT dimerisation assay and served as a benchmark control for the screens.

3.4.3 Virtual Drug Screen of putative NS1 inhibitors

We identified a nanomolar inhibitor of DENV infectious virus particle production using computational drug screening. With an NS1 crystal structure (PDB accession code: 7K93(330)), the NS1 dimerisation interface was interrogated for binding pockets using a blind docking screen with QuickVina-W, and a molecular dynamics simulation using GROMACS allowed for visualisation of these static pockets as dynamic structures. Using QuickVina-2, 7.8 million compounds from the ZINC20 ultralarge chemical database were tested for an interaction with two binding pockets within the dimerisation interface, against 7 NS1 structures representing the molecular dynamics simulation as well as the original static structure.

Of the top 30 hits identified at each of the binding pockets, we were able to purchase a total of 25 compounds, one of which did not dissolve in DMSO. These compounds were tested in a medium-throughput assay using our Huh-7.5-adapted DENV2-NS1-mScarlet reporter virus. This assay revealed Compound V2.3 as a potent inhibitor of DENV spread with minimal cytotoxicity. The antiviral efficacy of Compound V2.3 was shown to most strongly impair infectious virus particle production, with an IC_{50} of 599 nm, and only a minor inhibitory impact on viral RNA replication.

As Compound V2.3 was expected to bind at a dimerisation interface, we utilised the NanoBiT® Protein:Protein interaction assay to test for a reduction of NS1 dimerisation. However, even when tested at a concentration of 40 µM, dimerization-associated luminescence was not significantly to be reduced. As these assays were only performed in a single format, with inhibitors applied at 16 hours post-transfection, further testing using this and other NS1 dimerization assays may be required to definitely rule out an effect of Compound V2.3 on NS1 dimerization. The NanoLuc luciferase thermal shift assay (NaLTSA) also failed to demonstrate an interaction of Compound V2.3 with NS1. We therefore do not have sufficient evidence to state that Compound V2.3 is an interactor or inhibitor of NS1, as opposed to an inhibitor of other aspect(s) of the DENV lifecycle. Future experiments, including surface plasmon resonance and x-ray crystallography will be performed to characterise the potential binding of Compound V2.3 to NS1. The pocket of NS1 which with which this compound is predicted to bind shows high amino acid conservation. If this site is genuinely the target of Compound V2.3, its strong conservation across DENV serotypes and related orthoflaviviruses may support

the potential effectiveness of the compound against other DENV serotypes and related orthoflaviviruses and a relatively high genetic barrier to drug resistance.

Compound V2.3 is a potent inhibitor of infectious particle production and is predicted to bind NS1 at the dimerisation interface. Further research into the antiviral mechanism of action of this compound is warranted to unambiguously confirm the predicted interaction of the protein and ligand, and medicinal chemistry and computational modelling will be used to improve the antiviral efficacy and safety profile of the compound.

3.5 Summary

The aim of this chapter was to identify NS1-specific inhibitors of DENV. Three novel approaches were taken to achieve this. A luciferase-based thermal shift assay was developed, using our DENV2-NS1-NLuc reporter virus, to identify compounds which interact with NS1. A dimerisation assay was developed to identify inhibitors of NS1 dimerisation, and a virtual screen was performed with the same goal. The thermal shift assay and dimerisation assay were each selected due to their scalability, which would allow for high-throughput compound screening. Each *in vitro* screen was performed initially with 3,378 drug-like compounds, then structural analogues were tested in follow up screens.

Likely due to technical errors while screening, the hit compounds from the NanoBiT® Protein:Protein interaction screen were shown to be false positives. These hits were not investigated further. Interestingly, the NaLTSA high-throughput screen also appears to have produced false positives that stabilise NanoLuc luciferase rather than NS1 protein. Before validating an interaction with NS1, these compounds were tested for antiviral activity, revealing a group of structural analogues which inhibited DENV growth. Follow up experiments identified the lead hit, Compound 14, as a potent inhibitor of infectious particle production. Confocal microscopy studies revealed an effect of Compound 14 on E protein conformational epitope recognition, as well as on ER architecture. These effects will be further examined in future studies.

The virtual screen for inhibitors of NS1 dimerisation identified a compound, named Compound V2.3, which inhibits infectious particle production with nanomolar activity. Despite Compound V2.3 being predicted to bind the dimerisation interface of NS1, it did not appear to decrease NS1 dimerisation as determined using the NS1 NanoBiT dimerization assay. Additionally, the NaLTSA showed no evidence for an interaction of Compound V2.3 with NS1. Biophysical techniques including x-ray crystallography and surface plasmon resonance will be used to further explore the potential protein:ligand interaction of NS1 with Compound V2.3. If this interaction is confirmed, future studies will focus on characterising this interaction, and computational chemistry will be utilised to improve the binding and antiviral efficacy of the drug. If this interaction cannot be confirmed, structural analogues will be tested to optimise the compound for antiviral efficacy, and further experiments will be designed to explore the mechanism of action of this class of compound.

Chapter 4: Understanding viral determinants of dengue virus tropism and investigating the possibility of *Wolbachia*-resistant dengue virus

4.1.1 Introduction

The release of *Aedes* mosquitoes infected with specific *Wolbachia* strains has resulted in significant decreases in DENV infection rates in infection-prone areas spanning multiple countries(375). However, breakthrough infections still occur in communities that are otherwise protected via the *Wolbachia* strategy. While there is a significant reduction in DENV transmission potential for *Wolbachia*-infected mosquitoes, complete blocking does not occur(233). The interplay between the *Aedes* mosquitoes and *Wolbachia* genomes in the context of DENV blocking has been studied, and no evidence suggests evolution of either will hinder the success of *Wolbachia* programs(376, 377). However, the potential for DENV to evolve resistance against *Wolbachia*-mediated blocking has not been fully explored(242). Under experimental conditions, the DENV1 Envelope E203K and E384K mutants have displayed increased fitness in *w*Mel-infected *Aedes aegypti* mosquitoes(378). However, a reduction of viral fitness in *Wolbachia*-free mosquitoes is observed. Whether *Wolbachia*-resistant DENV will emerge in regions in which *Wolbachia*-infected mosquitoes have been released is unknown.

We sought to identify *Wolbachia*-resistant DENV2 mutants using deep mutational scanning. As discussed previously, deep mutational scanning is a technique that utilises deep sequencing technology in combination with a library of mutant genes or genomes produced by random or directed mutagenesis to probe the functional effects of mutations of many or all nucleotides within a gene or genome. Using a DENV2 infectious clone (16681), a pool of DENV2 mutants spanning prM, Envelope and NS1 was generated. The library of mutants was selected for fitness in cell culture using a mosquito cell line, C6/36, to ensure replication competency, and will soon be passaged in *w*Mel- and *w*AlbB-infected mosquitoes, as well as *Wolbachia*-free mosquitoes, to identify mutations which confer *Wolbachia* resistance. These libraries were also utilised in experiments to identify viral determinants of species-specific tropism of DENV2 replication in mosquito and human cell lines, however the results were inconclusive and further experiments will be required to identify mutations of interest.

Additionally, we prepared NS1-specific mutant libraries for a full-length DENV2 infectious clone as well as the corresponding DENV2 subgenomic replicon. Additional experiments with

these mutant viral genome libraries will allow for demarcation of residues required for viral RNA replication and for infectious particle production, in both human and mosquito cell lines.

4.2.1 Generation of a library of DENV2 mutants spanning prM, Envelope and NS1

4.2.2 Results

Multiple strategies were attempted for the construction of a library of DENV2 mutants spanning prM, Envelope and NS1. Initially, we sought to purchase a pool of mutated DNA fragments spanning the unique *Sal*I to *Kas*I restriction enzyme sites of the DENV2 (strain 16681) infectious clone pFK-DVs, as the prM, E and NS1 genes are present within this region (Figure 4.1.1). The ThermoFisher Scientific Gene Art Controlled Randomisation Service allows synthesis of a DNA region with a defined mutation rate. However, ThermoFisher Scientific were unsuccessful in the construction of this library due to a high frequency of recombination events in the synthesised regions. Our next strategy for the generation of mutants was to utilise an error-prone DNA polymerase, as discussed in Section 1.23, or the adapted review on deep mutational scanning. The region to be mutated is large (~3500 nucleotides). Accordingly, to allow for easier identification and quantification of mutations within a single genome and reduce the likelihood of introduction of multiple mutations in a single PCR-amplified DNA fragment, we aimed to achieve the mutagenesis in subsections of the ~3500 region. Initially, a strategy using multiple overlap extension PCRs was attempted(379) (Figure 4.1.2). The region between restriction enzyme recognition sites for *Sal*I and *Kas*I was split into 4 sections of ~900 nucleotides in length. Each section was amplified using primers with an overlap between subregions, using either Q5® High-Fidelity DNA Polymerase to minimise introduction of mutations, or with the error-prone DNA polymerase Mutazyme II. Subregions were labelled A, B, C and D if amplified with Q5, or a, b, c and d if amplified with Mutazyme II. Multiple overlap extension PCR would then allow production of aBCD, AbCD, ABcD and ABCd DNA fragments, which could then be reintroduced into the digested pFK-DVs backbone either by standard restriction enzyme cloning or DNA Assembly. While the multiple overlap extension PCR appeared to produce combined fragments of the expected size, due to inefficient cloning and unexplained restriction enzyme digest patterning, this method was deemed unsuitable for production of the library.

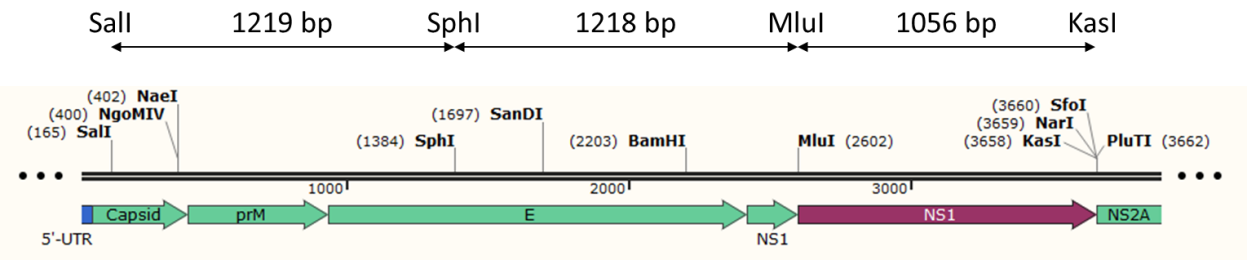

Figure 4.1.1: Schematic of the DENV2 infectious clone pFK-DVs, displaying the 5' UTR, capsid, prM, E, NS1 and NS2A. Distances between the restriction enzyme digest recognition sites for *Sal*I, *Sph*I, *Mlu*I and *Kas*I are displayed.

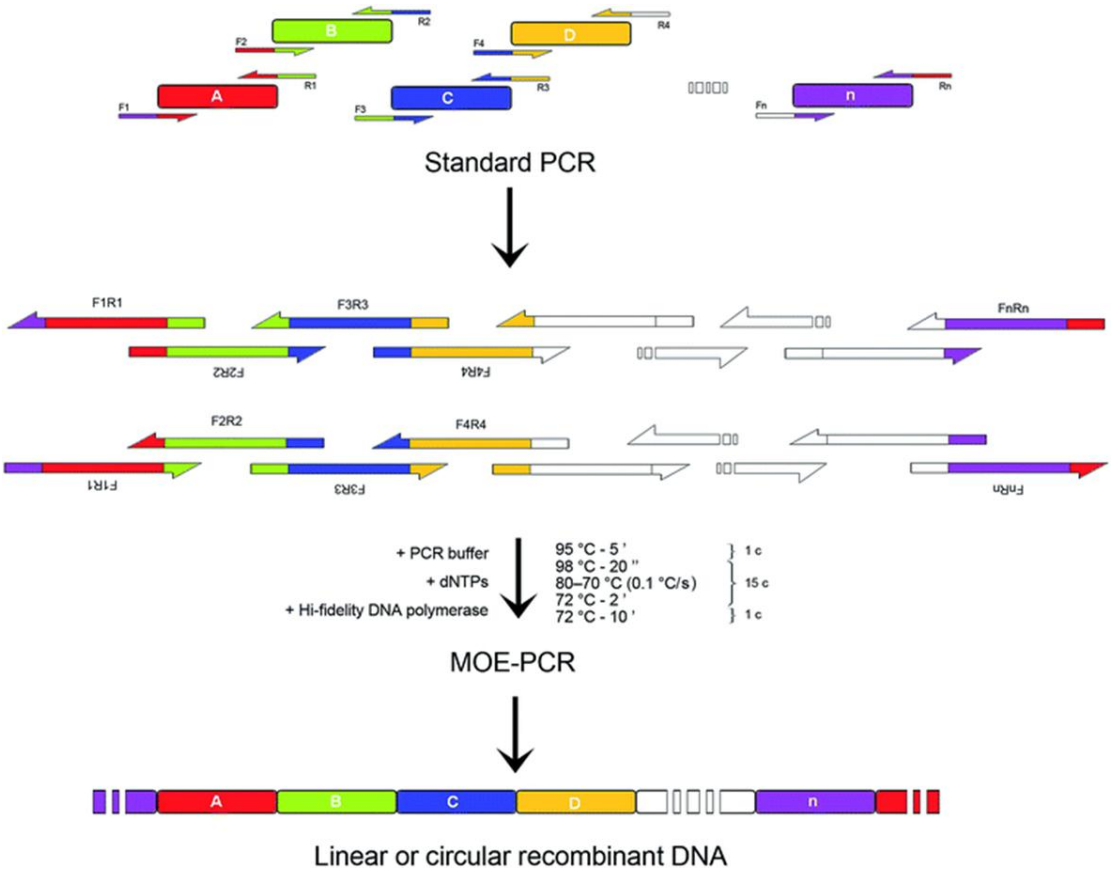

Figure 4.1.2: Schematic diagram illustrating the process of hybridising fragments using Multiple Overlap Extension PCR (MOE-PCR). In the Standard PCR cycle, Each DNA fragment is amplified using primers which allow for hybridisation with the adjacent DNA fragments. In MOE-PCR, amplification occurs using each amplified fragment as the template, allowing for construction of linear or circular recombinant DNA containing all DNA fragments in the correct order and orientation. Source: (380).

Between the *Sal*I and *Kas*I restriction enzyme recognition sites, additional sites for *Sph*I and *Mlu*I are present. Genomic regions from *Sal*I to *Sph*I and *Sph*I to *Mlu*I restriction sites each span ~1200 nucleotides, while the region between *Mlu*I and *Kas*I restriction sites spans ~1050 nucleotides (Figure 4.1.1). We attempted amplification of these 3 regions with the error-prone DNA polymerase Mutazyme II. To generate mutations in a region at a specific frequency, the number of amplification cycles, as well as the amount of DNA input can be modified(381). For this project, to reduce the occurrence of confounding epistatic mutations, and allow for the determination of single mutants promoting resistance to *Wolbachia*, we aimed for an average of 0-2 mutants per DNA fragment. As pFK-DVs is a large plasmid and multiple repetitive sequences are present, it was not practical to amplify each of the three regions (*Sal*I to *Sph*I, *Sph*I to *Mlu*I and *Mlu*I to *Kas*I) using Mutazyme II and the entire plasmid as the template, due in part to the large mass of DNA required to introduce a small number of mutations per kilobase. Instead, three unique DNA fragments of approximately 2000 base pairs were amplified using Q5® High-Fidelity DNA Polymerase, to generate a template for each of the three regions. These ~2000 base pair DNA fragments were then amplified using Mutazyme II. Primers utilised initially were designed to allow for reinsertion into pFK-DVs via NEBuilder HiFi DNA Assembly, however this approach did not yield successfully transformed NEB® Stable Competent *E. coli*. Standard restriction cloning by ligation was similarly unsuccessful. In contrast, an indirect approach involving amplification of these mutant fragments with primers designed to facilitate insertion of each fragment into a digested pUC57 shuttle vector via NEBuilder HiFi DNA Assembly was highly efficient, and it was therefore decided to use this shuttle vector approach towards generation of corresponding mutant libraries. Following testing of several conditions, a 19 cycle Mutazyme II PCR with 175 nanograms of target DNA was selected for production of DNA fragments with 0-2 mutations present. After their insertion, DNA fragments were sequenced in these pUC57-*Sal*I-*Sph*I, pUC57-*Sph*I-*Mlu*I and pUC57-*Mlu*I-*Kas*I vectors for analysis of mutational frequency.

Ligation products for the three mutant DNA regions inserted into correspondingly digested pUC57 shuttle vectors were then transformed into NEB® Stable Competent *E. coli*. Bacteria were grown on 15 cm ampicillin-containing LB agar plates, and all colonies were pooled in Luria broth before purification of the plasmid, with each of the three final vectors purified separately. Plasmids from individual colonies were also purified, and the presence of each

subregion (*Sal*I to *Sph*I, *Sph*I to *Mlu*I and *Mlu*I to *Kas*I) was confirmed via restriction enzyme digest and gel electrophoresis (Figure 4.1.3), before sequencing to ensure presence of mutations. Approximately 5,000,000 clones were purified for each subregion, as inferred by colony counting for serially diluted transformed bacteria for each transformation.

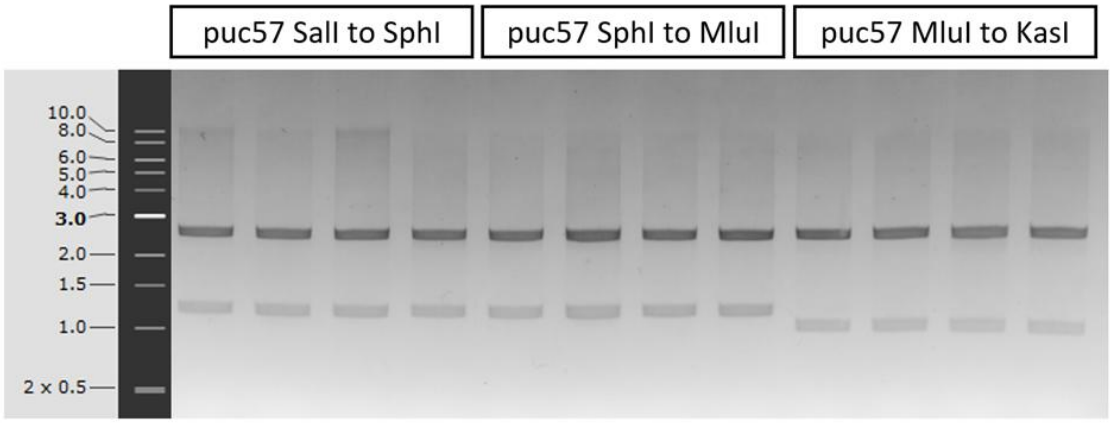

Figure 4.1.3: Purified pUC57 clones with each mutated subregion inserted. Each clone was digested with the corresponding restriction enzymes. Bands represent expected sizes of the inserted subregions (1219, 1218 and 1056 base pairs for *Sal*I to *Sph*I, *Sph*I to *Mlu*I and *Mlu*I to *Kas*I, respectively). 1 Kb Plus DNA ladder used. 4 individual clones for each insertion are displayed. Visualised by gel electrophoresis.

To reintroduce these mutated DNA fragments into pFK-DVs, we initially attempted to employ NEBuilder HiFi DNA Assembly. Despite the absence of colonies in the backbone-only control transformation, only ~50% of colonies contained the insert upon inspection via diagnostic restriction enzyme digest (Figure 4.1.4). We then attempted insertion by restriction cloning, in which each of the three pUC57 libraries (containing mutated *Sal*I to *Sph*I, *Sph*I to *Mlu*I and *Mlu*I to *Kas*I fragments) were digested with their corresponding restriction enzymes, and inserted into pFK-DVs plasmid that was also digested with those respective enzymes. This ligation was optimised for each reaction, with backbone:insert molar ratios of 1:1, 1:3 and 1:3 for *Sal*I/*Sph*I, *Sph*I/*Mlu*I and *Mlu*I/*Kas*I fragments, respectively, and a large-scale transformation successfully generated 100,000 to 200,000 uniquely transformed plasmids per subregion, which were separately purified. Due to the instability of the DENV2 cDNA genome in *E. coli*, recombination of the plasmid can occur(382). This event can typically be observed by a size difference between bacterial colonies harbouring recombined (large) or intact (small)

plasmid. To minimise the frequency of unwanted recombination events, transformations were optimised to a 30 °C, 40 hour incubation, which was observed to result in fewer large colonies. However, as many recombined colonies remained, each larger colony was removed physically with a pipette tip prior to collection. Recombined colonies were selected for removal by identifying and marking any colonies visible at 24 hours post-transformation. An *Eco*RI restriction enzyme digest of purified plasmid from each subregion transformation resulted in DNA banding patterns that closely reflected those of similarly digested wild-type pFK-DVs, with the exception of a faint band present at ~3.5 kb for the *Sph*I to *Mlu*I and *Mlu*I to *Kas*I subregions, which likely represents a minimal amount of remaining recombined plasmid (Figure 4.1.5). The overall process is outlined in Figure 4.1.6. The final mutation rates for each region were 0.6, 1.1 and 0.7 mutants for the *Sal*I to *Sph*I, *Sph*I to *Mlu*I and *Mlu*I to *Kas*I subregions, respectively (Table 4.1.1).

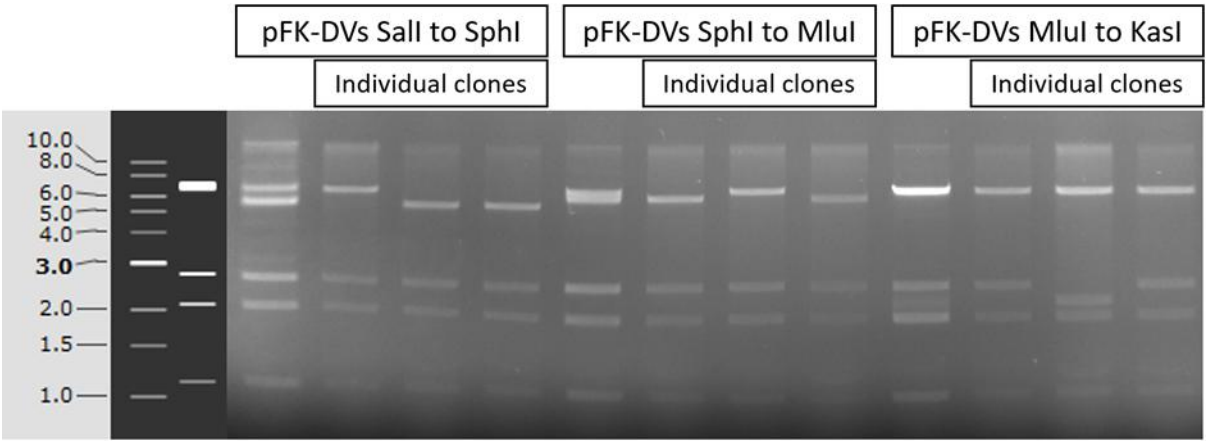

Figure 4.1.4: Mutant libraries and uniquely transformed bacterial colonies produced by PCR-amplified pUC57 *Sal*I-*Sph*I, *Sph*I-*Mlu*I and *Mlu*I-*Kas*I regions inserted into a digested pFK-DVs backbone, via NEBuilder HiFi DNA Assembly. For each subregion, the pooled library is shown, followed by three purified clones. 1 Kb DNA ladder (NEB) was used to approximate the sizes of DNA fragments. A separate simulated restriction digest ladder shows the theoretical banding pattern of pFK-DVs when digested with *Eco*RI. DNA bands were separated and visualised by agarose gel electrophoresis.

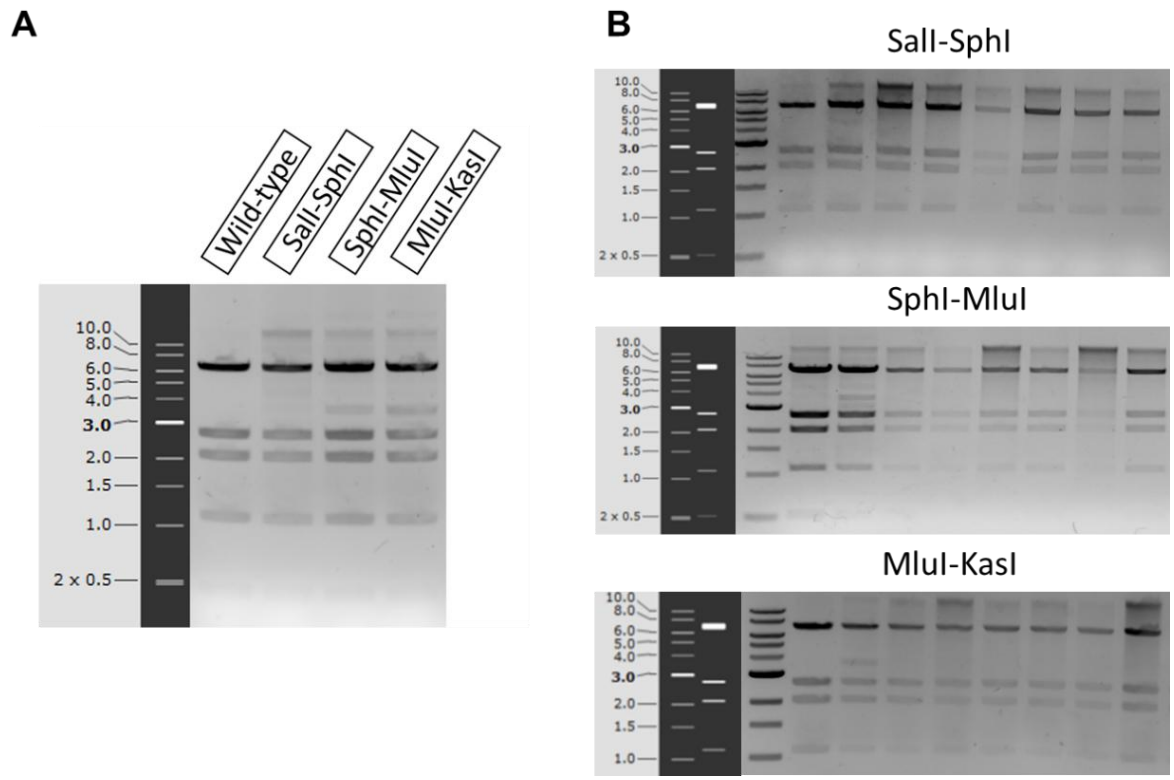

Figure 4.1.5: A) Purified, combined final pFK-DVs mutant libraries and comparative wild-type pFK-DVs digested with restriction enzyme *Eco*RI. B) Individual purified pFK-DVs clones with mutated regions inserted at the specified restriction enzyme digest sites. Samples were digested with restriction enzyme *Eco*RI. 1 Kb DNA ladder (NEB) was used to approximate the sizes of DNA fragments. A separate simulated restriction digest ladder shows the theoretical banding pattern of pFK-DVs when digested with *Eco*RI. DNA bands were separated and visualised by agarose gel electrophoresis.

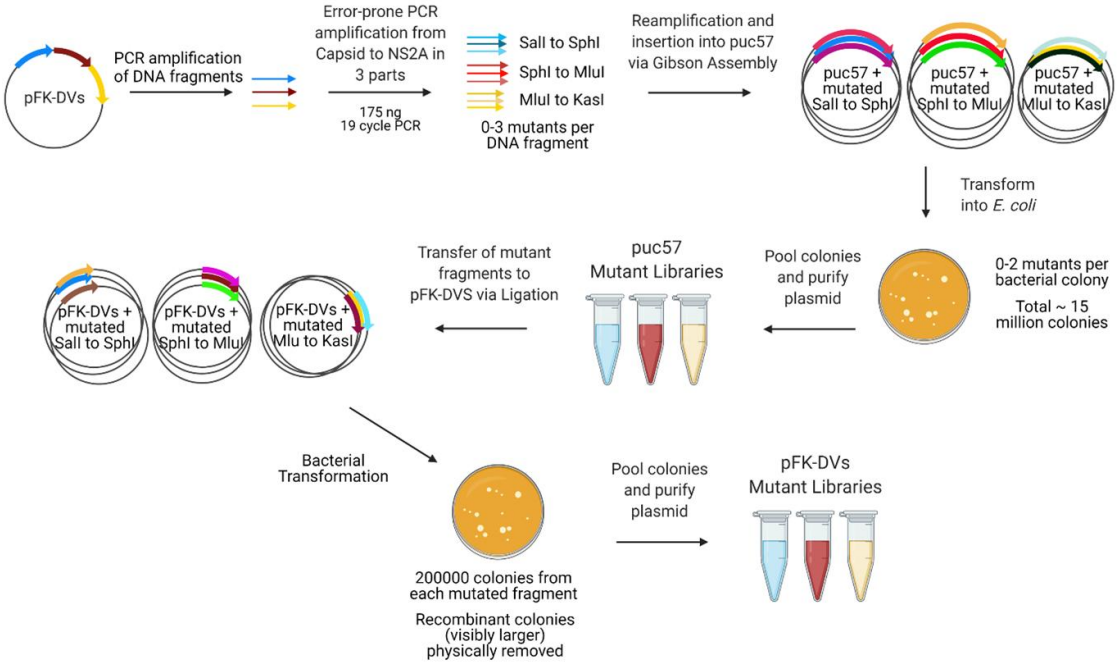

Figure 4.1.6: Outline of the pFK-DVs mutant library generation cloning process

Table 4.1.1: Mutants present in pFK-DVs mutated regions from a selection of clones.

Clone	1	2	3	4	5	6	7	8	9	10	Average
SalI to SphI Mutant Count	1	3	0	0	0	0	1	0	0	1	0.6
SphI to MluI Mutant Count	0	3	0	1	1	0	4	0	0	2	1.1
MluI to KasI Mutant Count	1	1	0	0	0	1	0	2	1	1	0.7

Each pooled plasmid library was linearised and used as a template for *in vitro* RNA transcription using the SP6 RNA Polymerase, alongside wild-type pFK-DVs. Wild-type DENV2 RNA and RNA from the three mutated DENV2 libraries was then individually transfected into C6/36 cells. The wild-type DENV2 and DENV2 library with mutations spanning *Sal*I to *Sph*I showed an approximate 10-fold higher infectious virus titre across 48-144 hours post-transfection, as compared to the *Sph*I/*Mlu*I and *Mlu*I/*Kas*I DENV2 mutant libraries, as determined via focus forming assays (Figure 4.1.7).

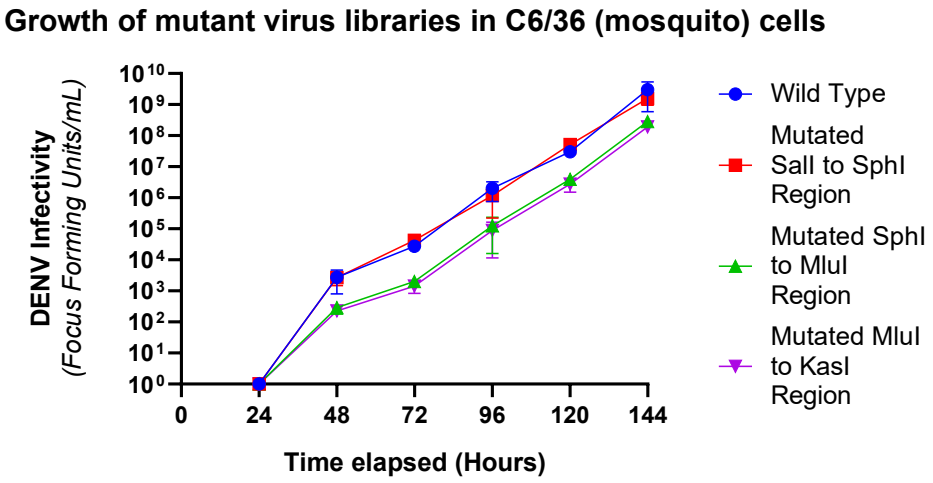

Figure 4.1.7: Kinetics of infectious virus production by wild-type DENV2 and mutant DENV2 libraries. I*n vitro* transcribed RNA for wild-type DENV2 and DENV2 mutant libraries was transfected into C6/36 cells. At the indicated time points cell culture supernatant samples were collected and stored at -80 °C, prior to determination of infectivity by focus-forming assays. Data are means ± S.D. (n = 3).

Following the demonstration that each mutant library displayed similar degrees of mutation and enabled comparable infectious virus production levels, the mutant libraries were combined in equimolar amounts, linearised and used as a template for *in vitro* RNA transcription. This RNA was transfected into both Huh7.5 and C6/36 cells, alongside wild-type DENV2 RNA. At 6 days post-transfection, virus-containing supernatants were collected (p0), and titrated using naïve Huh7.5 cells (Table 4.1.2). Viruses were successively passaged onto naïve Huh7.5 or C6/36 cells at an M.O.I. of 0.1, with titration of infectivity performed using Huh-7.5 cells. After collection of virus-containing supernatants, total RNA was extracted from remaining cell monolayers. Together, RNA was collected from the initial *in vitro* RNA transcription reaction, and from cell monolayers for the transfected cells (p0), and subsequent infections p1, p2 and p3.

Table 4.1.2: Infectious virus titres of mutant library DENV2 and wild-type DENV2 following transfection and passage experiments, as determined by focus forming assays using Huh7.5 cells.

	Wild Type 1	Wild Type 2	Wild Type 3	Mutant Library 1	Mutant Library 2	Mutant Library 3
C6/36						
p0	1.5*10^6	2.92*10^6	4.92*10^6	9.17*10^5	8*10^5	1.67*10^6
p1	1.92*10^8	1.25*10^8	2.17*10^8	7.42*10^7	8.42*10^7	9.33*10^7
p2	2.75*10^6	-	-	3*10^6	2*10^6	2.75*10^6
Huh7.5						
p0	1.67*10^6	-	-	2.17*10^6	2.67*10^6	2.83*10^6
p1	2*10^6	-	-	1.25*10^6	1*10^6	1.5*10^6
p2	2.5*10^6	-	-	4.25*10^6	2.25*10^6	3.75*10^6

4.2.3 Sequencing of DENV2 mutant libraries following passage in Huh-7.5 and C6/36 cells

4.2.4 Results

For the following results, all Oxford Nanopore Technology sample preparation and sequence analysis was performed by Dr Chaturaka Rodrigo, Associate Professor Rowena Bull and David Agapiou (UNSW, Sydney, Australia). All Illumina short-read sample preparation and sequence analysis was performed by Veronica Perera, Dr Kathryn Edenborough and Dr Johanna Fraser (Monash University, Melbourne, Australia).

Firstly, we sought to analyse the mutational landscape of the virus in both the mammalian and insect cell lines. Purified RNA from Huh7.5 and C6/36 cells following the initial transfection (p0), the first infection passage (p1), the third infection passage (p3) and the *in vitro*-transcribed RNA inputs were sent to collaborators at UNSW for analysis via Oxford Nanopore Technology (ONT) sequencing. ONT was selected to allow for identification of epistatic mutations across the entire DENV2 genome(383). Reverse transcriptase was used to generate cDNA from the purified RNA, and near full-length amplicons were generated by PCR, as per published protocol(383). Gel electrophoresis was used to detect amplification (Figure 4.2.1) and, following gel purification of bands and regions that corresponded to the expected size of full-length amplicons, the samples were submitted for ONT sequencing. Table 4.2.1 displays the DNA concentration of the prepared samples. Unfortunately, the resulting ONT data was unusable for the purpose of this study due to low read counts, making variant and epistasis analysis inconclusive. The DNA concentrations were much lower than expected, indicating poor amplification from cDNA. This could be resultant of the RNA template being of low quality, the reverse-transcriptase reaction being inefficient, or due to issues with the long-range PCR reaction. As the virus was quantified via focus forming assay (Table 4.1.2) and Sanger sequencing was used to ensure acceptable numbers of mutations (Table 4.1.1), it is unlikely that the sequencing issues arose before extraction of RNA from infectious virus-

containing supernatant. These samples are currently being prepared for Illumina sequencing, in which the DENV2 genome will be amplified in 6 regions.

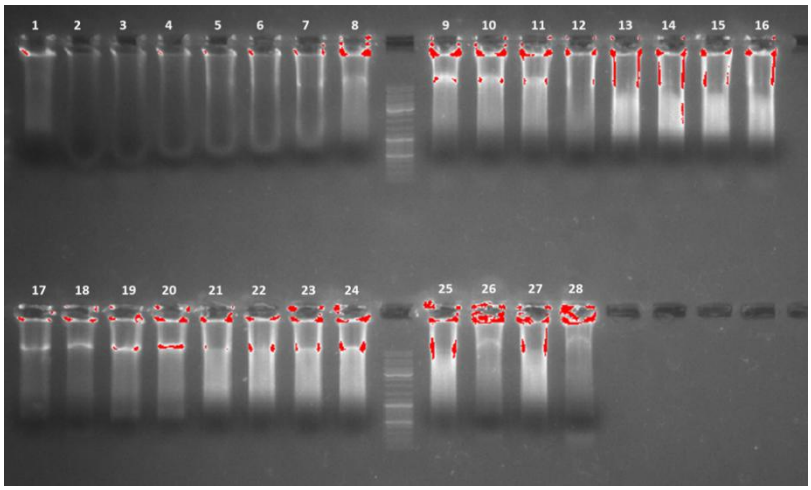

Figure 4.2.1: Agarose gel electrophoretic analysis of full-length DENV genome amplicons, prepared for mutational frequency analysis using Oxford Nanopore Technology. Huh-7.5 cells and C6/36 cells were transfected with wild-type DENV2 or mutant library DENV2 RNA, generated using *in vitro* RNA transcription, then supernatants were collected, clarified and used to infect naïve cell lines. This was repeated two additional times. At 6 days post-infection/post-transfection, total RNA was purified from cell monolayers. Following RT-PCR, near full-length amplicons were visualised via gel electrophoresis prior to gel purification of amplicons for ONT sequencing (red highlighting indicates saturated pixels).

Table 4.2.1: DNA concentrations of full-length DENV genome amplicons, prepared for mutational frequency analysis using Oxford Nanopore Technology

	Sample	Concentration (ng/µL)
1	C6/36-WT-P0	1.9
2	C6/36-ML1-P0	1.6
3	C6/36-ML2-P0	1.7
4	C6/36-ML3-P0	1.5
5	Huh7.5-WT-P0	3.9
6	Huh7.5-ML1-P0	0
7	Huh7.5-ML2-P0	4.9
8	Huh7.5-ML3-P0	4
9	C6/36-WT-P1	3.6
10	C6/36-ML1-P1	4.1
11	C6/36-ML2-P1	4.4
12	C6/36-ML3-P1	2.9
13	Huh7.5-WT-P1	12
14	Huh7.5-ML1-P1	8.5
15	Huh7.5-ML2-P1	6.4
16	Huh7.5-ML3-P1	8.5
17	C6/36-WT-P3	3.2
18	C6/36-ML1-P3	4.2
19	C6/36-ML2-P3	2
20	C6/36-ML3-P3	2
21	Huh7.5-WT-P3	14.3
22	Huh7.5-ML1-P3	8
23	Huh7.5-ML2-P3	8.7
24	Huh7.5-ML3-P3	8.3
25	C6/36-WT-Input-RNA	13.5
26	C6/36-ML-Input-RNA	4.1
27	Huh7.5-WT-Input-RNA	9.2
28	Huh7.5-ML-Input-RNA	2.8

While ONT sequencing of these samples was unsuccessful, infectious virus (p1) was sent to collaborators at Monash University for studies that ultimately sought to identify mutations in prM, E and/or NS1 that altered the sensitivity of DENV to *Wolbachia*-mediated suppression. Performed by Veronica Perera from Monash University, this infectious virus was further propagated in the Aag2 insect cell line for 7 days. For sequencing sample preparation, RNA was extracted from infectious supernatant and used as template for cDNA synthesis, as detailed in Section 2.32. High-fidelity PCR using two pools of primers was then used to amplify the entire genome, and resulting amplicons were processed for purification and size selection, as detailed in Section 2.32. After normalising concentration of samples, DNA was tagmented,

dual indices were added and samples were again subjected to purification and size selection. A commercially available library quantification system for Illumina platforms was then used to allow standardisation of concentration across samples. The library was denatured with a 1% PhiX spike-in, and samples were then loaded into an Illumina MiSeq sequencer and the standard sequencing protocol was followed.

After trimming of paired-end reads, as described (384), and removal of PCR primers and low quality regions as described in reference (385), Illumina paired reads were mapped to the DENV2 genome (NC_ 001474.2). Regions with <100 reads per location were excluded, then variants were identified using Geneious software. When detecting variants at >10% frequency across the genome, 22 variants in wild-type DENV2 were identified and 42 variants in the DENV2 mutant library were identified. Repeating the analysis for variants at >1% frequency, 119 variants in wild-type DENV2 were identified, and 211 variants were identified in the DENV2 mutant library (Figure 4.2.2). While this number of mutants was lower than expected, the virus had been amplified in C6/36 cells for 12 days and in Aag2 cells for a further 7 days, which would likely result in the removal of less fit variants that were present in the *in vitro*-transcribed RNA input. Multiple mutations appeared throughout the genome in both the wild-type DENV2 and DENV2 mutant library, outside of the areas which were deliberately mutated. Surprisingly, 5 additional mutations were identified throughout the NS3 gene in the mutant library, at >10% frequency, compared to wild-type DENV2. Whether these were rescue mutations, selected in response to mutants in the prM-E-NS1 region, or adaptive mutations to the Aag2 cell line which did not happen to occur in the wild-type infection, is unknown. Due to time constraints, mosquito infections using the C6/36 p1 supernatants, for both wild-type and mutated virus, remain to be performed.

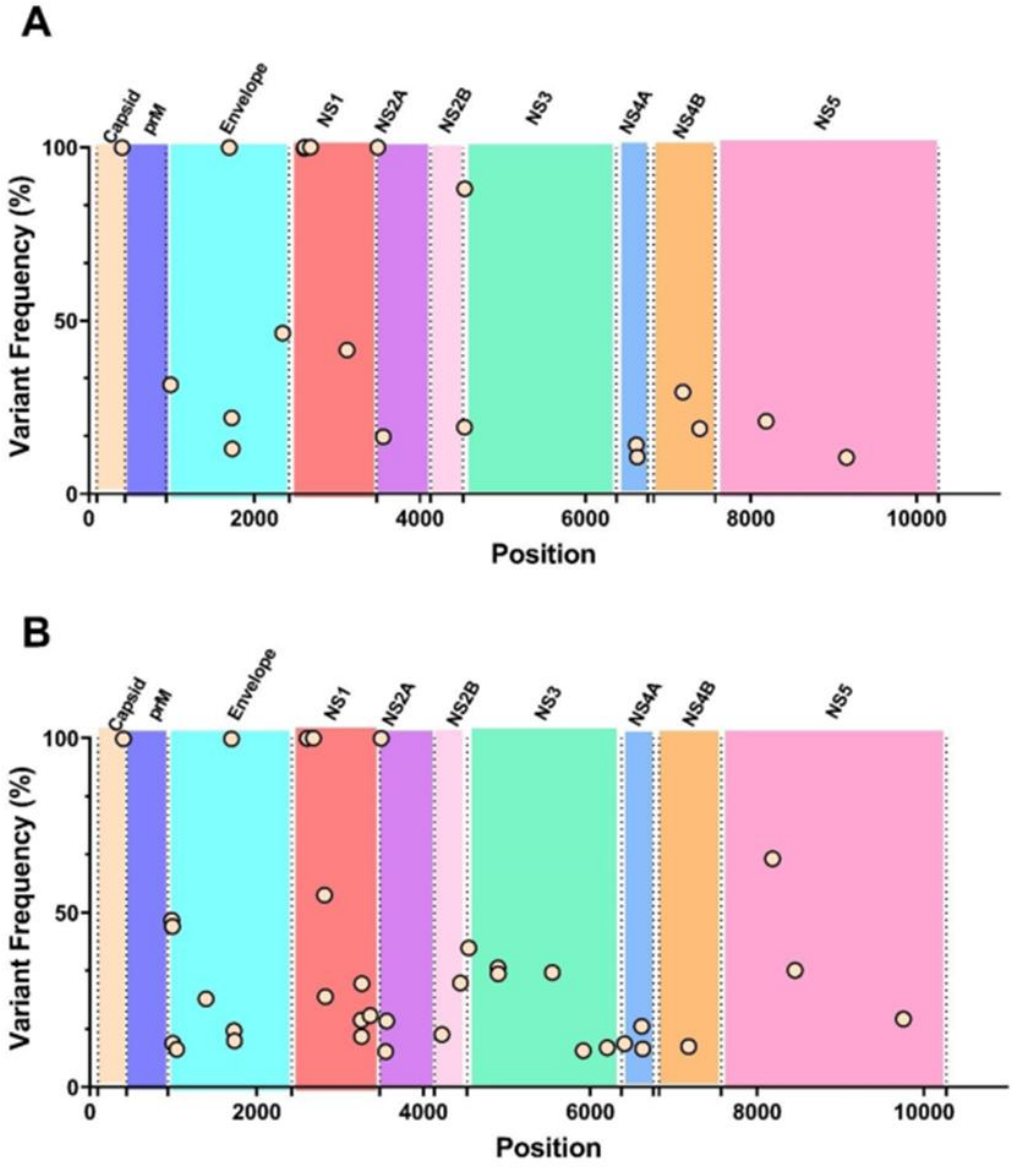

Figure 4.2.2: Frequency of mutations in DENV2 wild-type (A) and mutant library (B) virus stocks. DENV wild-type and mutant IVT RNA libraries were transfected into C6/36 cells. At 6 d.p.i., supernatants were collected, titred in Huh7.5 cells via focus forming assay and used to infect naïve C6/36 cells at an MOI of 0.1. The virus was then further propagated in *Aag2* cells for 7 days. RNA was harvested from the infectious supernatant, with reverse transcription utilised to generate cDNA. PCR amplicons were then generated and sequenced via Illumina short-read sequencing. The reads were mapped to the DENV2 genome (strain 16681) and all SNPs, insertions and deletions above a 10% threshold were identified and displayed. Variant frequency is displayed on the y-axis, and nucleotide position along the DENV2 genome is displayed on the x-axis.

4.2.5 Generation of a library of NS1 mutants for the DENV2 full-length infectious clone and a DENV2 subgenomic replicon

4.2.6 Results

In addition to the E, prM and NS1 mutant library, mutant libraries were also prepared to allow for identification of residues of NS1 that are required for infectious particle production and/or viral RNA replication. As mentioned previously, there have been several mutational analyses of specific NS1 residues, examining their importance in dimerisation(164-166), viral RNA replication and virus production(145), NS1 secretion(364) and NS1 interaction with endothelial cells(169). However, these studies have generally focussed on small subsets of NS1 residues, typically selected based on disulphide bonding sites, glycosylated residues, hydrophobicity, or NS1 conservation between dengue serotypes and other orthoflavivirus species. To examine the involvement of NS1 residues in both viral RNA replication and infectious particle production, we prepared additional mutant libraries for pFK-DVs, a full-length DENV2 infectious clone (strain 16681), and for pFK-sgDVs, a derivative DENV2 subgenomic replicon of the same strain. In each case, mutants were introduced in NS1 using error-prone PCR.

As these libraries were constructed using similar methods to those employed in the generation of the E, prM and NS1 mutant libraries described above, the approaches employed in the preparation of the NS1-specific mutant libraries are only briefly described below. For pFK-DVs, restriction enzymes *Bam*HI and *Kas*I were used to isolate a DNA fragment containing the entire NS1-coding sequence and the flanking regions encoding the C-terminus of E (a.a. 423-485) and the N-terminus of NS2A (a.a. 1-62). This 1455 bp fragment was then amplified with Mutazyme II DNA polymerase, using 250 ng of template DNA and a 30 cycle PCR, as per manufacturer's protocol. The resulting amplicon was gel purified, digested with *Bam*HI and *Kas*I and inserted into similarly digested pUC57 shuttle vector via restriction cloning and ligation as detailed in Section 2.28. Ligation products were transformed into NEB® Stable Competent *E. coli* cells *en masse* and plasmid DNA was extracted. Following liberation of the NS1-encoding DNA fragment via restriction digest (*Bam*HI/*Kas*I) and high fidelity amplification of the corresponding pFK-DVs backbone, NEBuilder HiFi DNA Assembly was then used to assemble the desired full-length pFK-DVs plasmid containing the mutagenized NS1-encoding region. Three libraries were individually prepared, featuring ~578000, 866000 and 713000 colonies. Sanger sequencing analysis revealed that 4/15 clones from uniquely transformed

bacterial colonies contained mutations (1-4 mutations per clone), with 5 colonies tested per library (Table 4.3.1).

Table 4.3.1: Number of mutations present in pFK-DVs NS1 from a selection of clones across the three libraries.

Clone	1	2	3	4	5	Average
First Library Mutant Count	1	0	4	1	1	1.4
Second Library Mutant Count	0	0	1	1	1	0.6
Third Library Mutant Count	2	0	0	1	2	1

Due to the unavailability of the same unique restriction sites, a different approach was used for pFK-sgDVS-R2A NS1 mutant library construction. Firstly, error prone PCR was employed to yield a fragment encoding mutagenized NS1, the upstream 2A protease cleavage site and C-terminus of E (a.a. 461-485) and downstream N-terminus of NS2A (a.a. 1-62). This amplicon was gel purified and digested using restriction enzymes *Age*I and *Kas*I, allowing for direct reinsertion into the similarly digested pFK-sgDVs-R2A backbone by ligation. The ligation product was electroporated into electrocompetent *E.coli* cells *en masse*, before pooling of bacterial colonies and plasmid DNA extraction. Three plasmid DNA libraries were prepared that were derived from approximately 150,000 bacterial colonies each.

For full-length DENV2, wild-type pFK-DVs and each pFK-DVs-derived mutant library were linearised and used as a templates for *in vitro* RNA transcription. RNA products were then purified and transfected into Huh7.5 cells for analysis of infectious virus production. Huh7.5 cells were transfected with RNA from the three mutant libraries as well as wild type DENV2. Supernatant samples were collected at 24, 48, 72, 96 and 120 hours post-transfection, and titred by focus forming assay using Huh7.5 cells. The mutant libraries produced replication competent, infectious virus, although showed a slight reduction in fitness for the first 96 hours when compared to wild type DENV2 (Figure 4.3.1 A).

As the subgenomic replicon DENV2 clone is incapable of infectious particle production, a *Renilla* luciferase assays were performed to measure replication competence of the respective subgenomic replicon mutant RNA pools. Wild type pFK-sgDVs-R2A, the mutant libraries and a GND mutant (viral RNA replication-incompetent) were linearised and used as a template for *in vitro* RNA transcription. RNA samples were then purified and transfected into Huh7.5 cells.

Renilla luciferase activity was measured in parallel samples that were lysed and frozen at 3, 24, 48 and 72 hours post-transfection. As demonstrated, replicon-encoded luciferase activities were comparable for each mutant library and the wildtype control, with the exception of a moderate but appreciable reduction of viral replication levels for each of the mutant libraries compared to the wildtype replicon at 48 hours post-transfection, indicating robust but slightly attenuated replication of mutant subgenomic replicon pools (Figure 4.3.1 B).

In future experiments, these libraries will be further used in transfection experiments, with full-length samples to be passaged once into naïve Huh-7.5 cells. Through analysis of mutant variant abundance via RT-PCR and NGS analysis, it is hoped that the resulting data will enable mapping of the *in vitro* functional significance of a large number of NS1 residues in Huh-7.5 cells, and enable demarcation of residues that are required for viral RNA replication from those required for infectious particle production.

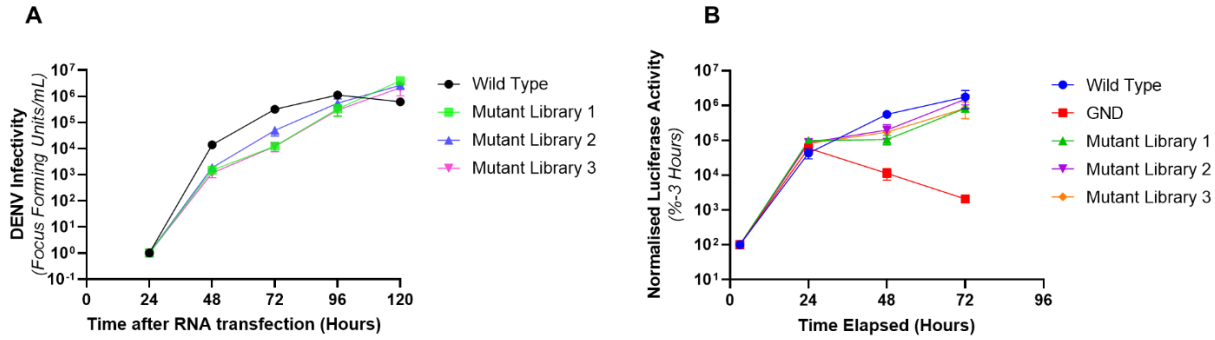

Figure 4.3.1: Assessment of growth of the NS1-focussed pFK-DVs and pFK-sgDVs-R2a mutant libraries. A) Wild type and mutant pFK-DVs libraries were linearised and used as a template for *in vitro* RNA transcription. The RNA was then transfected into Huh-7.5 cells. At 3, 24, 48, 72, 96 and 120 hours post-transfection, supernatant samples were collected and stored at -80 °C, prior to analysis of virus infectivity by focus forming assays. Data are means ±S.D. (n=3). B) Wild type and mutant pFK-sgDVs-R2A subgenomic replicon libraries, as well as the replication-incompetent GND mutant, were linearised and used as a template for *in vitro* RNA transcription. The RNA was then purified and transfected into Huh-7.5 cells. Cell monolayers were harvested at 3, 24, 48, 72 and 96 hours post-transfection. *Renilla* luciferase levels were determined and expressed as a percentage of average values for each group at 3-h time points. Data are means ± SD (n=3).

4.3 Discussion

The use of *Wolbachia*-infected mosquitoes has been incredibly successful in reducing the spread of dengue virus in multiple countries(235, 375, 386, 387). Research has demonstrated that the *Wolbachia* genome is stable in *Aedes aegypti* mosquitoes(377), and the fitness of mosquito hosts that diminish *Wolbachia*-mediated blocking is impaired, indicating that changes to the *Aedes aegypti* genome are not likely to hinder the success of *Wolbachia* programs(240). Due to the propensity of RNA viruses to adapt to antiviral pressures, there is potential for dengue virus to overcome *Wolbachia*-mediated suppression. It has previously been shown using a serial passage system that the E protein mutant E203K is positively selected in the presence of the *w*Mel *Wolbachia* strain, however this mutation is accompanied by a decrease in viral replicative fitness in the absence of *w*Mel, compared to the wild-type virus(251). Whether this decrease in fitness can be rescued with additional mutations has not yet been investigated and it is possible that multiple viral mutations that alter the susceptibility of DENV to *Wolbachia*-mediated suppression remain to be identified.

We sought to identify DENV mutations in the E, prM and NS1 genes which may confer resistance to *Wolbachia*-based suppression. Unlike the serial-passage system(251), we utilised error-prone PCR to generate libraries of mutant DENV. These virus libraries were passaged in both human (Huh-7.5) and *Aedes albopictus* mosquito (C6/36) cells. Supernatant from the C6/36 cells was then used to infect Aag2 cells, an *Aedes aegypti*-derived clonal mosquito cell line(388). Illumina short-read sequencing was then used for the analysis of viral RNA collected from the Aag2 supernatant. The analysis revealed higher mutational frequency from the mutant virus library compared to the wild type library.

A 77% increase in variant frequency in passaged mutant library viral RNA samples compared to wild-type viral RNA samples was observed when a threshold variant frequency of 10% was applied. This variant frequency in passaged mutant library viral samples, compared to wild-type samples, increased to 90% when the threshold variant frequency was lowered to 1%. Due to time constraints, studies utilising the C6/36-grown, once-passaged ‘p1’ virus stocks to infect mosquitoes have not yet been performed. In future experiments, the p1 virus will be passaged through *Aedes aegypti* mosquitoes 20 times, for both *Wolbachia*-infected and *Wolbachia*-free mosquitoes, using both *w*Mel and *w*AlbB strains of *Wolbachia*. Illumina short-read sequencing will be used to identify variants which specifically confer resistance to

Wolbachia-mediated suppression, demarcated from variants which increase general replicative fitness in mosquitoes. These variants will then be reinserted into the DENV2 infectious clone, and their resistance to *Wolbachia* will be verified.

In addition to the identification of *Wolbachia*-resistant variants, we also aimed to identify viral determinants of DENV2 host species tropism in human and mosquito cell lines using the same mutant libraries. As stated, wild type and mutant DENV2 libraries were passaged in both Huh-7.5 and C6/36 cell lines multiple times. RNA was harvested from the transfected cells (p0), as well as from the 1st passage (p1) and 3rd passage (p3), and from the input RNA from the *in vitro* transcription reaction. ONT sequencing was selected to allow for interrogation of near-full length DENV2 genomes, ensuring that epistatic mutations would not cause confounding effects. Unfortunately, this sequencing was unsuccessful, with an average read count of ~500 per sample. As such, this data was not reliable for further analysis. As the mutational frequency of multiple clones had been tested by Sanger sequencing (Table 4.1.1), and the libraries showed production of viral particles by focus forming assay (Table 4.1.2), it appears that the issues with sequencing arose during the preparation of RNA or cDNA, or during the sequencing reaction. RNA was extracted from virus-containing supernatant using a standard phenol-chloroform method with the TRIzol reagent. While 260/280 ratios indicated successful extraction of high-quality RNA in each sample, specific viral RNA extraction kits would likely yield viral RNA with higher consistency in quality, and allow for greater removal of contaminants such as PCR-inhibitors, phenol, guanidine or other reagents. As the long PCR was performed by collaborators prior to sequencing, this was not optimised to ensure efficient amplification of samples. While we sought to sequence the entire DENV2 genome from individual amplicons to allow analysis of epistatic effects, future ONT-based studies of this nature may benefit from the sequencing of smaller viral amplicons that are more reliable and efficient to generate. While the sequencing approach employed here has been successfully utilised to generate consensus viral genome sequences from patient samples(389), it may not be well-suited for quantitative viral variant analysis given inefficient amplification of full-length virus sequences and potential associated confounding effects. We will be repeating NGS analysis of these samples using Illumina short-read sequencing, and individual mutants of interest will be reintroduced into the pFK-DVs vector to analyse their impact on viral fitness in C6/36 and Huh7.5 cells.

To analyse the contribution of each NS1 residue to both infectious particle production and viral RNA replication, we constructed libraries containing NS1 mutants in both the DENV2 full-length infectious clone, pFK-DVs, as well as the corresponding subgenomic replicon, pFK-sgDVs-R2A. While these libraries were tested for viral replicative fitness, no further experimentation or sequencing was performed due to time constraints. Huh7.5 and C6/36 cells will be transfected with these libraries, alongside wild type RNA, and for the full-length virus we will perform one subsequent passage. Using Illumina sequencing and comparisons of variant frequencies in resulting viral sequences compared to initial 'input' viral sequences, it is hoped that these studies will generate a map of the functional significance of a large number of NS1 residues, in mammalian and mosquito cells, demarcating residues required for viral RNA replication from those that are required for infectious particle production. Mutant residues of significance, revealed by the sequencing results, will be reintroduced into full-length and subgenomic replicon DENV clones, and their impact on the viral lifecycle will be investigated.

5 Final Discussion

Despite causing a major global health burden each year, there is not yet an approved antiviral treatment for patients suffering dengue illness. While the highly promising antiviral, JNJ-1802(390), is progressing through human clinical trials, the recommended treatment for patients suffering with dengue infection remains as supportive treatment. While the vaccine Dengvaxia is available, it is only recommended for individuals who have already been infected with DENV(7). More recently, the live attenuated tetravalent dengue vaccine, QDENGA, has been approved for use in Indonesia, the EU and the UK(9). Long term studies will further reveal the safety and efficacy of this vaccine. The unique approach of releasing *Wolbachia*-harbouring mosquitoes in dengue-prone areas has shown significant promise in decreasing local cases, however there exists the possibility that DENV will adapt and overcome *Wolbachia*-mediated suppression. There is a clear need for further research into therapeutics, prophylactics and biocontrol strategies against DENV. This will require targeted research into antivirals and vaccines, as well as greater understanding of the lifecycle of dengue virus both *in vitro* and *in vivo*.

Due to the importance of NS1 in the viral lifecycle of DENV, we attempted to identify small molecule compounds that specifically target NS1 using three unique screening approaches. We identified multiple compounds with antiviral properties and in some instances we characterised the stage(s) of the lifecycle they impaired, but were not able to demonstrate an interaction between these ligands with NS1.

Our first attempt at identifying NS1-interacting compounds utilised a Nanoluciferase-tagged DENV2 reporter virus in a high-throughput luminescence-based thermal shift assay. In a high-throughput screen of 3,378 compounds belonging to 1,126 drug-like scaffolds, 22 hits from three unique scaffold families of structural analogues were identified as modulators of the denaturation profile of the NS1-NLuc fusion protein. Among these hits, multiple compounds were shown to have antiviral properties. However, validation experiments demonstrated that the modulation of the denaturation profile of NS1-NLuc was likely due to an interaction with NLuc rather than a specific interaction with NS1. We hypothesised that the antiviral activity of these compounds is a coincidence, and not a reflection of the success of the high-throughput screen. In further experiments, the most promising candidate, Compound 14, was shown to be a potent inhibitor of infectious particle production, but not of viral RNA replication.

Confocal microscopy studies revealed that during an infection using the DENV2-NS1-mScarlet reporter virus, mature E protein was not detectable in a portion of Compound 14-treated, DENV2-infected cells, when probing with a monoclonal anti-Envelope antibody. Further experimentation using both the conformation-specific anti-Envelope monoclonal antibody and a polyclonal anti-Envelope antibody, that likely recognises both mature and immature forms of Envelope protein, revealed a Compound 14-induced dose-dependent effect on the recognition of mature E protein.

Future experiments will determine the exact mechanism of action through which Compound 14 inhibits infectious particle production of DENV2, and the specific effect of Compound 14 on the maturation of E protein. It has been shown previously that E protein epitope accessibility is altered in DPM1-deficient cells(391). DPM1 is required for the dolichylphosphate mannose biosynthesis pathway, which facilitates proper glycosylation of glycoproteins(366). We hypothesise that Compound 14 may have direct or indirect effects on *N*-linked glycosylation of E protein, and future studies will be performed to determine where in the glycosylation pathway, if at all, Compound 14 is exerting an effect.

Also observed in cells lacking mature E protein, was a web-like localisation for total E protein, as well as for the ER. It has previously been shown that knockout of the Atlastin (ATL) protein family, which are determinants of ER tubule structure, results in a similar ER morphology(367, 368). Additionally, knockdown of the Atlastin protein family has been shown to inhibit orthoflavivirus RNA replication and/or infectious virus particle production(370). Knockdown of ATL3, specifically, has been shown to reduce infectious particle production, but not viral RNA replication of DENV and ZIKV(370). Further mechanistic studies will be required to untangle the role of Compound 14 in alteration of ER morphology and glycosylation of E protein and the relationship, if any, between the similar effects of Compound 14 treatment and ATL3 knockdown on ER morphology and infectious virus production. While striking, Compound 14-mediated disruption of ER morphology and E protein maturation was only evident in a minor proportion of DENV-infected cells. Given the more pronounced effects of Compound 14 on infectious virus production, it is possible that the observable effects of Compound 14 on ER morphology and E protein maturation are reflective of less striking, but still functionally important, effects of Compound 14 on ER morphology and E protein maturation across the entire treated cell population. Alternatively, it is possible that at any

given time, only a fraction of infected cells are actively involved in virus particle production and that the disruptive effects of Compound 14 on ER morphology and E protein maturation are most apparent in the subpopulation of cells that are actively engaged in virus particle production. Furthermore, it is plausible that there are other major mechanisms of action through which Compound 14 exerts its antiviral effects that remain to be characterised. Further studies are required to determine the exact mechanism(s) of action of Compound 14.

Next, we developed a NanoBiT® Protein:Protein interaction system to monitor NS1 dimerisation via measurement of luminescence associated with structural complementation of NS1-SmBiT and NS1-LgBiT fusion proteins. This system was applied towards a high-throughput screen of 3,378 drug-like compounds from 1,126 drug scaffold families to identify potential inhibitors of NS1 dimerisation. Partly due to technical errors during the high-throughput screening of compounds, we were unsuccessful in identifying inhibitors of NS1 dimerisation. The first two screens, with one data point for each compound tested, showed poor reproducibility and this was largely attributed to obvious unexpected inaccuracies ('drift effects') in automated liquid handling during these screens. A validation screen was then performed using the results of the first two screens. For the initial two primary screens, from each 'scaffold' of ~30 compounds, 3 compounds were tested. For the validation screen, scaffolds featuring at least one hit in both initial screens were selected to be fully tested. Unfortunately, the three hits from this validation screen were not shown to be inhibitors of NS1 dimerisation in follow up NanoBiT experiments. In regard to the small number of hits identified, it is likely that the confounding liquid handling problems encountered during the initial screens contributed towards selection of false positive hits, such that the validation screen featured compounds that were limited in structural diversity. Beyond unanticipated liquid handling problems encountered during the primary screens, as discussed previously, there were also marked differences in raw luminescence readings between control groups in the two repeated primary screens that likely arose due to differences in the transient transfection efficiencies achieved in each of the two repeated primary screening experiments. When repeating this screen, we will utilise monoclonal cell lines stably expressing NS1-SmBiT and NS1-LgBiT to decrease well-to-well, plate-to-plate and screen-to-screen variations in luminescence signals that may otherwise be attributable to heterogenous and variable transfection efficiencies. It is also highly relevant to note that, for the NS1 dimerisation screen

and the NaLTSA screen, we lacked a positive control inhibitor and, accordingly, we were not able to fully validate or optimise the functional dynamic ranges of each assay in the context of a small molecule inhibitor screen experimental format. The availability of such an NS1 inhibitor would have been highly valuable to assess screen quality and plate-to-plate and experiment-to-experiment variations and benchmark hits against. In the absence of such a validated small molecule inhibitor, future experiments and screens of this nature may benefit from the inclusion of known NS1-binding compounds such as PG545(201) and the previously mentioned NS1-targetting peptides(334) as additional controls that are expected to bind to NS1 and possibly alter NS1 dimerisation efficiency.

Finally, we applied the newly established warpDOCK pipeline(353) to identify compounds which interact with NS1 *in silico*. A blind docking screen against monomeric NS1 revealed two potential binding pockets within the NS1 dimerisation interface. A 500 nanosecond all-atom molecular dynamics simulation was performed to identify 7 representative conformations of NS1, including that of the high-resolution crystal structure (PDB: 4O6B), for further screening. An ultra-large library of 7.8 million drug-like, commercially available compounds was then tested for binding within the two binding pockets. From the top 30 hits at each site, 25 hits overall were purchased, with 24 of these compounds found to be soluble in DMSO. Utilising live cell imaging with the DENV2-NS1-mScarlet reporter virus, we analysed the antiviral efficacy and cytotoxicity of each compound over 72 hours. The top hit, Compound V2.3, was shown in further experiments to have nanomolar efficacy for inhibition of infectious particle production. This potent activity was assumed to be a consequence of an interaction between NS1 and Compound V2.3. However, analysis of this possibility using the NaLTSA did not demonstrate NS1-specific modulation of the NS1-NLuc denaturation profile. It should be noted that Compound V2.3-mediated stabilisation was observed for both DENV2-NS1-NLuc detergent lysates and the NLuc control lysates, indicating an unexpected effect of Compound V2.3 on Nanoluciferase activity and its susceptibility to thermal denaturation. This effect may be masking a *bona fide* interaction between Compound V2.3 and NS1. Assuming that Compound V2.3 specifically and directly interacts with NS1 and given the availability of purified NS1 protein and newly developed Compound V2.3 analogues with improved potency and properties in our laboratory ongoing experiments will utilise surface plasmon resonance to confirm this interaction, and x-ray crystallography will be used to characterise the nature of

this interaction at atomic resolution. Also of note was the lack of inhibition of NS1 dimerisation by Compound V2.3, despite its predicted localisation within the dimerisation interface. This may be a result of the compound binding at the interface, yet not having any impact on NS1 dimerisation, or may indicate that the compound does not bind at the NS1 dimerisation interface. Along with Compound 14, to determine if Compound V2.3 is a bona fide inhibitor of NS1, we will select for and sequence resistant variants by sequential passaging of DENV2 in the presence of increasing inhibitor concentrations. The results of this experiment would inform further mechanistic studies.

In addition to further investigation into the mechanism of action of Compound 14 and Compound V2.3, and enhancement of antiviral and cytotoxic properties via a medicinal chemistry approach, testing of these compounds in a murine challenge model and validating their effectiveness *in vivo* would demonstrate if the compounds are suitable for further development. Experiments utilising type I and II receptor deficient mice (AG129) to determine protection against DENV infection or DENV-induced pathogenesis would inform the significance of these compounds as anti-DENV agents.

Programs involving the large-scale release of *Wolbachia*-infected mosquitoes in dengue-prone areas have been highly successful in combatting dengue virus infections in numerous regions worldwide(392). These *Wolbachia*-infected mosquitoes have a decreased capacity for transmitting DENV to people, and their introduction into a wild mosquito population can result in long term establishment of *Wolbachia* in the area due to 'cytoplasmic incompatibility'; a process whereby the bacterium confers a reproductive advantage to *Wolbachia*-carry female mosquitoes (393). It has recently been shown that serial passage of DENV1 in *Wolbachia*-carrying *Ae. Aegypti* mosquitoes results in the frequent selection of two major mutations in the Envelope protein, E203K and E384K (251). While further studies are required, the authors of this work suggested that E203K, in particular, may contribute to evasion of *Wolbachia*-mediated virus blocking. We sought to identify *Wolbachia*-resistant DENV2 mutants using deep mutational scanning. Pools of DENV2 mutants spanning genes E, prM and NS1 were prepared using an error-prone DNA polymerase, then passaged in C6/36 and Aag2 cells in collaboration with the research group of Dr Johnanna Fraser (Monash University). NGS analysis of these pools, after repeated passaging, demonstrated the presence of additional mutants, generally within E, NS1 and surprisingly NS3. Due to time constraints,

we were unable to perform *in vivo* experiments with the mutant libraries. In future experiments, the mutant libraries will be passaged through *Aedes aegypti* mosquitoes, either *Wolbachia*-free, or infected with *Wolbachia* strains *wMel* or *wAlbB*. After passaging through 20 generations of mosquito, NGS will be used to determine DENV2 mutants with increased fitness, specifically in *Wolbachia*-infected mosquitoes, as opposed to mosquito-adaptive mutations that are unrelated to *Wolbachia*-mediated selective pressures. Of note will be DENV2 mutants which confer resistance to *wMel*, not *wAlbB*, and vice-versa, as this information may be relevant to the overall *Wolbachia* biocontrol program.

Dengue virus is known to exist as a dynamic population, circulating between insect and mammalian hosts(394). To be successful, the virus must replicate efficiently in both hosts. Beneficial mutations within a mosquito host may not always be beneficial in humans, and vice-versa. During the course of this project, Dolan *et al* reported the findings of a study involving serial passaging of DENV2 in Huh7 (human) and C6/36 (mosquito) cells to elucidate the fitness landscape in these alternative hosts(395). This resulted in the identification of many host-specific mutations that contribute to the replicative fitness of DENV in these divergent host cells. However, as the effects of these mutations were not individually tested, it remains unclear which mutations are essential for adaption of DENV to efficient replication and spread in human and mosquito host cells. We sought to address similar questions using a different approach to examine the host-specific genetic fitness landscape of DENV. Mutant virus IVT RNA libraries of DENV2, bearing mutations in prM-E-NS1 that were generated using an error-prone DNA polymerase, and wild type DENV2 IVT RNA were transfected into Huh7.5 and C6/36 cells, and resulting infectious virus progeny were each passaged three times. At each stage, RNA from the cell monolayer was harvested, then prepared for long read sequencing using Oxford Nanopore Technology. This was chosen specifically to allow for analysis of long-range epistatic mutations. However, likely due to technical challenges in preparation of high-quality genome-length amplicons from these samples and subsequent sequencing library preparation, the sequencing data was of insufficient quality for meaningful interpretation. To overcome some of these potential issues, the respective RNA samples may be analysed again using short-read Illumina sequencing. Based on the results, we hope to identify mutations which are beneficial for replicative fitness in one host, but deleterious in the other, with a specific focus on NS1. Single DENV2 mutants will then be reintroduced into the cloned

infectious DENV2 genome, and differences in their replicative fitness in different host cells will be characterised. While interesting from an academic standpoint, determinants of tropism have also previously been used to develop attenuated vaccines. Deep mutational scanning of ZIKV E protein led to the identification of two mutants, 316Q and 461G, which are beneficial in C6/36 cells but deleterious in Vero (primate) cells(320). A 316Q/461G virus was shown to provide complete protection against a ZIKV lethal challenge in IFNAR$^{-/-}$ mice, demonstrating the utility of identifying tropic factors(395). Understanding viral determinants of host species tropism is also important in antiviral drug development programs. For example, antivirals targeting a region of DENV2 that is critical to viral replication in both human and mosquito hosts will be more effective, as there will likely be less evolutionary flexibility to mutate and evade the inhibitor and less risk of transmission of resistance if the resistance mutation(s) cause a reduced replicative fitness in mosquito hosts.

Focussing on NS1, we also prepared NS1-based mutant libraries for a DENV2 full length infectious clone (strain 16681), and a derivative DENV subgenomic replicon. These libraries were demonstrated to be replication-competent and were subjected to selection in human (Huh-7.5) and mosquito (C6/36) host cells, with cellular RNA samples collected, awaiting future RT-PCR and NGS analysis. These studies will allow for the generation of a map of NS1 residues that are required for viral RNA replication and those that are required for both RNA replication and infectious virus particle production. Individual mutants of interest will then be introduced into the DENV2 infectious clone pFK-DVs and replicon pFK-sgDVs-R2A for analysis of altered viral fitness. Again, these results will highlight residues of importance to the DENV lifecycle, revealing areas for which targeting of antiviral strategies may be more effective, due to a limited evolutionary space for which DENV can mutate and develop resistance.

Overall, we have taken multiple approaches to further the effort against DENV, with a focus on NS1. We have utilised novel methods including a virtual drug screen and a Nanoluciferase-based thermal shift assay to identify two compounds which display antiviral activity against DENV *in vitro*, and will continue to develop these drugs through medicinal chemistry approaches, and ensure their validity as potential therapeutics with *in vivo* experiments. We have generated multiple mutant libraries of the DENV NS1 gene using both the full-length infectious clone pFK-DVs and the subgenomic replicon pFK-sgDVs-R2A, which will be used to identify variants of interest in viral replication and infectious particle production, and

potentially inform future studies on antiviral therapeutics or prophylactics by providing information on the genetic flexibility of the DENV genome. Mutant libraries generated for the investigation of *Wolbachia* escape mutants may inform field-based surveillance programs for variants of concern, while also examining the overall selective pressure exerted by *Wolbachia* on the DENV genome.

Appendices

Appendix I: Primers used in this thesis.

Generation of pTRIPZ NS1-LgBiT expression construct:

E_NS1_pTRIPZ_FWD	tagtgaaccgtcagatcgcaccaccatgAGCACCTCACTGTCTGTG
E_NS1_pTRIPZ_REV	tccccgagccAGCTGTGACCAAGGAGTTG
LgBiT_pTRIPZ_FWD	ggtcacagctggctcggggATGGTCTTCACACTCGAAG
LgBiT_pTRIPZ_REV	aaaacccggcgcggaggccactaGTTGATGGTTACTCGGAAC

Generation of pLenti6 NS1-LgBiT expression construct:

E_NS1_pLENTI6_FWD	TCCATAGAAGACACCGACTCTAGAGgatccctcgaattcgctaccaccatgagcacctcactgtctgtg
E_NS1_pLENTI6_REV	tccccgagccagctgtgaccaaggagttg
LgBiT_pLENTI6_FWD	ggtcacagctggctcggggatggtcttcacactcgaag
LgBiT_pLENTI6_REV	TTAGGGATAGGCTTACCTTCGAACCGCGGGCCCTCTAGACTCGAgttaGTTGATGGTTACTCGGAACAG

Generation of pLenti6 NS1-CyOFP1 expression construct:

E_NS1_pLenti_FWD	GTGGTTCAAAGTTTTTTTCTTCCATTTCAGGTGTCGTGAcGTACGccaccatgagcacctcactgtctgt
E_NS1_pLenti_REV	TCCTCGCCCTTGCTCACCATccccgagccagctgtgaccaaggagt
CyOFP1_pLenti_FWD	tcaactccttggtcacagctggctcggggATGGTGAGCAAGGGC
CyOFP1_pLenti_REV	ACCGCATGTTAGCAGACTTCCTCTGCCCTCTCCACTGCCtgtacaCTTGTACAGCTCGTCCA

Generation of pTRIPZ NS1-NLuc expression construct:

E_NS1_pTRIPZ_FWD	AGAGCTCGTTTAGTGAACCGTCAGATCGCACCGGTccaccatgagcacctcactgtctgt
E_NS1_pTRIPZ_REV	GAGTGTGAAGACCATccccgagccagctgtgaccaagga
NLuc_pTRIPZ_FWD	tccttggtcacagctggctcggggATGGTCTTCACACTCGAAGA
NLuc_pTRIPZ_REV	GGGAGGCGCCAAAACCCGGCGCGGAGGCCACGCGTTTACGCCAGAATGCGTTCGC

Generation of pLenti6 NS1 expression construct:

E_NS1_pLenti6_FWD	TCCATAGAAGACACCGACTCTAGAGGATCCaccatgagcacctcactgtctg
E_NS1_pLenti6_REV	CCTTCGAACCGCGGGCCCTCTAGACTCGAGttaagctgtgaccaaggag

Site directed mutagenesis:

DENV2 NS4B L52F:

DENV_NS4B_FWD	TCCAGTTACGCTGGAGTCTGAGGCTCGTCCTGAATGGTACatcacggctagcatcc
DENV_NS4B_REV	GATTTAAATGGTCAGTATTGAGCACGCGTGATATCTAGAGcatcatgttgtacacacatgttt
DENV_L52F_fwd_SDM	gaattttcaatgctatgtctaaacattggtgtaacaaatgttgtggc
DENV_L52F_rev_SDM	gccacaacatttgttacaccaatgtttagacatagcattgaaaattc

DENV2 NS1 T164S:

DENV_NS1_FWD_SDM	tttgtggaatccgctcagtaacgcgtct
DENV_NS1_T164S_REV_SDM	ttcaattttagccatatattggtgCtgaatactccaaagccatagtcttc
DENV_NS1_T164S_FWD_SDM	aagactatggctttggagtattcaGcaccaatatatggctaaaattgaaagaaa
DENV_NS1_REV_SDM	cctatgtcatccgtcatagtggcgcctaccataacc

Mutant Library Preparation (*Wolbachia* project):

Four fragment (ABCD) approach:

Full length A-D	WMP_CprMENS1_A_FP1	agagaaaccgcgtgtcgactgtg
	WMP_CprMENS1_D_RP1	ccgtcatagtggcgcctaccataac
Fragment A	WMP_CprMENS1_A_FP1	agagaaaccgcgtgtcgactgtg
	WMP_CprMENS1_A_RP1	ggtttgtttttgccatcgtcgtcacacag
Fragment B	WMP_CprMENS1_B_FP1	gaacatggaagctgtgtgacgacgatg
	WMP_CprMENS1_B_RP1	ggtttgtttttgccatcgtcgtcacacag
Fragment C	WMP_CprMENS1_C_FP1	caatagttatcagagtgcaatatgaaggggacgg
	WMP_CprMENS1_C_RP1	ggttatgagactctgtagagagcatttttgctttgc
Fragment D	WMP_CprMENS1_D_FP1	catggggcaaagcaaaaatgctctctacaga
	WMP_CprMENS1_D_RP1	ccgtcatagtggcgcctaccataac

Preparation of large, mutated regions as template for further amplification:

Fragment 1 (SalI/SphI)	WMP_Frag1_FWD	CAGATGCGTAAGGAGAAAATACCGCATCAGtcgactgtgcaacag
	WMP_Frag1_REV	ggagagccgtccccttcatattgc
Fragment 2 (SphI/MluI)	WMP_Frag2_FWD	gaacatggaagctgtgtgacgacgatg
	WMP_Frag2_REV	ggttatgagactctgtagagagcatttttgctttgc
Fragment 3 (MluI/KasI)	WMP_Frag3_FWD	caatagttatcagagtgcaatatgaaggggacgg
	WMP_Frag3_REV	TACGCCAAGCTTGCATGCAGGCCTCTGCAGgcgcctaccataacc

Amplification of large fragments with overhangs allowing for insertion into SalI/SphI, SphI/MluI or MluI/KasI-digested puc57 shuttle vector:

SalI to SphI	WMP_gib_saltosph_puc_fwd	GCGTAAGGAGAAAATACCGCATCAGgagaaaccgcgtgtcg
	WMP_gib_saltosph_puc_rev	ACCATGATTACGCCAAGCTTGCATGgtcatttccgactgcatg
SphI to MluI	WMP_gib_sphtomlu_puc_fwd	GCGTAAGGAGAAAATACCGCATCAGcaggggaagagcatgc
	WMP_gib_sphtomlu_puc_rev	ACCATGATTACGCCAAGCTTGCATGgattctccagacgcgttac
MluI to KasI	WMP_gib_mlutokas_puc_fwd	GCGTAAGGAGAAAATACCGCATCAGaatccgctcagtaacgc
	WMP_gib_mlutokas_puc_rev	TACGCCAAGCTTGCATGCAGGCCTCTGCAGgcgcctaccataacc

Amplification of full-length dengue virus for analysis by Oxford Nanopore Technology:

5’ UTR – 3’ UTR	ONT_FWD	AGAGAAACCGCGTGTCGACT
	ONT_REV	TCTGTGCCTGGAATGATGCT

Primer pools used by Monash University to amplify DENV for NGS:

Pool 1:

Forward Primer Name	Forward Primer Sequence	Reverse Primer Name	Reverse Primer Sequence
DV2-400bp-F1	GTCTACGTGGACCRACAAAG	DV2-400bp-R1	ACGATCATGTGTGGTTCTCC
DV2-400bp-F3	GGGTTCAGGAAAGAGATYGG	DV2-400bp-R3	GCCCCTTCTGATGACATCC
DV2-400bp-F5	GTATCAGGAGGRAGYTGGGT	DV2-400bp-R5	CCATGTTTTCCTGTGTCATTWCC
DV2-400bp-F7	TGGTCACTTTCAAAAATCCYCA	DV2-400bp-R7	CGAATGGAGGTTCTGCTTCTAT
DV2-400bp-F9	TCCACCAAGTYTTYGGAGC	DV2-400bp-R9	TCTGGTGTTATTTGTYTCCACAT
DV2-400bp-F11-Ver2	AAYCACACCTTTCTYATTGATGG	DV2-400bp-R11-Ver2	CCWTCGCAGARATCRAAGTCCAT
DV2-400bp-F13	AATGGTGCTGYCGATCTTG	DV2-400bp-R13	TCATCAATTCCTTGGAGGTCA
DV2-400bp-F15	GACCTCCAAGGAATTRATGATG	DV2-400bp-R15	GCCACTAATGGWCCTGTCAT
DV2-400bp-F17	GGATTGCTAGTGATCTCAGGA	DV2-400bp-R17	CCAGAGATACRGCRCCTAT
DV2-400bp-F19**	TCCAGGAGCRGGAAARAC	DV2-400bp-R19**	ACGAACGCTCAGGGATTTC
DV2-400bp-F21	AGACGCTGCATGAAACCAG	DV2-400bp-R21	ATCAAAACACCACYTTCTGTCT
DV2-400bp-F23	GGTAGACTTCCAACWTTCATGAC	DV2-400bp-R23	TCTCGTTTGCCATGGTTGC
DV2-400bp-F25	TGTCAAAAATGGAYATYGGAG	DV2-400bp-R25	AATGTTAGCCATTGACACYGC
DV2-400bp-F27-Ver2	GGAGAAACGGACCAYCAYGC	DV2-400bp-R27-Ver2	GATTCCTCACCAARGCTCCTCC
DV2-400bp-F29	TGGCACTATGAYCAAGAYCA	DV2-400bp-R29	CACATGTTTCACACTTYCCTTC
DV2-400bp-F31	AAGGAGGAGCMATGTAYGC	DV2-400bp-R31	TCCACTGATGGCCATTCTTG
DV2-400bp-F31 - Ver 2	AAGGAGGAGCMATGTAYAC		
DV2-400bp-F33	TYCCATGCAGAAAYCAAGATGA	DV2-400bp-R33	GGATGTTCTTTGCCCAKGT
DV2-400bp-F35	AGAAAACCCATGGATGGAAGA	DV2-400bp-R35	CCTCCTCAGGTGGAGCTAC

Pool 2:

Forward Primer Name	Forward Primer Sequence	Reverse Primer Name	Reverse Primer Sequence
DV2-400bp-F2	GCTAAGCTTAACGTAGTTCTAACAG	DV2-400bp-R2	ACGATCATGTGTGGTTCTCC
DV2-400bp-F4	AGAAGAGAAAAAAGATCAGTGGC	DV2-400bp-R4	TTGGCTTCCGTTTTTRTCAGTTC
DV2-400bp-F6	GCATTGTGACCTGTGCTATGT	DV2-400bp-R6	TCTGTGGCTCCTGTGAGTG
DV2-400bp-F8-Ver2	AAATAGCAGAAACACAACATGGAAC	DV2-400bp-R8-Ver2	GCTRCGTGARTTCATTCCTATCC
DV2-400bp-F10	GCAYACGTGGACAGARCA	DV2-400bp-R10	GYGAGTTCCAAGCTCTRTT
DV2-400bp-F12	CACCCTCTGGAGYAATGRAGT	DV2-400bp-R12	TCGTGTCCTGAGCATTTCYTC
DV2-400bp-F14-Ver2	TGCTYAGGACCCGARTRGGAA	DV2-400bp-R14-Ver2	GTGCAGCTCACYTTCCATGC
DV2-400bp-F16	CATGGCAGTYGGGATGGT	DV2-400bp-R16	GTGAAGGGACRTCCCACA
DV2-400bp-F16 Ver-2	CATGGCAGTYGGGATGGG		
DV2-400bp-F18	CTCGAAGGAGAATGGAAGGA	DV2-400bp-R18	CTCTGAGAGCTTCYTCCATTTC
DV2-400bp-F20	TTTCAACTCGAGTRGAGATGGG	DV2-400bp-R20	CCTCTTCTTTGYGCTGCRCT
DV2-400bp-F22-Ver2	TAYCGCTTGAGAGGRGARGC	DV2-400bp-R22-Ver2	CATYCCCAGGGTCATYTTYCC
DV2-400bp-F24	TGCTCATTCCAGARCCAGAAAA	DV2-400bp-R24	TCCTGGCCCTATRATRGCRTA
DV2-400bp-F26	ATGATGAGGACYACATGGGC	DV2-400bp-R26	CAATAGTATGACCAGCCYCC
DV2-400bp-F28	ACACCCAATTTTGCRTAAARGT	DV2-400bp-R28	ACCATGGATGATGCTGATCC
DV2-400bp-F30-Ver2	AYGAGAACAAGTGGAARTCRGC	DV2-400bp-R30-Ver2	TRTCCATTACTGTKCCTCTTGG
DV2-400bp-F32	GACAGATGGAGGGAGAAGGA	DV2-400bp-R32	CCACATTTGGGCGTAAGACTT
DV2-400bp-F34	TCCCATCACAYTGGGTTCC	DV2-400bp-R34	ATGGCTTAATCCGACCTGAC

Appendix II: General solutions and buffers used in this thesis

1 x Phosphate-buffered-saline (PBS) solution

1 x Tris-glycine-SDS (TGS) buffer

1 x Tris-buffered-saline (TBS) buffer

1 x Tris-acetate-EDTA (TAE) buffer

Glacial acetic acid

NaCl

Ampicillin 1 mg/ml

Dimethyl sulfoxide (DMSO)

Kanamycin 1 mg/ml

Luria agar

Luria Broth

Sodium dodecyl sulfate (SDS)

Tris solutions (varying pH and concentrations)

EDTA (varying pH and concentrations)

Sodium deoxycholate

NP-40

Dithiothreitol (DTT)

Bromophenol blue

Glycerol

Glycine

Penicillin/streptomycin

Trypan blue

Trypsin-EDTA

Foetal calf serum (FCS)

Bovine serum albumin

Acetone

Methanol

Tween® 20

2-mercaptoethanol

Agarose

Bovine serum albumin (BSA)

Solution:	Components/Recipe
Acetone:methanol	1 Litre: 500 mL acetone 500 mL methanol
1 x Phosphate-buffered-saline (PBS) solution	1 Litre: 8 g NaCl 0.2 g KCl 1.44 g Na_2HPO_4 KH_2PO_4 H_2O
1 x Tris-glycine-SDS (TGS) buffer	1 Litre: 3.02 g tris base 14.4 g glycine pH to 8.80 1 g SDS H_2O
1 x Tris-buffered-saline (TBS) buffer	1 Litre: 2.4 g tris base 8.8 g NaCl pH to 7.6 H_2O
1 x Tris-acetate-EDTA (TAE) buffer	1 Litre: 4.85 g tris base 1.14 mL glacial acetic acid 20 mL 0.5M EDTA (pH 8.0) H_2O
Luria Broth	1 Litre: 10 g tryptone 10 g NaCl 5 g yeast extract H_2O
Luria Agar	1 Litre: 10 g tryptone 10 g NaCl 5 g yeast extract 20 g agar H_2O
1% Bovine Serum Albumin (PBST)	1 Litre: 10 g bovine serum albumin 990 mL PBST

Cell freeze mix	1 Litre 500 mL complete mammalian cell culture medium 300 mL Foetal calf serum 200 mL DMSO
1% Agarose	1 Litre: 10 g agarose 990 mL 1 x TAE buffer
PBS-T	1 Litre: 0.1% Tween® 20 1 L PBS
TBS-T	1 Litre: 0.1% Tween® 20 1 L TBS
SDS-PAGE reducing loading buffer	50 mL: 6.25 mL of 0.5 M Tris-HCl, pH 6.8 18.75 mL Glycerol (80%) 10 mL SDS (10% w/v) 2.5 mL 2-mercaptoethanol 2.5 mL bromophenol blue (1% w/v) H_2O
SDS-PAGE non-reducing loading buffer	50 mL: 6.25 mL of 0.5 M Tris-HCl, pH 6.8 18.75 mL Glycerol (80%) 2.5 mL 2-mercaptoethanol 2.5 mL bromophenol blue (1% w/v) H_2O
RIPA lysis buffer	100 mL: 3.75 mL of 4M NaCL 0.5 g deoxycholate 1 mL of 10% SDS 1 mL of NP-40 5 mL of 1M Tris H_2O
Mammalian cell culture medium	500 mL DMEM 50 mL FCS 5 mL Pen/Strep
Insect cell culture medium	500 mL Basal Media E 10 – 50 mL FCS 5 mL MEM non-essential amino acids 5 mL sodium pyruvate 5 mL L-GlutaMAX

Appendix III: Antibodies used in this thesis

Antibodies:

Primary Antibodies	Dilution	Supplier
Mouse anti-β-actin (A5441)	1: (Western blotting)	Sigma
Rabbit anti-NS4B (GTX103349)	1: (Immunofluorescent staining)	GeneTex
Mouse anti-NS3 (GT2811)	1: (Immunofluorescent staining)	GeneTex
Mouse anti-NS1 (4G4) hybridoma supernatant	1: (Immunofluorescent staining) 1: (Western blotting)	Jody Peters & Roy Hall, University of Queensland
Mouse anti-E (D1-4G2-4-15) hybridoma supernatant	1: 1000 (Immunofluorescent staining)	ATCC
Mouse anti-capsid (6F3.1) hybridoma supernatant	1: (Immunofluorescent staining)	John Aaskov, Queensland University of Technology
Rabbit anti-E (GTX127277)	1: (Immunofluorescent staining)	GeneTex
Secondary Antibodies		
IRDye® 800CW Goat anti-Mouse IgG Secondary Antibody	1:20000 (Western blotting)	Li-Cor
IRDye® 680LT Goat anti-Rabbit IgG Secondary Antibody	1:20000 (Western blotting)	Li-Cor
Alexa-Fluor 488 Dye	1:200 (Immunofluorescent staining – confocal microscopy) 1:500 (Immunofluorescent staining – general microscopy)	Thermo Fisher Scientific
Alexa-Fluor 555 Dye	1:200 (Immunofluorescent staining – confocal microscopy) 1:500 (Immunofluorescent staining – general microscopy)	Thermo Fisher Scientific

Appendix IV: Plasmids maps

pFK-DVs:

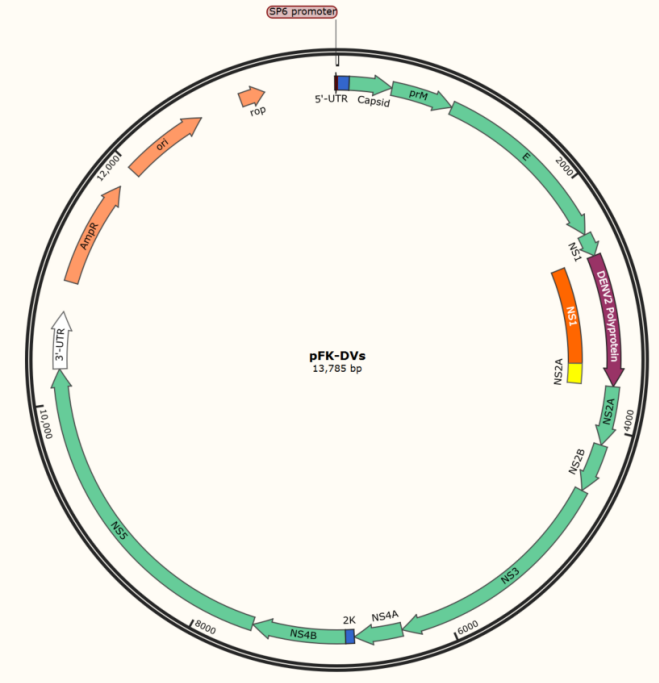

pFK-sgDVs-R2A

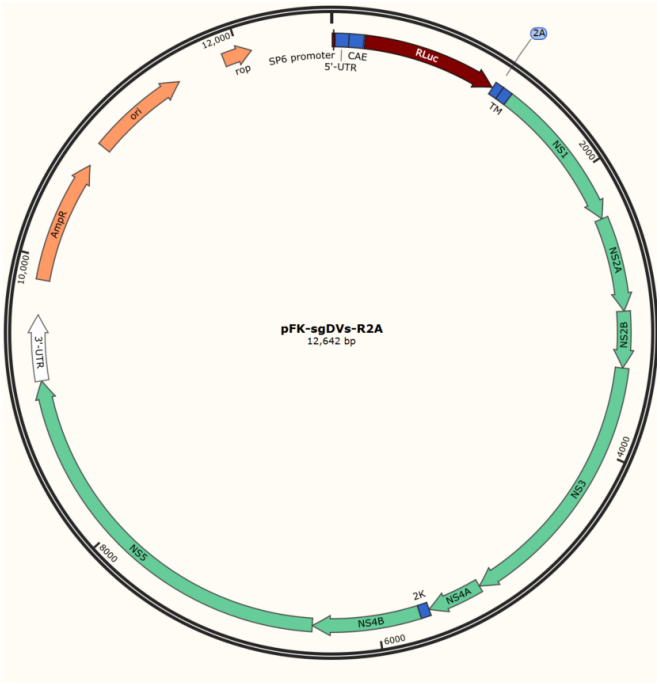

pFK-DVs-NS1-mScarlet

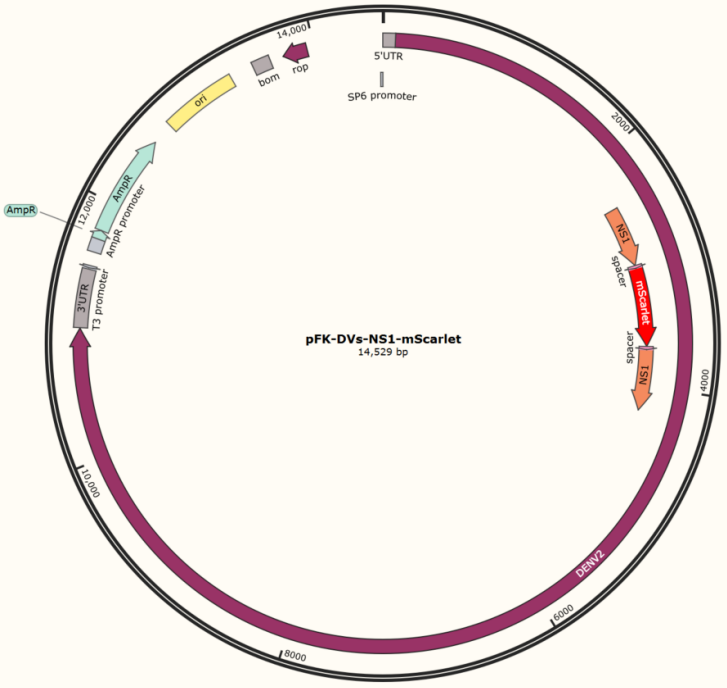

pFK-DVs-NS1-NLuc

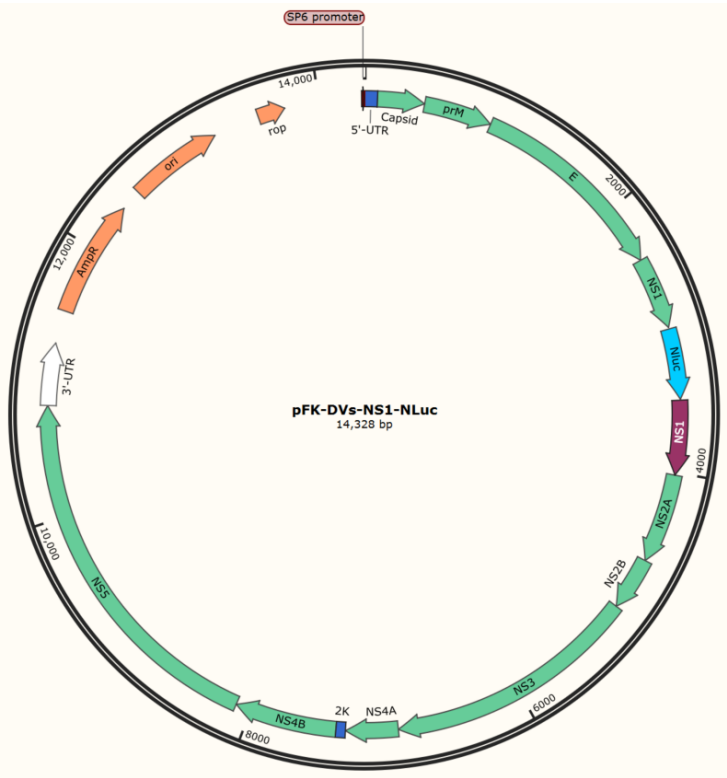

pLenti NS1-LgBiT

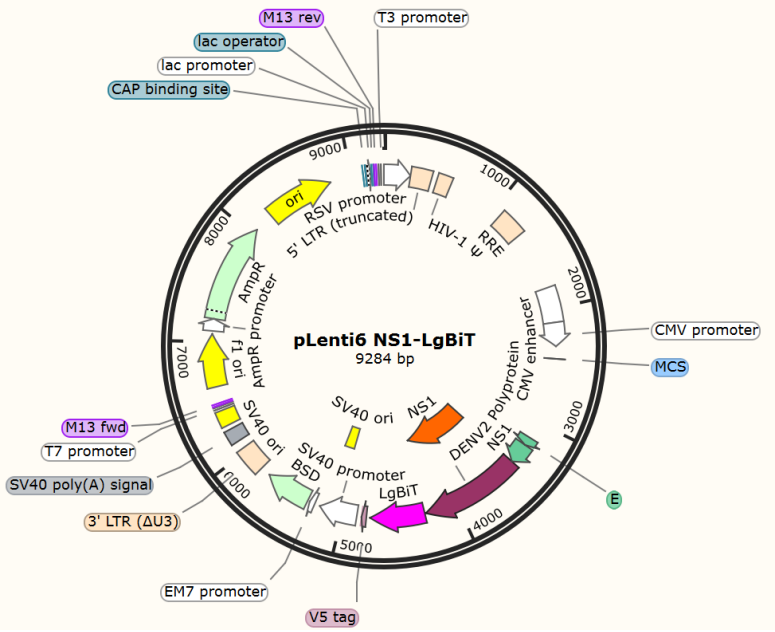

pLenti6 NS1-SmBiT

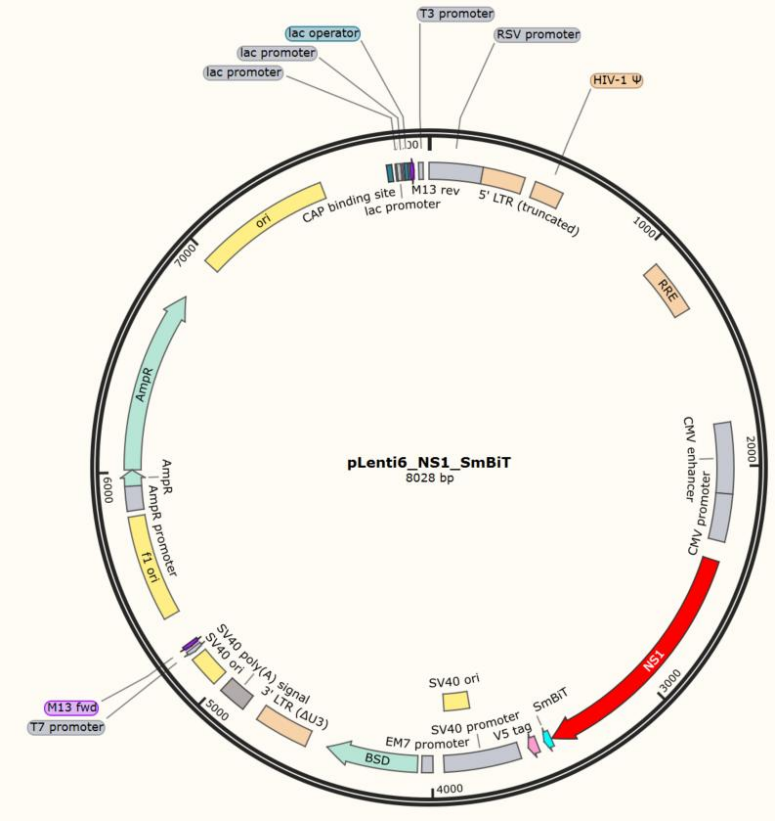

pUC57

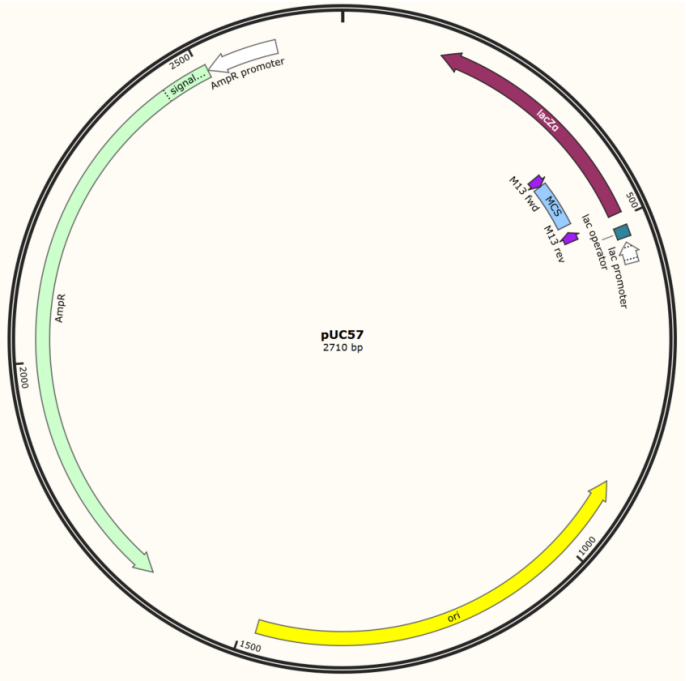
pUC57
2710 bp
2500
signal...
AmpR promoter
lacZα
500
M13 fwd
MCS
M13 rev
lac operator
lac promoter
AmpR
2000
1000
ori
1500

viruses

MDPI

Review

Applications of Deep Mutational Scanning in Virology

Thomas D. Burton and Nicholas S. Eyre *

College of Medicine and Public Health, Flinders University, Bedford Park, SA 5042, Australia; burt0181@flinders.edu.au
* Correspondence: nicholas.eyre@flinders.edu.au

Abstract: Several recently developed high-throughput techniques have changed the field of molecular virology. For example, proteomics studies reveal complete interactomes of a viral protein, genome-wide CRISPR knockout and activation screens probe the importance of every single human gene in aiding or fighting a virus, and ChIP-seq experiments reveal genome-wide epigenetic changes in response to infection. Deep mutational scanning is a relatively novel form of protein science which allows the in-depth functional analysis of every nucleotide within a viral gene or genome, revealing regions of importance, flexibility, and mutational potential. In this review, we discuss the application of this technique to RNA viruses including members of the Flaviviridae family, Influenza A Virus and Severe Acute Respiratory Syndrome Coronavirus 2. We also briefly discuss the reverse genetics systems which allow for analysis of viral replication cycles, next-generation sequencing technologies and the bioinformatics tools that facilitate this research.

Keywords: deep mutational scanning; virology; virus; hepatitis; Zika; Dengue; Influenza; SARS-CoV-2

Citation: Burton, T.D.; Eyre, N.S. Applications of Deep Mutational Scanning in Virology. *Viruses* **2021**, *13*, 1020. https://doi.org/10.3390/v13061020

Academic Editor: Roy A. Hall

Received: 29 March 2021
Accepted: 26 May 2021
Published: 28 May 2021

1. Introduction

In its essence, deep sequencing is a tool that allows the sequencing of a genomic region multiple times. Deep mutational scanning (DMS) is a technique that utilises deep sequencing technology in combination with a library of mutant genes or genomes produced by random mutagenesis to probe the functional effects of mutations at every single nucleotide position within a gene or genome, linking genotype to phenotype in a single high-throughput experiment. This technique has been applied to various proteins to reveal residue-specific information regarding many aspects of protein biology. For example, under certain conditions, replacement of a yeast gene with a mutant library of a human orthologue can allow for determination of mutants which impact growth, and may be linked to human disease [1,2]. Unbiased selection and identification of mutants with improved properties or activities for specific requirements, such as increased solubility, have furthered the field of protein engineering [3]. Numerous other applications have also been pursued through DMS, including construction of complete functional activity landscapes of genes [4,5], establishment of quantitative evolutionary models [6,7], and contributions to structural biology [8,9]. In this review, we will predominantly focus on how DMS has been applied to the study of viral replicative fitness and immune evasion in the context of infectious virus replication cycles.

First, we should consider how residues and genomic regions of importance have been analysed by point mutagenesis in the past. Many studies have utilised alanine substitution to reveal residues or regions of importance in a viral protein. Commonly, residues for mutation are selected by analysis of protein structure, conservation with other isolates or strains, or amino acid biophysical properties [10,11]. Alternatively, large regions of interest may be interrogated by alanine scanning mutagenesis as a less targeted approach [12,13]. Alanine mutagenesis is the preferred substitution, as alanine features an inert, non-bulky methyl functional group, and does not alter main-chain conformation [14]. In these studies, mutants of interest are typically loss-of-function mutants, as this is indicative of the absense

of a functionally important residue. Experiments attempting to generate adaptive or gain-of-function mutations often rely on serial passages of a virus in cell culture or animal models [15–17], relying on an error-prone viral polymerase to generate mutants. A limiting factor is that combinations of mutations that may be required to enhance viral fitness in a given host may not be realised within the system. This method can also be time consuming as multiple rounds of infection are required. In regard to analysis of the impact of amino acid substitutions on viral protein function or viral replicative fitness, DMS can allow the substitution of a given residue with all possible amino acids, increasing the probability of identifying gain-of-function mutations that otherwise require more than one nucleotide substitution.

DMS studies in virology are generally performed using a three-step approach. First, a mutant library of a gene or genome of interest is prepared, ideally with genetic variants encoding every single possible residue change within the sequence of interest. Second, a selective pressure is applied to the library, enabling the enrichment of mutations that encode a selective advantage and the removal of deleterious mutations. Finally, the frequency of mutations within the library is quantified via next-generation sequencing (NGS) and compared before and after the application of the selective pressure. In studies of viral replicative fitness, a mutant with a cost to fitness will be selected against, while an enhancing mutant, for example, an antiviral escape mutant, will become enriched. Selective pressures, such as drug/antibody presence, stimulation of antiviral innate immunity, growth in cell types of different species, and binding potential to a host receptor have been applied to studies of many viral genes. Analysis of variants through DMS has enabled evolutionary studies, escape mutant predictions, attenuated vaccine construction and other applications. In this review, we will discuss various DMS strategies and how they have been applied in virology, with a focus on the *Flaviviridae* family of viruses, Influenza Virus A (IAV) and Severe Acute Respiratory Syndrome Coronavirus 2 (SARS-CoV-2). DMS studies of RNA viruses have been made possible through the development of reverse genetics systems, or easily modified infectious clones, and advances in sequencing technologies, which we will discuss herein.

1.1. Influenza A

As members of the *Orthomyxoviridae* family, IAVs are negative-sense single-stranded RNA (-ssRNA) viruses [18]. Influenza strains vary from seasonal variants which cause a significant health care burden, to pandemics such as the Spanish Flu which killed an estimated 50 million people from 1918 to 1919 [19]. Influenza circulates not only in the human population, but in species such as birds, pigs and cats [20]. Two major obstacles towards effective Influenza protection and treatment are antigenic shift and antigenic drift, which are mechanisms which, through mutation or gene reassortment, can functionally change Influenza biology. Antigenic drift, which also applies to other viruses such as *Flaviviridae* and *Coronaviridae* family members, is the accumulation of point mutations due to the error-prone virally encoded RNA-dependent RNA polymerase used to generate new copies of the genome during replication [21]. Antigenic shift allows the formation of new Influenza subtypes through reassortment of surface antigens haemagglutinin (HA) or neuraminidase (NA) and is facilitated by the segmented genome of Influenza. Antigenic shift occurs when an animal is infected with two or more different strains of Influenza virus, enabling reassortment of HA and NA viral RNA segments and leading to a novel Influenza strain to which the population is completely naïve [21]. This resulted in the first pandemic of the 21st Century: swine-origin IAV [22]. The prediction of mutant strains of IAV that are likely to arise is therefore imperative for prophylaxis and control, and the predictive power of DMS can be utilised for the identification of animal viruses with zoonotic potential, or to predict escape mutants that are insensitive to otherwise effective adaptive immune responses or antiviral therapies.

1.2. Flaviviridae

The *Flaviviridae* family of RNA viruses comprises multiple positive-sense single-stranded RNA (+ssRNA) enveloped viruses, including hepatitis C virus (HCV), Dengue virus (DENV) and Zika virus (ZIKV) [23]. These viruses have enormous impact around the globe, with DENV alone infecting approximately 390 million people each year [24]. For most *Flaviviridae* (and viruses in general), no therapeutics or vaccines exist, with exceptions for vaccines being yellow fever virus [25] and Japanese encephalitis virus [26]. In addition to furthering our understanding of basic *Flaviviridae* biology, DMS has enabled the construction of a vaccine candidate for ZIKV, which will be discussed later.

1.3. SARS-CoV-2

The *Coronaviridae* family of positive-sense single-stranded RNA (+ssRNA) viruses features several clinically relevant viruses including Middle East respiratory syndrome-related coronavirus (MERS-CoV), Severe Acute Respiratory Syndrome Coronavirus (SARS-CoV), and the current pandemic SARS-CoV-2, all of which have emerged in the past two decades [27], as well as common cold-causing viruses such as HCoV-OC43 [28]. There is currently a major global research effort to develop therapeutics and vaccines against SARS-CoV-2 which ideally target regions of the virus that are incapable of mutational escape, which would otherwise reduce the effectiveness of the treatment. DMS has been employed to determine how mutants will affect SARS-CoV-2 neutralisation.

2. Reverse Genetics Systems to Study RNA Viruses

Due to the absence of DNA in the lifecycle of RNA viruses, the construction of cDNA clones of infectious RNA viruses has become an incredibly important tool in studying their lifecycle. Generally, a reverse genetics system is comprised of genomic viral RNA that is reverse-transcribed into cDNA and then cloned into a plasmid, allowing for stable propagation of a virus genome within bacteria or yeast. The plasmid can then be easily manipulated by standard molecular methods, with the introduction of mutations and tags, or the removal of segments of the genome [29].

There are multiple key requirements for an infectious (+)RNA virus cDNA clone. A common approach involves incorporation of a DNA-dependent RNA polymerase promoter at the 5′ end of a cloned viral genome to enable in vitro transcription of infectious viral RNA via a corresponding RNA polymerase, with or without a type I 5′ cap structure, if required. This is commonly achieved using bacteriophage promoters/polymerases such as those of T7 and SP6. Produced RNA can then be purified and transfected into cells to initiate the viral replication cycle. A constitutive promoter such as a human cytomegalovirus [HCMV] promoter can also be utilised, with viral RNA produced by host Polymerase II after direct transfection of a full length cDNA clone into cells. As it is necessary to produce viral RNA with precise ends, a self-cleaving hepatitis delta or hammerhead ribozyme or a T7 terminator sequence may be added to the 3′ end of the viral genome to enable generation of authentic 3′ ends [30,31]. Alternatively, a unique restriction endonuclease site can be inserted at the 3′ end for plasmid linearization [32]. Some of the limitations of these plasmid systems are instability in bacteria, due to the presence of cryptic bacterial promoters and other factors leading to recombination during growth, and poor plasmid yields [33]. As the preparation of mutant libraries involving plasmid clones of viral cDNA often requires the pooling of a large number of bacterial colonies, it is important in DMS studies to have a plasmid with both minimal recombination, to ensure that recombination of the plasmid in bacteria does not affect cell culture experiments/analysis, as well as high transformation efficiency to ensure that a library of sufficient mutational diversity can be prepared. For these reasons, several bacterium-free approaches such as circular polymerase extension reaction (CPER) [34] and yeast artificial chromosome (YAC) approaches, including transformation-associated recombination (TAR) cloning in *Saccharomyces cerevisiae* [35], have also been employed to enable efficient propagation and manipulation of (+)RNA virus cDNA clones. Similarly, bacterial artificial chromosome (BAC) systems and modified

plasmid DNA clones with features designed to minimise viral cDNA recombination and toxicity in bacteria have also been applied to various reverse genetics systems for (+)RNA viruses [31]. The reliability and ease of manipulation of viral cDNA using these systems are important determinants of the success of DMS experiments.

Many significant hurdles were encountered during the construction of an Influenza reverse genetics system. The Influenza genome comprises eight negative-sense ssRNA segments [18]. Due to the negative-sense genome, the viral RNA is not sufficient for initiation of viral replication, with the presence of multiple viral proteins being required to begin the viral lifecycle [18]. The eight vRNAs must colocalise with this protein machinery within the nucleus for initiation of infection [18]. Many reverse genetics systems have been developed to overcome these difficulties, with the two main categories comprising helper virus-dependent and -independent systems. Please see the review by Neumann et al. for a more in-depth analysis of the history of Influenza reverse genetics systems [36]; and for detailed documentation of these systems, please see the review by Engelhardt et al. [37].

Reverse genetics systems exist for many Flaviviridae species. Unlike Influenza A, the construction of infectious clones for *Flaviviridae* was, at the time, hindered more by the lack of available technologies such as high-fidelity PCR, instead of the fundamental biology of the virus. Construction of these systems is often considered as relatively straightforward although, as detailed above, challenges in genome construction due to repetitive elements, toxicity in *E. coli* and associated instability and recombination in *E. coli* are well-documented. For a history of Flavivirus reverse genetics systems, please see the review by Aubry et al. [31].

A reverse genetics system has recently been developed for SARS-CoV-2 [35]. However, as no DMS experiments have been performed to date using a reverse genetics system for the virus, we will not discuss this further. However, we highlight this as a potential area for future DMS studies.

Reverse genetics systems have traditionally been used in low-throughput mutational studies, to analyse the effect of single point mutations. Coupling reverse genetics with deep sequencing and random mutagenesis has allowed for high-throughput mutational studies, with analysis of hundreds of thousands of mutants being made possible in a single experiment. In the following sections, we discuss the technologies which have been essential in enabling DMS studies.

3. Next-Generation Sequencing

Advances in next-generation sequencing (NGS) have been crucial to the development of DMS as a tool in the field of molecular virology. The first generation of sequencing consisted mainly of Sanger sequencing and the Maxam and Gilbert technique. The second generation of sequencing introduced mass parallelisation of reactions. The current generation of sequencers enable real-time, single molecule sequencing [38]. We will discuss three commonly used platforms in DMS studies; Pacific Biosciences (PacBio) Single Molecule Real-Time (SMRT) sequencing, Oxford Nanopore Technologies (ONT) real-time sequencing, and the Illumina short-read sequencing-by-synthesis technology, which is part of the second generation of sequencing. [39]. For further in-depth detailing of the latest advances in NGS, please see the review by Goodwin et al. [40].

3.1. Single-Molecule Long-Read Sequencing

Produced by Pacific Biosciences, PacBio SMRT technology (henceforth referred to as SMRT) utilises a sequencing by synthesis approach. Initially, the DNA is fragmented into pieces several kilobases in length and the addition of hairpin adaptors to the DNA results in the formation of a circular SMRTbell DNA conformation. Next, the circular DNA is introduced to a flow cell lined with picolitre wells with a transparent bottom (a zero-mode waveguide) and a DNA polymerase enzyme fixed to the bottom of the well. The polymerase then incorporates a fluorescently tagged nucleotide into the elongating DNA strand, and the fluorescent signal emitted by the individual nucleotide being incorporated

is recorded by a camera. Finally, each fluorophore is cleaved by the polymerase and diffuses before the next read occurs. A major advantage of this technology is that the circular SMRTbell DNA conformation allows for many rounds of sequencing of a single DNA fragment, producing an accurate circular consensus sequence [41] (Figure 1).

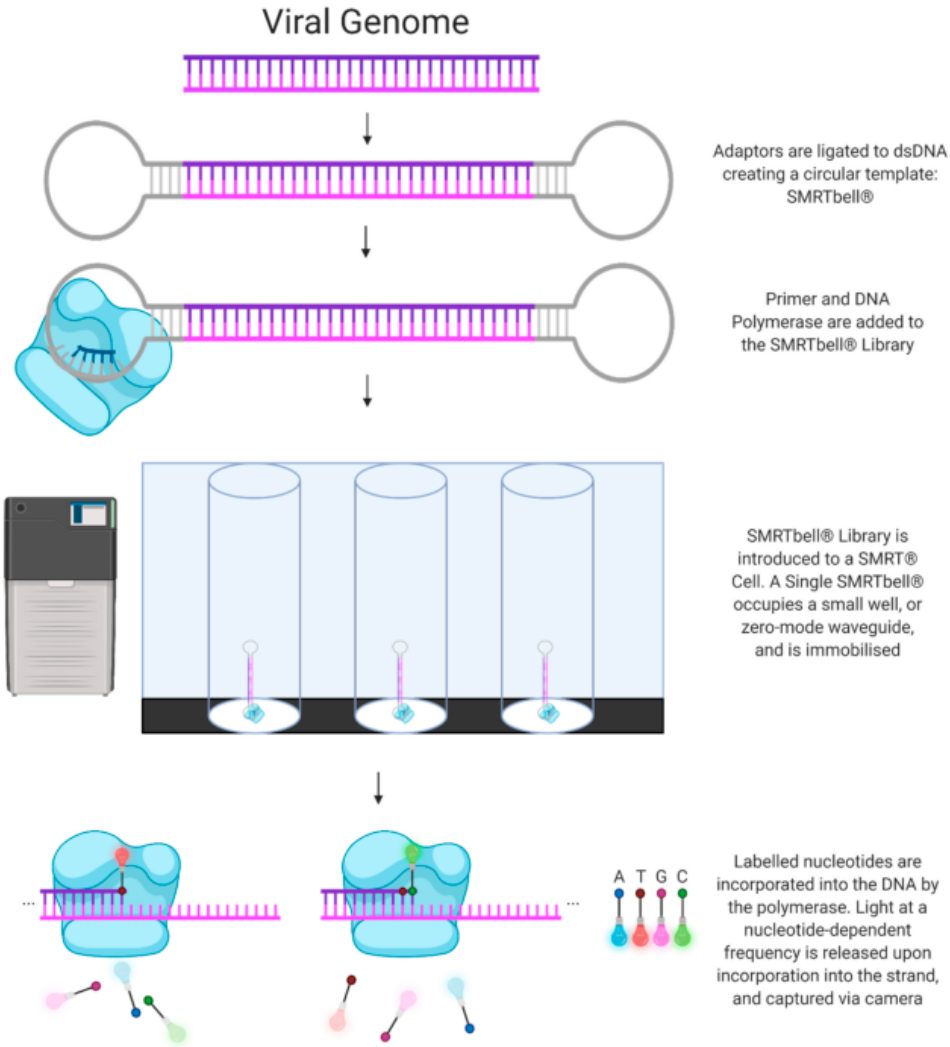

Figure 1. Next-Generation Sequencing: PacBio SMRT Technology.

The Oxford Nanopore system (henceforth referred to as ONT) sequences DNA in a unique manner. DNA is fragmented into pieces of several kilobases in length, then a motor protein and a hairpin adaptor are added to either side of the DNA. A leader sequence directs the DNA to a pore embedded in an electrically resistant membrane, and the motor protein allows ssDNA to be pulled through the aperture of the pore. Simultaneously, an electric current passes through the pore protein. As the ssDNA passes through the pore, a

characteristic disruption of the electrical current occurs, dependent on the multiple bases present in the pore. By analysis of this disruption, a DNA sequence can be identified by its unique 'k-mer', which can be translated into a sequence (for example, AAGT will have a distinct disruption compared to AGAT). The hairpin adaptor allows for bidirectional sequencing of the DNA fragment, and the read from the forward and reverse strands can be used to generate a consensus sequence [42] (Figure 2).

3.2. Illumina Sequencing by Synthesis

Used in Illumina sequencing instruments, DNA molecules are sheared to ≤300 base pair fragments then ligated to adapter sequences which allow for hybridisation to complementary oligonucleotides present in nanowells across a patterned flow cell. The DNA fragments are amplified via bridge amplification, resulting in clonal clusters of DNA. Subsequent addition and imaging of fluorophore-labelled terminator nucleotides allows for highly parallel sequencing [43] (Figure 3).

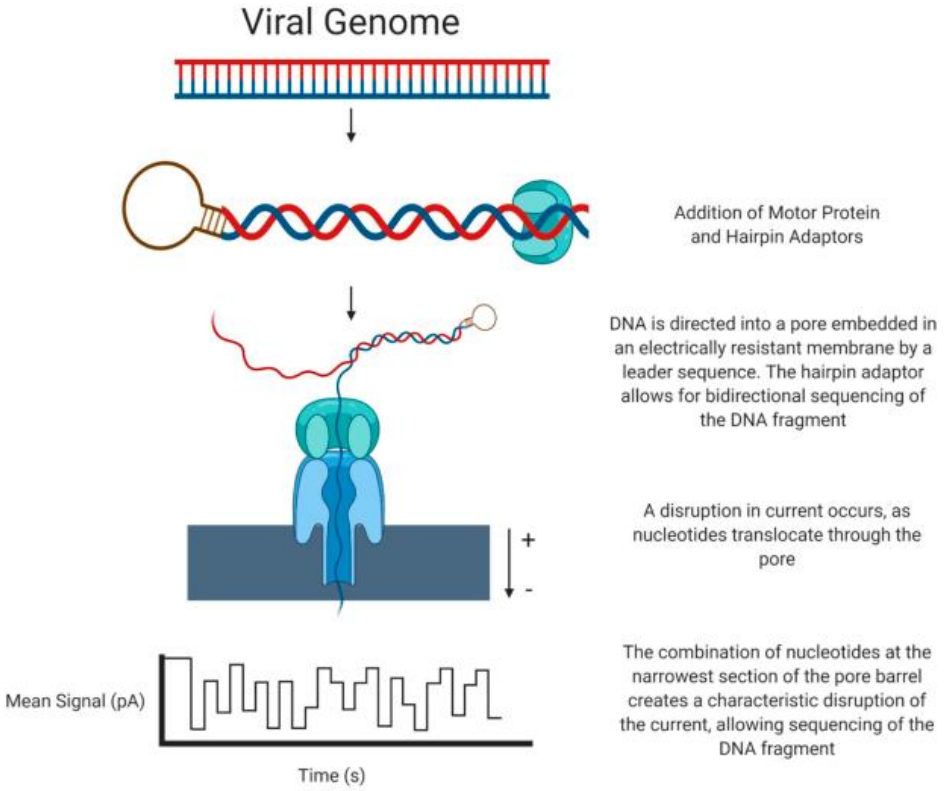

Figure 2. Next-Generation Sequencing: Oxford Nanopore Technology.

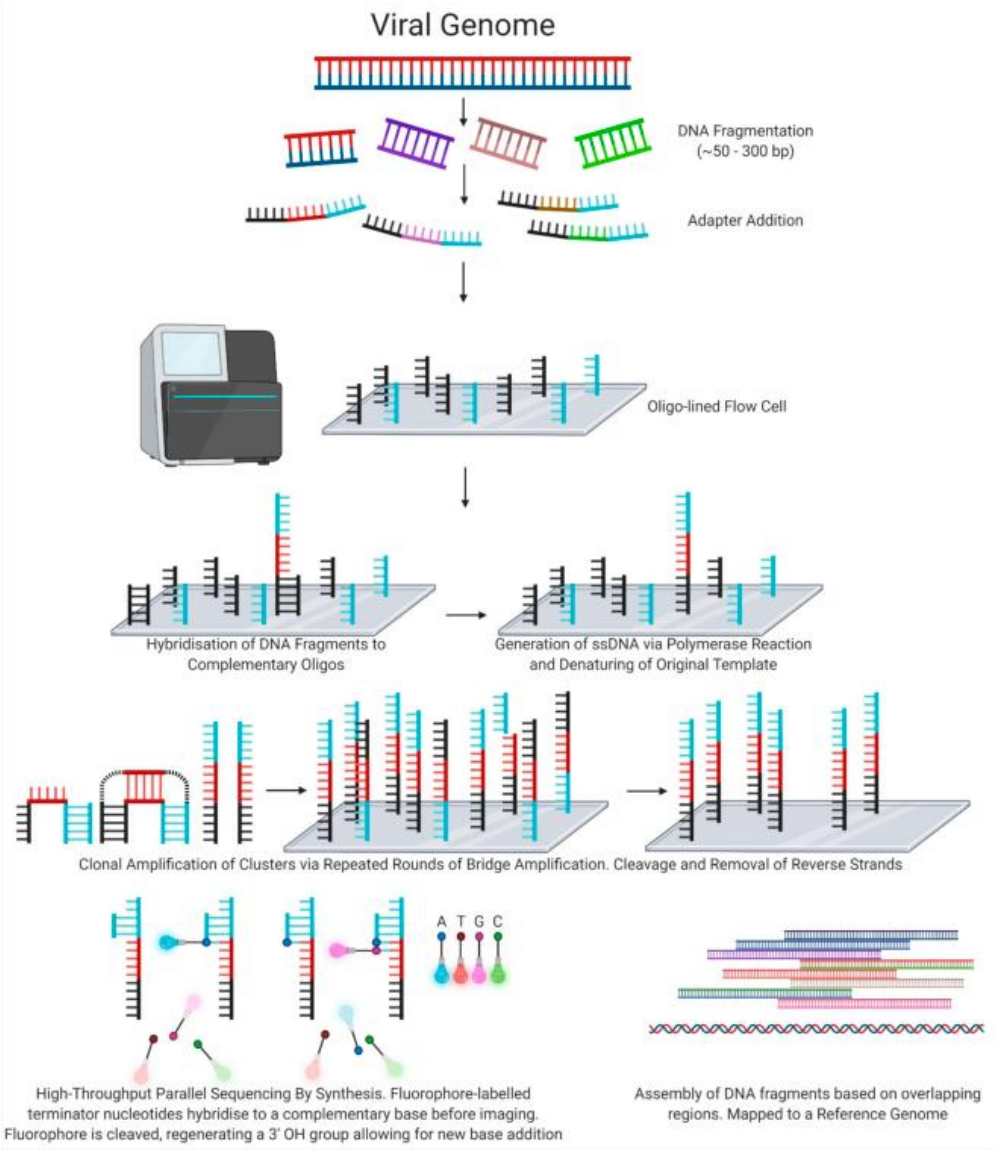

Figure 3. Next-Generation Sequencing: Illumina short-read technology.

3.3. Next-Generation Sequencing Technologies: A Comparison

The main limitation of Illumina short-read technology in DMS studies is the short-read length. Viral segments for analysis are often much longer than the read length of the instrument. If two distant mutants are present in a single viral genome, and a specific phenotype is observed, it is difficult to determine without further experimentation if they are acting in a pairwise manner or if a single mutation is wholly responsible for

the phenotype. Thus, pairwise epistatic mutations are not always resolvable using short-read technology. A partial solution to this problem is to create multiple adjacent mutant libraries of short lengths, 'tiling' across a gene, to restrict epistatic mutations to within a readable window [44]. Alternatively, subassembly can be utilised. In this approach, tagging each template molecule with a unique DNA barcode or 'unique molecular identifier' (UMI) allows for the grouping and analysis of multiple short reads on the basis of their original template molecule [45]. Resolution of distant mutants is only possible using third generation long-read sequencing strategies, offered by both SMRT and ONT.

Of the long-read sequencing platforms, SMRT is far more common than ONT in DMS studies, likely attributed to its higher accuracy. The circular SMRTbell DNA conformation allows for increased sequencing depth (how often a base is sequenced on average) to form a consensus sequence, as the SMRTbell can be repeatedly sequenced. Errors in PacBio sequencing are distributed randomly, and therefore the accuracy increases with increased reads of a single SMRTbell molecule [46]. Oxford Nanopore sequencing utilises dsDNA fragments, but does not allow continuous sequencing. A consensus sequence can be formed by sequencing one strand of dsDNA, followed immediately by the complementary strand, referred to as $1D^2$ sequencing, though the accuracy is somewhat limited compared to PacBio and Illumina strategies [46]. Interestingly, a recent study has reported a high-throughput amplicon sequencing approach that combines UMIs with PacBio or ONT to enable generation of high-accuracy single-molecule consensus sequences for large DNA regions [47]. This and similar approaches will help to overcome compromises in accuracy that have previously been associated with the above long-read sequencing strategies. To date, however, Illumina sequencing remains the most commonly used platform in DMS studies due to its cost-effectiveness and high levels of accuracy.

4. Deep Mutational Scanning: Library Construction

As mentioned previously, the first step in a DMS experiment is the construction of a mutant library. Multiple approaches have been developed and applied to mutant library generation, which we will briefly describe below.

The simplest and most cost-effective method is error-prone PCR. In this method, one or more polymerases are employed to exponentially amplify a region of DNA, with initial template amount and cycle number varied to optimise mutation rate [48]. *Taq* DNA polymerase, a popular error-prone polymerase, has a reaction buffer-dependent mutation rate of roughly 8×10^{-6} errors/nucleotide [49]. However, the use of Taq polymerase alone in library construction is limited by the mutants generated being dominated by AT $\rightarrow$ GC transitions and AT $\rightarrow$ TA transversions, at approximately 2–4x the mutation rate of G and C residues. A polymerase named Mutazyme DNA polymerase has a 2–4x stronger preference for GC $\rightarrow$ AT transitions and GC $\rightarrow$ TA transversions [50]. In combination, these enzymes can be used to produce a relatively unbiased mutant library with a somewhat controllable mutation rate. A major drawback of this method is that not all amino acid residues are accessible with single-nucleotide polymorphisms [51]. Additionally, this technique can often result in multiple mutations present in a single DNA fragment that can confound results, especially when using short-read sequencing strategies as mentioned earlier.

First described in virology studies by the Bloom lab in an Influenza nucleoprotein (NP) study, synthetic oligonucleotides were designed to contain a randomised triplet for each codon present in the gene, with 16 leading and lagging nucleotides that anneal specifically to the NP gene, as well as the reverse complement of these oligonucleotides. Using a series of joining PCR steps and restriction enzyme cloning, a product pool containing all possible amino acid mutations of NP was cloned into an Influenza reverse genetics system [6]. When designing oligonucleotides with randomised triplets, codon usage should be considered. NNK degeneracy (N: Ade/Cyt/Gua/Thy, K: Gua/Thy) encodes all amino acids, while NDT (N: Ade/Cyt/Gua/Thy, D: Ade/Gua/Thy, T: Thy) and DBK (D: Ade/Gua/Thy, B: Cyt/Gua/Thy, K: Gua/Thy) each encode 12 amino acids, feature no stop codons and exhibit all major biophysical types, while potentially decreasing workload. However,

with decreased coverage, the amount of interesting variants will also be reduced [52]. This method is more costly compared to the error-prone PCR method, but can be used to generate libraries with complete mutational coverage.

A synthetic approach to mutant library generation is also available. Gene synthesis begins with oligonucleotide construction. These are designed such that adjacent oligonucleotides in the final product contain overlapping sequences. The overlap results in a DNA duplex which, through an assembly reaction with DNA polymerase, results in the construction of the gene of interest [53]. Multiple methods allow for controlled or randomised insertion of mutants into a gene. For example, the "Spiked Genes" method uses oligonucleotides spiked, or interspersed, with mutants to create a pooled mutant fragment [54]. Synthetic construction of multiple types of mutant libraries is possible through commercially available gene synthesis services. Available mutant library types include controlled randomised libraries, scanning alanine mutagenesis libraries, scanning codon mutagenesis libraries and others.

An additional type of mutant library discussed in this review is the transposon insertion library. This is facilitated by a transposase protein, such as Tn5, Tn7 or MuA that recognizes the ends of a transposon, or a mobile DNA element, and forms a protein-DNA complex termed the 'transpososome'. This complex catalyses cleavage of target DNA at a random site (although evidence of insertion bias exists [55]), and joining reactions allow for the introduction of the transposon into a DNA template. For many applications, the transposon is engineered to feature an antibiotic resistance gene, allowing for selection of genetic elements with successful transposon integration. In these systems the transposon also features two identical restriction enzyme sites on each end of the DNA element. Upon purification, the now-unique plasmids are digested with the required restriction enzyme. Gel electrophoresis allows for the removal of the majority of the introduced DNA element by size separation, with a small insertion remaining after ligation of the plasmid backbone [56,57]. High-throughput random mutagenesis of a cloned viral genome paired with deep scanning allows for incredibly powerful studies which can probe regions of genomic flexibility and functionality.

5. Standard Deep Mutational Scanning Experiment Methodology

DMS experiments often follow a similar methodology. Using a reverse genetics system, a mutant virus library is generated via a method such as randomised mutagenesis, controlled site-saturation mutagenesis, or transposon mutagenesis. This library is often initially amplified using bacteria, with a higher number of uniquely transformed plasmids translating to increased mutational diversity. This library is transfected into cells, allowing for the propagation of RNA replication-competent viral genomes, as well as production of viral particles. Infection of naïve cells with virus-containing cell culture supernatants allows for propagation of genomes which are capable of both RNA replication and infectious particle production. Variant analysis by NGS is then key to identifying specific variants which are present at higher or lower levels at certain stages of the viral lifecycle in comparison to the initial input (Figure 4).

While not a major focus in this review, it is important to note that DMS studies of individually expressed proteins have been highly informative, particularly in the context of the interactions of viral glycoproteins with host receptors or neutralising antibodies. For example, angiotensin-converting enzyme 2 (ACE2), the host receptor for SARS-CoV-2 [58], has been analysed for mutants which enhance binding to the spike glycoprotein, to explore the use of an engineered soluble ACE2 as a potential therapeutic [59,60]. The binding of computer-generated miniprotein inhibitors [61] and ACE2 decoys [62] to the spike glycoprotein has also been effectively optimised using DMS. A similar strategy was used to optimise affinity and specificity of a computationally designed protein that targets H1N1 Influenza haemagglutinin [63,64].

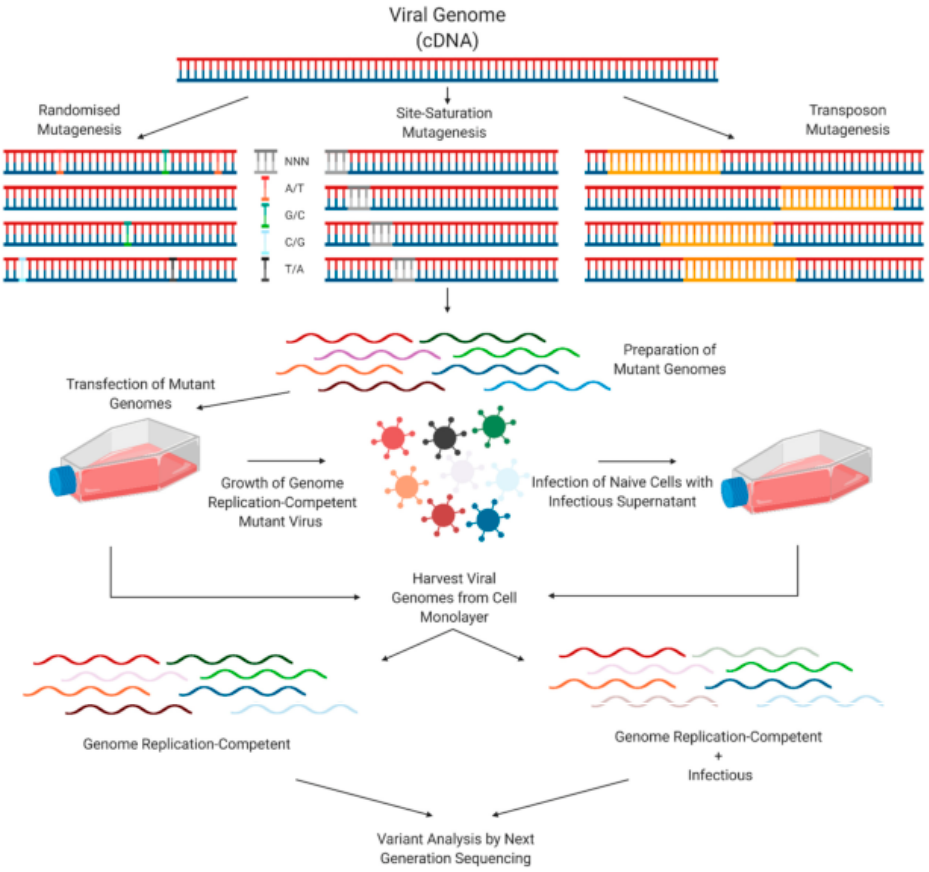

Figure 4. Standard methodology of a DMS experiment.

6. Bioinformatic Tools for Deep Mutational Scanning Data Analysis and Visualisation

Multiple software packages are available which facilitate variant analysis. 'dms_tools' [65] and 'Enrich2' [66] calculate amino acid preferences under a selective pressure. 'dms-view' allows straightforward visualisation of DMS data in the context of a protein structure [67]. 'MaveDB' (multiplex assays of variant effect database) provides a tool for sharing DMS data analyses.

7. Deep Mutational Scanning Experiments

In this section, we will briefly describe several past applications of DMS in virology, focussing on *Flaviviridae* family viruses, IAV and SARS-CoV-2. Transposon mutagenesis has been applied to several viruses to identify genomic regions tolerant to small insertions. An insertion with minimal impact on fitness indicates genomic flexibility, or high mutability, at a specific area, which may allow for adaptation of the virus to a new environment. Disruption of function from an insertion may also reveal a region of functionality within a gene or protein. The identification of a region of insertional tolerance is often exploited by incorporation of epitope tags or reporter genes for further research. DMS projects focussing on single-nucleotide polymorphisms and codon mutagenesis have focussed on

several biological aspects, including identifying determinants of viral tropism, epistatic interactions, drug and antibody escape mutants, and residues critical to several biological functions. It is important to note that the following summary is not a comprehensive list of all DMS scanning projects. DMS has also been applied to viruses including Norovirus [68], Venezuelan equine encephalitis virus [69], Measles virus [70], Paramyxoviruses [71], foot-and-mouth disease virus [72], Epstein–Barr virus [73] and Human immunodeficiency virus [74–79], and as mentioned previously, we focus mainly on studies of viral replicative fitness and immune evasion.

7.1. Hepatitis C Virus (HCV)

7.1.1. Transposon Analysis

In a comprehensive early study by Remenyi et al., the Mu-transposon system was used to insert 15 nucleotide (nt) sequences (of which 10 nt are transposon derived and 5 nt are duplicated target sites) into an HCV plasmid based on the chimeric sequence of genotype 2a J6 and JFH1 viruses [80]. This mutant library was propagated in human hepatoma Huh-7.5.1 cells, then passaged onto naïve Huh-7.5.1 cells to separately analyse genomes capable of viral RNA replication and infectious particle production. Regions tolerant to an insertion illustrate flexibility at the genomic level, and potentially highlight a region non-essential for in vitro growth. P7 and non-structural protein 2 (NS2), each coordinators of virus assembly [81], and envelope protein 2 (E2) were identified as potential areas for insertion of a tag or small peptide with minimal costs to replicative fitness due to the regions of high genomic flexibility uncovered. The impact of NS4B transposon insertions on infectious particle production helped to reveal a previously unknown functional region of NS4B which was suggested to play a role in the viral lifecycle post-RNA replication.

In a subsequent study by the same group, a similar methodology was used to assess insertions that confer sensitivity to the antiviral cytokine Interferon alpha (IFN-α) [82]. After two rounds of passage in Huh-7.5.1 cells in the presence or absence of IFN-α, it was observed that mutants conferring sensitivity to IFN-α were clustered in p7, the 3′ untranslated region (UTR) and non-structural protein 5A (NS5A), which is important for viral replication, infectious virus particle production and modulation of host cell signalling [83]. Eight IFN-α sensitive p7 insertion mutants were constructed for validation, and revealed the role of p7 in immune evasion. An interferon-stimulated gene (ISG) cDNA expression library screen demonstrated that 13 of these ISGs were particularly antiviral against viruses with mutant p7 in comparison to wild-type p7. Amongst these ISGs, IFI6-16 was identified as a major target of p7-mediated immune evasion. Coimmunoprecipitation was then used to show a direct interaction between p7 and IFI6-16, which was previously unknown. Each of these DMS studies furthered understanding of the roles of HCV proteins in infection.

7.1.2. Variant Analysis

In an important application of DMS towards understanding emergence of viral resistance to antiviral drugs Qi et al. applied high-throughput variant analysis towards understanding resistance to Daclatasvir [84]; a potent inhibitor of NS5A [85]. An NS5A mutant library of the J6/JFH1 strain (genotype 2a) was prepared and passaged in Huh7.5.1 cells in the presence or absence of daclatasvir over 2 passages, before analysis by NGS. Drug selection resulted in selection of drug-resistant mutants at NS5A residues 28, 31, 38, 92 and 93, and increased drug resistance of some mutants at four additional residues. These escape mutants can be used to identify daclatasvir-resistant strains of HCV [86]. In support of this methodology, many of these resistance mutations have been identified in numerous in vitro and clinical studies of HCV resistance to Daclatasvir and related inhibitors [87].

7.2. Zika Virus (ZIKV)

7.2.1. Transposon Analysis

In the first published study involving high-throughput mutational analysis of ZIKV a transposon insertion mutant library was generated for the ZIKV MR-766 strain [88]. Human embryonic kidney 293T (HEK 293T) cells were used to propagate the virus, then naïve African green monkey kidney Vero cells were infected with viral supernatants over two rounds. The first pool of selected viral RNA, reflecting viral RNA replication requirements in HEK 293T cells, showed high levels of flexibility in the structural proteins Envelope (E), precursor membrane (prM) and capsid (C), and also non-structural protein 1 (NS1), which is essential for ER remodelling and RNA replication [89]. The third pool, consisting of infectious particle production-competent genomes, displayed most flexibility in the structural proteins. Some insertions present in NS1 rendered the virus incapable of infectious particle production while enhancing viral RNA replication capacity. In this context, an insertion after amino acid 174 resulted in >650-fold enrichment in the initial HEK 293T cell viral RNA population compared to the input RNA library yet was not present in the Vero cell populations. Together, this study revealed regions of genetic rigidity in the ZIKV genome across multiple lifecycle stages.

7.2.2. Variant Analysis

Envelope

Several mutational analyses of the ZIKV Envelope (E) protein have been performed. An envelope mutant library for the MR766 ZIKV strain was constructed by Sourisseau et al. to examine how mutants affect viral neutralisation by monoclonal antibodies [90]. The MR-766 strain was first tested for the effects of mutations on viral fitness, with a focus on infectious particle production in Vero cells. After validation, mutational antigenic profiling was performed, whereby the selective pressure of a neutralising antibody results in the enrichment of escape mutants present in the mutant library. Two antibodies were used in this screen; ZKA64, which binds domain III of recombinant E protein, and ZKA185 which neutralises ZIKV without interaction with E protein, or any confirmed epitope [91]. Domain III of E protein is responsible for binding the cellular receptor, and is a common target of potent ZIKV-neutralising antibodies [92]. The mutant ZIKV library was subjected to these antibodies individually. ZKA64 and ZKA185 treatment resulted in strong selection of several mutations that corresponded to sites within E, with mutants selected by ZKA64 present on envelope domain III, and mutants selected by ZKA185 present on envelope domain II. Antibody escape resistance mutations A333T and T335E for ZKA64, and D67A and K118R for ZKA185, were confirmed in follow-up neutralisation assays, illustrating the usefulness and accuracy of mutational antigenic profiling for escape mutant predictions, and demonstrating that antibody escape mutants can appear outside the receptor binding domain.

The impact of Envelope on tropism using ZIKV strain PRVABC59 has also been examined [93]. This study analysed mutant library growth in three cell types: C6/36 cells, derived from *Aedes albopictus* larvae, A549 adenocarcinomic human epithelial cells and hCMEC/D3 cells, a human blood–brain barrier endothelial cell line. NGS analysis revealed that a mutation at N154, an N-linked glycosylation site on the ZIKV envelope protein, resulted in a significantly higher fitness of ZIKV in mosquito cells, but not in human cells. Additionally, ablation of glycosylation through mutations surrounding the N154 position enhanced viral entry into C6/36 cells, resulting in increased levels of viral replication. DC-SIGN is a known viral entry factor for ZIKV that is not expressed in 293T cells such that overexpression of DC-SIGN in 293T cells enhances ZIKV infection [94]. A comparison between wild-type ZIKV and ZIKV glycosylation mutants showed that, with overexpression of DC-SIGN, infection of 293T cells by the glycosylation mutant ZIKV was significantly diminished compared to wild-type ZIKV, demonstrating the requirement of N-linked glycosylation of E in viral entry into mammalian cells, despite the resultant loss of fitness in mosquito cells.

In a similar study into cell tropism, a mutant library for the C-terminal of the E protein of ZIKV (PRVABC59) was prepared and grown in Vero and C6/36 cells for 8 and 13 days, respectively, to identify host-adaptive substitutions [95]. In C6/36 cells, mutants K316Q and S461G were preferentially selected. The K316Q/S461G virus replicated less efficiently in a selection of human cell lines, with lower levels of cytotoxicity compared to wild type, while no change was seen in C6/36 and Aag2 mosquito cell lines. This combinatorial mutant was determined to decrease the thermal stability of E, and as mosquito cell lines are typically grown at a lower temperature (28 °C) than human cell lines, the effect was not observed in the mosquito cell line. ZIKV infection can result in severe developmental defects in the brain [96]. The K316Q/S461G virus was used to infect induced-pluripotent stem cell-derived human brain organoids. Development of these organoids infected with the K316Q/S461G virus greatly decreased growth retardation in comparison to wild-type ZIKV. Infection of interferon alpha receptor knockout mice showed attenuated infection by the K316Q/S461G virus, and protection against a later wild-type ZIKV infection, indicating its potential as an attenuated vaccine candidate.

7.3. Dengue Virus (DENV)

Transposon Analysis

To identify regions of genetic flexibility in DENV, our group applied the Mu transposase system to generate a library of mutants containing single random 15 nt insertions in a serotype 2 Dengue virus (DENV-2) genome (strain 16681) [97]. Analysing both viral RNA replication and infectious particle production in Huh7.5 cells, non-structural protein NS1, required for RNA replication [98] and virus assembly [10], as well as structural protein capsid (C) demonstrated highest tolerance to the insertions. Lowest tolerance of insertions was seen in structural protein prM and non-structural protein 2A (NS2A), which is essential for virus assembly [99]. Across the genome, flexibility peaked at the C termini for C, E, NS1, NS2B and NS4B, and at the N termini of NS3 and NS4B. These experiments allowed for the tagging of NS1 with epitope tags and reporter proteins including FLAG, APEX2 and NLuc, with minimal loss of viral fitness in Huh7.5 cells.

A similar transposon mutagenesis study of DENV-2 (16681) was performed by Perry et al. [100]. This study identified regions of genetic flexibility and enabled identification of well-tolerated insertion sites within non-structural protein 4B (NS4B), which is involved in membrane rearrangements [101], and C, which were utilised to create a DENV-2 clone expressing HA-tagged capsid, incapable of infectious particle production, and a replication-competent infectious DENV-2 clone expressing HA-tagged NS4B. Together, these studies identified regions of genetic flexibility within DENV-2 and exploited this information to generate infectious reporter virus tools.

7.4. Influenza A Virus (IAV)

7.4.1. Transposon Analysis

Transposon mutagenesis has also been applied to great effect with the Influenza (H1N1) A/Puerto Rico/8/1934 strain [102]. Mutagenized viral genome segments were transfected into HEK 293T cells, then viruses were passaged onto naïve Madin–Darby canine kidney (MDCK) cells for two rounds. NGS analysis revealed that two genes were tolerant to insertions; haemagglutinin (HA), an attachment factor and membrane fusion protein [103], and non-structural protein 1, responsible for immune evasion [104]. The mutant library was then grown in embryonated chicken eggs, to determine how the library would perform under different environmental pressures. HA features a head and stalk domain [105]. In chicken eggs, insertions in the head of HA were preserved, while mutants present in the stalk domain were not tolerated. Analysis of these HA head insertion mutants showed no loss of fitness and were found to occur at antigenic sites. The authors hypothesised that this flexibility may reflect a strategy in evasion of host immune systems.

7.4.2. Variant Analysis

Hemagglutinin and Neuraminidase

A major focus of IAV research is the functional analysis of NA, which aids virus budding, and HA, as antigenic variation of these proteins is responsible for the limited protection that vaccines provide against IAV infection [106]. Using a HA mutant library, Thyagarajan et al. illustrated that the antigenic sites of Influenza (H1N1) A/WSN/1933 HA are most tolerant to mutations, providing an explanation for Influenza's rapid antigenic evolution [107]. Similar effects were also reported in DMS studies by Wu et al. [108] and Boud et al. [109]. Influenza (H3N2) A/Perth/16/2009 HA has also been subject to analysis by DMS [110]. Interestingly, from these studies, mutational tolerance was demonstrated to be higher in the HA head for H1N1 Influenza strains, while mutational tolerance was higher in the HA stalk of H3N2 [110]. H3 virus DMS data was therefore shown to not be suitable for prediction of H1 virus evolution, while similarly H1 virus DMS data was not useful for prediction of H3 virus evolution.

Continuing research into HA and its immunogenicity, Doud et al. analysed the effects of single HA mutations on broad and narrow antibody neutralisation [111]. Broad neutralising antibodies are capable of neutralising multiple strains of a virus subtype, or neutralising multiple types of Influenza virus, due to their targeting of conserved regions of proteins, while narrow antibodies are strain specific [112]. Wild-type Influenza (H1N1) A/WSN/1933 was shown to be neutralised by broad anti-RBS and anti-stalk antibodies, and narrow anti-head antibodies. Doud et al. prepared HA mutant libraries of a lab-adapted Influenza (H1N1) A/WNS/1933 strain carrying green fluorescent protein in the PB1 segment and demonstrated that narrow anti-head antibodies as well as broad anti-RBS antibodies were highly susceptible to single mutation escape mutants, while broad anti-stalk antibodies were highly resistant to escape mutants.

Expanding on the single-strain studies of HA, multiple H3N2 IAV strains were investigated for strain-specific HA properties in a recent study by Wu et al. [113]. Five major antigenic sites (A-E) exist for H3N2 HA [114]. To investigate antigenic site B, mutant libraries of H3N2 strains A/Hong Kong/1/1968, A/Bangkok/1/1979, A/Beijing/353/1989, A/Moscow/10/1999, A/Brisbane/10/2007, and A/North Dakota/26/2016 were prepared. These libraries featured specific mutants of the HA receptor binding site at residues 156, 158, 159, 190, 193 and 196; each of which are known to affect receptor binding and viral fitness [115–118]. A local fitness landscape of each mutant for each strain was constructed, by transfection of the libraries into HEK 293T cells, and subsequent passage of the resultant virus onto MDCK-SIAT1 cells. Analysis of the fitness landscape of these strains illustrated that evolutionary constraints at these residues has changed during the natural evolution of H3N2, indicating that deep mutational scanning data is not always suitable for extrapolation across strains.

In another application of DMS to understand the evolution of IAV resistance to antiviral selective pressures, Wu et al. investigated the antiviral therapeutic Oseltamivir [119], which targets NA of various IAV strains [120]. Oseltamivir treatment has resulted in the generation of Influenza (H1N1) H274Y neuraminidase mutants which decrease sensitivity of the enzyme to oseltamivir. Despite fitness costs associated with the H274Y mutant, the mutant has quickly become widespread [121]. Studying the Influenza (H1N1) A/WSN/1933 virus with the H274Y mutant present, Wu et al. prepared a NA mutant library. After successive passages in A549 cells, four mutants were discovered which either fully (R194G, E214D) or partially (L250P, F239Y) restore H247Y A/WSN/1933 virus to wild-type fitness levels without restored susceptibility to oseltamivir. This study illustrates the power of DMS to understand and predict drug-resistant mutant strains and second site mutations that restore fitness of otherwise attenuated drug-resistant virus strains.

Polymerase

Another IAV machinery that has been the subject of DMS studies is the viral polymerase. One of the most comprehensive studies of this nature involved analysis of adap-

tation of the complex from avian to human cells by Soh et al. [122]. The core of the Influenza virus RNA polymerase consists of the polymerase acidic protein (PA) C-terminal domain, polymerase basic protein 1 (PB1) and the N-terminal of polymerase basic protein 2 (PB2) [123]. PB2 is a known virulence determinant [124] and it has been shown that a single amino acid substitution (E627K) allows avian IAV to replicate efficiently in mammalian cells [125]. Bioinformatics analyses reviewing IAV sequence databases have revealed other mutants which have facilitated host adaptation in the past [126,127]. However, these databases are likely incomplete and limited to past outbreaks. To address these ambiguities, Soh et al. constructed a PB2 mutant library to reveal mutants of Influenza (H7N9) A/Green-winged Teal/Ohio/175/1986 PB2 which improve either polymerase activity or viral replication in human A549 cells in comparison to avian embryo CCL141 cells, to predict mutants which may allow expansion of transmission towards mammalian species. Thirty-three previously undescribed adaptive mutants were discovered. These adaptive mutations were clustered in patches, potentially revealing regions of PB2 responsible for host cell interactions.

Ozawa et al. applied a novel DMS approach to investigate avian Influenza polymerase mutant residues of PA, PB1 and PB2, and their effect on host range [128]. A virus possessing vRNA of both avian Influenza (H5N1) A/Muscovy duck/Vietnam/TY93/2007 and a laboratory-adapted Influenza (H1N1) A/WSN/33, including a partial HA deletion mutant featuring GFP was constructed. Growth of the virus was therefore limited to HA-expressing cell lines. Mutant libraries were generated for PA, PB1 and PB2. The mutant virus library was grown in 293-HA cells, and the highest GFP-expressing 293-HA cells were individually sorted by flow cytometry for infection of naïve MDCK-HA cells. Analysis of expression of matrix protein by quantitative reverse transcription PCR was used to identify 90 viruses for further analysis by deep sequencing. After additional testing, 11 mutants were further characterised in lung and bronchial epithelial cells as well as chicken fibroblast cells, for viral kinetics and polymerase activity, and then for viral replication and pathogenesis in mice, identifying multiple mutants which may increase virulence in mammals.

Continuing the molecular interrogation of PA, Wu et al. coupled DMS with in silico mutant stability predictions to identify functional regions of Influenza (H1N1) A/WSN/1933 PA [129]. A PA mutant library of this strain was used to infect A549 cells, allowing identification of both functionally and structurally important residues. In addition, a protein stability predictor, Rosetta, was used to identify residues of structural importance [130]. Pairing these methods of analysis allowed exclusion of structurally important residues from residues that were deemed to be deleterious by DMS, isolating only functional effects. The study identified multiple residues of PA which abolish polymerase activity with no detectable destabilization effect, as well as residues with little impact on polymerase activity, but a substantial decrease in infectious particle production. While most mutational studies focus on conserved regions for protein functionality, which can exclude species- and strain-specific functional residues, this study by Wu et al. illustrated an unbiased means of determining residues that are strictly functionally important, as opposed to structurally important.

Assorted Viral Proteins and DMS Applications

Another application of DMS that is gaining attention involves analysis of viral determinants of sensitivity to innate immune responses. As an example of this, Ashenberg et al. explored resistance to the antiviral host factor MxA [131]. IAV nucleoprotein (NP) forms the viral ribonucleoprotein complex with vRNA and the heterotrimeric RNA-dependent RNA polymerase, and acts as an elongation factor [123,132]. Antiviral host factor MxA is known to suppress viral transcription through its interaction with polymerase PB2 subunit and NP [133]. IAV strains have been identified which either block interferon-induced production of MxA, or, through adaptive mutations, directly confer resistance to MxA [134,135]. Ashenberg et al. determined the impact of all mutant NP residues of Influenza (H3N2) A/Aichi/2/1968 on MxA resistance in MDCK-SIAT1 canine kidney cells

either wild type or constitutively expressing MxA. Twenty nine mutants impacting MxA resistance were identified via the screen, with further analysis identifying mutants which increase sensitivity, or increase resistance.

Viral resistance and sensitivity to the antiviral effects of interferons (IFNs) is another emerging application of DMS methodology, as exemplified by a recent study by Du et al. [136]. Many interactions between IAV and the host immune system, as well as host evasion strategies, have long been a focus of interest [137]. Du et al. performed a genome-wide mutant screen for Influenza (H1N1) A/WNS/1933 to discover mutants that alter interferon sensitivity. Virus was grown first in HEK 293T cells, then passaged in A549 cells in the presence or absence of type 1 interferon pre- and post-infection, directly prior to analysis of mutant abundance. Twenty six missense mutations that decreased relative fitness under interferon treatment were randomly selected for further analysis. Eight mutants from viral polymerase subunit PB2, matrix protein M1 and non-structural protein 1 were chosen for further investigation, and then combined to create an interferon-sensitive virus. This mutant IAV showed no attenuation in IFN-deficient Vero cells, but significant attenuation in IFN-competent A549 cells compared to the wild-type IAV strain. Additionally, the virus was attenuated in IFN-competent mice and ferrets, but not IFN AR-/- mice, and acted as an attenuated vaccine, protecting mice and ferrets from broad viral challenges. This study therefore allowed the identification of potential attenuated vaccine candidates.

Further exploring IAV's capacity to evade immunity, Wu et al. constructed a mutant library for the vRNA segment of Influenza (H1N1) A/WSN/1933 which encodes NS1 [138], given the critical role of NS1 as an antagonist of the innate immune response [137]. The virus was passaged in the presence or absence of type I interferon in A549 cells. Multiple SNPs displayed >2-fold higher interferon sensitivity compared to WT virus. In particular, D92Y of NS1 showed 12-fold higher sensitivity to the interferon treatment. This mutant was demonstrated to disrupt a hydrophobic pocket on NS1, which appeared to be critical for anti-interferon activity. Further research demonstrated a critical role for the domain in inhibition of RIG-I ubiquitination, a requirement for functional interferon signalling [139].

DMS is an ideal technique for discovery of single-residue changes that impact on viral fitness. However, it can be challenging to investigate paired mutants of significance, even if the mutants happen to be present on a single genome within a DMS experiment dataset. Wu et al. combined a high-throughput genetic study with analysis of naturally occurring sequences to identify a compensatory mutation in matrix protein M1 of IAV [140]. M1 acts as an endoskeleton for the virus [141] and aids virus budding [142]. Transfection of HEK 293T cells with Influenza (H1N1) A/WNS/1933 with a mutant M segment, followed by infection of A549 cells allowed identification of deleterious mutants. Thirteen deleterious mutants were validated, and it was found that 3 of these were prevalent in nature, including M1 Q214H. The software CAPS (Coevolution analysis using protein sequences) allows for identification of co-evolving amino acids with a time-dependent analysis of the evolution of pairs of amino acids from a changing sequence [143]. The analysis using CAPS revealed that M1 214 coevolves with residues 121, 207, 209 and 214. The A209T mutation was found to be compensatory for Q214H, revealing a novel pairwise epistatic interaction.

7.5. Severe Acute Respiratory Syndrome Coronavirus 2 (SARS-CoV-2)

Variant Analysis

The recent devastating outbreak of SARS-CoV-2 prompted the application of DMS to investigation of binding of the viral spike protein to the angiotensin-converting enzyme 2 (ACE2) receptor [144]. Specifically, this study explored the effects of all amino acid mutations of the receptor-binding domain (RBD) of a Wuhan-Hu-1 SARS-CoV-2 isolate on its interaction with angiotensin-converting enzyme 2 (ACE2) to identify potential targets of future antiviral strategies [145]. Two mutant libraries were prepared and expressed in a yeast-surface display platform. RBD mutant expression was measured using a fluorescent tag and sorted by flow cytometry based on expression levels into bins for analysis by deep

sequencing. ACE2 binding was then measured by incubation of cells with fluorescently labelled ACE2, which was separated by flow cytometry into bins for further deep sequencing. Analysis revealed considerable mutational tolerance of RBD for ACE2 binding and normal expression levels. Mutants enhancing affinity for ACE2 were found at RBD sites Q493, Q498 and N501. After publication, the SARS-CoV-2 variant VOC-202012/01, containing an N501Y mutant, spread rapidly throughout the UK and South Africa, indicating the real-world applicability of DMS [146]. In a follow up study, these RBD mutant libraries were tested for escape from 10 human monoclonal antibodies [147]. Escape mutants were identified using the yeast display platform model, with FACS determining ACE2 binding levels. Most escape mutants appeared at the receptor-binding motif, where ACE2/RBD contact residues are present. Negative-stain electron microscopy was used to determine antigenic regions of the RBD for each antibody. This information allowed prediction of effective antibody cocktails which do not allow enrichment of escape mutants

8. Concluding Remarks

DMS is an incredibly powerful tool for rapid and high-throughput mutational analysis of viral proteins and genomes, and the above studies have illustrated the plethora of applications that DMS offers to virology. DMS has allowed the construction of attenuated vaccines, evolutionary studies, identification of functional regions of proteins, prediction of mutants that increase host range and many other applications. As the feasibility of NGS increases due to decreases in the cost of such studies, we will likely have a very detailed view of the impact of point mutations for many viral genes. We hope that the recent development of bioinformatic tools and databases which facilitate visualisation and sharing of gathered DMS data will enable and encourage researchers to utilise existing data for further experimentation, akin to the Protein Data Bank. The DMS-based discovery of a SARS-CoV-2 N501 RBD mutant with enhanced ACE2-binding affinity, prior to its natural appearance as a highly trasmissible variant reinforces the utility of DMS. However, it also illustrates the need for strict biosafety measures in the field, in order to prevent the accidental or intentional release of laboratory-created gain-of-function mutants. It has been suggested that publication of specific gain-of-function mutations should be regulated to ensure they are not recreated and misused, with data available on request. Alternatively, as some have argued, studies which may produce gain-of-function mutations in viruses with pandemic potential should be carefully scrutinised and regulated. For additional reading, we refer to two Editorials for further thoughts on the ethical considerations of gain-of-function experiments [148,149].

Author Contributions: Conceptualization, N.S.E.; investigation, T.D.B.; writing—original draft preparation, T.D.B.; figure preparation, T.D.B.; writing—review and editing, T.D.B. and N.S.E.; supervision, N.S.E.; funding acquisition, N.S.E. All authors have read and agreed to the published version of the manuscript.

Funding: This research was funded by the National Health and Medical Research Council (NHMRC) of Australia, awarded to N.SE. (APP1163662).

Data Availability Statement: Figures are created with BioRender.com.

Conflicts of Interest: The authors declare no conflict of interest.

References

1. Fowler, D.M.; Stephany, J.J.; Fields, S. Measuring the activity of protein variants on a large scale using deep mutational scanning. *Nat. Protoc.* **2014**, *9*, 2267–2284. [CrossRef] [PubMed]
2. Livesey, B.J.; Marsh, J.A. Using deep mutational scanning to benchmark variant effect predictors and identify disease mutations. *Mol. Syst. Biol.* **2020**, *16*. [CrossRef] [PubMed]
3. Klesmith, J.R.; Bacik, J.-P.; Wrenbeck, E.E.; Michalczyk, R.; Whitehead, T.A. Trade-offs between enzyme fitness and solubility illuminated by deep mutational scanning. *Proc. Natl. Acad. Sci. USA* **2017**, *114*, 2265–2270. [CrossRef] [PubMed]
4. Li, C.; Qian, W.; MacLean, C.J.; Zhang, J. The fitness landscape of a tRNA gene. *Science* **2016**, 352, 837–840. [CrossRef] [PubMed]

5. Sarkisyan, K.S.; Bolotin, D.A.; Meer, M.V.; Usmanova, D.R.; Mishin, A.S.; Sharonov, G.V.; Ivankov, D.N.; Bozhanova, N.G.; Baranov, M.S.; Soylemez, O.; et al. Local fitness landscape of the green fluorescent protein. *Nature* **2016**, *533*, 397–401. [CrossRef]
6. Bloom, J.D. An Experimentally Determined Evolutionary Model Dramatically Improves Phylogenetic Fit. *Mol. Biol. Evol.* **2014**, *31*, 1956–1978. [CrossRef]
7. Canale, A.S.; Cote-Hammarlof, P.A.; Flynn, J.M.; Bolon, D.N. Evolutionary mechanisms studied through protein fitness landscapes. *Curr. Opin. Struct. Biol.* **2018**, *48*, 141–148. [CrossRef]
8. Newberry, R.W.; Leong, J.T.; Chow, E.D.; Kampmann, M.; DeGrado, W.F. Deep mutational scanning reveals the structural basis for α-synuclein activity. *Nat. Chem. Biol.* **2020**, *16*, 653–659. [CrossRef]
9. Adkar, B.V.; Tripathi, A.; Sahoo, A.; Bajaj, K.; Goswami, D.; Chakrabarti, P.; Swarnkar, M.K.; Gokhale, R.S.; Varadarajan, R. Protein Model Discrimination Using Mutational Sensitivity Derived from Deep Sequencing. *Structure* **2012**, *20*, 371–381. [CrossRef]
10. Scaturro, P.; Cortese, M.; Chatel-Chaix, L.; Fischl, W.; Bartenschlager, R. Dengue Virus Non-structural Protein 1 Modulates Infectious Particle Production via Interaction with the Structural Proteins. *PLoS Pathog.* **2015**, *11*, e1005277. [CrossRef]
11. Wang, W.; Guan, M.; Liu, Y.; Xu, Q.; Peng, H.; Liu, X.; Tang, Z.; Zhu, Y.; Wu, D.; Ren, H.; et al. Alanine scanning mutagenesis of hepatitis C virus E2 cysteine residues: Insights into E2 biogenesis and antigenicity. *Virology* **2014**, *448*, 229–237. [CrossRef] [PubMed]
12. Urabe, M.; Hasumi, Y.; Kume, A.; Surosky, R.T.; Kurtzman, G.J.; Tobita, K.; Ozawa, K. Charged-to-Alanine Scanning Mutagenesis of the N-Terminal Half of Adeno-Associated Virus Type 2 Rep78 Protein. *J. Virol.* **1999**, *73*, 2682–2693. [CrossRef] [PubMed]
13. Murray, C.L.; Jones, C.T.; Tassello, J.; Rice, C.M. Alanine Scanning of the Hepatitis C Virus Core Protein Reveals Numerous Residues Essential for Production of Infectious Virus. *J. Virol.* **2007**, *81*, 10220–10231. [CrossRef]
14. Lefevre, F. Alanine-stretch scanning mutagenesis: A simple and efficient method to probe protein structure and function. *Nucleic Acids Res.* **1997**, *25*, 447–448. [CrossRef] [PubMed]
15. Dolan, P.T.; Taguwa, S.; Rangel, M.A.; Acevedo, A.; Hagai, T.; Andino, R.; Frydman, J. Principles of dengue virus evolvability derived from genotype-fitness maps in human and mosquito cells. *eLife* **2021**, *10*. [CrossRef] [PubMed]
16. Ilyushina, N.A.; Khalenkov, A.M.; Seiler, J.P.; Forrest, H.L.; Bovin, N.V.; Marjuki, H.; Barman, S.; Webster, R.G.; Webby, R.J. Adaptation of Pandemic H1N1 Influenza Viruses in Mice. *J. Virol.* **2010**, *84*, 8607–8616. [CrossRef]
17. Choi, E.-J.; Lee, Y.J.; Lee, J.-M.; Kim, Y.-J.; Choi, J.-H.; Ahn, B.; Kim, K.; Han, M.G. The effect of mutations derived from mouse-adapted H3N2 seasonal influenza A virus to pathogenicity and host adaptation. *PLoS ONE* **2020**, *15*, e0227516. [CrossRef]
18. Bouvier, N.M.; Palese, P. The biology of influenza viruses. *Vaccine* **2008**, *26*, D49–D53. [CrossRef]
19. Phillips, H. The Recent Wave of 'Spanish' Flu Historiography. *Soc. Hist. Med.* **2014**, *27*, 789–808. [CrossRef]
20. Ducatez, M.; Webster, R.; Webby, R. Animal influenza epidemiology. *Vaccine* **2008**, *26*, D67–D69. [CrossRef]
21. Kim, H.; Webster, R.G.; Webby, R.J. Influenza Virus: Dealing with a Drifting and Shifting Pathogen. *Viral Immunol.* **2018**, *31*, 174–183. [CrossRef] [PubMed]
22. Novel Swine-Origin Influenza A (H1N1) Virus Investigation Team. Emergence of a Novel Swine-Origin Influenza A (H1N1) Virus in Humans. *N. Engl. J. Med.* **2009**, *360*, 2605–2615. [CrossRef]
23. Barrows, N.J.; Campos, R.K.; Liao, K.-C.; Prasanth, K.R.; Soto-Acosta, R.; Yeh, S.-C.; Schott-Lerner, G.; Pompon, J.; Sessions, O.M.; Bradrick, S.S.; et al. Biochemistry and Molecular Biology of Flaviviruses. *Chem. Rev.* **2018**, *118*, 4448–4482. [CrossRef] [PubMed]
24. Bhatt, S.; Gething, P.W.; Brady, O.J.; Messina, J.P.; Farlow, A.W.; Moyes, C.L.; Drake, J.M.; Brownstein, J.S.; Hoen, A.G.; Sankoh, O.; et al. The global distribution and burden of dengue. *Nat. Cell Biol.* **2013**, *496*, 504–507. [CrossRef] [PubMed]
25. Chen, L.H.; Wilson, M.E. Yellow fever control: Current epidemiology and vaccination strategies. *Trop. Dis. Travel Med. Vaccines* **2020**, *6*, 1. [CrossRef] [PubMed]
26. Hegde, N.R.; Gore, M.M. Japanese encephalitis vaccines: Immunogenicity, protective efficacy, effectiveness, and impact on the burden of disease. *Hum. Vaccines Immunother.* **2017**, *13*, 1320–1337. [CrossRef] [PubMed]
27. Munster, V.; Koopmans, M.; Van Doremalen, N.; Van Riel, D.; De Wit, E. A Novel Coronavirus Emerging in China—Key Questions for Impact Assessment. *N. Engl. J. Med.* **2020**, *382*, 692–694. [CrossRef] [PubMed]
28. Lau, S.K.P.; Lee, P.; Tsang, A.K.L.; Yip, C.C.Y.; Tse, H.; Lee, R.A.; So, L.-Y.; Lau, Y.-L.; Chan, K.-H.; Woo, P.C.Y.; et al. Molecular Epidemiology of Human Coronavirus OC43 Reveals Evolution of Different Genotypes over Time and Recent Emergence of a Novel Genotype due to Natural Recombination. *J. Virol.* **2011**, *85*, 11325–11337. [CrossRef]
29. Stobart, C.C.; Moore, M.L. RNA virus Reverse Genetics and Vaccine Design. *Viruses* **2014**, *6*, 2531–2550. [CrossRef]
30. Walpita, P.; Flick, R. Reverse genetics of negative-stranded RNA viruses: A global perspective. *FEMS Microbiol. Lett.* **2005**, *244*, 9–18. [CrossRef]
31. Aubry, F.; Nougairède, A.; Gould, E.A.; de Lamballerie, X. Flavivirus reverse genetic systems, construction techniques and applications: A historical perspective. *Antivir. Res.* **2015**, *114*, 67–85. [CrossRef]
32. Yun, S.-I.; Kim, S.-Y.; Rice, C.M.; Lee, Y.-M. Development and Application of a Reverse Genetics System for Japanese Encephalitis Virus. *J. Virol.* **2003**, *77*, 6450–6465. [CrossRef]
33. Willemsen, A.; Zwart, M.P. On the stability of sequences inserted into viral genomes. *Virus Evol.* **2019**, *5*, vez045. [CrossRef] [PubMed]
34. Edmonds, J.; Van Grinsven, E.; Prow, N.; Bosco-Lauth, A.; Brault, A.C.; Bowen, R.A.; Hall, R.A.; Khromykh, A.A. A Novel Bacterium-Free Method for Generation of Flavivirus Infectious DNA by Circular Polymerase Extension Reaction Allows Accurate Recapitulation of Viral Heterogeneity. *J. Virol.* **2012**, *87*, 2367–2372. [CrossRef] [PubMed]

35. Thao, T.T.N.; Labroussaa, F.; Ebert, N.; V'kovski, P.; Stalder, H.; Portmann, J.; Kelly, J.; Steiner, S.; Holwerda, M.; Kratzel, A.; et al. Rapid reconstruction of SARS-CoV-2 using a synthetic genomics platform. *bioRxiv* **2020**. [CrossRef]
36. Neumann, G. Influenza Reverse Genetics—Historical Perspective. *Cold Spring Harb. Perspect. Med.* **2020**, a038547. [CrossRef]
37. Engelhardt, O.G. Many ways to make an influenza virus—Review of influenza virus reverse genetics methods. *Influenza Other Respir. Viruses* **2012**, *7*, 249–256. [CrossRef]
38. Heather, J.M.; Chain, B. The sequence of sequencers: The history of sequencing DNA. *Genomics* **2016**, *107*, 1–8. [CrossRef] [PubMed]
39. Lee, H.; Gurtowski, J.; Yoo, S.; Nattestad, M.; Marcus, S.; Goodwin, S.; Richard McCombie, W.; Schatz, M.C. Third-generation sequencing and the future of genomics. *bioRxiv* **2016**. [CrossRef]
40. Goodwin, S.; McPherson, J.D.; McCombie, W.R. Coming of age: Ten years of next-generation sequencing technologies. *Nat. Rev. Genet.* **2016**, *17*, 333–351. [CrossRef]
41. Eid, J.; Fehr, A.; Gray, J.; Luong, K.; Lyle, J.; Otto, G.; Peluso, P.; Rank, D.; Baybayan, P.; Bettman, B.; et al. Real-Time DNA Sequencing from Single Polymerase Molecules. *Science* **2009**, *323*, 133–138. [CrossRef] [PubMed]
42. Clarke, J.; Wu, H.-C.; Jayasinghe, L.; Patel, A.; Reid, S.; Bayley, H. Continuous base identification for single-molecule nanopore DNA sequencing. *Nat. Nanotechnol.* **2009**, *4*, 265–270. [CrossRef] [PubMed]
43. Bentley, D.R.; Balasubramanian, S.; Swerdlow, H.P.; Smith, G.P.; Milton, J.; Brown, C.G.; Hall, K.P.; Evers, D.J.; Barnes, C.L.; Bignell, H.R.; et al. Accurate whole human genome sequencing using reversible terminator chemistry. *Nat. Cell Biol.* **2008**, *456*, 53–59. [CrossRef] [PubMed]
44. Wrenbeck, E.E.; Faber, M.; Whitehead, T.A. Deep sequencing methods for protein engineering and design. *Curr. Opin. Struct. Biol.* **2017**, *45*, 36–44. [CrossRef] [PubMed]
45. Hiatt, J.B.; Patwardhan, R.P.; Turner, E.; Lee, C.; Shendure, J. Parallel, tag-directed assembly of locally derived short sequence reads. *Nat. Methods* **2010**, *7*, 119–122. [CrossRef] [PubMed]
46. Amarasinghe, S.L.; Su, S.; Dong, X.; Zappia, L.; Ritchie, M.E.; Gouil, Q. Opportunities and challenges in long-read sequencing data analysis. *Genome Biol.* **2020**, *21*, 1–16. [CrossRef] [PubMed]
47. Karst, S.M.; Ziels, R.M.; Kirkegaard, R.H.; Sørensen, E.A.; McDonald, D.; Zhu, Q.; Knight, R.; Albertsen, M. High-accuracy long-read amplicon sequences using unique molecular identifiers with Nanopore or PacBio sequencing. *Nat. Methods* **2021**, *18*, 165–169. [CrossRef]
48. Cirino, P.C.; Mayer, K.M.; Umeno, D.; Arnold, F.H.; Georgiou, G. Generating Mutant Libraries Using Error-Prone PCR. In *Directed Evolution Library Creation*; Arnold, F.H., Georgiou, G., Eds.; Humana Press: Totowa, NJ, USA, 2003; pp. 3–9.
49. Cline, J. PCR fidelity of pfu DNA polymerase and other thermostable DNA polymerases. *Nucleic Acids Res.* **1996**, *24*, 3546–3551. [CrossRef]
50. Vanhercke, T.; Ampe, C.; Tirry, L.; Denolf, P. Reducing mutational bias in random protein libraries. *Anal. Biochem.* **2005**, *339*, 9–14. [CrossRef]
51. Miyazaki, K.; Arnold, F.H. Exploring Nonnatural Evolutionary Pathways by Saturation Mutagenesis: Rapid Improvement of Protein Function. *J. Mol. Evol.* **1999**, *49*, 716–720. [CrossRef]
52. Reetz, M.T.; Carballeira, J.D. Iterative saturation mutagenesis (ISM) for rapid directed evolution of functional enzymes. *Nat. Protoc.* **2007**, *2*, 891–903. [CrossRef]
53. Hughes, R.A.; Ellington, A.D. Synthetic DNA Synthesis and Assembly: Putting the Synthetic in Synthetic Biology. *Cold Spring Harb. Perspect. Biol.* **2017**, *9*, a023812. [CrossRef] [PubMed]
54. Cárcamo, E.; Roldán-Salgado, A.; Osuna, J.; Bello-Sanmartin, I.; Yáñez, J.A.; Saab-Rincón, G.; Viadiu, H.; Gaytán, P. Spiked Genes: A Method to Introduce Random Point Nucleotide Mutations Evenly throughout an Entire Gene Using a Complete Set of Spiked Oligonucleotides for the Assembly. *ACS Omega* **2017**, *2*, 3183–3191. [CrossRef] [PubMed]
55. Green, B.; Bouchier, C.; Fairhead, C.; Craig, N.L.; Cormack, B.P. Insertion site preference of Mu, Tn5, and Tn7 transposons. *Mob. DNA* **2012**, *3*, 3. [CrossRef] [PubMed]
56. Savilahti, H.; Rice, P.A.; Mizuuchi, K. The phage Mu transpososome core: DNA requirements for assembly and function. *EMBO J.* **1995**, *14*, 4893–4903. [CrossRef] [PubMed]
57. Haapa, S.; Taira, S.; Heikkinen, E.; Savilahti, H. An efficient and accurate integration of mini-Mu transposons in vitro: A general methodology for functional genetic analysis and molecular biology applications. *Nucleic Acids Res.* **1999**, *27*, 2777–2784. [CrossRef]
58. Hoffmann, M.; Kleine-Weber, H.; Schroeder, S.; Krüger, N.; Herrler, T.; Erichsen, S.; Schiergens, T.S.; Herrler, G.; Wu, N.-H.; Nitsche, A.; et al. SARS-CoV-2 Cell Entry Depends on ACE2 and TMPRSS2 and Is Blocked by a Clinically Proven Protease Inhibitor. *Cell* **2020**, *181*, 271–280.e8. [CrossRef]
59. Chan, K.K.; Dorosky, D.; Sharma, P.; Abbasi, S.A.; Dye, J.M.; Kranz, D.M.; Herbert, A.S.; Procko, E. Engineering human ACE2 to optimize binding to the spike protein of SARS coronavirus 2. *Science* **2020**, *369*, 1261–1265. [CrossRef]
60. Heinzelman, P.; Romero, P.A. Discovery of human ACE2 variants with altered recognition by the SARS-CoV-2 spike protein. *bioRxiv* **2020**. [CrossRef]
61. Cao, L.; Goreshnik, I.; Coventry, B.; Case, J.B.; Miller, L.; Kozodoy, L.; Chen, R.E.; Carter, L.; Walls, A.C.; Park, Y.-J.; et al. De novo design of picomolar SARS-CoV-2 miniprotein inhibitors. *Science* **2020**, *370*, eabd9909-431. [CrossRef]
62. Linsky, T.W.; Vergara, R.; Codina, N.; Nelson, J.W.; Walker, M.J.; Su, W.; Barnes, C.O.; Hsiang, T.-Y.; Esser-Nobis, K.; Yu, K.; et al. De novo design of potent and resilient hACE2 decoys to neutralize SARS-CoV-2. *Science* **2020**, *370*, eabe0075. [CrossRef]

63. Whitehead, T.A.; Chevalier, A.; Song, Y.; Dreyfus, C.; Fleishman, S.J.; De Mattos, C.; Myers, C.A.; Kamisetty, H.; Blair, P.; Wilson, I.A.; et al. Optimization of affinity, specificity and function of designed influenza inhibitors using deep sequencing. *Nat. Biotechnol.* **2012**, *30*, 543–548. [CrossRef] [PubMed]
64. Fleishman, S.J.; Whitehead, T.A.; Ekiert, D.C.; Dreyfus, C.; Corn, J.E.; Strauch, E.-M.; Wilson, I.A.; Baker, D. Computational Design of Proteins Targeting the Conserved Stem Region of Influenza Hemagglutinin. *Science* **2011**, *332*, 816–821. [CrossRef] [PubMed]
65. Bloom, J.D. Software for the analysis and visualization of deep mutational scanning data. *BMC Bioinform.* **2015**, *16*, 168. [CrossRef] [PubMed]
66. Rubin, A.; Gelman, H.; Lucas, N.; Bajjalieh, S.M.; Papenfuss, A.T.; Speed, T.P.; Fowler, D.M. A statistical framework for analyzing deep mutational scanning data. *Genome Biol.* **2017**, *18*, 150. [CrossRef] [PubMed]
67. Hilton, S.K.; Huddleston, J.; Black, A.; North, K.; Dingens, A.S.; Bedford, T.; Bloom, J.D. *dms-view*: Interactive visualization tool for deep mutational scanning data. *bioRxiv* **2020**. [CrossRef]
68. Thorne, L.; Bailey, D.; Goodfellow, I. High-Resolution Functional Profiling of the Norovirus Genome. *J. Virol.* **2012**, *86*, 11441–11456. [CrossRef] [PubMed]
69. Beitzel, B.F.; Bakken, R.R.; Smith, J.M.; Schmaljohn, C.S. High-Resolution Functional Mapping of the Venezuelan Equine Encephalitis Virus Genome by Insertional Mutagenesis and Massively Parallel Sequencing. *PLoS Pathog.* **2010**, *6*, e1001146. [CrossRef]
70. Fulton, B.O.; Sachs, D.; Beaty, S.M.; Won, S.T.; Lee, B.; Palese, P.; Heaton, N.S. Mutational Analysis of Measles Virus Suggests Constraints on Antigenic Variation of the Glycoproteins. *Cell Rep.* **2015**, *11*, 1331–1338. [CrossRef]
71. Ikegame, S.; Beaty, S.M.; Stevens, C.; Won, S.T.; Park, A.; Sachs, D.; Hong, P.; Lee, B.; Thibault, P.A. Genome-wide transposon mutagenesis of paramyxoviruses reveals constraints on genomic plasticity. *PLoS Pathog.* **2020**, *16*, e1008877. [CrossRef]
72. Herod, M.R.; Loundras, E.-A.; Ward, J.C.; Tulloch, F.; Rowlands, D.J.; Stonehouse, N.J. Employing transposon mutagenesis to investigate foot-and-mouth disease virus replication. *J. Gen. Virol.* **2015**, *96*, 3507–3518. [CrossRef] [PubMed]
73. Procko, E.; Berguig, G.Y.; Shen, B.W.; Song, Y.; Frayo, S.; Convertine, A.J.; Margineantu, D.; Booth, G.; Correia, B.E.; Cheng, Y.; et al. A Computationally Designed Inhibitor of an Epstein-Barr Viral Bcl-2 Protein Induces Apoptosis in Infected Cells. *Cell* **2014**, *157*, 1644–1656. [CrossRef]
74. Luo, Y.; Jacobs, E.Y.; Greco, T.M.; Mohammed, K.D.; Tong, T.; Keegan, S.; Binley, J.M.; Cristea, I.M.; Fenyö, D.; Rout, M.; et al. HIV–host interactome revealed directly from infected cells. *Nat. Microbiol.* **2016**, *1*, 16068. [CrossRef] [PubMed]
75. Haddox, H.K.; Dingens, A.S.; Bloom, J.D. Experimental Estimation of the Effects of All Amino-Acid Mutations to HIV's Envelope Protein on Viral Replication in Cell Culture. *PLoS Pathog.* **2016**, *12*, e1006114. [CrossRef] [PubMed]
76. Haddox, H.K.; Dingens, A.S.; Hilton, S.K.; Overbaugh, J.; Bloom, J.D. Mapping mutational effects along the evolutionary landscape of HIV envelope. *eLife* **2018**, *7*. [CrossRef] [PubMed]
77. Dingens, A.S.; Haddox, H.K.; Overbaugh, J.; Bloom, J.D. Comprehensive Mapping of HIV-1 Escape from a Broadly Neutralizing Antibody. *Cell Host Microbe* **2017**, *21*, 777–787.e4. [CrossRef]
78. Dingens, A.S.; Arenz, D.; Weight, H.; Overbaugh, J.; Bloom, J.D. An Antigenic Atlas of HIV-1 Escape from Broadly Neutralizing Antibodies Distinguishes Functional and Structural Epitopes. *Immunity* **2019**, *50*, 520–532.e3. [CrossRef]
79. Dingens, A.S.; Pratap, P.; Malone, K.; Hilton, S.K.; Ketas, T.; Cottrell, C.A.; Overbaugh, J.; Moore, J.P.; Klasse, P.J.; Ward, A.B.; et al. High-resolution mapping of the neutralizing and binding specificities of polyclonal rabbit serum elicited by HIV Env trimer immunization. *bioRxiv* **2020**. [CrossRef]
80. Remenyi, R.; Qi, H.; Su, S.-Y.; Chen, Z.; Wu, N.C.; Arumugaswami, V.; Truong, S.; Chu, V.; Stokelman, T.; Lo, H.-H.; et al. A Comprehensive Functional Map of the Hepatitis C Virus Genome Provides a Resource for Probing Viral Proteins. *mBio* **2014**, *5*, e01469-14. [CrossRef]
81. Alazard-Dany, N.; Denolly, S.; Boson, B.; Cosset, F.-L. Overview of HCV Life Cycle with a Special Focus on Current and Possible Future Antiviral Targets. *Viruses* **2019**, *11*, 30. [CrossRef]
82. Qi, H.; Chu, V.; Wu, N.C.; Chen, Z.; Truong, S.; Brar, G.; Su, S.-Y.; Du, Y.; Arumugaswami, V.; Olson, C.A.; et al. Systematic identification of anti-interferon function on hepatitis C virus genome reveals p7 as an immune evasion protein. *Proc. Natl. Acad. Sci. USA* **2017**, *114*, 2018–2023. [CrossRef] [PubMed]
83. Ross-Thriepland, D.; Harris, M. Hepatitis C virus NS5A: Enigmatic but still promiscuous 10 years on! *J. Gen. Virol.* **2015**, *96*, 727–738. [CrossRef] [PubMed]
84. Qi, H.; Olson, C.A.; Wu, N.C.; Ke, R.; Loverdo, C.; Chu, V.; Truong, S.; Remenyi, R.; Chen, Z.; Du, Y.; et al. A Quantitative High-Resolution Genetic Profile Rapidly Identifies Sequence Determinants of Hepatitis C Viral Fitness and Drug Sensitivity. *PLoS Pathog.* **2014**, *10*, e1004064. [CrossRef] [PubMed]
85. Gao, M.; Nettles, R.E.; Belema, M.; Snyder, L.B.; Nguyen, V.N.; Fridell, R.A.; Serrano-Wu, M.H.; Langley, D.R.; Sun, J.-H.; Ii, D.R.O.; et al. Chemical genetics strategy identifies an HCV NS5A inhibitor with a potent clinical effect. *Nat. Cell Biol.* **2010**, *465*, 96–100. [CrossRef]
86. Scheel, T.; Gottwein, J.; Mikkelsen, L.S.; Jensen, T.B.; Bukh, J. Recombinant HCV Variants With NS5A From Genotypes 1–7 Have Different Sensitivities to an NS5A Inhibitor but Not Interferon-α. *Gastroenterology* **2011**, *140*, 1032–1042.e6. [CrossRef]
87. Wyles, D.L.; Luetkemeyer, A.F. Understanding Hepatitis C Virus Drug Resistance: Clinical Implications for Current and Future Regimens. *Top. Antivir. Med.* **2017**, *25*, 103–109.
88. Fulton, B.O.; Sachs, D.; Schwarz, M.C.; Palese, P.; Evans, M.J. Transposon Mutagenesis of the Zika Virus Genome Highlights Regions Essential for RNA Replication and Restricted for Immune Evasion. *J. Virol.* **2017**, *91*, e00698-17. [CrossRef]

89. Cì, Y.; Liu, Z.-Y.; Zhang, N.-N.; Niu, Y.; Yang, Y.; Xu, C.; Yang, W.; Qin, C.-F.; Shi, L. Zika NS1–induced ER remodeling is essential for viral replication. *J. Cell Biol.* **2020**, *219*. [CrossRef]
90. Sourisseau, M.; Lawrence, D.J.P.; Schwarz, M.C.; Storrs, C.H.; Veit, E.C.; Bloom, J.D.; Evans, M.J. Deep Mutational Scanning Comprehensively Maps How Zika Envelope Protein Mutations Affect Viral Growth and Antibody Escape. *J. Virol.* **2019**, *93*. [CrossRef]
91. Stettler, K.; Beltramello, M.; Espinosa, D.A.; Graham, V.; Cassotta, A.; Bianchi, S.; Vanzetta, F.; Minola, A.; Jaconi, S.; Mele, F.; et al. Specificity, cross-reactivity, and function of antibodies elicited by Zika virus infection. *Science* **2016**, *353*, 823–826. [CrossRef]
92. Yang, M.; Dent, M.; Lai, H.; Sun, H.; Chen, Q. Immunization of Zika virus envelope protein domain III induces specific and neutralizing immune responses against Zika virus. *Vaccine* **2017**, *35*, 4287–4294. [CrossRef] [PubMed]
93. Gong, D.; Zhang, T.-H.; Zhao, D.; Du, Y.; Chapa, T.J.; Shi, Y.; Wang, L.; Contreras, D.; Zeng, G.; Shi, P.-Y.; et al. High-Throughput Fitness Profiling of Zika Virus E Protein Reveals Different Roles for Glycosylation during Infection of Mammalian and Mosquito Cells. *iScience* **2018**, *1*, 97–111. [CrossRef] [PubMed]
94. Hamel, R.; Dejarnac, O.; Wichit, S.; Ekchariyawat, P.; Neyret, A.; Luplertlop, N.; Perera-Lecoin, M.; Surasombatpattana, P.; Talignani, L.; Thomas, F.; et al. Biology of Zika Virus Infection in Human Skin Cells. *J. Virol.* **2015**, *89*, 8880–8896. [CrossRef]
95. Setoh, Y.X.; Amarilla, A.A.; Peng, N.Y.; Griffiths, R.E.; Carrera, J.; Freney, M.E.; Nakayama, E.; Ogawa, S.; Watterson, D.; Modhiran, N.; et al. Determinants of Zika virus host tropism uncovered by deep mutational scanning. *Nat. Microbiol.* **2019**, *4*, 876–887. [CrossRef] [PubMed]
96. Wen, Z.; Song, H.; Ming, G.-L. How does Zika virus cause microcephaly? *Genes Dev.* **2017**, *31*, 849–861. [CrossRef] [PubMed]
97. Eyre, N.S.; Johnson, S.M.; Eltahla, A.A.; Aloi, M.; Aloia, A.L.; McDevitt, C.A.; Bull, R.A.; Beard, M.R. Genome-Wide Mutagenesis of Dengue Virus Reveals Plasticity of the NS1 Protein and Enables Generation of Infectious Tagged Reporter Viruses. *J. Virol.* **2017**, *91*, e01455-17. [CrossRef]
98. Fan, J.; Liu, Y.; Yuan, Z. Critical role of Dengue Virus NS1 protein in viral replication. *Virol. Sin.* **2014**, *29*, 162–169. [CrossRef]
99. Xie, X.; Zou, J.; Zhang, X.; Zhou, Y.; Routh, A.L.; Kang, C.; Popov, V.L.; Chen, X.; Wang, Q.-Y.; Dong, H.; et al. Dengue NS2A Protein Orchestrates Virus Assembly. *Cell Host Microbe* **2019**, *26*, 606–622.e8. [CrossRef]
100. Perry, J.W.; Chen, Y.; Speliotes, E.; Tai, A.W. Functional Analysis of the Dengue Virus Genome Using an Insertional Mutagenesis Screen. *J. Virol.* **2018**, *92*, 02085–02117. [CrossRef]
101. Nemésio, H.; Palomares-Jerez, F.; Villalaín, J. NS4A and NS4B proteins from dengue virus: Membranotropic regions. *Biochim. Biophys. Acta BBA Biomembr.* **2012**, *1818*, 2818–2830. [CrossRef] [PubMed]
102. Heaton, N.S.; Sachs, D.; Chen, C.-J.; Hai, R.; Palese, P. Genome-wide mutagenesis of influenza virus reveals unique plasticity of the hemagglutinin and NS1 proteins. *Proc. Natl. Acad. Sci. USA* **2013**, *110*, 20248–20253. [CrossRef] [PubMed]
103. Russell, C.J.; Hu, M.; Okda, F.A. Influenza Hemagglutinin Protein Stability, Activation, and Pandemic Risk. *Trends Microbiol.* **2018**, *26*, 841–853. [CrossRef] [PubMed]
104. Haye, K.; Burmakina, S.; Moran, T.; García-Sastre, A.; Fernández-Sesma, A. The NS1 Protein of a Human Influenza Virus Inhibits Type I Interferon Production and the Induction of Antiviral Responses in Primary Human Dendritic and Respiratory Epithelial Cells. *J. Virol.* **2009**, *83*, 6849–6862. [CrossRef] [PubMed]
105. Kirkpatrick, E.; Qiu, X.; Wilson, P.C.; Bahl, J.; Krammer, F. The influenza virus hemagglutinin head evolves faster than the stalk domain. *Sci. Rep.* **2018**, *8*, 10432. [CrossRef] [PubMed]
106. Krammer, F.; Palese, P. Advances in the development of influenza virus vaccines. *Nat. Rev. Drug Discov.* **2015**, *14*, 167–182. [CrossRef] [PubMed]
107. Thyagarajan, B.; Bloom, J.D. The inherent mutational tolerance and antigenic evolvability of influenza hemagglutinin. *eLife* **2014**, *3*, e03300. [CrossRef]
108. Wu, N.C.; Young, A.P.; Al-Mawsawi, L.Q.; Olson, C.A.; Feng, J.; Qi, H.; Chen, S.-H.; Lu, I.-H.; Lin, C.-Y.; Chin, R.G.; et al. High-throughput profiling of influenza A virus hemagglutinin gene at single-nucleotide resolution. *Sci. Rep.* **2015**, *4*, 4942. [CrossRef]
109. Doud, M.B.; Bloom, J.D. Accurate Measurement of the Effects of All Amino-Acid Mutations on Influenza Hemagglutinin. *Viruses* **2016**, *8*, 155. [CrossRef]
110. Lee, J.M.; Huddleston, J.; Doud, M.B.; Hooper, K.A.; Wu, N.C.; Bedford, T.; Bloom, J.D. Deep mutational scanning of hemagglutinin helps predict evolutionary fates of human H3N2 influenza variants. *Proc. Natl. Acad. Sci. USA* **2018**, *115*, E8276–E8285. [CrossRef]
111. Doud, M.B.; Lee, J.M.; Bloom, J.D. How single mutations affect viral escape from broad and narrow antibodies to H1 influenza hemagglutinin. *Nat. Commun.* **2018**, *9*, 1386. [CrossRef]
112. Laursen, N.S.; Wilson, I.A. Broadly neutralizing antibodies against influenza viruses. *Antivir. Res.* **2013**, *98*, 476–483. [CrossRef] [PubMed]
113. Wu, N.C.; Otwinowski, J.; Thompson, A.J.; Nycholat, C.M.; Nourmohammad, A.; Wilson, I.A. Major antigenic site B of human influenza H3N2 viruses has an evolving local fitness landscape. *Nat. Commun.* **2020**, *11*, 1233. [CrossRef] [PubMed]
114. Lee, M.-S.; Chen, J.S.-E. Predicting Antigenic Variants of Influenza A/H3N2 Viruses. *Emerg. Infect. Dis.* **2004**, *10*, 1385–1390. [CrossRef] [PubMed]
115. Wu, N.C.; Thompson, A.J.; Xie, J.; Lin, C.-W.; Nycholat, C.M.; Zhu, X.; Lerner, R.A.; Paulson, J.C.; Wilson, I.A. A complex epistatic network limits the mutational reversibility in the influenza hemagglutinin receptor-binding site. *Nat. Commun.* **2018**, *9*, 1264. [CrossRef]
116. Chen, L.-M.; Blixt, O.; Stevens, J.; Lipatov, A.S.; Davis, C.T.; Collins, B.E.; Cox, N.J.; Paulson, J.C.; Donis, R.O. In vitro evolution of H5N1 avian influenza virus toward human-type receptor specificity. *Virology* **2012**, *422*, 105–113. [CrossRef]

117. Imai, M.; Watanabe, T.; Hatta, M.; Das, S.C.; Ozawa, M.; Shinya, K.; Zhong, G.; Hanson, A.; Katsura, H.; Watanabe, S.; et al. Experimental adaptation of an influenza H5 HA confers respiratory droplet transmission to a reassortant H5 HA/H1N1 virus in ferrets. *Nat. Cell Biol.* **2012**, *486*, 420–428. [CrossRef]
118. Parker, L.; Wharton, S.A.; Martin, S.R.; Cross, K.; Lin, Y.; Liu, Y.; Feizi, T.; Daniels, R.S.; McCauley, J.W. Effects of egg-adaptation on receptor-binding and antigenic properties of recent influenza A (H3N2) vaccine viruses. *J. Gen. Virol.* **2016**, *97*, 1333–1344. [CrossRef]
119. Wu, N.C.; Young, A.P.; Dandekar, S.; Wijersuriya, H.; Al-Mawsawi, L.Q.; Wu, T.-T.; Sun, R. Systematic Identification of H274Y Compensatory Mutations in Influenza A Virus Neuraminidase by High-Throughput Screening. *J. Virol.* **2012**, *87*, 1193–1199. [CrossRef] [PubMed]
120. Lew, W.; Chen, X.; Kim, C.U. Discovery and Development of GS 4104 (oseltamivir) An Orally Active Influenza Neuraminidase Inhibitor. *Curr. Med. Chem.* **2000**, *7*, 663–672. [CrossRef]
121. Hurt, A.C.; Ernest, J.; Deng, Y.-M.; Iannello, P.; Besselaar, T.G.; Birch, C.; Buchy, P.; Chittaganpitch, M.; Chiu, S.-C.; Dwyer, D.; et al. Emergence and spread of oseltamivir-resistant A(H1N1) influenza viruses in Oceania, South East Asia and South Africa. *Antivir. Res.* **2009**, *83*, 90–93. [CrossRef] [PubMed]
122. Soh, Y.S.; Moncla, L.H.; Eguia, R.; Bedford, T.; Bloom, J.D. Comprehensive mapping of adaptation of the avian influenza polymerase protein PB2 to humans. *eLife* **2019**, *8*, 8. [CrossRef] [PubMed]
123. Velthuis, A.J.W.T.; Fodor, A.J.W.T.V.E. Influenza virus RNA polymerase: Insights into the mechanisms of viral RNA synthesis. *Nat. Rev. Genet.* **2016**, *14*, 479–493. [CrossRef]
124. Boivin, S.; Cusack, S.; Ruigrok, R.W.H.; Hart, D.J. Influenza a Virus Polymerase: Structural Insights into Replication and Host Adaptation Mechanisms. *J. Biol. Chem.* **2010**, *285*, 28411–28417. [CrossRef]
125. Subbarao, E.K.; London, W.; Murphy, B.R. A single amino acid in the PB2 gene of influenza a virus is a determinant of host range. *J. Virol.* **1993**, *67*, 1761–1764. [CrossRef]
126. Mänz, B.; De Graaf, M.; Mögling, R.; Richard, M.; Bestebroer, T.M.; Rimmelzwaan, G.F.; Fouchier, R.A.M. Multiple Natural Substitutions in Avian Influenza A Virus PB2 Facilitate Efficient Replication in Human Cells. *J. Virol.* **2016**, *90*, 5928–5938. [CrossRef]
127. Miotto, O.; Heiny, A.T.; Tan, T.W.; August, J.T.; Brusic, V. Identification of human-to-human transmissibility factors in PB2 proteins of influenza A by large-scale mutual information analysis. *BMC Bioinform.* **2008**, *9*, S18. [CrossRef] [PubMed]
128. Taft, A.S.; Ozawa, M.; Fitch, A.; DePasse, J.V.; Halfmann, P.J.; Hill-Batorski, L.; Hatta, M.; Friedrich, T.C.; Lopes, T.J.S.; Maher, E.A.; et al. Identification of mammalian-adapting mutations in the polymerase complex of an avian H5N1 influenza virus. *Nat. Commun.* **2015**, *6*, 7491. [CrossRef]
129. Wu, N.C.; Olson, C.A.; Du, Y.; Le, S.; Tran, K.; Remenyi, R.; Gong, D.; Al-Mawsawi, L.Q.; Qi, H.; Wu, T.-T.; et al. Functional Constraint Profiling of a Viral Protein Reveals Discordance of Evolutionary Conservation and Functionality. *PLoS Genet.* **2015**, *11*, e1005310. [CrossRef]
130. Das, R.; Baker, D. Macromolecular Modeling with Rosetta. *Annu. Rev. Biochem.* **2008**, *77*, 363–382. [CrossRef]
131. Ashenberg, O.; Padmakumar, J.; Doud, M.B.; Bloom, J.D. Deep mutational scanning identifies sites in influenza nucleoprotein that affect viral inhibition by MxA. *PLoS Pathog.* **2017**, *13*, e1006288. [CrossRef] [PubMed]
132. Turrell, L.; Lyall, J.W.; Tiley, L.S.; Fodor, E.; Vreede, F.T. The role and assembly mechanism of nucleoprotein in influenza A virus ribonucleoprotein complexes. *Nat. Commun.* **2013**, *4*, 1591. [CrossRef]
133. Turan, K. Nuclear MxA proteins form a complex with influenza virus NP and inhibit the transcription of the engineered influenza virus genome. *Nucleic Acids Res.* **2004**, *32*, 643–652. [CrossRef] [PubMed]
134. Mänz, B.; Dornfeld, D.; Götz, V.; Zell, R.; Zimmermann, P.; Haller, O.; Kochs, G.; Schwemmle, M. Pandemic Influenza A Viruses Escape from Restriction by Human MxA through Adaptive Mutations in the Nucleoprotein. *PLoS Pathog.* **2013**, *9*, e1003279. [CrossRef] [PubMed]
135. Hale, B.G.; Albrecht, R.A.; García-Sastre, A. Innate immune evasion strategies of influenza viruses. *Future Microbiol.* **2010**, *5*, 23–41. [CrossRef] [PubMed]
136. Du, Y.; Xin, L.; Shi, Y.; Zhang, T.-H.; Wu, N.C.; Dai, L.; Gong, D.; Brar, G.; Shu, S.; Luo, J.; et al. Genome-wide identification of interferon-sensitive mutations enables influenza vaccine design. *Science* **2018**, *359*, 290–296. [CrossRef] [PubMed]
137. Van De Sandt, C.E.; Kreijtz, J.H.C.M.; Rimmelzwaan, G.F. Evasion of Influenza A Viruses from Innate and Adaptive Immune Responses. *Viruses* **2012**, *4*, 1438–1476. [CrossRef]
138. Wu, N.C.; Young, A.P.; Al-Mawsawi, L.Q.; Olson, C.A.; Feng, J.; Qi, H.; Luan, H.H.; Li, X.; Wu, T.-T.; Sun, R. High-Throughput Identification of Loss-of-Function Mutations for Anti-Interferon Activity in the Influenza A Virus NS Segment. *J. Virol.* **2014**, *88*, 10157–10164. [CrossRef]
139. Loo, Y.-M.; Gale, M. Immune Signaling by RIG-I-like Receptors. *Immunity* **2011**, *34*, 680–692. [CrossRef]
140. Wu, N.C.; Du, Y.; Le, S.; Young, A.P.; Zhang, T.-H.; Wang, Y.; Zhou, J.; Yoshizawa, J.M.; Dong, L.; Li, X.; et al. Coupling high-throughput genetics with phylogenetic information reveals an epistatic interaction on the influenza A virus M segment. *BMC Genom.* **2016**, *17*, 46. [CrossRef]
141. Hilsch, M.; Goldenbogen, B.; Sieben, C.; Höfer, C.T.; Rabe, J.P.; Klipp, E.; Herrmann, A.; Chiantia, S. Influenza A Matrix Protein M1 Multimerizes upon Binding to Lipid Membranes. *Biophys. J.* **2014**, *107*, 912–923. [CrossRef]
142. Liu, H.; Grantham, M.L.; Pekosz, A. Mutations in the Influenza A Virus M1 Protein Enhance Virus Budding To Complement Lethal Mutations in the M2 Cytoplasmic Tail. *J. Virol.* **2017**, *92*, e00858-17. [CrossRef]
143. Fares, M.A.; McNally, D. CAPS: Coevolution analysis using protein sequences. *Bioinformatics* **2006**, *22*, 2821–2822. [CrossRef]

144. Starr, T.N.; Greaney, A.J.; Hilton, S.K.; Ellis, D.; Crawford, K.H.; Dingens, A.S.; Navarro, M.J.; Bowen, J.E.; Tortorici, M.A.; Walls, A.C.; et al. Deep Mutational Scanning of SARS-CoV-2 Receptor Binding Domain Reveals Constraints on Folding and ACE2 Binding. *Cell* **2020**, *182*, 1295–1310.e20. [CrossRef] [PubMed]
145. Yan, R.; Zhang, Y.; Li, Y.; Xia, L.; Guo, Y.; Zhou, Q. Structural basis for the recognition of SARS-CoV-2 by full-length human ACE2. *Science* **2020**, *367*, 1444–1448. [CrossRef] [PubMed]
146. Liu, H.; Zhang, Q.; Wei, P.; Chen, Z.; Aviszus, K.; Yang, J.; Downing, W.; Jiang, C.; Liang, B.; Reynoso, L.; et al. The basis of a more contagious 501Y.V1 variant of SARS-CoV-2. *Cell Res.* **2021**. [CrossRef] [PubMed]
147. Greaney, A.J.; Starr, T.N.; Gilchuk, P.; Zost, S.J.; Binshtein, E.; Loes, A.N.; Hilton, S.K.; Huddleston, J.; Eguia, R.; Crawford, K.H.D.; et al. Complete mapping of mutations to the SARS-CoV-2 spike receptor-binding domain that escape antibody recognition. *bioRxiv* **2020**. [CrossRef]
148. Casadevall, A.; Imperiale, M.J. Risks and Benefits of Gain-of-Function Experiments with Pathogens of Pandemic Potential, Such as Influenza Virus: A Call for a Science-Based Discussion. *mBio* **2014**, *5*, e01730-14. [CrossRef]
149. Imperiale, M.J.; Casadevall, A. Rethinking Gain-of-Function Experiments in the Context of the COVID-19 Pandemic. *mBio* **2020**, *11*. [CrossRef]

viruses

MDPI

Article

Identification of sulfone-containing compounds that impair dengue virus infectious particle production

Thomas D Burton[1], Gustavo Bracho, Tom Avery, Marie Lowe, Amanda L Aloia, Michael R Beard? Jillian M Carr and Nicholas S Eyre [2,*]

[1] Flinders University; tom.darcy.burton@gmail.com
[2] Flinders University; nicholas.eyre@flinders.edu.au
* Correspondence: nicholas.eyre@flinders.edu.au

Abstract: Dengue virus (DENV) is the most common mosquito-borne viral disease and is responsible for a major public health burden in tropical and subtropical regions around the world. Despite this, there are no approved antiviral therapeutics available. We sought to discover novel inhibitors of DENV non-structural protein 1 (NS1) using a Nanoluciferase-based thermal shift assay in conjunction with a Nanoluciferase-tagged dengue reporter virus (DENV2-NS1-NLuc) in a high-throughput compound screen of 3,378 drug-like compounds. While we were unable to unambiguously identify NS1-targeting compounds, validation studies revealed a collection of structurally related compounds which inhibit DENV infection in a hepatoma cell culture model. Following testing of 37 structurally related analogues, we identified a lead compound (PubChem CID: 50839998) which had minimal impact on viral RNA replication and cell viability but inhibited infectious particle production at low micromolar concentrations. Examination of the impact of this compound on viral protein localization by confocal microscopy revealed dose-dependent reductions in the detection of mature Envelope (E) protein, consistent with the observed inhibition of infectious virus production. Further investigation into the mechanism of action of this compound is warranted to determine its exact molecular target(s), while testing of a wider range of structural analogues may enable identification of related compounds with greater efficacy and lower cytotoxicity.

Keywords: dengue, virus, flavivirus, Flaviviridae, Nanoluciferase, NaLTSA, antiviral, therapeutics, Envelope, NS1, non-structural protein 1.

Citation: Lastname, F.; Lastname, F.; Lastname, F. Title. *Viruses* **2022**, *14*, x. https://doi.org/10.3390/xxxxx

Academic Editor: Firstname Lastname

Received: date
Accepted: date
Published: date

Publisher's Note: MDPI stays neutral with regard to jurisdictional claims in published maps and institutional affiliations.

1. Introduction

Dengue virus (DENV) is a positive sense single-stranded RNA virus of the Flavivirus genus within the *Flaviviridae* family. DENV is primarily transmitted by *Aedes aegypti* mosquitoes and is estimated to infect approximately 390 million people each year, leading to approximately 25,000 deaths as a result of severe dengue[1,2]. The only licensed dengue vaccine, Dengvaxia®, is moderately effective but is only recommended for use in individuals who have previously been infected with DENV, given that it can increase the severity of DENV infections in seronegative individuals[3]. Importantly, no antiviral therapeutics against DENV infection have been approved[4], although a recently described inhibitor of the NS3-NS4B interaction shows promise[5]. The standard treatment for DENV related disease is supportive care, illustrating the urgent need for further research and development to identify safe and effective antiviral therapies[6].

The DENV genome encodes 3 structural proteins, Envelope (E), capsid and precursor membrane (prM), which are present in assembled virions[7], and 7 non-structural proteins that are involved in viral RNA replication, infectious virus particle production, immune evasion and pathogenesis[8]. The non-enzymatic, dimeric non-structural protein 1 (NS1) is indispensable for the replication of the viral RNA genome and assembly of new viral particles[9], and the secreted hexameric form of NS1 aids immune evasion and leads to the endothelial dysfunction that is a hallmark of severe dengue illness[10].

Previous efforts to identify inhibitors of NS1 function have led to the development of NS1-targeting peptides[11] and NS1 neutralising antibodies[12], as well as a glycosaminoglycan analogue which inhibits NS1-induced endothelial monolayer permeability[13]. However, no small molecule compounds have been identified which display antiviral properties through an interaction with NS1. To address this, we developed a novel antiviral compound screening approach based on the NanoLuc luciferase Thermal Shift Assay (NaLTSA)[14], to identify NS1-binding small molecules.

Thermal shift assays (TSA) exploit the principle that a protein bound to a ligand is likely to be more stable than the same unbound protein, and this will result in increased resistance to denaturation at high temperatures[15]. In a NaLTSA, denaturation of a protein is monitored via measurement of coelenterazine-derived Luminescence that is generated by a Nanoluciferase (NLuc) reporter protein that is fused to a protein of interest. As the protein of interest denatures upon heat treatment, NLuc also denatures, resulting in decreased luminescence. If a ligand is bound to the protein of interest, the denaturation profile of the fusion protein is expected to change, observable by a modified luminescence output[14]. We recently combined insertional mutagenesis with next-generation sequencing[16], a variation of deep mutational scanning[17], to identify regions of genetic flexibility within the DENV genome that may be exploited in the generation of infectious tagged reporter viruses. This enabled us to generate several DENV derivatives that encode reporter protein or epitope tags inserted within the NS1 protein, including a variant that featured insertion of NLuc within NS1 with minimal impact on replicative fitness in a cell culture model. Here, we applied this DENV2-NS1-NLuc virus to the development of a NaLTSA that allows for a luminescence-based measurement of NS1 thermal stability and is amenable to high-throughput screening (HTS) for NS1-binding compounds.

Using this assay, we screened 3,378 drug-like compounds from a scaffold-based library for compounds that limited heat-induced reductions in NLuc activity, using lysates prepared from Huh-7.5 cells that were transfected with *in vitro* transcribed RNA for the DENV2-NS1-NLuc reporter construct. These screens identified 22 hits from 3 scaffold families as candidate NS1-interacting compounds. While we were unable to verify these

hits as NS1-interactors, likely due to their stabilisation of NLuc, hit validation studies nonetheless identified a group of structural analogues with antiviral properties, with the lead candidate displaying low micromolar antiviral activity and minimal cytotoxicity. Here, we describe a sulfone-containing group of compounds, specifically Compound 14 (PubChem CID: 50839998), which inhibit DENV2 infectious particle production and perturb the detection and localisation of mature E protein. We propose that derivatives of Compound 14 with improved antiviral potency and safety warrant further investigation, as does the exact mechanisms involved in the effect of these compounds on infectious DENV particle production.

2. Materials and Methods

Cell Culture

Huh-7.5 cells were generously provided by Charles M. Rice (Rockefeller University, New York, USA). Vero cells were provided by Jillian M. Carr (Flinders University, Adelaide, Australia) as were subgenomic DENV replicon-harbouring Vero-sgDVS-GFP cells, which were developed using plasmids from Theodore C. Pierson (National Institute of Allergy and Infectious Diseases, Maryland, United States of America). These cell lines were maintained in Dulbecco's Modified Eagle Medium (DMEM; Thermo Fisher Scientific) with 10% (v/v) Foetal Bovine Serum (FBS) and Penicillin/Streptomycin and incubated at 37°C and 5% CO_2. C6/36 cells, also provided by Jillian M. Carr, were maintained in Basal Medium Eagle (BME) with 10% Foetal Bovine Serum (FBS), 100 U/ml Penicillin, 100 μg/ml streptomycin and supplemented with nonessential amino acids, GlutaMAX and sodium pyruvate and cultured in a humidified incubator at 28°C and 5% CO_2.

Viruses and plasmids

pFK-DVs, containing the full length DENV2 genome (strain 16681), was kindly provided by Ralf Bartenschlager (University of Heidelberg, Heidelberg, Germany)[18]. pFK-DVs-NS1-NLuc and pFK-DVs-NS1-mScarlet have been previously described[16]. A laboratory-adapted variant of pFK-DVs-NS1-mScarlet was provided by Siena Centofanti and Steve Johnson (Flinders University, Adelaide, Australia), unpublished. To generate virus stocks, DNA plasmids were linearised using restriction enzyme *Xba*I (NEB), then used as a template for *in vitro* RNA synthesis with the mMESSAGE mMACHINE™ SP6 Transcription Kit (Thermo Fisher Scientific), as per manufacturer's instructions. Viral RNA was purified using TRIsure (Bioline) and transfected into cells using DMRIE-C transfection reagent (Thermo Fisher Scientific), according to manufacturer's instructions.

Antibodies

Primary antibodies used for Western blotting and/or immunofluorescent staining include mouse anti-β-actin (Sigma, A5441), rabbit anti-NS4B (GeneTex, GTX103349), mouse anti-NS3 (GeneTex, GT2811), mouse anti-NS1 (mAb 4G4, generously provided by Jody Peters and Roy Hall, University of Queensland), mouse anti-E (ATCC, mAB D1-4G2-4-15), rabbit anti-E (GeneTex, GTX127277), and mouse anti-capsid (mAb 6F3.1, provided by John Aaskov, Queensland University of Technology, 6F3.1). Secondary antibodies used for immunofluorescent staining include conjugates of Alexa Fluor 488, 555, and 647 dyes (Thermo Fisher Scientific). Goat anti-Mouse IRDye®-800CW (LI-COR Biosciences) was used for Western blotting.

NanoLuc luciferase thermal shift assay

Huh-7.5 cells were seeded at 2 x 10^5 cells/well in a 6-well tray. 24 hours later, DENV2-NS1-NLuc RNA was transfected into cells using DMRIE-C (Thermo Fisher Scientific), according to manufacturer's instructions. After 3 hours, the media was replaced with DMEM containing 10% FCS and Penicillin/Streptomycin. 72 hours later, all cells were reseeded into 75 cm^2 flasks (1 flask per 3 wells) and grown until confluent at 6 days post-transfection. Supernatants were removed and cells washed once with PBS. To prepare lysates, PBS was removed and ice-cold NP-40 lysis buffer (1% NP-40, 150 mM NaCl, 50 mM Tris [pH 8.0]) containing 1:100 protease inhibitor cocktail (Sigma-Aldrich cat. No. P8340) was added to the cell monolayer at 5 mL/flask, then flasks were incubated for 5 minutes at 4°C. The lysate was collected and homogenised by repeatedly passing the mixture through a 25-gauge syringe, approximately 25 times. The debris was then

removed by centrifugation at 10,000 x g for 5 minutes at 4°C. Clarified lysates were then aliquoted and stored at -80°C. Control samples were prepared in a similar manner, except that Huh-7.5 cells were transfected with an expression plasmid encoding unfused NLuc[19], and lysates were prepared at 24 hours post-transfection.

To perform the assay, DENV2-NS1-NLuc lysate was thawed on ice, then diluted 1 in 10 in OptiMEM (Thermo Fisher Scientific). For each compound for testing, 45 µL of lysate/OptiMEM and 5 µL of a compound in DMSO was added to each tube in a capped PCR strip tube (8-strip format). The entire strip was incubated at room temperature for 2 hours while rocking. The strip tube was transferred to a gradient-enabled PCR machine and incubated from 40 - 54°C or 56 - 70°C for 3 minutes, before immediately being removed and returned to room temperature. 25 µL was then transferred to a white walled 96-well plate. A 25 µL solution of OptiMEM with 1:100 NanoLuc substrate was added and mixed, then incubated at room temperature for 10 minutes. Luminescence was then measured using a Cytation 5 Cell Imaging Multimode Reader (BioTek), with luminescence values expressed as a percentage of those of the samples treated at 40°C.

NaLTSA high-throughput screening

For high throughput screening, 40 nl of each compound from the Open Scaffold collection from Compounds Australia (Griffith University, Australia) at 5 mM (in DMSO) was dispensed into each well of 384-well PCR plates (Bio-Rad, cat. No. HSP3801) in triplicate. For negative controls, 40 nl of DMSO was plated for 40 wells/plate (columns 1, 24 and half of 23), while methyl-beta-cyclodextrin (MβCD, Sigma-Aldrich) served as a technical positive control and, for this, 530 nl of MβCD at 50 mM (in DMSO) was plated into 8 wells/plate (second half of column 23). Lysates were diluted 1 in 10 in OptiMEM (Thermo Fisher Scientific), as above, and to each well 20 µl of diluted lysate was added before mixing by agitation and incubation at room temperature for 2 hours. Plates were subjected to heat denaturation in a Bio-Rad S1000 thermal cycler by incubating at 54 °C for 5 mins, then 24 °C for 2 mins. During this time, 9 µl of Nanoluc substrate (Nanoluciferase Assay, Promega), pre-diluted 1 in 100 in OptiMEM, was added to each well of a 384-well opaque assay plate (OptiPlate, PerkinElmer) and then 9 µl of heat-denatured lysate was added to each well. Plates were then shaken, incubated for 18 mins and luminescence was measured using an EnSight Multimode Plate Reader (PerkinElmer). Data was analysed using TIBCO Spotfire software (PerkinElmer) on a per plate basis. In most instances the Z-prime value was approximately 0.85, the MβCD:DMSO signal was approximately 2.1 and the %CV values were 5-10%.

Indirect immunofluorescent labelling

Cell monolayers were washed with PBS, then fixed by incubation with ice-cold acetone:methanol (1:1) for 5 minutes at 4°C. Cells were then washed with PBS and incubated with 5% (w/v) Bovine Serum Albumin (BSA; Sigma-Aldrich) diluted in PBS for 30 minutes at room temperature. The BSA solution was removed and replaced with primary antibody diluted appropriately in 1% w/v BSA in PBS. Samples were then incubated for 1 hour at room temperature. Cells were then washed with PBS, and incubated with Alexa Fluor-488, -555 or -647 conjugated secondary antibody diluted (1 in 200) in 1% (w/v) BSA in PBS for 1 hour in the dark at 4°C. Cells were then washed with PBS. Where appropriate, cells were incubated for 10 minutes in 1 µg/mL DAPI (Sigma-Aldrich) in PBS at 4°C or for 15 minutes in 50 µM DRAQ5 in PBS at room temperature to stain the nucleus. To stain the endoplasmic reticulum, cells were incubated for 30 minutes in 25 nM IraZolve-ER Blue™ in PBS at room temperature and washed in PBS. Cells were imaged immediately or stored at 4°C prior to imaging.

Live cell imaging

Live cell imaging was performed using the Sartorius IncuCyte® SX5 Live-Cell Analysis Instrument. Huh7.5 cells were seeded into black-walled PerkinElmer 96-well PhenoPlate-96 microplates at 2 x 10^4 cells/well and, after 24 hours, infected with DENV2-NS1-mScarlet (MOI ~0.1) with/without treatment. The plate was transferred to the IncuCyte® SX5 and cultured at 37°C and 5% CO_2 for the length of the experiment. Phase contrast and red fluorescent channels were imaged at specified intervals over 72 hours. Analysis was performed using the IncuCyte 2021C Basic Analyzer tool.

Automated fluorescence microscopy

Huh-7.5 cells were cultured overnight in 96-well black wall imaging plates (PhenoPlate-96, PerkinElmer), infected with DENV2 (MOI: ~0.1) and returned to culture. After 42 hours, cells were fixed and stained for indirect immunofluorescence. Samples were then imaged using a Cytation 5 Cell Imaging Multimode Reader (BioTek) using a 10× or 4× objective and appropriate fluorescent filters and settings. Infection levels were calculated from stitched images using the Gen5 Software, as follows. Total cell numbers were enumerated based on nuclei that were DAPI-stained to define the 'primary mask', while infected cells were identified by using uninfected cells to enable thresholding of anti-Capsid immunofluorescent staining within a 'secondary mask' that included and expanded upon the primary mask. The percentage of infected cells was determined for each well and expressed as a percentage of average values for those of DMSO-treated controls.

Western blotting

Cell monolayers were washed with ice-cold PBS before lysis with RIPA buffer (150 mM NaCl, 1% [v/v] NP-40, 0.5% [w/v] sodium deoxycholate, 0.1% [w/v] SDS, 50 mM Tris, pH 8.0) containing mammalian protease inhibitor cocktail (Sigma-Aldrich). Cells were lysed for 30 minutes at 4°C, then transferred to microcentrifuge tubes and frozen at -20°C. Samples were thawed and centrifuged at 15,000 × g for 15 minutes, and supernatants were then transferred to new tubes, with the cell debris discarded. When probing for NS1, non-reducing sample buffer was added, while other primary antibodies required reducing sample buffer. Samples were heated at 95°C for 5 minutes, before separation by SDS-PAGE using 4-20% Tris-HCl pre-cast gels (Bio-Rad). Proteins were transferred to nitrocellulose membranes using a Trans-Blot® Turbo™ Transfer System (Bio-Rad).

Membranes were washed in PBS containing 0.1% [v/v] Tween-20 (PBS-T), then blocked for approximately 60 minutes in 5% (w/v) skim milk in PBS-T at room temperature (RT). Membranes were then incubated overnight with primary antibody diluted in 5% skim milk in PBS-T at 4°C. Membranes were washed in PBS-T for 3 × 5 minutes, incubated with IRDye®-800CW -conjugated secondary antibody (1:20,000) in PBS-T for one hour at RT, then washed 3 × 5 minutes in PBS-T. The LI-COR Odyssey® Imaging System was used to image the membranes. Fluorescence was recorded at both 700 and 800 nm. Image Studio Lite software was used for quantification purposes.

Focus forming assays of viral infectivity

Virus infectivity was determined by focus-forming assays, as described previously[20]. Briefly, Huh-7.5 cells were seeded into 96-well plates at 2 x 10^4 cells/well and cultured overnight. Following preparation of 10-fold serial dilutions of virus-containing supernatants, cells were infected using 40 μL/well of each diluted inoculum. Cells were then

cultured for 3 hours, washed once with PBS and returned to culture in normal media for 72 h, prior to fixation and indirect immunofluorescent labelling using anti-Capsid or anti-Envelope primary antibodies. Infected cell foci were enumerated and virus infectivity was expressed as focus-forming units (FFU) per mL.

Viral RNA Replication Assay

Subgenomic replicon-harbouring Vero-sgDVS-GFP cells were used to determine levels of viral RNA replication. Vero-sgDVs-GFP cells were seeded into 96-well white-walled plates at 2 x 10^4 cells/well and cultured overnight. After 24, 48 or 72 hours of treatment, cells were washed once with PBS, and GFP signal was measured using the BioTek Cytation 5 Cell Imaging Multimode Reader (Agilent). Cells were then fixed with acetone:methanol and stained with DAPI, then measured using the same instrument. The fluorescent GFP signal was normalised to fluorescent signal from DAPI.

Confocal Microscopy

8-well #1.5H glass-bottom chamber slides (μ-Slide; Ibidi) were coated with 0.2% (w/v) gelatin in PBS for 1 hour, before washing with PBS and seeding with Huh7.5 cells at 5 × 10^4 cells/well. After culture and treatments, cells were fixed and stained by indirect immunofluorescence, as described above. Imaging was performed using a ZEISS LSM880 Fast Airyscan confocal microscope system using a 63× (N.A. 1.4) Plan-Apochromat oil immersion objective. Appropriate laser lines (405, 488, 561 and 633 nm) were used at 2% of maximal power, with master gain settings adjusted to enable signal visualisation with minimal saturation. Pinhole size was set to 1.0 Airy units for the longest-wavelength fluorophore and matched for all tracks. Images were primarily captured using Z-stack or tile scan options. Images were analysed and processed using the ZEISS Zen Blue version 3.2 software. For colocalisation analysis, Bezier regions of interest were drawn around fluorescently labelled cells and Pearson's correlation coefficients were determined for each cell.

3. Results

To identify inhibitors of DENV NS1 function, we developed a luminescence-based target engagement assay compatible with high-throughput screening. The NanoLuc luciferase thermal shift assay[14] was utilised in conjunction with a previously described DENV2-NS1-NLuc reporter virus[16], allowing for the coupling of a luminescent signal with the folded state of NS1 protein (Supplementary Figure 1). A library of 3,378 drug-like compounds was tested for stabilisation of NS1-NLuc, which ultimately led to the identification of a group of candidate DENV inhibitors.

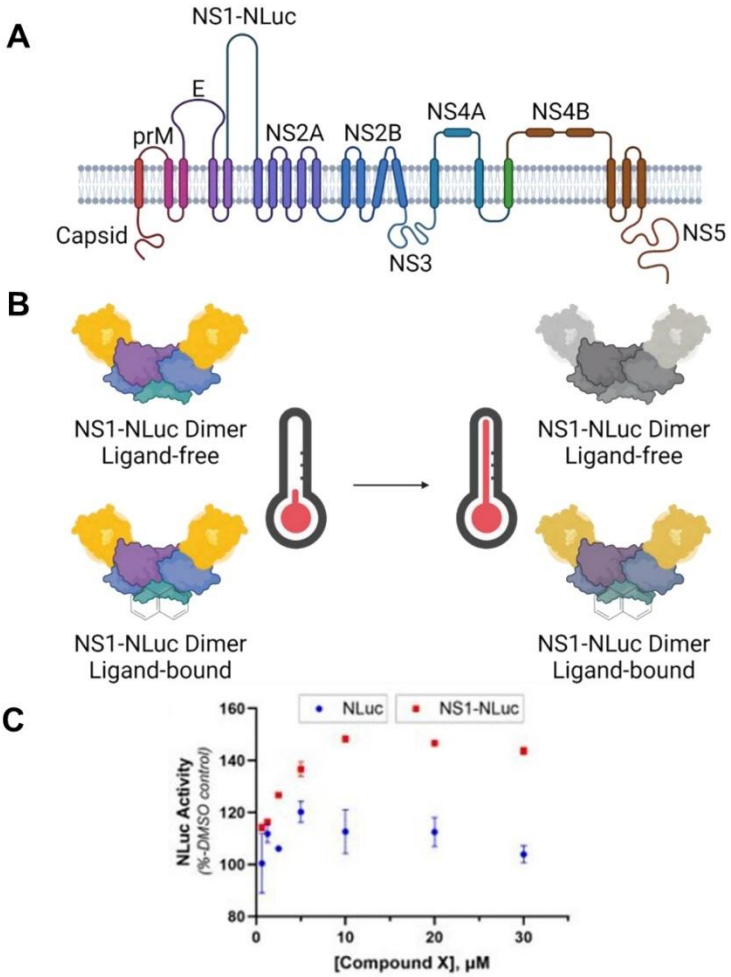

Supplementary Figure 1: A) Topology of a single DENV polypeptide chain. The elongated NS1 represents insertion of the Nanoluciferase protein[21]. B) Principle of the NALTSA. As temperature rises, a bound ligand modifies the denaturation profile of the protein. The coupled Nanoluciferase protein allows a luminescence-based measurement of the folded state of the protein of interest. Decreased colour reflects a theoretical

decrease in luminescence. C) Theoretical plot for a compound which displays a concentration-dependent NS1-specific stabilisation effect.

Detergent lysates of Huh7.5 hepatoma cells that had been transfected with DENV2-NS1-NLuc reporter virus RNA were applied to 384-well plates that contained compounds from a scaffold-based library. For each of 1,226 distinct drug-like scaffolds, 1 compound was tested at a final concentration of 10 μM, with triplicate data points for each compound and two identical repeat screens. DMSO (0.2% [v/v]) served as a carrier control for compound effects while methyl-beta cyclodextrin (MβCD, 5 mM final concentration) served as a technical positive control for stabilization of NanoLuc activity. Following incubation at room temperature with compounds, samples were heat-treated at 55°C for 5 minutes using a thermal cycler. A fraction of each sample was then transferred to a 384-well white-walled plate containing NanoLuc substrate and incubated at room temperature before measurement of luminescence. Hits were defined as compounds which increased relative luminescence levels to >130% of that of the DMSO controls or decreased luminescence by >40%. Overall, these screens were designed to identify compounds which either stabilise or destabilise NS1 upon binding, known as N-ligands, or U-ligands, respectively[22]. In total, 15 hits were recorded, with 8 N-ligands and 7 U-ligands (Supplementary Figure 2). On average, Z′ values were approximately 0.85 and %CV values for controls were generally less than 5%, indicating strong reproducibility of the primary screening data.

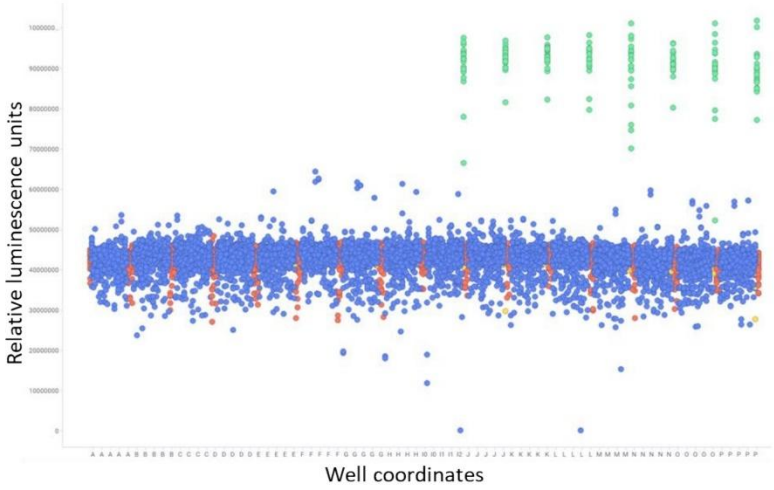

Supplementary Figure 2: Identification of compounds which increase/decrease stabilisation of NS1-NLuc in a NALTSA. Lysate from Huh7.5 cells infected with the DENV2-NS1-NLuc reporter virus was added to 3,378 pre-dispensed drug-like compounds, with compounds at a final concentration of 10 μM. The positive control, MβCD, was dissolved in water and at a final concentration of 5 mM. After incubation of each compound with lysate at room temperature for 2 hours, followed by a 5 minute heat treatment at 50°C, an aliquot was transferred from each well to a white-walled plate with 9 μL of prepared Nano-Glo® assay substrate. After an 18 minute incubation, luminescence was measured for all wells. Blue represents drug-like compounds, n=2 per compound, Orange represents DMSO control wells, Yellow represents empty wells and Green represents the MβCD positive control wells.

For each of these hits, 28-30 structural analogues from the relevant scaffolds were tested in a subsequent screen of the same format, such that a total of 427 compounds were analysed. As shown in Supplementary Table 1, 21 compounds satisfied N-ligand criteria (>130% of DMSO control), while one compound satisfied U-ligand criteria (<40% of DMSO control). These 22 compounds were then tested for antiviral activity and for a concentration-dependent effect on NS1 thermal stabilisation, with lysates from Huh7.5 cells transfected with an NLuc expression plasmid used as a control for NS1-independent NLuc stabilisation.

Supplementary Table 1: Potential NS1-interacting compounds identified using a high-throughput NaLTSA drug screen. Avg(%DMSO) indicates the increase or decrease in relative luminescence units compared to the DMSO control.

Compound	QCL_SAMPLE_NUMBER	increase/decrease	Avg(%DMSO)	SCAFFOLD_ID	COMPOUND_ID	found_in
1	SN00775760	increase	134.05	SC002718	Z54316000	both replicates validation screen
2	SN00776650	increase	132.7	SC005543	Z57238485	both replicates validation screen
3	SN00776652	increase	137.71	SC005543	Z57238504	both replicates validation screen
4	SN00776653	increase	135.87	SC005543	Z57382940	both replicates validation screen
5	SN00776654	increase	133.86	SC005543	Z57238109	both replicates validation screen
6	SN00776655	increase	141.38	SC005543	Z57238119	both replicates validation screen
7	SN00776667	increase	169.68	SC005543	Z319215790	both replicates validation screen
8	SN00776672	increase	135.86	SC005543	Z335452708	both replicates validation screen
9	SN00784185	increase	144.55	CL1050	C066-4659	both replicates validation screen
10	SN00794051	increase	141.93	CL8321	J023-0485	both replicates validation screen
11	SN00795388	increase	132.71	CL9224	L356-0243	both replicates validation screen
12	SN00797921	increase	141.21	CL7988	M071-0013	both replicates validation screen
13	SN00797922	increase	145.2	CL7988	M071-0019	both replicates validation screen
14	SN00797925	increase	132.05	CL7988	M071-0045	both replicates validation screen
15	SN00797928	increase	142.6	CL7988	M071-0080	both replicates validation screen
16	SN00797930	increase	143.76	CL7988	M071-0086	both replicates validation screen
17	SN00797933	increase	131.07	CL7988	M071-0113	both replicates validation screen
18	SN00797940	increase	133.36	CL7988	M071-0220	both replicates validation screen
19	SN00776666	increase	130.38	SC005543	Z317045570	rep1 validation screen
20	SN00795375	increase	131.6	CL9224	L356-0003	rep2 validation screen
21	SN00795385	increase	131.51	CL9224	L356-0222	rep2 validation screen
22	SN00785809	decrease	43.03	CL7499	D116-0230	both replicates validation screen

To test the antiviral efficacy of the 22 hits, each compound was pre-plated into black walled 96-well plates, and Huh7.5 cells in a DENV2-containing medium (MOI: ~0.7) were directly seeded onto the compounds to achieve final compound concentrations ranging from 0.5 to 40 μM. After 42 hours, the cells were fixed and labelled by indirect immunofluorescence using an anti-Capsid antibody and counterstained with the nuclear fluorescent dye DAPI. A DAPI-based cell count was used for a measurement of cytotoxicity. The percentage of cells infected with DENV2 was calculated using automated imaging and analysis software, whereby a threshold of fluorescence intensity in an area surrounding each DAPI-identified cell was utilised to differentiate between infected and non-infected cells. This revealed a potential antiviral scaffold (Compounds Australia scaffold CL7988) represented by compounds 12 – 18; all of which displayed comparable levels of antiviral activity and cytotoxicity, relative to DMSO-treated controls (Figure 1, with structures, IC_{50} and CC_{50} and selectivity index shown in Supplementary Figure 3).

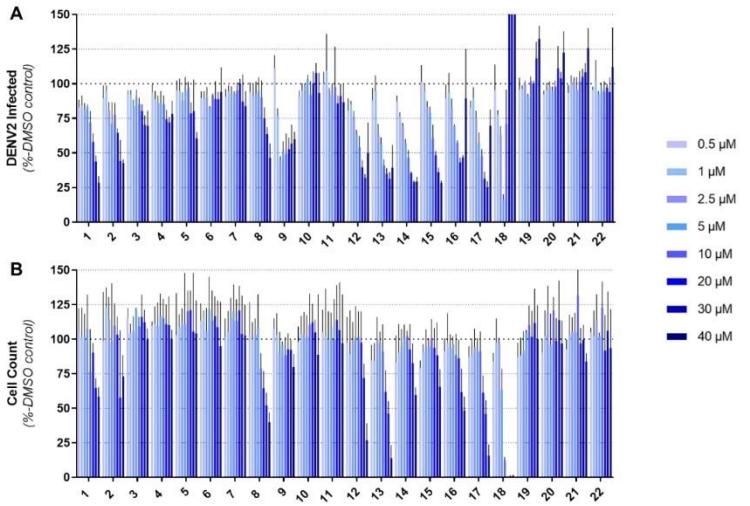

Figure 1: Dose-response analysis of the antiviral effects of the top 22 hits from the NaLTSA screen. 96-well plates were purchased from Compounds Australia with pre-dispensed drugs present at concentrations ranging from 0.5 to 40 µM. Huh7.5 cells were infected with DENV2 at an MOI of 0.7, with a final DMSO/compound concentration of 0.8%. Cells were incubated with compound and virus for 42 hours, then fixed, labelled by an anti-Capsid antibody and counterstained with DAPI. Percentage of cells infected (A) and cell count (B) were calculated via automated immunofluorescence microscopy with the Cytation 5 Cell Imaging Multi-Mode Reader. N=4 per condition. Error bars represent ± SD.

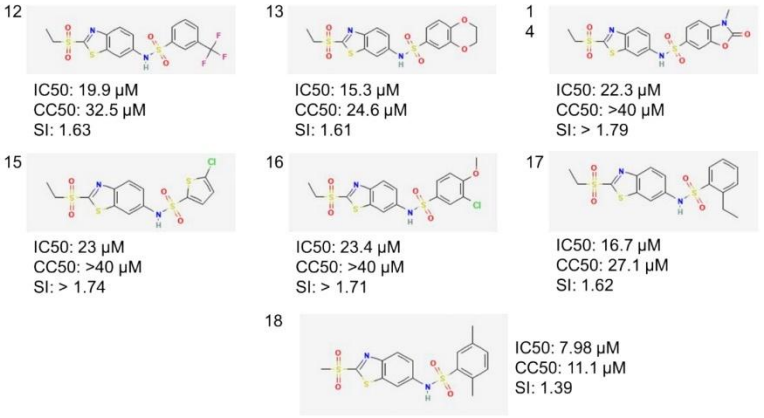

Supplementary Figure 3: Structure of compounds 12 – 18, with IC50 and CC50 as calculated from the assay presented in Figure 1. All structures are present in the Compounds Australia CL7998 scaffold of structural analogues.

The 22 hits were also analysed for thermal stabilisation of the aforementioned DENV2-NS1-NLuc- and NLuc-expressing Huh7.5 lysates for 7 concentrations ranging from 1 μM to 30 μM. While these results generally supported specific NS1-stabilisation (not shown), subsequent NaLTSA experiments with compounds 12, 14 and 18 that involved a fixed compound concentration (20 μM) and a gradient of temperatures ranging from 40-70°C revealed largely indistinguishable NaLTSA profiles of NS1-NLuc and NLuc lysates (Supplementary Figure 4 and Supplementary Table 2), indicating that these compounds interfere with NanoLuc activity. As such, we cannot conclude that our hits interact with NS1 or modify NS1 stability.

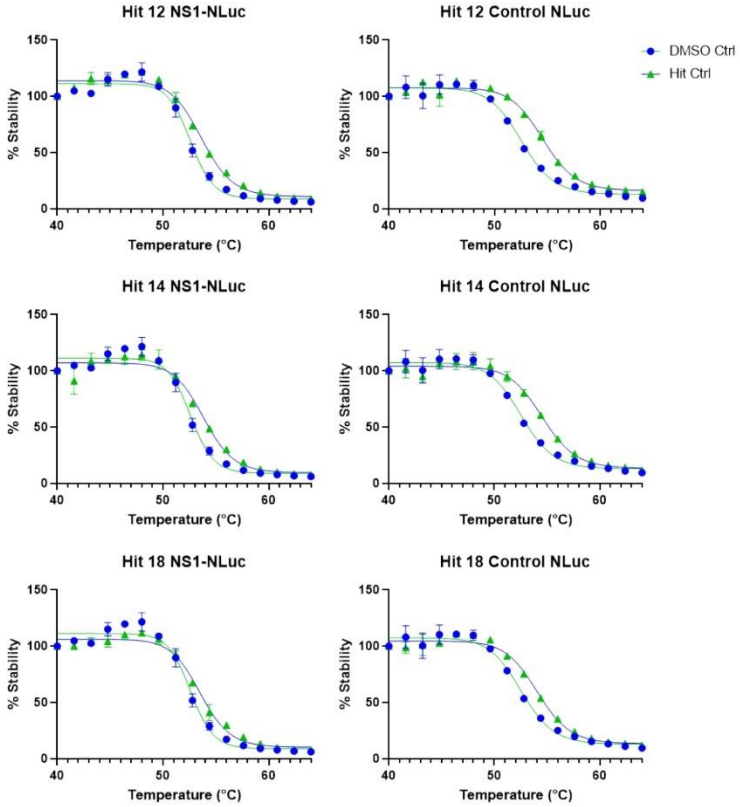

Supplementary Figure 4: Determination of NS1 interaction of 3 top hits from the high-throughput NaLTSA screen. Lysate collected from Huh7.5 cells transfected with DENV2-NS1-NLuc RNA, or with NLuc alone, were treated with DMSO or the stated compound for 2 hours at a final concentration of 20 μM at room temperature, then heat treated for 3 minutes at varying temperatures. After cooling to room temperature, the samples were transferred to a 96-well white-walled plate containing Nano-Glo assay substrate, and luminescence was recorded. Measurements are presented as a % of the luminescence recorded for the 40°C treatment. N=2 per temperature point. Sigmoidal 4PL regression model displayed.

Supplementary Table 2: Validation of the stabilisation effect of 20 μM hit compounds from the high-throughput NaLTSA screen. Numbers represent temperature at which luminescence equates to 50% of the value recorded at 40°C, as modelled by a sigmoidal 4PL regression model.

	NS1-NLuc (°C)		NLuc (°C)		Compound Stabilisation (°C)		NS1 stabilisation net effect (°C)
	DMSO	Compound	DMSO	Compound	ΔNS1-NLuc	ΔNLuc	(ΔNS1-NLuc) – (ΔNLuc)
Hit 12	52.61	53.66	52.55	54.57	1.05	2.02	-0.97
Hit 14	52.61	53.84	52.61	53.53	1.23	0.92	0.31
Hit 18	52.55	54.09	52.55	54.55	1.54	2	-0.46

While this scaffold appeared to possess antiviral properties, the antiviral efficacy of the compounds in this immunofluorescence-based assay was modest. Amongst these compounds, 'Compound 14' was identified to display the best compromise of antiviral activity and toxicity, with a CC_{50} greater than 40 μM and an IC_{50} of 22.3 μM (Supplementary Figure 3). Given that the 42 hour immunofluorescence-based assay may favour identification of antiviral compounds that impair early events in the viral replication cycle and viral RNA replication, we reasoned that if Compound 14 and related analogues inhibit infectious particle production or secretion, such an effect may be under-represented in this assay. To address this possibility, Huh-7.5 cells were treated with a 10 μM concentration of Compounds 12 and 14, previously shown to display low levels of cytotoxicity, and infected with DENV2. Supernatants were collected for measurement of viral infectivity. A decrease in infectivity of approximately 80% was seen from Compound 14 compared to the control. Dose-response analysis of Compound 14 using this assay format demonstrated dose-dependent reduction of infectivity, with an IC_{50} value of 1.13 μM (Figure 2), demonstrating a strong effect of Compound 14 on DENV infectious particle production.

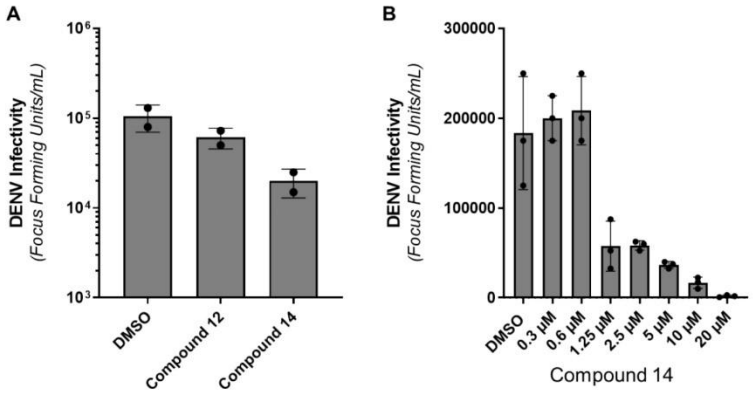

Figure 2: Analysis of the inhibition of infectious particle production by Compounds 12 and 14. Huh7.5 cells were infected with DENV2 at an MOI of 0.1 and treated with the indicated compound at a final concentration of 10 μM. 72 hours later, supernatant was collected and frozen. Naïve Huh7.5 cells were then infected with 1 in 10 serial dilutions of the supernatant. Supernatant was removed at 3 hours, cells were washed with PBS and cell culture medium was added. 72 hours later, cells were fixed and labelled by anti-Capsid antibody. Wells containing countable numbers of foci were identified to calculate the Focus Forming Units of the supernatant. N=2 for graph A, N=3 for graph B. Error bars represent ± SD.

Next, we screened 37 commercially available structural analogues of Compound 14, with the aim of exploring varied ring system electronics, general structural changes and structures with reduced logP (a measure of lipophilicity[23]). While none of these analogues displayed improved antiviral activity or reduced toxicity in comparison to Compound 14, it was noteworthy that changes to the 2-ethylsulfonyl group on the benzothiazole core resulted in increased toxicity or abrogated antiviral activity

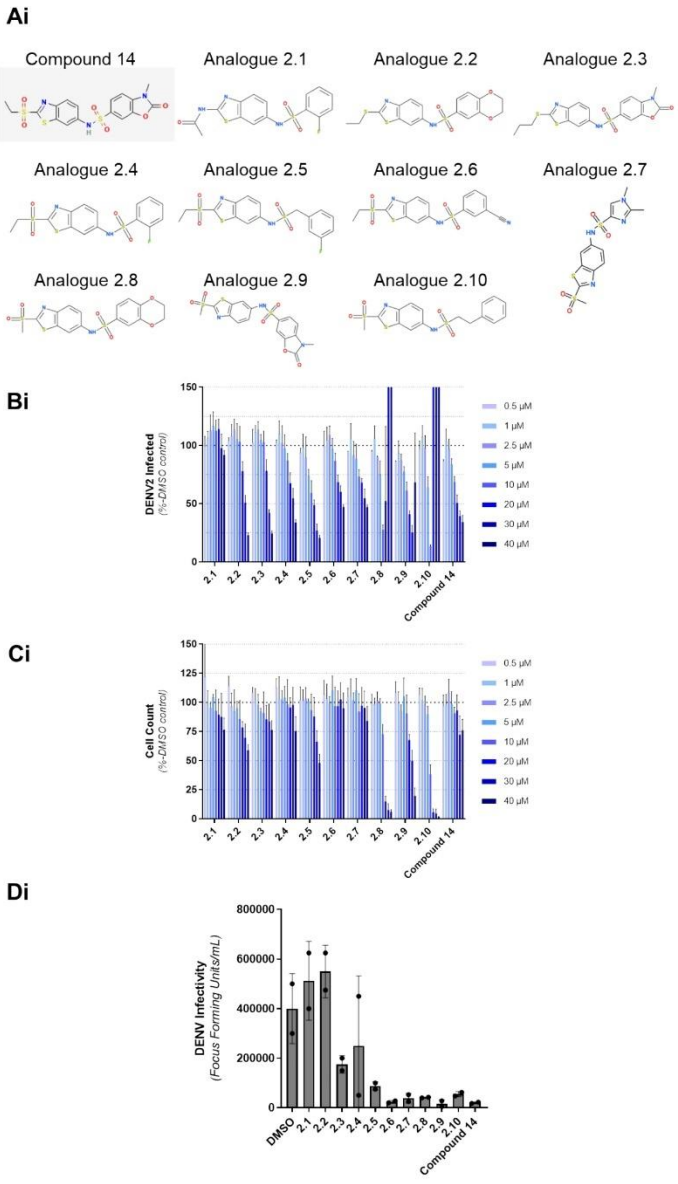

403

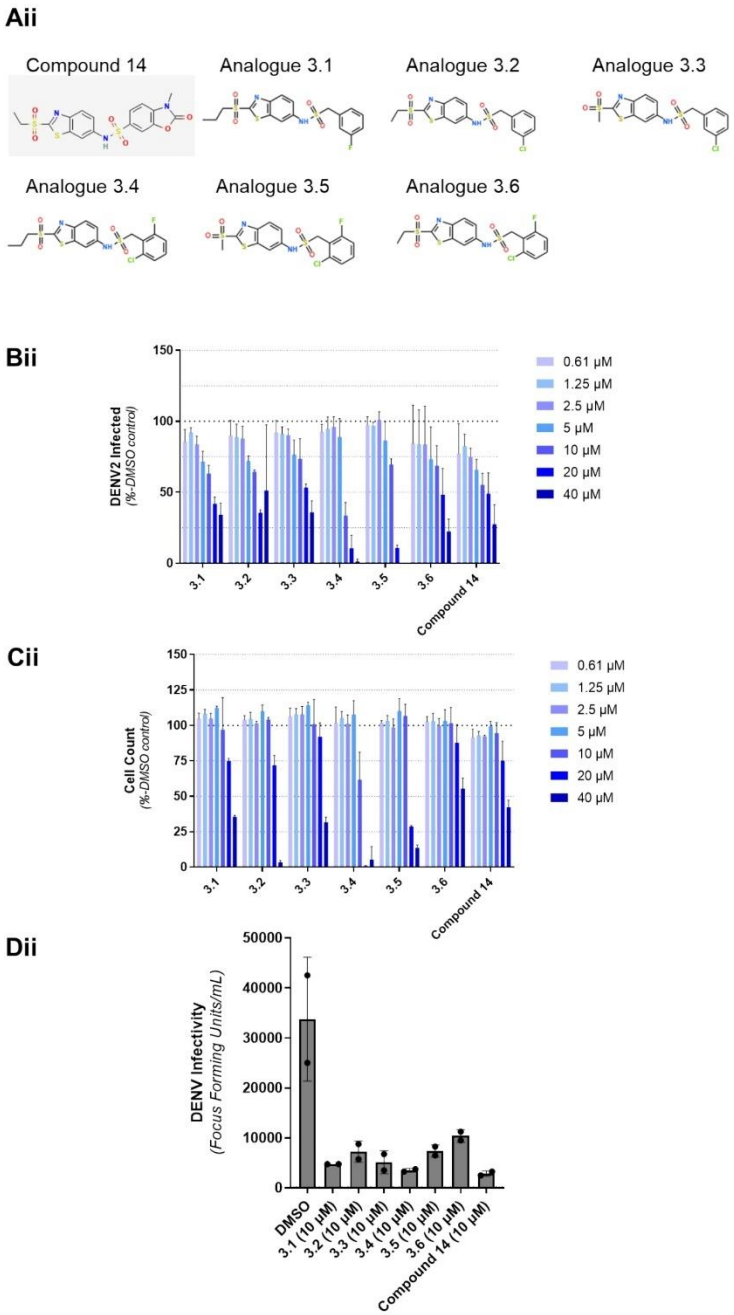
Aii
Compound 14
Analogue 3.1
Analogue 3.2
Analogue 3.3
Analogue 3.4
Analogue 3.5
Analogue 3.6
Bii
DENV2 Infected
(%-DMSO control)
150
100
50
0
3.1
3.2
3.3
3.4
3.5
3.6
Compound 14
0.61 µM
1.25 µM
2.5 µM
5 µM
10 µM
20 µM
40 µM
Cii
Cell Count
(%-DMSO control)
150
125
100
75
50
25
0
3.1
3.2
3.3
3.4
3.5
3.6
Compound 14
0.61 µM
1.25 µM
2.5 µM
5 µM
10 µM
20 µM
40 µM
Dii
DENV Infectivity
(Focus Forming Units/mL)
50000
40000
30000
20000
10000
0
DMSO
3.1 (10 µM)
3.2 (10 µM)
3.3 (10 µM)
3.4 (10 µM)
3.5 (10 µM)
3.6 (10 µM)
Compound 14 (10 µM)

404

405

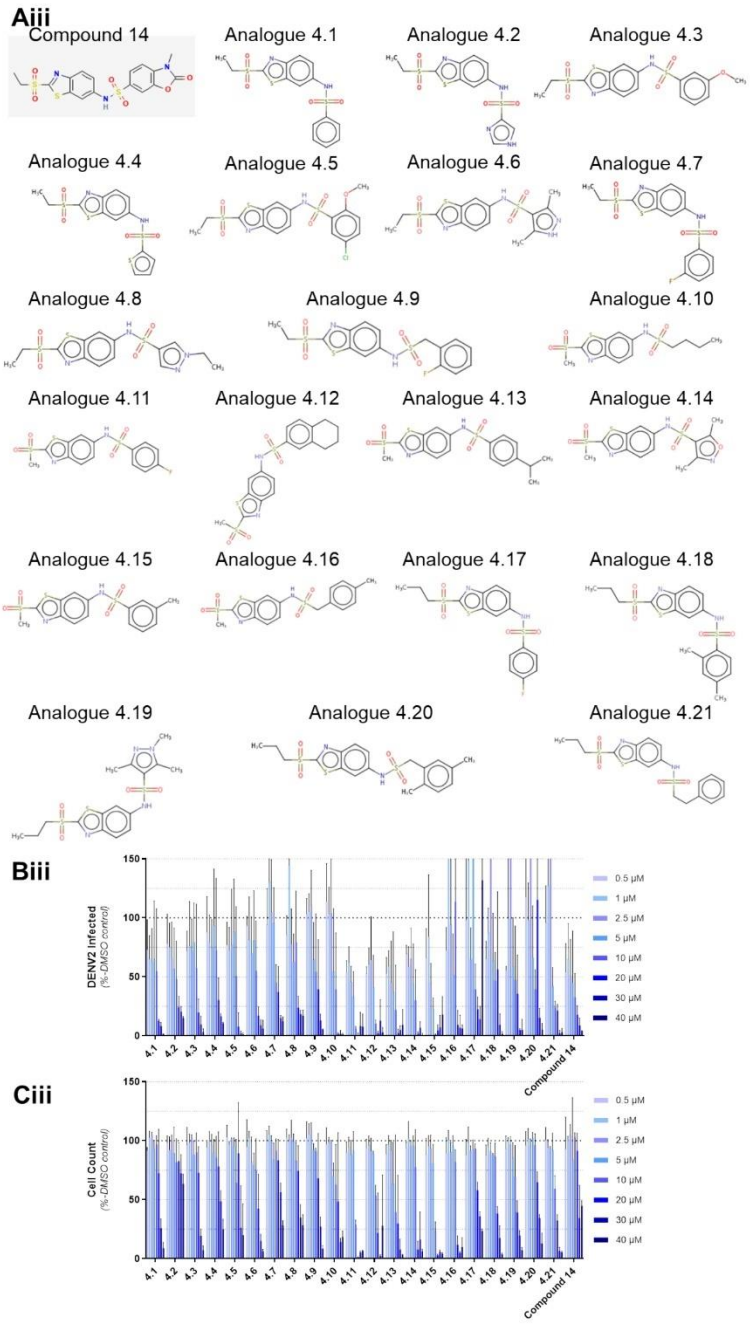
Aiii
Compound 14
Analogue 4.1
Analogue 4.2
Analogue 4.3
Analogue 4.4
Analogue 4.5
Analogue 4.6
Analogue 4.7
Analogue 4.8
Analogue 4.9
Analogue 4.10
Analogue 4.11
Analogue 4.12
Analogue 4.13
Analogue 4.14
Analogue 4.15
Analogue 4.16
Analogue 4.17
Analogue 4.18
Analogue 4.19
Analogue 4.20
Analogue 4.21
Biii
DENV2 Infected (%-DMSO control)
Ciii
Cell Count (%-DMSO control)
0.5 µM
1 µM
2.5 µM
5 µM
10 µM
20 µM
30 µM
40 µM
Compound 14

406

Supplementary Figure 5: Dose-response analysis of the antiviral effects of structural analogues 2.1 – 2.10, 3.1 – 3.6 and 4.1 – 4.21 via infectivity assay, and analysis of the inhibition of infectious particle production by compounds 2.1 – 2.10 and 3.1 – 3.6 via focus forming assay. A) Compound structures. B/C) Infectivity assays: Huh7.5 cells were coinfected/treated with DENV2 at an MOI of 0.7, and stated compounds present at concentrations ranging from 0.5 to 40 μM then incubated for 42 hours. Cells were fixed, labelled by anti-Capsid antibody and counterstained with DAPI. Cell count and the percentage of cells infected were calculated via automated immunofluorescence microscopy with the Cytation 5 Cell Imaging Multi-Mode Reader. N=4 per condition. D) Inhibition of infectious particle production: Huh7.5 cells were infected with DENV2 at an MOI of 0.1 and treated with the indicated compound at a 10 μM final concentration. 72 hours later, supernatant was collected and frozen. Naïve Huh7.5 cells were then infected with 1 in 10 serial dilutions of the supernatant. Supernatant was removed at 3 hours, cells were washed with PBS and fresh cell culture medium was added. 72 hours later, cells were fixed and labelled by anti-Capsid antibody. Wells containing countable numbers of foci were identified to calculate the Focus Forming Units of the supernatant. N=2 per condition. Not performed for compounds 4.1 – 4.21. Error bars represent ± SD.

Due to the significant effect of Compound 14 on infectious particle production, we next sought to analyse the impact of the drug on the spread of DENV2 via live cell imaging using a derivative of a DENV2-NS1-mScarlet reporter virus [16], which has been adapted to improve its replicative fitness (Centofanti S, Johnson SM and Eyre NS, unpublished data). Huh7.5 cells in 96-well imaging plates were infected with the adapted DENV2-NS1-mScarlet reporter virus at a low MOI and treated with Compound 14 at concentrations ranging from 0.313 μM to 20 μM. Automated imaging every hour for 72 hours was performed, capturing mScarlet fluorescence to monitor DENV2 infection levels and phase contrast images to monitor cell health growth (Figure 3). Quantitative analysis of the mScarlet fluorescence revealed dose-dependent inhibition of viral spread, with an IC_{50} of 8.15 μM.

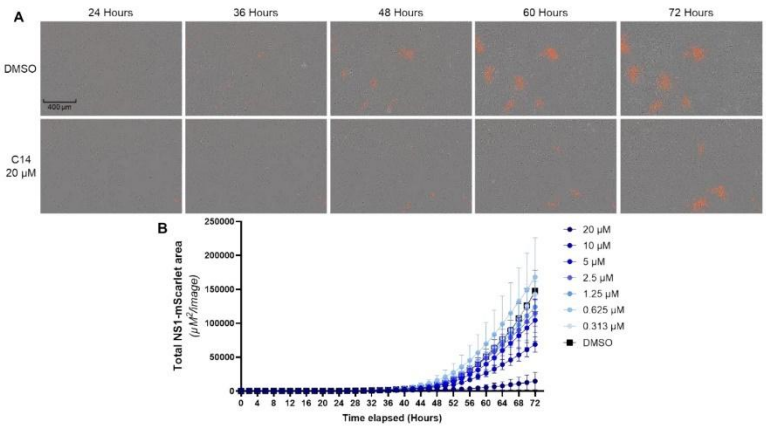

Figure 3: Dose-response analysis of the inhibition of foci growth by Compound 14. Huh7.5 cells in a black-walled 96 well plate were treated with DMSO or Compound 14 at concentrations ranging from 0.313 μM to 20 μM and infected with DENV2-NS1-mScarlet at an MOI of 0.05 and placed in an Incucyte® Live-Cell Analysis System. A) Phase and Red channel pictures were taken every hour for 72 hours. Each image is representative of 5 captured fields of view. Scale bar measures 400 μm. B) Images from all

wells and all timepoints were analysed for the total area containing red signal as a proxy measurement for NS1-mScarlet translation. N=4 wells per data point, calculated from all 5 images. Error bars represent ± SD.

To confirm the inhibition of DENV2 by Compound 14 in an orthogonal assay, we pre-treated Huh-7.5 cells for 20 hours with Compound 14 at concentrations ranging from 0.625 μM to 20 μM, then infected the cells with DENV2. Twenty-four hours later, the cells were lysed and analysed by Western Blot for levels of NS3. Quantification of NS3 showed a dose-dependent decrease in protein level, with NS3 protein levels reduced by approximately 80% in cells that were treated with Compound 14 at 20 μM (Figure 4). This 24 hour viral growth experiment is consistent with a direct impact of Compound 14 on the first replication lifecycle of DENV2 in cells, potentially through decreased virus entry, translation or early replication events.

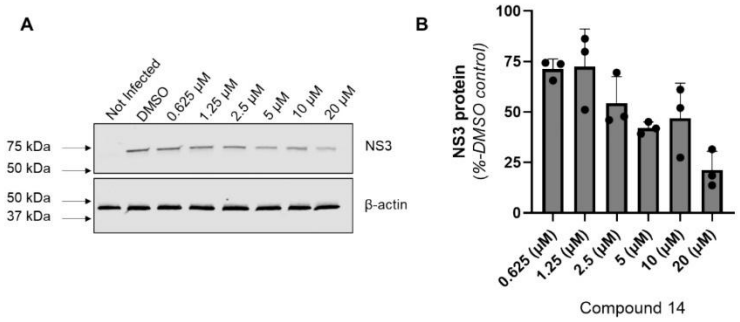

Figure 4: Dose-response analysis of Compound 14 on DENV2 NS3 protein levels. A) Huh7.5 cells were seeded and treated with Compound 14 at for 20 hours, then treated with Compound 14 and infected with DENV2 at an MOI of 3.6. After 24 hours, cells were lysed using RIPA buffer and samples were analysed via immunoblotting with the indicated antibodies and visualised with fluorescent secondary antibodies using the Odyssey® DLx Imaging System. B) Image quantification was performed using Image Studio Lite. N=3 independent experiments. Error bars represent ± SD.

To explore the effect of Compound 14 on viral RNA replication, we utilised a DENV subgenomic replicon, which allows for the study of self-replicating non-structural proteins of dengue in the absence of the structural proteins. Vero cells with a stably incorporated GFP-tagged DENV subgenomic replicon[24] were seeded into 96 well plates and treated with Compound 14 for 24, 48 and 72 hours at concentrations ranging from 0.313 μM to 20 μM. The NS3-NS4B inhibitor JNJ-A07 was used as a positive control for inhibition of viral RNA replication, at a concentration 45 times greater than the reported IC_{50}[5]. At 24, 48 and 72 hours, the positive control showed a reduction in fluorescent signal, normalised to cell number, of 30%, 67% and 80% respectively. The 20 μM Compound 14 resulted in a decrease of 14%, 22% and 24% at the same respective time points (Figure 5). While each of these decreases were statistically significant, dengue antivirals reported to inhibit viral RNA replication with similar levels of anti-DENV activity to Compound 14 display much greater effects in comparable experiments[25]. Due to the weak impact of the treatment of Compound 14 on viral RNA replication, we do not suspect that the significant decrease in infectious particle production seen in our previous experiments is a result of inhibited RNA replication.

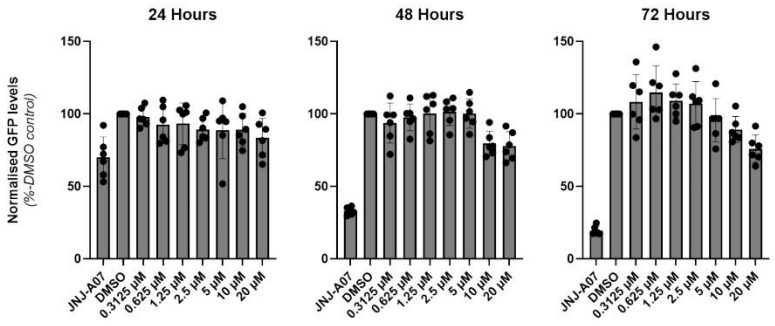

Figure 5: Temporal and dose-response analysis of Compound 14 on viral RNA replication. Vero cells stably expressing a DENV subgenomic replicon containing GFP were treated with JNJ-A07 at 35 nM or Compound 14 at the specified concentrations for 24, 48 or 72 hours. At the end of each incubation, whole well green fluorescence was measured, then cells were fixed and counterstained with DAPI. Whole well blue fluorescence was used as an indirect measurement of cell count/confluency, allowing normalisation of viral RNA replication (GFP signal) to cell count (DAPI signal). Results are representative of two identical plates, prepared at the same time. N=6. Error bars represent ± SD.

To identify an effect of Compound 14 on the localisation of viral proteins, Huh7.5 cells were seeded in glass chamber slides, infected with DENV2-NS1-mScarlet at an MOI of 0.3 and treated with Compound 14 at 20 µM, or DMSO. 48 hours later, the cells were fixed and labelled with a rabbit anti-NS4B antibody and mouse anti-E or anti-Capsid antibodies for analysis via confocal microscopy. No clear difference was seen for the localisation of NS4B, capsid or NS1-mScarlet when comparing Compound 14 to the DMSO treatment (Figure 6A). However, analysis of cells stained for E and NS4B unexpectedly revealed cells expressing both NS1-mScarlet and NS4B, but with E protein at levels equal to non-infected cells (Figure 6B). To confirm these results, we performed multiple tile scans of DMSO- and Compound 14-treated cells, all of which showed multiple cells expressing NS1-mScarlet and NS4B but with a background level signal for E protein (data not shown). Colocalisation analysis of 65 DMSO-treated and 119 Compound 14-treated cells from the tile scans displayed a significant decrease in colocalisation of NS1-mScarlet and E protein in response to the Compound 14 treatment (Figure 6C). The conformation specific 4G2 anti-E antibody used for this experiment targets the fusion loop of domain II (EDII)[26].

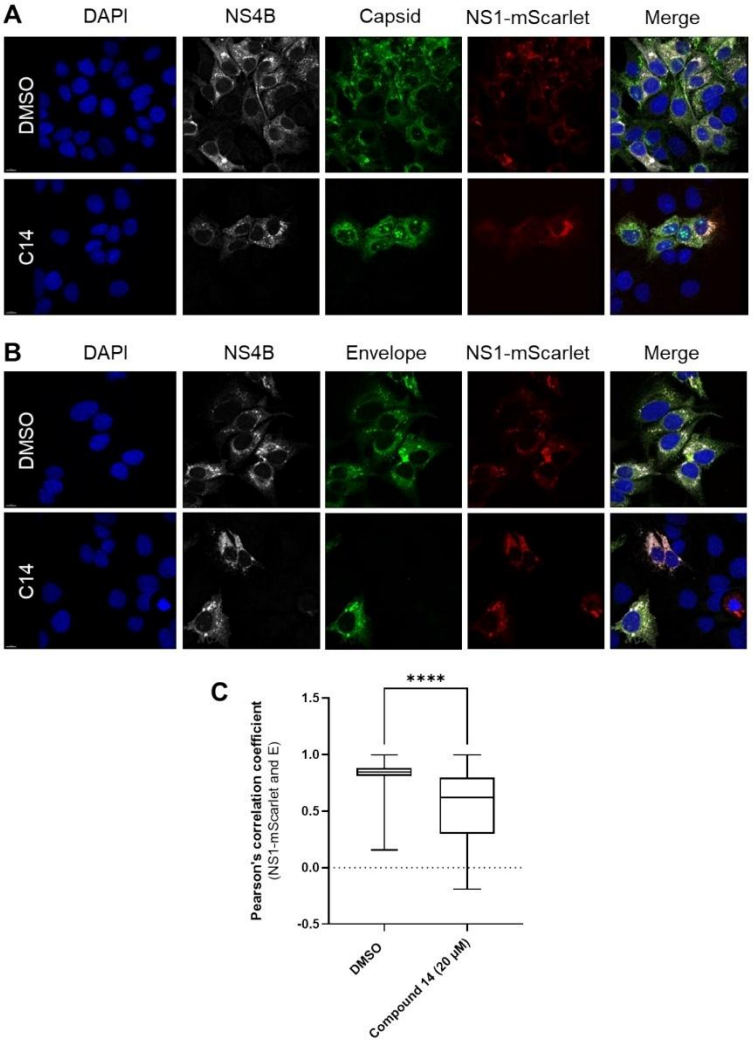

Figure 6: The effect of Compound 14 on the colocalisation of viral proteins. Huh7.5 cells were seeded in glass chamber slides and infected with DENV2-NS1-mScarlet at an MOI of 0.3 and treated with DMSO or Compound 14, then incubated for 48 hours. Cells were fixed, labelled by anti-NS4B and anti-Capsid (A) or anti-Envelope (B) antibodies and counterstained with DAPI, then visualised via confocal microscopy. Scale bar measures 10 μm. C) Box and whisker plot representing cells from the same well as those visualised in Figure 6B. Colocalisation was calculated with Zeiss Zen Blue software. The box and whisker plot represents 65 DMSO-treated cells and 119 Compound 14-treated cells.

To further quantify the reduced levels of mature, detectable E protein in DENV2-infected cells, Huh7.5 cells were simultaneously infected with DENV2-NS1-mScarlet and treated with serial dilutions of Compound 14 in a 96-well plate. 48 hours later, cells were

fixed and stained with anti-E primary antibody and DAPI. Using automated immunofluorescence imaging and fluorescence intensity thresholds, cells with NS1, or NS1 AND mature E, were counted. To calculate the portion of infected cells with NS1 and detectable E, the following calculation was performed (Equation 1):

$$\frac{Cells\ with\ both\ NS1\ AND\ mature\ E}{Cells\ with\ NS1} \quad (520)$$

Figure 7B shows a clear decrease in the proportion of infected cells with mature E protein detected with the conformation specific anti-E antibody, as Compound 14 concentration increases. Images from this experiment are shown in Supplementary Figure 7, with each image representative of one of 56 images stitched together to encompass the entire well. We hypothesised that this effect was a result of E protein not fully maturing in a portion of the infected cell population, affecting epitope accessibility. This effect has been observed previously with the 4G2 monoclonal anti-E antibody in response to knockout of a host gene, and was attributed to E protein misfolding[27].

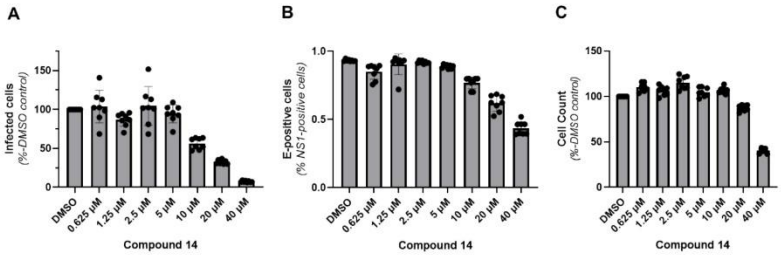

Figure 7: Dose-response quantification of E- and NS1-mScarlet-displaying cells. Huh7.5 cells were seeded in a 96-well plate then infected with DENV2-NS1-mScarlet at an MOI of 0.3 and treated with DMSO or Compound 14. After 48 hours, cells were fixed, labelled by anti-E antibody (4G2) and counterstained with DAPI. Automated immunofluorescent imaging with the Cytation 5 Cell Imaging Multi-Mode Reader was used to capture whole well images, then identify cells with specific viral proteins above a specified fluorescence threshold. A) Infected cells as determined by NS1-mScarlet detection, presented as a percentage of the DMSO control. B) The portion of NS1-mScarlet-positive cells in which E protein was detected. C) Cell count as a percentage of the DMSO control. N=6. Error bars represent ± SD.

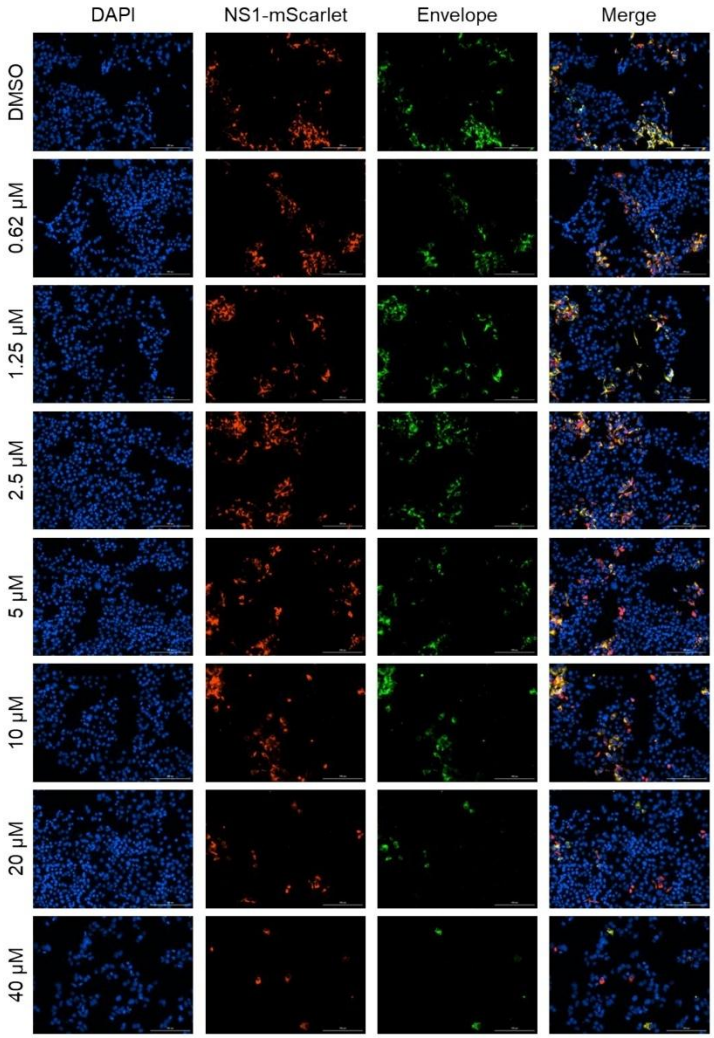

Supplementary Figure 6: Images from the dose-response quantification of E- and NS1-mScarlet-expressing cells from Figure 7. Huh7.5 cells were infected with DENV2-NS1-mScarlet at an MOI of 0.3 and treated with DMSO or Compound 14. After 48 hours, cells were fixed, labelled by anti-Envelope antibody and counterstained with DAPI. Automated immunofluorescent imaging with the Cytation 5 Cell Imaging Multi-Mode Reader was used to capture whole well images by stitching a montage of images. The images presented are representative of this montage. Scale bar measures 200 µM.

To probe for conformations of E protein which may not be visualised by the conformation-specific monoclonal antibody (4G2), we also performed further immunolabelling experiments using a polyclonal anti-E antibody that is expected to recognise immature and mature forms of E protein. Huh-7.5 cells were infected with wild-type DENV2 at an MOI of 0.1 and treated with Compound 14 and DMSO. After 48 hours, cells were fixed

and labelled with both the monoclonal anti-E antibody and the polyclonal anti-E antibody, as well as the endoplasmic reticulum dye IraZolve-ER Blue™ (white) and the DNA stain DRAQ5™ (blue). Confocal analysis revealed distinct subpopulations of infected cells, with mature E protein visualised by both the monoclonal and polyclonal anti-E antibodies, and immature E protein visualised by only the polyclonal anti-E antibody. Figure 8A displays tile scans of Compound 14 and DMSO-treated cells. Infected cells with immature E protein were seen in both treatments, although the ratio of these cells compared to cells expressing mature E protein appeared higher in Compound 14-treated cells. Additionally, we observed a portion of Compound 14-treated cells displaying web-like localisation patterns of both immature E protein and the endoplasmic reticulum, which was not observed in any DMSO-treated cells. An example of this is highlighted in Figure 8B.

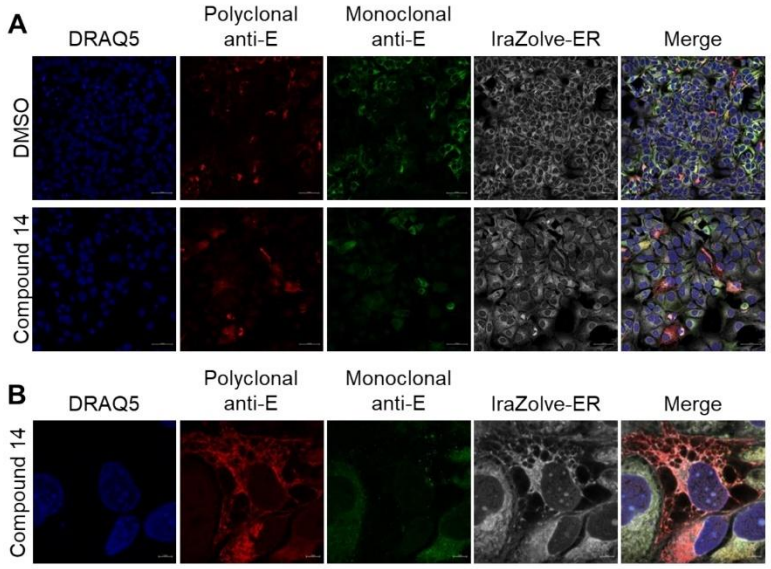

Figure 8: The effect of Compound 14 on the post-translational modification of E protein and the endoplasmic reticulum during DENV infection. Huh7.5 cells were seeded in a glass chamber slide and infected with DENV2 at an MOI of 0.1 with the addition of DMSO or Compound 14 (20 μM) and incubated for 48 hours. Cells were fixed and stained with the specified antibodies or dye, then visualised via confocal microscopy. A) 3x3 tile scan images. Scale bar measures 50 μm. B) Close-up image of cells. Scale bar measures 5 μm.

To confirm that this impact on the maturation of E protein was related to the Compound 14 treatment, we infected Huh7.5 cells in a 96-well plate with DENV2 at an MOI of 0.1 and treated with DMSO and Compound 14 at concentrations of 5 μM, 10 μM and 20 μM. 48 hours later, cells were fixed and stained with the polyclonal and monoclonal anti-E antibodies, as well as DAPI. Automated immunofluorescent imaging with the Cytation 5 Cell Imaging Multi-Mode Reader was used to capture whole well images, then count infected cells with immature E and mature E protein, as visualised by the polyclonal anti-E antibody, as well as infected cells with mature E protein as visualised by the monoclonal anti-E antibody. To calculate the portion of infected cells with mature E protein, the following calculation was performed (Equation 2):

$$\frac{Cells\ with\ mature\ E}{Cells\ with\ E}$$

Figure 9B shows that the portion of cells with mature E protein decreases as the concentration of Compound 14 increases. Images from this experiment are shown in Figure 9D with each image representative of one of 20 images stitched together to encompass the entire well.

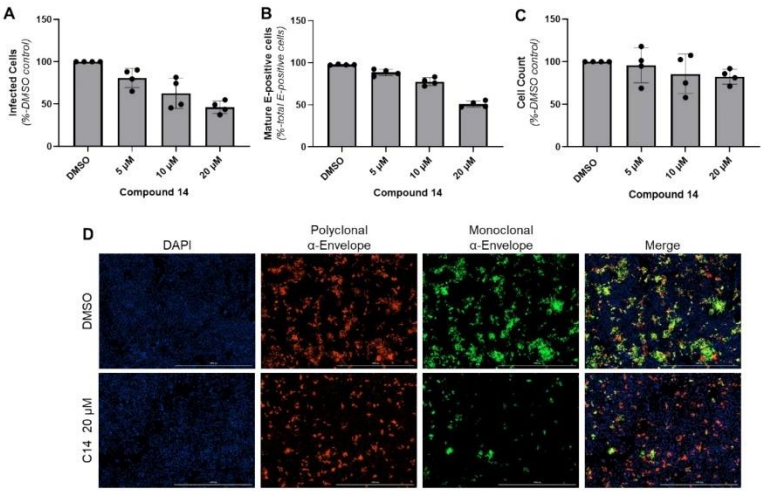

Figure 9: Dose-response quantification of infected cells visualised by polyclonal and monoclonal anti-E antibodies. Huh7.5 cells were infected with DENV2 at an MOI of 0.1 and treated with DMSO or Compound 14. After 48 hours, cells were fixed, labelled with the specified antibodies and counterstained with DAPI. Automated immunofluorescent imaging with the Cytation 5 Cell Imaging Multi-Mode Reader was used to capture whole well images, then identify cells above a specified fluorescent threshold for each marker. A) Infected cells as determined by detection with the polyclonal anti-E antibody, presented as a percentage of the DMSO control. B) Infected cells with mature E protein detected by the monoclonal anti-Envelope antibody (4G2), presented as a portion of the total infect cell population as detected by the polyclonal anti-E antibody. C) Cell count as a percentage of the DMSO control. N=4. Error bars represent ± SD. D) Representative images of graphs A-C. Scale bar measures 1000 µm.

2. Discussion

Despite significant advances in the development of promising antiviral drug candidates, there remains no available treatment for patients suffering from dengue fever, besides supportive care. The goal of this study was to identify NS1-specific inhibitors using a Nanoluciferase-based thermal shift assay. While we were unable to verify an interaction with NS1, we did identify a group of structurally related compounds which inhibit DENV and, to our knowledge, have not been previously studied for their antiviral properties. Compound 14 was identified as the most promising candidate amongst the compounds tested when considering efficacy and cytotoxicity and was shown to reduce infectious particle production with an IC_{50} of 1.1 µM. While multiple structural analogues were also subsequently tested, Compound 14 remained the most effective candidate. While subgenomic replicon experiments indicated a slight impact of Compound 14 on

viral RNA replication, the small effect is unlikely to reflect its marked inhibition of infectious particle production.

Confocal microscopy was employed to investigate the impact of Compound 14 treatment on the localisation of viral proteins in cells that were infected with the DENV2-NS1-mScarlet reporter virus. Interestingly, we found that Compound 14 treatment frequently resulted in an inability to detect E protein when visualised with the monoclonal anti-E antibody 4G2 in cells expressing both NS1 and NS4B. This antibody targets domain II of Envelope protein (EDII)[26], which is required for binding to the host cell receptor DC-SIGN[28], and is known to detect a conformational epitope, suggesting that E protein misfolding and/or failure to mature may be caused by Compound 14 treatment. Using automated immunofluorescent microscopy, these effects were observed to be dose-dependent in nature, with Compound 14 treatment at 20 μM resulting in an approximately 40% reduction in detection of mature E protein in cells that express NS1-mScarlet, relative to vehicle-treated controls. To further investigate this phenomenon, we probed wild-type DENV2-infected cells with both the 4G2 monoclonal anti-E antibody and a polyclonal anti-E antibody. As the concentration of Compound 14 was increased, the number of infected cells that were positively labelled with both the conformation-specific monoclonal anti-E antibody and the conformation-insensitive polyclonal anti-E antibody decreased, indicating a Compound 14-induced effect on the recognition of mature E protein.

Targeting of specific host proteins has been previously reported to alter envelope epitope accessibility[27]. The ER-resident dolichol-phosphate mannose synthase (DMPS) complex is required for protein glycosylation and glycosylphosphatidylinositol anchor biosynthesis in the ER lumen[29]. Specifically, knockout of a subunit of this complex, DPM1, was shown to result in abnormal glycosylation of E protein. This was suggested to be the result of decreased epitope accessibility due to protein misfolding. In a similar manner, we hypothesise that Compound 14 may impact upon the folding and/or post-translational modification of E protein, and propose that the impact of Compound 14 on the glycosylation of E protein should be investigated in future studies.

Among the infected Compound 14-treated cells that lack mature E protein, confocal microscopy revealed web-like localisation patterns for E protein and the ER itself. Several proteins that are involved in regulation of ER morphology are known. Amongst these proteins, the atlastin protein family, including ATL1, which is predominantly localised to the Golgi, and ATL2 and ATL3, which are localised to the ER, are GTPases that are important determinants of ER tubule structure due to their role in the formation of three-way junctions, which connect the ER network of sheets and tubules[30,31]. Triple Atl1/2/3 knockout NIH-3T3 cells have been shown to display this disrupted ER network, or web-like pattern, caused by a reduction in the ER tubule fusion events which are required to generate these three-way junctions[32]. Relating to DENV, knockdown of ATL2 in DENV-infected A549 cells results in reduced viral titres and reduced intracellular viral RNA. Similar to our observed effects of Compound 14, knockdown of ATL3 results in reduced viral titres, but not viral RNA replication [33]. It is tempting to speculate that ATL2 knockdown and Compound 14 treatment have similar effects on ER morphology and further mechanistic studies of the impact of Compound 14 on ER architecture are warranted.

E protein has been shown to be the target of many experimental DENV antiviral small molecule drug candidates. The mechanism of action of these compounds includes inhibition of virus binding to cell receptors, cellular entry and fusion of viral envelopes with endosomal membranes to allow for nucleocapsid release[34]. A common target site within E protein is the conserved binding pocket in the hinge region between EDI and

EDII, which binds to the small detergent molecule N-octyl-β-D-glucoside (βOG)[35]. Interaction with this binding pocket with small molecule drug candidates has been demonstrated to inhibit a crucial step in membrane fusion[36,37], and multiple ligands that bind to this pocket have displayed antiviral activity[36,38-41]. Domain III of E protein is important for virus entry, as the domain recognizes host cell receptors[42]. Multiple receptors involved in virus entry have been identified, including glycosaminoglycans such as heparan sulfate[43]. The heparan binding motif, a positively charged region of EDIII, has since been successfully targeted with multiple negatively charged compounds, often glycosaminoglycan mimetics[44-47]. However, to our knowledge the impact of Compound 14 on the maturation of E protein and ER morphology in infected cells has not been reported for candidate inhibitors of E protein or other anti-DENV drug candidates, suggesting a novel mode of anti-DENV activity for Compound 14.

In summary, Compound 14 shows high efficacy in reducing infectious particle production and appears to disrupt post-translational processing/maturation and localisation of E. This study suggests that further investigation into its mechanism of action and exact molecular target(s) of Compound 14 is warranted and, specifically, it will be important to better understand the impact of Compound 14 on the morphology of the endoplasmic reticulum in DENV-infected cells and how this relates to the maturation of E. We hypothesise that the antiviral efficacy and safety profile of Compound 14 may be improved upon via further rational medicinal chemistry efforts.

References

1. Carrington, L.B.; Simmons, C.P. Human to mosquito transmission of dengue viruses. *Front Immunol* **2014**, *5*, 290, doi:10.3389/fimmu.2014.00290.
2. Bhatt, S.; Gething, P.W.; Brady, O.J.; Messina, J.P.; Farlow, A.W.; Moyes, C.L.; Drake, J.M.; Brownstein, J.S.; Hoen, A.G.; Sankoh, O.; et al. The global distribution and burden of dengue. *Nature* **2013**, *496*, 504-507, doi:10.1038/nature12060.
3. Thomas, S.J.; Yoon, I.K. A review of Dengvaxia®: development to deployment. *HUm Vaccin Immunother* **2019**, *15*, 2295-2314, doi:10.1080/21645515.2019.1658503.
4. Dighe, S.N.; Ekwudu, O.; Dua, K.; Chellappan, D.K.; Katavic, P.L.; Collet, T.A. Recent update on anti-dengue drug discovery. *Eur J Med Chem* **2019**, *176*, 431-455, doi:10.1016/j.ejmech.2019.05.010.
5. Kaptein, S.J.F.; Goethals, O.; Kiemel, D.; Marchand, A.; Kesteleyn, B.; Bonfanti, J.-F.; Bardiot, D.; Stoops, B.; Jonckers, T.H.M.; Dallmeier, K.; et al. A pan-serotype dengue virus inhibitor targeting the NS3–NS4B interaction. *Nature* **2021**, *598*, 504-509, doi:10.1038/s41586-021-03990-6.
6. Kularatne, S.A.; Dalugama, C. Dengue infection: Global importance, immunopathology and management. *Clinical Medicine* **2022**, *22*, 9-13, doi:10.7861/clinmed.2021-0791.
7. Perera, R.; Kuhn, R.J. Structural proteomics of dengue virus. *Curr Opin Microbiol* **2008**, *11*, 369-377, doi:10.1016/j.mib.2008.06.004.
8. Nasar, S.; Rashid, N.; Iftikhar, S. Dengue proteins with their role in pathogenesis, and strategies for developing an effective anti-dengue treatment: A review. *Journal of Medical Virology* **2020**, *92*, 941-955, doi:https://doi.org/10.1002/jmv.25646.
9. Scaturro, P.; Cortese, M.; Chatel-Chaix, L.; Fischl, W.; Bartenschlager, R. Dengue Virus Non-structural Protein 1 Modulates Infectious Particle Production via Interaction with the Structural Proteins. *PLoS Pathog* **2015**, *11*, e1005277, doi:10.1371/journal.ppat.1005277.
10. Libraty, D.H.; Young, P.R.; Pickering, D.; Endy, T.P.; Kalayanarooj, S.; Green, S.; Vaughn, D.W.; Nisalak, A.; Ennis, F.A.; Rothman, A.L. High circulating levels of the dengue virus nonstructural protein NS1 early in dengue illness correlate with the development of dengue hemorrhagic fever. *J Infect Dis* **2002**, *186*, 1165-1168, doi:10.1086/343813.
11. Songprakhon, P.; Thaingtamtanha, T.; Limjindaporn, T.; Puttikhunt, C.; Srisawat, C.; Luangaram, P.; Dechtawewat, T.; Uthaipibull, C.; Thongsima, S.; Yenchitsomanus, P.-t.; et al. Peptides targeting dengue viral nonstructural protein 1 inhibit dengue virus production. *Scientific Reports* **2020**, *10*, 12933, doi:10.1038/s41598-020-69515-9.
12. Modhiran, N.; Song, H.; Liu, L.; Bletchly, C.; Brillault, L.; Amarilla, A.A.; Xu, X.; Qi, J.; Chai, Y.; Cheung, S.T.M.; et al. A broadly protective antibody that targets the flavivirus NS1 protein. *Science* **2021**, *371*, 190-194, doi:10.1126/science.abb9425.
13. Modhiran, N.; Gandhi, N.S.; Wimmer, N.; Cheung, S.; Stacey, K.; Young, P.R.; Ferro, V.; Watterson, D. Dual targeting of dengue virus virions and NS1 protein with the heparan sulfate mimic PG545. *Antiviral Res* **2019**, *168*, 121-127, doi:10.1016/j.antiviral.2019.05.004.
14. Dart, M.L.; Machleidt, T.; Jost, E.; Schwinn, M.K.; Robers, M.B.; Shi, C.; Kirkland, T.A.; Killoran, M.P.; Wilkinson, J.M.; Hartnett, J.R.; et al. Homogeneous Assay for Target Engagement Utilizing Bioluminescent Thermal Shift. *ACS Medicinal Chemistry Letters* **2018**, *9*, 546-551, doi:10.1021/acsmedchemlett.8b00081.
15. Matulis, D.; Kranz, J.K.; Salemme, F.R.; Todd, M.J. Thermodynamic stability of carbonic anhydrase: measurements of binding affinity and stoichiometry using ThermoFluor. *Biochemistry* **2005**, *44*, 5258-5266, doi:10.1021/bi048135v.
16. Eyre, N.S.; Johnson, S.M.; Eltahla, A.A.; Aloi, M.; Aloia, A.L.; McDevitt, C.A.; Bull, R.A.; Beard, M.R. Genome-Wide Mutagenesis of Dengue Virus Reveals Plasticity of the NS1 Protein and Enables Generation of Infectious Tagged Reporter Viruses. *J Virol* **2017**, *91*, doi:10.1128/jvi.01455-17.
17. Burton, T.D.; Eyre, N.S. Applications of Deep Mutational Scanning in Virology. *Viruses* **2021**, *13*, 1020.

18. Fischl, W.; Bartenschlager, R. High-throughput screening using dengue virus reporter genomes. *Methods Mol Biol* **2013**, *1030*, 205-219, doi:10.1007/978-1-62703-484-5_17.
19. Eyre, N.S.; Aloia, A.L.; Joyce, M.A.; Chulanetra, M.; Tyrrell, D.L.; Beard, M.R. Sensitive luminescent reporter viruses reveal appreciable release of hepatitis C virus NS5A protein into the extracellular environment. *Virology* **2017**, *507*, 20-31, doi:https://doi.org/10.1016/j.virol.2017.04.003.
20. Eyre, N.S.; Johnson, S.M.; Eltahla, A.A.; Aloi, M.; Aloia, A.L.; McDevitt, C.A.; Bull, R.A.; Beard, M.R. Genome-Wide Mutagenesis of Dengue Virus Reveals Plasticity of the NS1 Protein and Enables Generation of Infectious Tagged Reporter Viruses. *Journal of Virology* **2017**, *91*, e01455-01417, doi:doi:10.1128/JVI.01455-17.
21. Tan, T.Y.; Fibriansah, G.; Kostyuchenko, V.A.; Ng, T.-S.; Lim, X.-X.; Zhang, S.; Lim, X.-N.; Wang, J.; Shi, J.; Morais, M.C.; et al. Capsid protein structure in Zika virus reveals the flavivirus assembly process. *Nature Communications* **2020**, *11*, 895, doi:10.1038/s41467-020-14647-9.
22. Cimmperman, P.; Baranauskiene, L.; Jachimoviciūte, S.; Jachno, J.; Torresan, J.; Michailoviene, V.; Matuliene, J.; Sereikaite, J.; Bumelis, V.; Matulis, D. A quantitative model of thermal stabilization and destabilization of proteins by ligands. *Biophys J* **2008**, *95*, 3222-3231, doi:10.1529/biophysj.108.134973.
23. Fujita, T.; Iwasa, J.; Hansch, C. A New Substituent Constant, π, Derived from Partition Coefficients. *Journal of the American Chemical Society* **1964**, *86*, 5175-5180, doi:10.1021/ja01077a028.
24. Ansarah-Sobrinho, C.; Nelson, S.; Jost, C.A.; Whitehead, S.S.; Pierson, T.C. Temperature-dependent production of pseudoinfectious dengue reporter virus particles by complementation. *Virology* **2008**, *381*, 67-74, doi:10.1016/j.virol.2008.08.021.
25. Ka, S.; Merindol, N.; Sow, A.A.; Singh, A.; Landelouci, K.; Plourde, M.B.; Pépin, G.; Masi, M.; Lecce, R.D.; Evidente, A.; et al. Amaryllidaceae Alkaloid Cherylline Inhibits the Replication of Dengue and Zika Viruses. *Antimicrobial Agents and Chemotherapy* **2021**, *65*, e00398-00321, doi:doi:10.1128/AAC.00398-21.
26. Crill, W.D.; Chang, G.J. Localization and characterization of flavivirus envelope glycoprotein cross-reactive epitopes. *J Virol* **2004**, *78*, 13975-13986, doi:10.1128/jvi.78.24.13975-13986.2004.
27. Labeau, A.; Simon-Loriere, E.; Hafirassou, M.-L.; Bonnet-Madin, L.; Tessier, S.; Zamborlini, A.; Dupré, T.; Seta, N.; Schwartz, O.; Chaix, M.-L.; et al. A Genome-Wide CRISPR-Cas9 Screen Identifies the Dolichol-Phosphate Mannose Synthase Complex as a Host Dependency Factor for Dengue Virus Infection. *Journal of Virology* **2020**, *94*, e01751-01719, doi:doi:10.1128/JVI.01751-19.
28. Pokidysheva, E.; Zhang, Y.; Battisti, A.J.; Bator-Kelly, C.M.; Chipman, P.R.; Xiao, C.; Gregorio, G.G.; Hendrickson, W.A.; Kuhn, R.J.; Rossmann, M.G. Cryo-EM Reconstruction of Dengue Virus in Complex with the Carbohydrate Recognition Domain of DC-SIGN. *Cell* **2006**, *124*, 485-493, doi:https://doi.org/10.1016/j.cell.2005.11.042.
29. Gandini, R.; Reichenbach, T.; Tan, T.-C.; Divne, C. Structural basis for dolichylphosphate mannose biosynthesis. *Nature Communications* **2017**, *8*, 120, doi:10.1038/s41467-017-00187-2.
30. Goyal, U.; Blackstone, C. Untangling the web: mechanisms underlying ER network formation. *Biochim Biophys Acta* **2013**, *1833*, 2492-2498, doi:10.1016/j.bbamcr.2013.04.009.
31. Rismanchi, N.; Soderblom, C.; Stadler, J.; Zhu, P.P.; Blackstone, C. Atlastin GTPases are required for Golgi apparatus and ER morphogenesis. *Hum Mol Genet* **2008**, *17*, 1591-1604, doi:10.1093/hmg/ddn046.
32. Zhao, G.; Zhu, P.-P.; Renvoisé, B.; Maldonado-Báez, L.; Park, S.H.; Blackstone, C. Mammalian knock out cells reveal prominent roles for atlastin GTPases in ER network morphology. *Experimental Cell Research* **2016**, *349*, 32-44, doi:https://doi.org/10.1016/j.yexcr.2016.09.015.

33. Neufeldt, C.J.; Cortese, M.; Scaturro, P.; Cerikan, B.; Wideman, J.G.; Tabata, K.; Moraes, T.; Oleksiuk, O.; Pichlmair, A.; Bartenschlager, R. ER-shaping atlastin proteins act as central hubs to promote flavivirus replication and virion assembly. *Nat Microbiol* **2019**, *4*, 2416-2429, doi:10.1038/s41564-019-0586-3.
34. Troost, B.; Smit, J.M. Recent advances in antiviral drug development towards dengue virus. *Current Opinion in Virology* **2020**, *43*, 9-21, doi:https://doi.org/10.1016/j.coviro.2020.07.009.
35. Modis, Y.; Ogata, S.; Clements, D.; Harrison, S.C. A ligand-binding pocket in the dengue virus envelope glycoprotein. *Proc Natl Acad Sci U S A* **2003**, *100*, 6986-6991, doi:10.1073/pnas.0832193100.
36. Schmidt, A.G.; Lee, K.; Yang, P.L.; Harrison, S.C. Small-Molecule Inhibitors of Dengue-Virus Entry. *PLOS Pathogens* **2012**, *8*, e1002627, doi:10.1371/journal.ppat.1002627.
37. Klein, D.E.; Choi, J.L.; Harrison, S.C. Structure of a dengue virus envelope protein late-stage fusion intermediate. *J Virol* **2013**, *87*, 2287-2293, doi:10.1128/jvi.02957-12.
38. Yang, J.-M.; Chen, Y.-F.; Tu, Y.-Y.; Yen, K.-R.; Yang, Y.-L. Combinatorial Computational Approaches to Identify Tetracycline Derivatives as Flavivirus Inhibitors. *PLOS ONE* **2007**, *2*, e428, doi:10.1371/journal.pone.0000428.
39. Poh, M.K.; Yip, A.; Zhang, S.; Priestle, J.P.; Ma, N.L.; Smit, J.M.; Wilschut, J.; Shi, P.-Y.; Wenk, M.R.; Schul, W. A small molecule fusion inhibitor of dengue virus. *Antiviral Research* **2009**, *84*, 260-266, doi:https://doi.org/10.1016/j.antiviral.2009.09.011.
40. Leal, E.S.; Adler, N.S.; Fernández, G.A.; Gebhard, L.G.; Battini, L.; Aucar, M.G.; Videla, M.; Monge, M.E.; Hernández de los Ríos, A.; Acosta Dávila, J.A.; et al. De novo design approaches targeting an envelope protein pocket to identify small molecules against dengue virus. *European Journal of Medicinal Chemistry* **2019**, *182*, 111628, doi:https://doi.org/10.1016/j.ejmech.2019.111628.
41. Zhou, Z.; Khaliq, M.; Suk, J.-E.; Patkar, C.; Li, L.; Kuhn, R.J.; Post, C.B. Antiviral Compounds Discovered by Virtual Screening of Small−Molecule Libraries against Dengue Virus E Protein. *ACS Chemical Biology* **2008**, *3*, 765-775, doi:10.1021/cb800176t.
42. Alen, M.M.F.; Schols, D. Dengue Virus Entry as Target for Antiviral Therapy. *Journal of Tropical Medicine* **2012**, *2012*, 628475, doi:10.1155/2012/628475.
43. Chen, Y.; Maguire, T.; Hileman, R.E.; Fromm, J.R.; Esko, J.D.; Linhardt, R.J.; Marks, R.M. Dengue virus infectivity depends on envelope protein binding to target cell heparan sulfate. *Nat Med* **1997**, *3*, 866-871, doi:10.1038/nm0897-866.
44. S, A.H.; Pujar, G.V.; Sethu, A.K.; Bhagyalalitha, M.; Singh, M. Dengue structural proteins as antiviral drug targets: Current status in the drug discovery & development. *European Journal of Medicinal Chemistry* **2021**, *221*, 113527, doi:https://doi.org/10.1016/j.ejmech.2021.113527.
45. Lin, Y.-L.; Lei, H.-Y.; Lin, Y.-S.; Yeh, T.-M.; Chen, S.-H.; Liu, H.-S. Heparin inhibits dengue-2 virus infection of five human liver cell lines. *Antiviral Research* **2002**, *56*, 93-96, doi:https://doi.org/10.1016/S0166-3542(02)00095-5.
46. Behnam, M.A.M.; Nitsche, C.; Boldescu, V.; Klein, C.D. The Medicinal Chemistry of Dengue Virus. *Journal of Medicinal Chemistry* **2016**, *59*, 5622-5649, doi:10.1021/acs.jmedchem.5b01653.
47. Lee, E.; Pavy, M.; Young, N.; Freeman, C.; Lobigs, M. Antiviral effect of the heparan sulfate mimetic, PI-88, against dengue and encephalitic flaviviruses. *Antiviral Research* **2006**, *69*, 31-38, doi:https://doi.org/10.1016/j.antiviral.2005.08.006.

References

1. Guzman MG, Halstead SB, Artsob H, Buchy P, Farrar J, Gubler DJ, Hunsperger E, Kroeger A, Margolis HS, Martínez E, Nathan MB, Pelegrino JL, Simmons C, Yoksan S, Peeling RW. 2010. Dengue: a continuing global threat. Nature reviews Microbiology 8:S7-S16.
2. Hasan S, Jamdar SF, Alalowi M, Al Ageel Al Beaiji SM. 2016. Dengue virus: A global human threat: Review of literature. Journal of International Society of Preventive & Community Dentistry 6:1-6.
3. Ajlan BA, Alafif MM, Alawi MM, Akbar NA, Aldigs EK, Madani TA. 2019. Assessment of the new World Health Organization's dengue classification for predicting severity of illness and level of healthcare required. PLoS Negl Trop Dis 13:e0007144.
4. Rocklöv J, Tozan Y. 2019. Climate change and the rising infectiousness of dengue. Emerging Topics in Life Sciences 3:133.
5. Guy B, Barrere B, Malinowski C, Saville M, Teyssou R, Lang J. 2011. From research to phase III: Preclinical, industrial and clinical development of the Sanofi Pasteur tetravalent dengue vaccine. Vaccine 29:7229-7241.
6. Halstead SB. 2017. Dengvaxia sensitizes seronegatives to vaccine enhanced disease regardless of age. Vaccine 35:6355-6358.
7. Thomas SJ, Yoon IK. 2019. A review of Dengvaxia®: development to deployment. Hum Vaccin Immunother 15:2295-2314.
8. Rivera L, Biswal S, Sáez-Llorens X, Reynales H, López-Medina E, Borja-Tabora C, Bravo L, Sirivichayakul C, Kosalaraksa P, Martinez Vargas L, Yu D, Watanaveeradej V, Espinoza F, Dietze R, Fernando L, Wickramasinghe P, Duarte MoreiraJr E, Fernando AD, Gunasekera D, Luz K, Venâncioda Cunha R, Rauscher M, Zent O, Liu M, Hoffman E, LeFevre I, Tricou V, Wallace D, Alera M, Borkowski A, group ftTs. 2021. Three-year Efficacy and Safety of Takeda's Dengue Vaccine Candidate (TAK-003). Clinical Infectious Diseases 75:107-117.
9. Mallapaty S. 2022. Dengue vaccine poised for roll-out but safety concerns linger. Nature 611:434-435.
10. Mustafa MS, Rasotgi V, Jain S, Gupta V. 2015. Discovery of fifth serotype of dengue virus (DENV-5): A new public health dilemma in dengue control. Med J Armed Forces India 71:67-70.
11. Bartenschlager R, Miller S. 2008. Molecular aspects of Dengue virus replication. Future Microbiol 3:155-65.
12. Kuhn RJ, Zhang W, Rossmann MG, Pletnev SV, Corver J, Lenches E, Jones CT, Mukhopadhyay S, Chipman PR, Strauss EG, Baker TS, Strauss JH. 2002. Structure of Dengue Virus: Implications for Flavivirus Organization, Maturation, and Fusion. Cell 108:717-725.
13. Guzman MG, Gubler DJ, Izquierdo A, Martinez E, Halstead SB. 2016. Dengue infection. Nature Reviews Disease Primers 2:16055.
14. Watterson D, Modhiran N, Young PR. 2016. The many faces of the flavivirus NS1 protein offer a multitude of options for inhibitor design. Antiviral Res 130:7-18.
15. Vasilakis N, Cardosa J, Hanley KA, Holmes EC, Weaver SC. 2011. Fever from the forest: prospects for the continued emergence of sylvatic dengue virus and its impact on public health. Nat Rev Microbiol 9:532-41.
16. Valentine MJ, Murdock CC, Kelly PJ. 2019. Sylvatic cycles of arboviruses in non-human primates. Parasites & Vectors 12:463.

17. Khin MM, Than KA. 1983. Transovarial transmission of dengue 2 virus by Aedes aegypti in nature. Am J Trop Med Hyg 32:590-4.
18. Rosen L, Shroyer DA, Tesh RB, Freier JE, Lien JC. 1983. Transovarial transmission of dengue viruses by mosquitoes: Aedes albopictus and Aedes aegypti. Am J Trop Med Hyg 32:1108-19.
19. Watts DM, Harrison BA, Pantuwatana S, Klein TA, Burke DS. 1985. Failure to detect natural transovarial transmission of dengue viruses by Aedes aegypti and Aedes albopictus (Diptera: Culicidae). J Med Entomol 22:261-5.
20. Ramalingam S, Shekhar KC, Pang T, Rampal L, Chew C, Ramakrishna K, Poon G, Lam S. 1986. Does transovarial transmission of dengue viruses occur in Malaysia. Trop Biomed 3:87-88.
21. Grunnill M, Boots M. 2015. How Important is Vertical Transmission of Dengue Viruses by Mosquitoes (Diptera: Culicidae)? Journal of Medical Entomology 53:1-19.
22. Estofolete CF, de Oliveira Mota MT, Bernardes Terzian AC, de Aguiar Milhim BHG, Ribeiro MR, Nunes DV, Mourão MP, Rossi SL, Nogueira ML, Vasilakis N. 2019. Unusual clinical manifestations of dengue disease – Real or imagined? Acta Tropica 199:105134.
23. Bhatt S, Gething PW, Brady OJ, Messina JP, Farlow AW, Moyes CL, Drake JM, Brownstein JS, Hoen AG, Sankoh O, Myers MF, George DB, Jaenisch T, Wint GRW, Simmons CP, Scott TW, Farrar JJ, Hay SI. 2013. The global distribution and burden of dengue. Nature 496:504-507.
24. Wilder-Smith A. 2012. Dengue infections in travellers. Paediatr Int Child Health 32 Suppl 1:28-32.
25. Srikiatkhachorn A, Mathew A, Rothman AL. 2017. Immune-mediated cytokine storm and its role in severe dengue. Semin Immunopathol 39:563-574.
26. Dayarathna S, Jeewandara C, Gomes L, Somathilaka G, Jayathilaka D, Vimalachandran V, Wijewickrama A, Narangoda E, Idampitiya D, Ogg GS, Malavige GN. 2020. Similarities and differences between the 'cytokine storms' in acute dengue and COVID-19. Scientific Reports 10:19839.
27. Hammond SN, Balmaseda A, Pérez L, Tellez Y, Saborío SI, Mercado JC, Videa E, Rodriguez Y, Pérez MA, Cuadra R, Solano S, Rocha J, Idiaquez W, Gonzalez A, Harris E. 2005. Differences in dengue severity in infants, children, and adults in a 3-year hospital-based study in Nicaragua. Am J Trop Med Hyg 73:1063-70.
28. Guzmán MG, Kouri G, Bravo J, Valdes L, Vazquez S, Halstead SB. 2002. Effect of age on outcome of secondary dengue 2 infections. Int J Infect Dis 6:118-24.
29. de Araújo TVB, Rodrigues LC, de Alencar Ximenes RA, de Barros Miranda-Filho D, Montarroyos UR, de Melo APL, Valongueiro S, de Albuquerque MdFPM, Souza WV, Braga C, Filho SPB, Cordeiro MT, Vazquez E, Di Cavalcanti Souza Cruz D, Henriques CMP, Bezerra LCA, da Silva Castanha PM, Dhalia R, Marques-Júnior ETA, Martelli CMT. 2016. Association between Zika virus infection and microcephaly in Brazil, January to May, 2016: preliminary report of a case-control study. The Lancet Infectious Diseases 16:1356-1363.
30. Verma R, Sharma P, Garg RK, Atam V, Singh MK, Mehrotra HS. 2011. Neurological complications of dengue fever: Experience from a tertiary center of north India. Ann Indian Acad Neurol 14:272-8.

31. St. John AL, Abraham SN, Gubler DJ. 2013. Barriers to preclinical investigations of anti-dengue immunity and dengue pathogenesis. Nature Reviews Microbiology 11:420-426.
32. Mazeaud C, Freppel W, Chatel-Chaix L. 2018. The Multiples Fates of the Flavivirus RNA Genome During Pathogenesis. Front Genet 9:595.
33. Villordo SM, Filomatori CV, Sánchez-Vargas I, Blair CD, Gamarnik AV. 2015. Dengue virus RNA structure specialization facilitates host adaptation. PLoS Pathog 11:e1004604.
34. Dong H, Chang DC, Xie X, Toh YX, Chung KY, Zou G, Lescar J, Lim SP, Shi PY. 2010. Biochemical and genetic characterization of dengue virus methyltransferase. Virology 405:568-78.
35. Polacek C, Friebe P, Harris E. 2009. Poly(A)-binding protein binds to the non-polyadenylated 3' untranslated region of dengue virus and modulates translation efficiency. Journal of General Virology 90:687-692.
36. Villordo SM, Alvarez DE, Gamarnik AV. 2010. A balance between circular and linear forms of the dengue virus genome is crucial for viral replication. Rna 16:2325-35.
37. Pijlman GP, Funk A, Kondratieva N, Leung J, Torres S, van der Aa L, Liu WJ, Palmenberg AC, Shi PY, Hall RA, Khromykh AA. 2008. A highly structured, nuclease-resistant, noncoding RNA produced by flaviviruses is required for pathogenicity. Cell Host Microbe 4:579-91.
38. Schuessler A, Funk A, Lazear HM, Cooper DA, Torres S, Daffis S, Jha BK, Kumagai Y, Takeuchi O, Hertzog P, Silverman R, Akira S, Barton DJ, Diamond MS, Khromykh AA. 2012. West Nile virus noncoding subgenomic RNA contributes to viral evasion of the type I interferon-mediated antiviral response. J Virol 86:5708-18.
39. Bidet K, Dadlani D, Garcia-Blanco MA. 2014. G3BP1, G3BP2 and CAPRIN1 are required for translation of interferon stimulated mRNAs and are targeted by a dengue virus non-coding RNA. PLoS Pathog 10:e1004242.
40. Gebhard LG, Filomatori CV, Gamarnik AV. 2011. Functional RNA elements in the dengue virus genome. Viruses 3:1739-56.
41. Zhang X, Jia R, Shen H, Wang M, Yin Z, Cheng A. 2017. Structures and Functions of the Envelope Glycoprotein in Flavivirus Infections. Viruses 9:338.
42. Harrison SC. 2008. Viral membrane fusion. Nat Struct Mol Biol 15:690-8.
43. Li L, Lok SM, Yu IM, Zhang Y, Kuhn RJ, Chen J, Rossmann MG. 2008. The flavivirus precursor membrane-envelope protein complex: structure and maturation. Science 319:1830-4.
44. Byk LA, Gamarnik AV. 2016. Properties and Functions of the Dengue Virus Capsid Protein. Annu Rev Virol 3:263-281.
45. Wang SH, Syu WJ, Hu ST. 2004. Identification of the homotypic interaction domain of the core protein of dengue virus type 2. J Gen Virol 85:2307-2314.
46. Samsa MM, Mondotte JA, Iglesias NG, Assuncao-Miranda I, Barbosa-Lima G, Da Poian AT, Bozza PT, Gamarnik AV. 2009. Dengue virus capsid protein usurps lipid droplets for viral particle formation. PLoS Pathog 5:e1000632.
47. Pong WL, Huang ZS, Teoh PG, Wang CC, Wu HN. 2011. RNA binding property and RNA chaperone activity of dengue virus core protein and other viral RNA-interacting proteins. FEBS Lett 585:2575-81.

48. Nasar S, Rashid N, Iftikhar S. 2020. Dengue proteins with their role in pathogenesis, and strategies for developing an effective anti-dengue treatment: A review. J Med Virol 92:941-955.
49. Rastogi M, Sharma N, Singh SK. 2016. Flavivirus NS1: a multifaceted enigmatic viral protein. Virology Journal 13:131.
50. Xie X, Zou J, Zhang X, Zhou Y, Routh AL, Kang C, Popov VL, Chen X, Wang QY, Dong H, Shi PY. 2019. Dengue NS2A Protein Orchestrates Virus Assembly. Cell Host Microbe 26:606-622.e8.
51. Muñoz-Jordan JL, Sánchez-Burgos GG, Laurent-Rolle M, García-Sastre A. 2003. Inhibition of interferon signaling by dengue virus. Proc Natl Acad Sci U S A 100:14333-8.
52. Xie X, Gayen S, Kang C, Yuan Z, Shi P-Y. 2013. Membrane Topology and Function of Dengue Virus NS2A Protein. Journal of Virology 87:4609-4622.
53. Mackenzie JM, Khromykh AA, Jones MK, Westaway EG. 1998. Subcellular Localization and Some Biochemical Properties of the Flavivirus Kunjin Nonstructural Proteins NS2A and NS4A. Virology 245:203-215.
54. Westaway EG, Mackenzie JM, Kenney MT, Jones MK, Khromykh AA. 1997. Ultrastructure of Kunjin virus-infected cells: colocalization of NS1 and NS3 with double-stranded RNA, and of NS2B with NS3, in virus-induced membrane structures. J Virol 71:6650-61.
55. Xie X, Zou J, Zhang X, Zhou Y, Routh AL, Kang C, Popov VL, Chen X, Wang Q-Y, Dong H, Shi P-Y. 2019. Dengue NS2A Protein Orchestrates Virus Assembly. Cell Host & Microbe 26:606-622.e8.
56. Ozden S, Poirier B. 1985. Dengue virus induced polypeptide synthesis. Archives of Virology 85:129-137.
57. Leung D, Schroder K, White H, Fang NX, Stoermer MJ, Abbenante G, Martin JL, Young PR, Fairlie DP. 2001. Activity of recombinant dengue 2 virus NS3 protease in the presence of a truncated NS2B co-factor, small peptide substrates, and inhibitors. J Biol Chem 276:45762-71.
58. Bazan JF, Fletterick RJ. 1989. Detection of a trypsin-like serine protease domain in flaviviruses and pestviruses. Virology 171:637-639.
59. Swarbrick CMD, Basavannacharya C, Chan KWK, Chan SA, Singh D, Wei N, Phoo WW, Luo D, Lescar J, Vasudevan SG. 2017. NS3 helicase from dengue virus specifically recognizes viral RNA sequence to ensure optimal replication. Nucleic Acids Res 45:12904-12920.
60. Xu S, Ci Y, Wang L, Yang Y, Zhang L, Xu C, Qin C, Shi L. 2019. Zika virus NS3 is a canonical RNA helicase stimulated by NS5 RNA polymerase. Nucleic Acids Research 47:8693-8707.
61. Li X-D, Deng C-L, Ye H-Q, Zhang H-L, Zhang Q-Y, Chen D-D, Zhang P-T, Shi P-Y, Yuan Z-M, Zhang B. 2016. Transmembrane Domains of NS2B Contribute to both Viral RNA Replication and Particle Formation in Japanese Encephalitis Virus. Journal of Virology 90:5735-5749.
62. Aguirre S, Luthra P, Sanchez-Aparicio MT, Maestre AM, Patel J, Lamothe F, Fredericks AC, Tripathi S, Zhu T, Pintado-Silva J, Webb LG, Bernal-Rubio D, Solovyov A, Greenbaum B, Simon V, Basler CF, Mulder LCF, García-Sastre A, Fernandez-Sesma A. 2017. Dengue virus NS2B protein targets cGAS for degradation and prevents mitochondrial DNA sensing during infection. Nature Microbiology 2:17037.

63. Lin C, Amberg SM, Chambers TJ, Rice CM. 1993. Cleavage at a novel site in the NS4A region by the yellow fever virus NS2B-3 proteinase is a prerequisite for processing at the downstream 4A/4B signalase site. Journal of Virology 67:2327-2335.
64. Miller S, Kastner S, Krijnse-Locker J, Bühler S, Bartenschlager R. 2007. The Non-structural Protein 4A of Dengue Virus Is an Integral Membrane Protein Inducing Membrane Alterations in a 2K-regulated Manner *. Journal of Biological Chemistry 282:8873-8882.
65. Mikulasova A, Gillespie LK, Ambrose RL, Aktepe TE, Trenerry AM, Liebscher S, Mackenzie JM. 2021. A Putative Lipid-Associating Motif in the West Nile Virus NS4A Protein Is Required for Efficient Virus Replication. Front Cell Dev Biol 9:655606.
66. Teo CS, Chu JJ. 2014. Cellular vimentin regulates construction of dengue virus replication complexes through interaction with NS4A protein. J Virol 88:1897-913.
67. Hung YF, Schwarten M, Schünke S, Thiagarajan-Rosenkranz P, Hoffmann S, Sklan EH, Willbold D, Koenig BW. 2015. Dengue virus NS4A cytoplasmic domain binding to liposomes is sensitive to membrane curvature. Biochim Biophys Acta 1848:1119-26.
68. McLean JE, Wudzinska A, Datan E, Quaglino D, Zakeri Z. 2011. Flavivirus NS4A-induced autophagy protects cells against death and enhances virus replication. J Biol Chem 286:22147-59.
69. Youn S, Li T, McCune BT, Edeling MA, Fremont DH, Cristea IM, Diamond MS. 2012. Evidence for a Genetic and Physical Interaction between Nonstructural Proteins NS1 and NS4B That Modulates Replication of West Nile Virus. Journal of Virology 86:7360-7371.
70. Zou J, Lee LT, Wang QY, Xie X, Lu S, Yau YH, Yuan Z, Shochat SG, Kang C, Lescar J, Shi P-Y. 2015. Mapping the Interactions between the NS4B and NS3 Proteins of Dengue Virus. Journal of Virology 89:3471-3483.
71. Muñoz-Jordán JL, Laurent-Rolle M, Ashour J, Martínez-Sobrido L, Ashok M, Lipkin WI, García-Sastre A. 2005. Inhibition of alpha/beta interferon signaling by the NS4B protein of flaviviruses. J Virol 79:8004-13.
72. Zou J, Xie X, Wang QY, Dong H, Lee MY, Kang C, Yuan Z, Shi PY. 2015. Characterization of dengue virus NS4A and NS4B protein interaction. J Virol 89:3455-70.
73. Miller S, Kastner S, Krijnse-Locker J, Bühler S, Bartenschlager R. 2007. The Non-structural Protein 4A of Dengue Virus Is an Integral Membrane Protein Inducing Membrane Alterations in a 2K-regulated Manner*. Journal of Biological Chemistry 282:8873-8882.
74. Płaszczyca A, Scaturro P, Neufeldt CJ, Cortese M, Cerikan B, Ferla S, Brancale A, Pichlmair A, Bartenschlager R. 2019. A novel interaction between dengue virus nonstructural protein 1 and the NS4A-2K-4B precursor is required for viral RNA replication but not for formation of the membranous replication organelle. PLoS Pathog 15:e1007736.
75. Liu L, Dong H, Chen H, Zhang J, Ling H, Li Z, Shi PY, Li H. 2010. Flavivirus RNA cap methyltransferase: structure, function, and inhibition. Front Biol (Beijing) 5:286-303.
76. El Sahili A, Lescar J. 2017. Dengue Virus Non-Structural Protein 5. Viruses 9:91.
77. De Maio FA, Risso G, Iglesias NG, Shah P, Pozzi B, Gebhard LG, Mammi P, Mancini E, Yanovsky MJ, Andino R, Krogan N, Srebrow A, Gamarnik AV. 2016. The Dengue Virus NS5 Protein Intrudes in the Cellular Spliceosome and Modulates Splicing. PLOS Pathogens 12:e1005841.

78. Hardy JM, Newton ND, Modhiran N, Scott CAP, Venugopal H, Vet LJ, Young PR, Hall RA, Hobson-Peters J, Coulibaly F, Watterson D. 2021. A unified route for flavivirus structures uncovers essential pocket factors conserved across pathogenic viruses. Nature Communications 12:3266.
79. Hobson-Peters J, Harrison JJ, Watterson D, Hazlewood JE, Vet LJ, Newton ND, Warrilow D, Colmant AMG, Taylor C, Huang B, Piyasena TBH, Chow WK, Setoh YX, Tang B, Nakayama E, Yan K, Amarilla AA, Wheatley S, Moore PR, Finger M, Kurucz N, Modhiran N, Young PR, Khromykh AA, Bielefeldt-Ohmann H, Suhrbier A, Hall RA. 2019. A recombinant platform for flavivirus vaccines and diagnostics using chimeras of a new insect-specific virus. Sci Transl Med 11.
80. Screaton G, Mongkolsapaya J, Yacoub S, Roberts C. 2015. New insights into the immunopathology and control of dengue virus infection. Nature Reviews Immunology 15:745-759.
81. van der Schaar HM, Rust MJ, Chen C, van der Ende-Metselaar H, Wilschut J, Zhuang X, Smit JM. 2008. Dissecting the Cell Entry Pathway of Dengue Virus by Single-Particle Tracking in Living Cells. PLOS Pathogens 4:e1000244.
82. Acosta EG, Castilla V, Damonte EB. 2009. Alternative infectious entry pathways for dengue virus serotypes into mammalian cells. Cellular Microbiology 11:1533-1549.
83. Diamond MS, Edgil D, Roberts TG, Lu B, Harris E. 2000. Infection of human cells by dengue virus is modulated by different cell types and viral strains. Journal of virology 74:7814-7823.
84. Modis Y, Ogata S, Clements D, Harrison SC. 2004. Structure of the dengue virus envelope protein after membrane fusion. Nature 427:313-319.
85. Smit JM, Moesker B, Rodenhuis-Zybert I, Wilschut J. 2011. Flavivirus cell entry and membrane fusion. Viruses 3:160-171.
86. Clyde K, Kyle JL, Harris E. 2006. Recent advances in deciphering viral and host determinants of dengue virus replication and pathogenesis. J Virol 80:11418-31.
87. Cervantes-Salazar M, Angel-Ambrocio AH, Soto-Acosta R, Bautista-Carbajal P, Hurtado-Monzon AM, Alcaraz-Estrada SL, Ludert JE, Del Angel RM. 2015. Dengue virus NS1 protein interacts with the ribosomal protein RPL18: this interaction is required for viral translation and replication in Huh-7 cells. Virology 484:113-26.
88. Mazeaud C, Freppel W, Chatel-Chaix L. 2018. The Multiples Fates of the Flavivirus RNA Genome During Pathogenesis. Frontiers in genetics 9:595-595.
89. Paranjape SM, Harris E. 2010. Control of Dengue Virus Translation and Replication, p 15-34. *In* Rothman AL (ed), Dengue Virus doi:10.1007/978-3-642-02215-9_2. Springer Berlin Heidelberg, Berlin, Heidelberg.
90. Chiu W-W, Kinney RM, Dreher TW. 2005. Control of translation by the 5'- and 3'-terminal regions of the dengue virus genome. Journal of virology 79:8303-8315.
91. Gallie DR. 1991. The cap and poly(A) tail function synergistically to regulate mRNA translational efficiency. Genes Dev 5:2108-16.
92. Mandl CW, Kunz C, Heinz FX. 1991. Presence of poly(A) in a flavivirus: significant differences between the 3' noncoding regions of the genomic RNAs of tick-borne encephalitis virus strains. Journal of virology 65:4070-4077.
93. Wells SE, Hillner PE, Vale RD, Sachs AB. 1998. Circularization of mRNA by Eukaryotic Translation Initiation Factors. Molecular Cell 2:135-140.

94. Alvarez DE, Lodeiro MF, Ludueña SJ, Pietrasanta LI, Gamarnik AV. 2005. Long-Range RNA-RNA Interactions Circularize the Dengue Virus Genome. Journal of Virology 79:6631.
95. Friebe P, Harris E. 2010. Interplay of RNA elements in the dengue virus 5' and 3' ends required for viral RNA replication. Journal of virology 84:6103-6118.
96. Welsch S, Miller S, Romero-Brey I, Merz A, Bleck CK, Walther P, Fuller SD, Antony C, Krijnse-Locker J, Bartenschlager R. 2009. Composition and three-dimensional architecture of the dengue virus replication and assembly sites. Cell Host Microbe 5:365-75.
97. Chatel-Chaix L, Bartenschlager R. 2014. Dengue virus- and hepatitis C virus-induced replication and assembly compartments: the enemy inside--caught in the web. J Virol 88:5907-11.
98. Miller S, Kastner S, Krijnse-Locker J, Buhler S, Bartenschlager R. 2007. The non-structural protein 4A of dengue virus is an integral membrane protein inducing membrane alterations in a 2K-regulated manner. J Biol Chem 282:8873-82.
99. You S, Padmanabhan R. 1999. A novel in vitro replication system for Dengue virus. Initiation of RNA synthesis at the 3'-end of exogenous viral RNA templates requires 5'- and 3'-terminal complementary sequence motifs of the viral RNA. J Biol Chem 274:33714-22.
100. Byk LA, Gamarnik AV. 2016. Properties and Functions of the Dengue Virus Capsid Protein. Annual review of virology 3:263-281.
101. Comas-Garcia M, Davis SR, Rein A. 2016. On the Selective Packaging of Genomic RNA by HIV-1. Viruses 8.
102. Pong W-L, Huang Z-S, Teoh P-G, Wang C-C, Wu H-N. 2011. RNA binding property and RNA chaperone activity of dengue virus core protein and other viral RNA-interacting proteins. FEBS Letters 585:2575-2581.
103. Ivanyi-Nagy R, Lavergne JP, Gabus C, Ficheux D, Darlix JL. 2008. RNA chaperoning and intrinsic disorder in the core proteins of Flaviviridae. Nucleic Acids Res 36:712-25.
104. Zhang Y, Corver J, Chipman PR, Zhang W, Pletnev SV, Sedlak D, Baker TS, Strauss JH, Kuhn RJ, Rossmann MG. 2003. Structures of immature flavivirus particles. The EMBO journal 22:2604-2613.
105. Yu IM, Zhang W, Holdaway HA, Li L, Kostyuchenko VA, Chipman PR, Kuhn RJ, Rossmann MG, Chen J. 2008. Structure of the Immature Dengue Virus at Low pH Primes Proteolytic Maturation. Science 319:1834.
106. Oliveira ERA, de Alencastro RB, Horta BAC. 2017. New insights into flavivirus biology: the influence of pH over interactions between prM and E proteins. Journal of Computer-Aided Molecular Design 31:1009-1019.
107. Cruz-Oliveira C, Freire JM, Conceição TM, Higa LM, Castanho MARB, Da Poian AT. 2015. Receptors and routes of dengue virus entry into the host cells. FEMS Microbiology Reviews 39:155-170.
108. Simanjuntak Y, Liang J-J, Lee Y-L, Lin Y-L. 2014. Repurposing of Prochlorperazine for Use Against Dengue Virus Infection. The Journal of Infectious Diseases 211:394-404.
109. Heaton NS, Perera R, Berger KL, Khadka S, LaCount DJ, Kuhn RJ, Randall G. 2010. Dengue virus nonstructural protein 3 redistributes fatty acid synthase to sites of viral replication and increases cellular fatty acid synthesis. Proceedings of the National Academy of Sciences 107:17345.

110. Heaton NS, Randall G. 2010. Dengue virus-induced autophagy regulates lipid metabolism. Cell Host Microbe 8:422-32.
111. Savidis G, McDougall WM, Meraner P, Perreira JM, Portmann JM, Trincucci G, John SP, Aker AM, Renzette N, Robbins DR, Guo Z, Green S, Kowalik TF, Brass AL. 2016. Identification of Zika Virus and Dengue Virus Dependency Factors using Functional Genomics. Cell Rep 16:232-246.
112. Campos RK, Wong B, Xie X, Lu YF, Shi PY, Pompon J, Garcia-Blanco MA, Bradrick SS. 2017. RPLP1 and RPLP2 Are Essential Flavivirus Host Factors That Promote Early Viral Protein Accumulation. J Virol 91.
113. Garcia M, Wehbe M, Leveque N, Bodet C. 2017. Skin innate immune response to flaviviral infection. Eur Cytokine Netw 28:41-51.
114. Srikiatkhachorn A, Mathew A, Rothman AL. 2017. Immune-mediated cytokine storm and its role in severe dengue. Seminars in immunopathology 39:563-574.
115. Mogensen TH. 2009. Pathogen recognition and inflammatory signaling in innate immune defenses. Clinical microbiology reviews 22:240-273.
116. Nasirudeen AM, Wong HH, Thien P, Xu S, Lam KP, Liu DX. 2011. RIG-I, MDA5 and TLR3 synergistically play an important role in restriction of dengue virus infection. PLoS Negl Trop Dis 5:e926.
117. Uno N, Ross TM. 2018. Dengue virus and the host innate immune response. Emerging microbes & infections 7:167-167.
118. Wang JP, Liu P, Latz E, Golenbock DT, Finberg RW, Libraty DH. 2006. Flavivirus activation of plasmacytoid dendritic cells delineates key elements of TLR7 signaling beyond endosomal recognition. J Immunol 177:7114-21.
119. Zhang Q, Lenardo MJ, Baltimore D. 2017. 30 Years of NF-kappaB: A Blossoming of Relevance to Human Pathobiology. Cell 168:37-57.
120. Morrison J, Garcia-Sastre A. 2014. STAT2 signaling and dengue virus infection. Jakstat 3:e27715.
121. Shaio MF, Chang FY, Hou SC. 1992. Complement pathway activity in serum from patients with classical dengue fever. Trans R Soc Trop Med Hyg 86:672-5.
122. Walport MJ. 2001. Complement. New England Journal of Medicine 344:1058-1066.
123. Avirutnan P, Punyadee N, Noisakran S, Komoltri C, Thiemmeca S, Auethavornanan K, Jairungsri A, Kanlaya R, Tangthawornchaikul N, Puttikhunt C, Pattanakitsakul SN, Yenchitsomanus PT, Mongkolsapaya J, Kasinrerk W, Sittisombut N, Husmann M, Blettner M, Vasanawathana S, Bhakdi S, Malasit P. 2006. Vascular leakage in severe dengue virus infections: a potential role for the nonstructural viral protein NS1 and complement. J Infect Dis 193:1078-88.
124. Ubol S, Masrinoul P, Chaijaruwanich J, Kalayanarooj S, Charoensirisuthikul T, Kasisith J. 2008. Differences in Global Gene Expression in Peripheral Blood Mononuclear Cells Indicate a Significant Role of the Innate Responses in Progression of Dengue Fever but Not Dengue Hemorrhagic Fever. The Journal of Infectious Diseases 197:1459-1467.
125. Mehlhop E, Ansarah-Sobrinho C, Johnson S, Engle M, Fremont DH, Pierson TC, Diamond MS. 2007. Complement protein C1q inhibits antibody-dependent enhancement of flavivirus infection in an IgG subclass-specific manner. Cell Host Microbe 2:417-26.

126. Boonnak K, Dambach KM, Donofrio GC, Tassaneetrithep B, Marovich MA. 2011. Cell type specificity and host genetic polymorphisms influence antibody-dependent enhancement of dengue virus infection. J Virol 85:1671-83.
127. Flipse J, Diosa-Toro MA, Hoornweg TE, van de Pol DP, Urcuqui-Inchima S, Smit JM. 2016. Antibody-Dependent Enhancement of Dengue Virus Infection in Primary Human Macrophages; Balancing Higher Fusion against Antiviral Responses. Sci Rep 6:29201.
128. Douradinha B, McBurney SP, Soares de Melo KM, Smith AP, Krishna NK, Barratt-Boyes SM, Evans JD, Nascimento EJM, Marques ETA. 2014. C1q binding to dengue virus decreases levels of infection and inflammatory molecules transcription in THP-1 cells. Virus Research 179:231-234.
129. Conde JN, Silva EM, Barbosa AS, Mohana-Borges R. 2017. The Complement System in Flavivirus Infections. Frontiers in Microbiology 8.
130. Puschnik AS, Majzoub K, Ooi YS, Carette JE. 2017. A CRISPR toolbox to study virus–host interactions. Nature Reviews Microbiology 15:351-364.
131. Maeder ML, Linder SJ, Cascio VM, Fu Y, Ho QH, Joung JK. 2013. CRISPR RNA–guided activation of endogenous human genes. Nature Methods 10:977-979.
132. Dukhovny A, Lamkiewicz K, Chen Q, Fricke M, Jabrane-Ferrat N, Marz M, Jung JU, Sklan EH. 2019. A CRISPR Activation Screen Identifies Genes That Protect against Zika Virus Infection. Journal of Virology 93:e00211-19.
133. Chou Y-C, Lai MM, Wu Y-C, Hsu N-C, Jeng K-S, Su W-C. 2015. Variations in genome-wide RNAi screens: lessons from influenza research. Journal of clinical bioinformatics 5:2-2.
134. Hafirassou ML, Meertens L, Umaña-Diaz C, Labeau A, Dejarnac O, Bonnet-Madin L, Kümmerer BM, Delaugerre C, Roingeard P, Vidalain P-O, Amara A. 2017. A Global Interactome Map of the Dengue Virus NS1 Identifies Virus Restriction and Dependency Host Factors. Cell Reports 21:3900-3913.
135. Mackenzie JM, Jones MK, Young PR. 1996. Immunolocalization of the Dengue Virus Nonstructural Glycoprotein NS1 Suggests a Role in Viral RNA Replication. Virology 220:232-240.
136. Winkler G, Maxwell SE, Ruemmler C, Stollar V. 1989. Newly synthesized dengue-2 virus nonstructural protein NS1 is a soluble protein but becomes partially hydrophobic and membrane-associated after dimerization. Virology 171:302-305.
137. Flamand M, Megret F, Mathieu M, Lepault J, Rey FA, Deubel V. 1999. Dengue Virus Type 1 Nonstructural Glycoprotein NS1 Is Secreted from Mammalian Cells as a Soluble Hexamer in a Glycosylation-Dependent Fashion. Journal of Virology 73:6104.
138. Somnuke P, Hauhart RE, Atkinson JP, Diamond MS, Avirutnan P. 2011. N-linked glycosylation of dengue virus NS1 protein modulates secretion, cell-surface expression, hexamer stability, and interactions with human complement. Virology 413:253-264.
139. Akey DL, Brown WC, Dutta S, Konwerski J, Jose J, Jurkiw TJ, DelProposto J, Ogata CM, Skiniotis G, Kuhn RJ, Smith JL. 2014. Flavivirus NS1 structures reveal surfaces for associations with membranes and the immune system. Science 343:881-5.
140. Gutsche I, Coulibaly F, Voss JE, Salmon J, d'Alayer J, Ermonval M, Larquet E, Charneau P, Krey T, Mégret F, Guittet E, Rey FA, Flamand M. 2011. Secreted dengue virus nonstructural protein NS1 is an atypical barrel-shaped high-density lipoprotein. Proc Natl Acad Sci U S A 108:8003-8.

141. Edeling MA, Diamond MS, Fremont DH. 2014. Structural basis of Flavivirus NS1 assembly and antibody recognition. Proc Natl Acad Sci U S A 111:4285-90.
142. Akey DL, Brown WC, Jose J, Kuhn RJ, Smith JL. 2015. Structure-guided insights on the role of NS1 in flavivirus infection. BioEssays : news and reviews in molecular, cellular and developmental biology 37:489-494.
143. Eyre NS, Johnson SM, Eltahla AA, Aloi M, Aloia AL, McDevitt CA, Bull RA, Beard MR. 2017. Genome-Wide Mutagenesis of Dengue Virus Reveals Plasticity of the NS1 Protein and Enables Generation of Infectious Tagged Reporter Viruses. Journal of Virology 91:e01455-17.
144. Płaszczyca A, Scaturro P, Neufeldt CJ, Cortese M, Cerikan B, Ferla S, Brancale A, Pichlmair A, Bartenschlager R. 2019. A novel interaction between dengue virus nonstructural protein 1 and the NS4A-2K-4B precursor is required for viral RNA replication but not for formation of the membranous replication organelle. PLoS pathogens 15:e1007736-e1007736.
145. Scaturro P, Cortese M, Chatel-Chaix L, Fischl W, Bartenschlager R. 2015. Dengue Virus Non-structural Protein 1 Modulates Infectious Particle Production via Interaction with the Structural Proteins. PLoS Pathog 11:e1005277.
146. Cervantes-Salazar M, Angel-Ambrocio AH, Soto-Acosta R, Bautista-Carbajal P, Hurtado-Monzon AM, Alcaraz-Estrada SL, Ludert JE, Del Angel RM. 2015. Dengue virus NS1 protein interacts with the ribosomal protein RPL18: This interaction is required for viral translation and replication in Huh-7 cells. Virology 484:113-126.
147. Gutsche I, Coulibaly F, Voss JE, Salmon J, Alayer J, Ermonval M, Larquet E, Charneau P, Krey T, Mégret F, Guittet E, Rey FA, Flamand M. 2011. Secreted dengue virus nonstructural protein NS1 is an atypical barrel-shaped high-density lipoprotein. Proceedings of the National Academy of Sciences 108:8003.
148. Beatty PR, Puerta-Guardo H, Killingbeck SS, Glasner DR, Hopkins K, Harris E. 2015. Dengue virus NS1 triggers endothelial permeability and vascular leak that is prevented by NS1 vaccination. Science Translational Medicine 7:304ra141.
149. Modhiran N, Watterson D, Muller DA, Panetta AK, Sester DP, Liu L, Hume DA, Stacey KJ, Young PR. 2015. Dengue virus NS1 protein activates cells via Toll-like receptor 4 and disrupts endothelial cell monolayer integrity. Science Translational Medicine 7:304ra142.
150. Thiemmeca S, Tamdet C, Punyadee N, Prommool T, Songjaeng A, Noisakran S, Puttikhunt C, Atkinson JP, Diamond MS, Ponlawat A, Avirutnan P. 2016. Secreted NS1 Protects Dengue Virus from Mannose-Binding Lectin–Mediated Neutralization. The Journal of Immunology 197:4053.
151. Vaughn DW, Green S, Kalayanarooj S, Innis BL, Nimmannitya S, Suntayakorn S, Endy TP, Raengsakulrach B, Rothman AL, Ennis FA, Nisalak A. 2000. Dengue viremia titer, antibody response pattern, and virus serotype correlate with disease severity. J Infect Dis 181:2-9.
152. Falconar AKI. 1997. The dengue virus nonstructural-1 protein (NS1) generatesantibodies to common epitopes on human blood clotting,integrin/adhesin proteins and binds to humanendothelial cells: potential implications in haemorrhagic fever pathogenesis. Archives of Virology 142:897-916.
153. Jayathilaka D, Gomes L, Jeewandara C, Jayarathna GSB, Herath D, Perera PA, Fernando S, Wijewickrama A, Hardman CS, Ogg GS, Malavige GN. 2018. Role of NS1

antibodies in the pathogenesis of acute dengue infection. bioRxiv doi:10.1101/348342:348342.
154. Martínez-Cuellar C, Lovera D, Galeano F, Gatti L, Arbo A. 2020. Non-structural protein 1 (NS1) of dengue virus detection correlates with severity in primary but not in secondary dengue infection. Journal of Clinical Virology 124:104259.
155. Hang VT, Nguyet NM, Trung DT, Tricou V, Yoksan S, Dung NM, Van Ngoc T, Hien TT, Farrar J, Wills B, Simmons CP. 2009. Diagnostic accuracy of NS1 ELISA and lateral flow rapid tests for dengue sensitivity, specificity and relationship to viraemia and antibody responses. PLoS Negl Trop Dis 3:e360.
156. Lin YS, Yeh TM, Lin CF, Wan SW, Chuang YC, Hsu TK, Liu HS, Liu CC, Anderson R, Lei HY. 2011. Molecular mimicry between virus and host and its implications for dengue disease pathogenesis. Exp Biol Med (Maywood) 236:515-23.
157. Jayathilaka D, Gomes L, Jeewandara C, Jayarathna GSB, Herath D, Perera PA, Fernando S, Wijewickrama A, Hardman CS, Ogg GS, Malavige GN. 2018. Role of NS1 antibodies in the pathogenesis of acute secondary dengue infection. Nat Commun 9:5242.
158. Chew BLA, Ngoh AQ, Phoo WW, Chan WKK, Ser Z, Lim SS, Weng MJG, Watanabe S, Choy MM, Low JG, Ooi EE, Sobota RM, Vasudevan SG, Luo D. 2022. Secreted dengue virus NS1 is predominantly dimeric and in complex with high-density lipoprotein. bioRxiv doi:10.1101/2022.04.06.487425:2022.04.06.487425.
159. Benfrid S, Park K-H, Dellarole M, Voss JE, Tamietti C, Pehau-Arnaudet G, Raynal B, Brûlé S, England P, Zhang X, Mikhailova A, Hasan M, Ungeheuer M-N, Petres S, Biering SB, Harris E, Sakuntabhai A, Buchy P, Duong V, Dussart P, Coulibaly F, Bontems F, Rey FA, Flamand M. 2022. Dengue virus NS1 protein conveys pro-inflammatory signals by docking onto high-density lipoproteins. EMBO reports 23:e53600.
160. Shu B, Ooi JSG, Tan AWK, Ng T-S, Dejnirattisai W, Mongkolsapaya J, Fibriansah G, Shi J, Kostyuchenko VA, Screaton GR, Lok S-M. 2022. CryoEM structures of the multimeric secreted NS1, a major factor for dengue hemorrhagic fever. Nature Communications 13:6756.
161. Bukrinsky MI, Mukhamedova N, Sviridov D. 2020. Lipid rafts and pathogens: the art of deception and exploitation: Thematic Review Series: Biology of Lipid Rafts. Journal of Lipid Research 61:601-610.
162. Coelho DR, Carneiro PH, Mendes-Monteiro L, Conde JN, Andrade I, Cao T, Allonso D, White-Dibiasio M, Kuhn RJ, Mohana-Borges R. 2021. ApoA1 Neutralizes Proinflammatory Effects of Dengue Virus NS1 Protein and Modulates Viral Immune Evasion. Journal of Virology 95:10.1128/jvi.01974-20.
163. Benfrid S, Park KH, Dellarole M, Voss JE, Tamietti C, Pehau-Arnaudet G, Raynal B, Brûlé S, England P, Zhang X, Mikhailova A, Hasan M, Ungeheuer MN, Petres S, Biering SB, Harris E, Sakuntabhai A, Buchy P, Duong V, Dussart P, Coulibaly F, Bontems F, Rey FA, Flamand M. 2022. Dengue virus NS1 protein conveys pro-inflammatory signals by docking onto high-density lipoproteins. EMBO reports 23:e53600.
164. Parrish CR, Woo WS, Wright PJ. 1991. Expression of the NS1 gene of dengue virus type 2 using vaccinia virus. Archives of Virology 117:279-286.
165. Pryor MJ, Wright PJ. 1993. The Effects of Site-Directed Mutagenesis on the Dimerization and Secretion of the NS1 Protein Specified by Dengue Virus. Virology 194:769-780.

166. Pryor MJ, Wright PJ. 1994. Glycosylation Mutants of Dengue Virus NS1 Protein. Journal of General Virology 75:1183-1187.
167. Dolan PT, Taguwa S, Rangel MA, Acevedo A, Hagai T, Andino R, Frydman J. 2021. Principles of dengue virus evolvability derived from genotype-fitness maps in human and mosquito cells. Elife 10.
168. Burton TD, Eyre NS. 2021. Applications of Deep Mutational Scanning in Virology. Viruses 13.
169. Lo NTN, Roodsari SZ, Tin NL, Wong MP, Biering SB, Harris E. 2022. Molecular Determinants of Tissue Specificity of Flavivirus Nonstructural Protein 1 Interaction with Endothelial Cells. Journal of Virology 96:e00661-22.
170. Perera R, Kuhn RJ. 2008. Structural proteomics of dengue virus. Curr Opin Microbiol 11:369-77.
171. Modis Y, Ogata S, Clements D, Harrison SC. 2004. Structure of the dengue virus envelope protein after membrane fusion. Nature 427:313-9.
172. Allison SL, Schalich J, Stiasny K, Mandl CW, Heinz FX. 2001. Mutational evidence for an internal fusion peptide in flavivirus envelope protein E. J Virol 75:4268-75.
173. Fritz R, Blazevic J, Taucher C, Pangerl K, Heinz FX, Stiasny K. 2011. The unique transmembrane hairpin of flavivirus fusion protein E is essential for membrane fusion. J Virol 85:4377-85.
174. Fritz R, Stiasny K, Heinz FX. 2008. Identification of specific histidines as pH sensors in flavivirus membrane fusion. J Cell Biol 183:353-61.
175. Perera-Lecoin M, Meertens L, Carnec X, Amara A. 2013. Flavivirus entry receptors: an update. Viruses 6:69-88.
176. Bressanelli S, Stiasny K, Allison SL, Stura EA, Duquerroy S, Lescar J, Heinz FX, Rey FA. 2004. Structure of a flavivirus envelope glycoprotein in its low-pH-induced membrane fusion conformation. Embo j 23:728-38.
177. Johnson AJ, Guirakhoo F, Roehrig JT. 1994. The envelope glycoproteins of dengue 1 and dengue 2 viruses grown in mosquito cells differ in their utilization of potential glycosylation sites. Virology 203:241-9.
178. Pokidysheva E, Zhang Y, Battisti AJ, Bator-Kelly CM, Chipman PR, Xiao C, Gregorio GG, Hendrickson WA, Kuhn RJ, Rossmann MG. 2006. Cryo-EM reconstruction of dengue virus in complex with the carbohydrate recognition domain of DC-SIGN. Cell 124:485-93.
179. Guirakhoo F, Hunt AR, Lewis JG, Roehrig JT. 1993. Selection and Partial Characterization of Dengue 2 Virus Mutants That Induce Fusion at Elevated pH. Virology 194:219-223.
180. Messer WB, de Alwis R, Yount BL, Royal SR, Huynh JP, Smith SA, Crowe JE, Doranz BJ, Kahle KM, Pfaff JM, White LJ, Sariol CA, de Silva AM, Baric RS. 2014. Dengue virus envelope protein domain I/II hinge determines long-lived serotype-specific dengue immunity. Proceedings of the National Academy of Sciences 111:1939-1944.
181. Rouvinski A, Dejnirattisai W, Guardado-Calvo P, Vaney MC, Sharma A, Duquerroy S, Supasa P, Wongwiwat W, Haouz A, Barba-Spaeth G, Mongkolsapaya J, Rey FA, Screaton GR. 2017. Covalently linked dengue virus envelope glycoprotein dimers reduce exposure of the immunodominant fusion loop epitope. Nat Commun 8:15411.
182. Guzman MG, Hermida L, Bernardo L, Ramirez R, Guillén G. 2010. Domain III of the envelope protein as a dengue vaccine target. Expert Review of Vaccines 9:137-147.

183. Chen Y, Maguire T, Hileman RE, Fromm JR, Esko JD, Linhardt RJ, Marks RM. 1997. Dengue virus infectivity depends on envelope protein binding to target cell heparan sulfate. Nat Med 3:866-71.
184. Hung JJ, Hsieh MT, Young MJ, Kao CL, King CC, Chang W. 2004. An external loop region of domain III of dengue virus type 2 envelope protein is involved in serotype-specific binding to mosquito but not mammalian cells. J Virol 78:378-88.
185. Crill WD, Roehrig JT. 2001. Monoclonal antibodies that bind to domain III of dengue virus E glycoprotein are the most efficient blockers of virus adsorption to Vero cells. J Virol 75:7769-73.
186. Stiasny K, Fritz R, Pangerl K, Heinz FX. 2011. Molecular mechanisms of flavivirus membrane fusion. Amino Acids 41:1159-1163.
187. Modis Y, Ogata S, Clements D, Harrison SC. 2003. A ligand-binding pocket in the dengue virus envelope glycoprotein. Proc Natl Acad Sci U S A 100:6986-91.
188. Schmidt AG, Lee K, Yang PL, Harrison SC. 2012. Small-Molecule Inhibitors of Dengue-Virus Entry. PLOS Pathogens 8:e1002627.
189. Klein DE, Choi JL, Harrison SC. 2013. Structure of a dengue virus envelope protein late-stage fusion intermediate. J Virol 87:2287-93.
190. Yang J-M, Chen Y-F, Tu Y-Y, Yen K-R, Yang Y-L. 2007. Combinatorial Computational Approaches to Identify Tetracycline Derivatives as Flavivirus Inhibitors. PLOS ONE 2:e428.
191. Poh MK, Yip A, Zhang S, Priestle JP, Ma NL, Smit JM, Wilschut J, Shi P-Y, Wenk MR, Schul W. 2009. A small molecule fusion inhibitor of dengue virus. Antiviral Research 84:260-266.
192. Leal ES, Adler NS, Fernández GA, Gebhard LG, Battini L, Aucar MG, Videla M, Monge ME, Hernández de los Ríos A, Acosta Dávila JA, Morell ML, Cordo SM, García CC, Gamarnik AV, Cavasotto CN, Bollini M. 2019. De novo design approaches targeting an envelope protein pocket to identify small molecules against dengue virus. European Journal of Medicinal Chemistry 182:111628.
193. Zhou Z, Khaliq M, Suk J-E, Patkar C, Li L, Kuhn RJ, Post CB. 2008. Antiviral Compounds Discovered by Virtual Screening of Small−Molecule Libraries against Dengue Virus E Protein. ACS Chemical Biology 3:765-775.
194. Alen MMF, Schols D. 2012. Dengue Virus Entry as Target for Antiviral Therapy. Journal of Tropical Medicine 2012:628475.
195. S AH, Pujar GV, Sethu AK, Bhagyalalitha M, Singh M. 2021. Dengue structural proteins as antiviral drug targets: Current status in the drug discovery & development. European Journal of Medicinal Chemistry 221:113527.
196. Lin Y-L, Lei H-Y, Lin Y-S, Yeh T-M, Chen S-H, Liu H-S. 2002. Heparin inhibits dengue-2 virus infection of five human liver cell lines. Antiviral Research 56:93-96.
197. Behnam MAM, Nitsche C, Boldescu V, Klein CD. 2016. The Medicinal Chemistry of Dengue Virus. Journal of Medicinal Chemistry 59:5622-5649.
198. Lee E, Pavy M, Young N, Freeman C, Lobigs M. 2006. Antiviral effect of the heparan sulfate mimetic, PI-88, against dengue and encephalitic flaviviruses. Antiviral Research 69:31-38.
199. Byrd CM, Dai D, Grosenbach DW, Berhanu A, Jones KF, Cardwell KB, Schneider C, Wineinger KA, Page JM, Harver C, Stavale E, Tyavanagimatt S, Stone MA, Bartenschlager R, Scaturro P, Hruby DE, Jordan R. 2013. A novel inhibitor of dengue

virus replication that targets the capsid protein. Antimicrob Agents Chemother 57:15-25.
200. Scaturro P, Trist IM, Paul D, Kumar A, Acosta EG, Byrd CM, Jordan R, Brancale A, Bartenschlager R. 2014. Characterization of the mode of action of a potent dengue virus capsid inhibitor. J Virol 88:11540-55.
201. Modhiran N, Gandhi NS, Wimmer N, Cheung S, Stacey K, Young PR, Ferro V, Watterson D. 2019. Dual targeting of dengue virus virions and NS1 protein with the heparan sulfate mimic PG545. Antiviral Res 168:121-127.
202. Modhiran N, Song H, Liu L, Bletchly C, Brillault L, Amarilla AA, Xu X, Qi J, Chai Y, Cheung STM, Traves R, Setoh YX, Bibby S, Scott CAP, Freney ME, Newton ND, Khromykh AA, Chappell KJ, Muller DA, Stacey KJ, Landsberg MJ, Shi Y, Gao GF, Young PR, Watterson D. 2021. A broadly protective antibody that targets the flavivirus NS1 protein. Science 371:190-194.
203. Biering SB, Akey DL, Wong MP, Brown WC, Lo NTN, Puerta-Guardo H, Tramontini Gomes de Sousa F, Wang C, Konwerski JR, Espinosa DA, Bockhaus NJ, Glasner DR, Li J, Blanc SF, Juan EY, Elledge SJ, Mina MJ, Beatty PR, Smith JL, Harris E. 2021. Structural basis for antibody inhibition of flavivirus NS1–triggered endothelial dysfunction. Science 371:194-200.
204. Rathore AP, Paradkar PN, Watanabe S, Tan KH, Sung C, Connolly JE, Low J, Ooi EE, Vasudevan SG. 2011. Celgosivir treatment misfolds dengue virus NS1 protein, induces cellular pro-survival genes and protects against lethal challenge mouse model. Antiviral Res 92:453-60.
205. Low JG, Sung C, Wijaya L, Wei Y, Rathore APS, Watanabe S, Tan BH, Toh L, Chua LT, Hou Y, Chow A, Howe S, Chan WK, Tan KH, Chung JS, Cherng BP, Lye DC, Tambayah PA, Ng LC, Connolly J, Hibberd ML, Leo YS, Cheung YB, Ooi EE, Vasudevan SG. 2014. Efficacy and safety of celgosivir in patients with dengue fever (CELADEN): a phase 1b, randomised, double-blind, placebo-controlled, proof-of-concept trial. Lancet Infect Dis 14:706-715.
206. Yusof R, Clum S, Wetzel M, Murthy HM, Padmanabhan R. 2000. Purified NS2B/NS3 serine protease of dengue virus type 2 exhibits cofactor NS2B dependence for cleavage of substrates with dibasic amino acids in vitro. J Biol Chem 275:9963-9.
207. Falgout B, Pethel M, Zhang YM, Lai CJ. 1991. Both nonstructural proteins NS2B and NS3 are required for the proteolytic processing of dengue virus nonstructural proteins. J Virol 65:2467-75.
208. Yang CC, Hsieh YC, Lee SJ, Wu SH, Liao CL, Tsao CH, Chao YS, Chern JH, Wu CP, Yueh A. 2011. Novel dengue virus-specific NS2B/NS3 protease inhibitor, BP2109, discovered by a high-throughput screening assay. Antimicrob Agents Chemother 55:229-38.
209. Umareddy I, Chao A, Sampath A, Gu F, Vasudevan SG. 2006. Dengue virus NS4B interacts with NS3 and dissociates it from single-stranded RNA. Journal of General Virology 87:2605-2614.
210. Umareddy I, Chao A, Sampath A, Gu F, Vasudevan SG. 2006. Dengue virus NS4B interacts with NS3 and dissociates it from single-stranded RNA. J Gen Virol 87:2605-2614.
211. Miller S, Sparacio S, Bartenschlager R. 2006. Subcellular localization and membrane topology of the Dengue virus type 2 Non-structural protein 4B. J Biol Chem 281:8854-63.

212. Zmurko J, Neyts J, Dallmeier K. 2015. Flaviviral NS4b, chameleon and jack-in-the-box roles in viral replication and pathogenesis, and a molecular target for antiviral intervention. Rev Med Virol 25:205-23.
213. Kaptein SJF, Goethals O, Kiemel D, Marchand A, Kesteleyn B, Bonfanti J-F, Bardiot D, Stoops B, Jonckers THM, Dallmeier K, Geluykens P, Thys K, Crabbe M, Chatel-Chaix L, Münster M, Querat G, Touret F, de Lamballerie X, Raboisson P, Simmen K, Chaltin P, Bartenschlager R, Van Loock M, Neyts J. 2021. A pan-serotype dengue virus inhibitor targeting the NS3–NS4B interaction. Nature 598:504-509.
214. Kesteleyn B, Bonfanti J-F, Bardiot D, De Boeck B, Goethals O, Kaptein SJF, Stoops B, Coesemans E, Fortin J, Muller P, Doublet F, Carlens G, Koukni M, Smets W, Raboisson P, Chaltin P, Simmen K, Loock MV, Neyts J, Marchand A, Jonckers THM. 2024. Discovery of JNJ-1802, a First-in-Class Pan-Serotype Dengue Virus NS4B Inhibitor. Journal of Medicinal Chemistry 67:4063-4082.
215. Goethals O, Kaptein SJF, Kesteleyn B, Bonfanti J-F, Van Wesenbeeck L, Bardiot D, Verschoor EJ, Verstrepen BE, Fagrouch Z, Putnak JR, Kiemel D, Ackaert O, Straetemans R, Lachau-Durand S, Geluykens P, Crabbe M, Thys K, Stoops B, Lenz O, Tambuyzer L, De Meyer S, Dallmeier K, McCracken MK, Gromowski GD, Rutvisuttinunt W, Jarman RG, Karasavvas N, Touret F, Querat G, de Lamballerie X, Chatel-Chaix L, Milligan GN, Beasley DWC, Bourne N, Barrett ADT, Marchand A, Jonckers THM, Raboisson P, Simmen K, Chaltin P, Bartenschlager R, Bogers WM, Neyts J, Van Loock M. 2023. Blocking NS3–NS4B interaction inhibits dengue virus in non-human primates. Nature doi:10.1038/s41586-023-05790-6.
216. Zou G, Chen YL, Dong H, Lim CC, Yap LJ, Yau YH, Shochat SG, Lescar J, Shi PY. 2011. Functional analysis of two cavities in flavivirus NS5 polymerase. J Biol Chem 286:14362-72.
217. Lim SP, Wen D, Yap TL, Yan CK, Lescar J, Vasudevan SG. 2008. A scintillation proximity assay for dengue virus NS5 2'-O-methyltransferase—kinetic and inhibition analyses. Antiviral Research 80:360-369.
218. Chung KY, Dong H, Chao AT, Shi P-Y, Lescar J, Lim SP. 2010. Higher catalytic efficiency of N-7-methylation is responsible for processive N-7 and 2'-O methyltransferase activity in dengue virus. Virology 402:52-60.
219. Lim SP, Sonntag LS, Noble C, Nilar SH, Ng RH, Zou G, Monaghan P, Chung KY, Dong H, Liu B, Bodenreider C, Lee G, Ding M, Chan WL, Wang G, Jian YL, Chao AT, Lescar J, Yin Z, Vedananda TR, Keller TH, Shi PY. 2011. Small molecule inhibitors that selectively block dengue virus methyltransferase. J Biol Chem 286:6233-40.
220. Jans DA, Martin AJ. 2018. Nucleocytoplasmic Trafficking of Dengue Non-structural Protein 5 as a Target for Antivirals, p 199-213. *In* Hilgenfeld R, Vasudevan SG (ed), Dengue and Zika: Control and Antiviral Treatment Strategies doi:10.1007/978-981-10-8727-1_15. Springer Singapore, Singapore.
221. Pryor MJ, Rawlinson SM, Butcher RE, Barton CL, Waterhouse TA, Vasudevan SG, Bardin PG, Wright PJ, Jans DA, Davidson AD. 2007. Nuclear localization of dengue virus nonstructural protein 5 through its importin alpha/beta-recognized nuclear localization sequences is integral to viral infection. Traffic 8:795-807.
222. Hannemann H, Sung PY, Chiu HC, Yousuf A, Bird J, Lim SP, Davidson AD. 2013. Serotype-specific differences in dengue virus non-structural protein 5 nuclear localization. J Biol Chem 288:22621-35.

223. Medin CL, Fitzgerald KA, Rothman AL. 2005. Dengue virus nonstructural protein NS5 induces interleukin-8 transcription and secretion. J Virol 79:11053-61.
224. Rawlinson SM, Pryor MJ, Wright PJ, Jans DA. 2009. CRM1-mediated nuclear export of dengue virus RNA polymerase NS5 modulates interleukin-8 induction and virus production. J Biol Chem 284:15589-97.
225. Wagstaff KM, Sivakumaran H, Heaton SM, Harrich D, Jans DA. 2012. Ivermectin is a specific inhibitor of importin α/β-mediated nuclear import able to inhibit replication of HIV-1 and dengue virus. Biochem J 443:851-6.
226. Low JG, Ooi EE, Vasudevan SG. 2017. Current Status of Dengue Therapeutics Research and Development. J Infect Dis 215:S96-s102.
227. Biering SB, Harris E. 2021. A step towards therapeutics for dengue. Nature 598:420-421.
228. Kenneson A, Beltrán-Ayala E, Borbor-Cordova MJ, Polhemus ME, Ryan SJ, Endy TP, Stewart-Ibarra AM. 2017. Social-ecological factors and preventive actions decrease the risk of dengue infection at the household-level: Results from a prospective dengue surveillance study in Machala, Ecuador. PLoS Negl Trop Dis 11:e0006150.
229. Moyes CL, Vontas J, Martins AJ, Ng LC, Koou SY, Dusfour I, Raghavendra K, Pinto J, Corbel V, David J-P, Weetman D. 2017. Contemporary status of insecticide resistance in the major Aedes vectors of arboviruses infecting humans. PLoS neglected tropical diseases 11:e0005625-e0005625.
230. Hoffmann AA, Montgomery BL, Popovici J, Iturbe-Ormaetxe I, Johnson PH, Muzzi F, Greenfield M, Durkan M, Leong YS, Dong Y, Cook H, Axford J, Callahan AG, Kenny N, Omodei C, McGraw EA, Ryan PA, Ritchie SA, Turelli M, O'Neill SL. 2011. Successful establishment of Wolbachia in Aedes populations to suppress dengue transmission. Nature 476:454-457.
231. Zabalou S, Riegler M, Theodorakopoulou M, Stauffer C, Savakis C, Bourtzis K. 2004. Wolbachia-induced cytoplasmic incompatibility as a means for insect pest population control. Proceedings of the National Academy of Sciences of the United States of America 101:15042.
232. McMeniman CJ, O'Neill SL. 2010. A virulent Wolbachia infection decreases the viability of the dengue vector Aedes aegypti during periods of embryonic quiescence. PLoS Negl Trop Dis 4:e748.
233. Flores HA, Taneja de Bruyne J, O'Donnell TB, Tuyet Nhu V, Thi Giang N, Thi Xuan Trang H, Thi Thuy Van H, Thi Long V, Thi Dui L, Le Anh Huy H, Thi Le Duyen H, Thi Van Thuy N, Thanh Phong N, Van Vinh Chau N, Thi Hue Kien D, Thuy Vi T, Wills B, O'Neill SL, Simmons CP, Carrington LB. 2020. Multiple Wolbachia strains provide comparative levels of protection against dengue virus infection in Aedes aegypti. PLoS pathogens 16:e1008433-e1008433.
234. O'Neill SL, Ryan PA, Turley AP, Wilson G, Retzki K, Iturbe-Ormaetxe I, Dong Y, Kenny N, Paton CJ, Ritchie SA, Brown-Kenyon J, Stanford D, Wittmeier N, Jewell NP, Tanamas SK, Anders KL, Simmons CP. 2018. Scaled deployment of Wolbachia to protect the community from dengue and other Aedes transmitted arboviruses. Gates Open Res 2:36.
235. Nazni WA, Hoffmann AA, NoorAfizah A, Cheong YL, Mancini MV, Golding N, Kamarul GMR, Arif MAK, Thohir H, NurSyamimi H, ZatilAqmar MZ, NurRuqqayah M, NorSyazwani A, Faiz A, Irfan FMN, Rubaaini S, Nuradila N, Nizam NMN, Irwan SM, Endersby-Harshman NM, White VL, Ant TH, Herd CS, Hasnor AH, AbuBakar R, Hapsah

DM, Khadijah K, Kamilan D, Lee SC, Paid YM, Fadzilah K, Topek O, Gill BS, Lee HL, Sinkins SP. 2019. Establishment of Wolbachia Strain wAlbB in Malaysian Populations of Aedes aegypti for Dengue Control. Curr Biol 29:4241-4248.e5.
236. Tantowijoyo W, Andari B, Arguni E, Budiwati N, Nurhayati I, Fitriana I, Ernesia I, Daniwijaya EW, Supriyati E, Yusdiana DH, Victorius M, Wardana DS, Ardiansyah H, Ahmad RA, Ryan PA, Simmons CP, Hoffmann AA, Rancès E, Turley AP, Johnson P, Utarini A, O'Neill SL. 2020. Stable establishment of wMel Wolbachia in Aedes aegypti populations in Yogyakarta, Indonesia. PLOS Neglected Tropical Diseases 14:e0008157.
237. Program WM. The World Mosquito Program's Wolbachia method. http://www.eliminatedengue.com/our-research/Wolbachia. Accessed
238. Huang B, Yang Q, Hoffmann AA, Ritchie SA, van den Hurk AF, Warrilow D. 2020. Wolbachia Genome Stability and mtDNA Variants in Aedes aegypti Field Populations Eight Years after Release. iScience 23:101572-101572.
239. Hoffmann AA, Iturbe-Ormaetxe I, Callahan AG, Phillips BL, Billington K, Axford JK, Montgomery B, Turley AP, O'Neill SL. 2014. Stability of the wMel Wolbachia Infection following invasion into Aedes aegypti populations. PLoS neglected tropical diseases 8:e3115-e3115.
240. Ford SA, Allen SL, Ohm JR, Sigle LT, Sebastian A, Albert I, Chenoweth SF, McGraw EA. 2019. Selection on Aedes aegypti alters Wolbachia-mediated dengue virus blocking and fitness. Nature Microbiology 4:1832-1839.
241. Carrington LB, Tran BCN, Le NTH, Luong TTH, Nguyen TT, Nguyen PT, Nguyen CVV, Nguyen HTC, Vu TT, Vo LT, Le DT, Vu NT, Nguyen GT, Luu HQ, Dang AD, Hurst TP, O'Neill SL, Tran VT, Kien DTH, Nguyen NM, Wolbers M, Wills B, Simmons CP. 2018. Field- and clinically derived estimates of Wolbachia-mediated blocking of dengue virus transmission potential in Aedes aegypti mosquitoes. Proceedings of the National Academy of Sciences 115:361.
242. Edenborough Kathryn M, Flores Heather A, Simmons Cameron P, Fraser Johanna E, Pierson Ted C. Using Wolbachia to Eliminate Dengue: Will the Virus Fight Back? Journal of Virology 95:e02203-20.
243. Geoghegan V, Stainton K, Rainey SM, Ant TH, Dowle AA, Larson T, Hester S, Charles PD, Thomas B, Sinkins SP. 2017. Perturbed cholesterol and vesicular trafficking associated with dengue blocking in Wolbachia-infected Aedes aegypti cells. Nat Commun 8:526.
244. Pan X, Zhou G, Wu J, Bian G, Lu P, Raikhel AS, Xi Z. 2012. Wolbachia induces reactive oxygen species (ROS)-dependent activation of the Toll pathway to control dengue virus in the mosquito <em>Aedes aegypti</em&gt. Proceedings of the National Academy of Sciences 109:E23.
245. Bhattacharya T, Newton ILG, Hardy RW. 2017. Wolbachia elevates host methyltransferase expression to block an RNA virus early during infection. PLoS Pathog 13:e1006427.
246. Lu P, Bian G, Pan X, Xi Z. 2012. Wolbachia induces density-dependent inhibition to dengue virus in mosquito cells. PLoS neglected tropical diseases 6:e1754-e1754.
247. Nainu F, Trenerry A, Johnson KN. 2019. Wolbachia-mediated antiviral protection is cell-autonomous. J Gen Virol 100:1587-1592.
248. Kurosu T. 2011. Quasispecies of dengue virus. Tropical medicine and health 39:29-36.

249. Sim S, Aw PP, Wilm A, Teoh G, Hue KD, Nguyen NM, Nagarajan N, Simmons CP, Hibberd ML. 2015. Tracking Dengue Virus Intra-host Genetic Diversity during Human-to-Mosquito Transmission. PLoS Negl Trop Dis 9:e0004052.
250. Sim S, Aw PPK, Wilm A, Teoh G, Hue KDT, Nguyen NM, Nagarajan N, Simmons CP, Hibberd ML. 2015. Tracking Dengue Virus Intra-host Genetic Diversity during Human-to-Mosquito Transmission. PLoS neglected tropical diseases 9:e0004052-e0004052.
251. Thi Hue Kien D, Edenborough KM, da Silva Goncalves D, Thuy Vi T, Casagrande E, Thi Le Duyen H, Thi Long V, Thi Dui L, Thi Tuyet Nhu V, Thi Giang N, Thi Xuan Trang H, Lee E, Donovan-Banfield Ia, Thi Thuy Van H, Minh Nguyet N, Thanh Phong N, Van Vinh Chau N, Wills B, Yacoub S, Flores H, Simmons CP. 2023. Genome evolution of dengue virus serotype 1 under selection by Wolbachia pipientis in Aedes aegypti mosquitoes. Virus Evolution doi:10.1093/ve/vead016.
252. Fowler DM, Stephany JJ, Fields S. 2014. Measuring the activity of protein variants on a large scale using deep mutational scanning. Nature protocols 9:2267-2284.
253. Livesey BJ, Marsh JA. 2020. Using deep mutational scanning to benchmark variant effect predictors and identify disease mutations. Molecular Systems Biology 16:e9380.
254. Klesmith JR, Bacik J-P, Wrenbeck EE, Michalczyk R, Whitehead TA. 2017. Trade-offs between enzyme fitness and solubility illuminated by deep mutational scanning. Proceedings of the National Academy of Sciences 114:2265-2270.
255. Li C, Qian W, Maclean CJ, Zhang J. 2016. The fitness landscape of a tRNA gene. Science 352:837.
256. Sarkisyan KS, Bolotin DA, Meer MV, Usmanova DR, Mishin AS, Sharonov GV, Ivankov DN, Bozhanova NG, Baranov MS, Soylemez O, Bogatyreva NS, Vlasov PK, Egorov ES, Logacheva MD, Kondrashov AS, Chudakov DM, Putintseva EV, Mamedov IZ, Tawfik DS, Lukyanov KA, Kondrashov FA. 2016. Local fitness landscape of the green fluorescent protein. Nature 533:397-401.
257. Bloom JD. 2014. An experimentally determined evolutionary model dramatically improves phylogenetic fit. Molecular biology and evolution 31:1956-1978.
258. Canale AS, Cote-Hammarlof PA, Flynn JM, Bolon DNA. 2018. Evolutionary mechanisms studied through protein fitness landscapes. Current Opinion in Structural Biology 48:141-148.
259. Newberry RW, Leong JT, Chow ED, Kampmann M, DeGrado WF. 2020. Deep mutational scanning reveals the structural basis for α-synuclein activity. Nature Chemical Biology 16:653-659.
260. Adkar BV, Tripathi A, Sahoo A, Bajaj K, Goswami D, Chakrabarti P, Swarnkar MK, Gokhale RS, Varadarajan R. 2012. Protein model discrimination using mutational sensitivity derived from deep sequencing. Structure 20:371-81.
261. Scaturro P, Cortese M, Chatel-Chaix L, Fischl W, Bartenschlager R. 2015. Dengue Virus Non-structural Protein 1 Modulates Infectious Particle Production via Interaction with the Structural Proteins. PLoS pathogens 11:e1005277-e1005277.
262. Wang W, Guan M, Liu Y, Xu Q, Peng H, Liu X, Tang Z, Zhu Y, Wu D, Ren H, Zhao P, Qi Z. 2014. Alanine scanning mutagenesis of hepatitis C virus E2 cysteine residues: Insights into E2 biogenesis and antigenicity. Virology 448:229-37.
263. Urabe M, Hasumi Y, Kume A, Surosky RT, Kurtzman GJ, Tobita K, Ozawa K. 1999. Charged-to-alanine scanning mutagenesis of the N-terminal half of adeno-associated virus type 2 Rep78 protein. Journal of virology 73:2682-2693.

264. Murray CL, Jones CT, Tassello J, Rice CM. 2007. Alanine Scanning of the Hepatitis C Virus Core Protein Reveals Numerous Residues Essential for Production of Infectious Virus. Journal of Virology 81:10220.
265. Lefèvre F, Rémy M-H, Masson J-M. 1997. Alanine-stretch scanning mutagenesis: a simple and efficient method to probe protein structure and function. Nucleic Acids Research 25:447-448.
266. Ilyushina NA, Khalenkov AM, Seiler JP, Forrest HL, Bovin NV, Marjuki H, Barman S, Webster RG, Webby RJ. 2010. Adaptation of Pandemic H1N1 Influenza Viruses in Mice. Journal of Virology 84:8607-8616.
267. Choi E-J, Lee YJ, Lee J-M, Kim Y-J, Choi J-H, Ahn B, Kim K, Han MG. 2020. The effect of mutations derived from mouse-adapted H3N2 seasonal influenza A virus to pathogenicity and host adaptation. PloS one 15:e0227516-e0227516.
268. Stobart CC, Moore ML. 2014. RNA Virus Reverse Genetics and Vaccine Design. Viruses 6:2531-2550.
269. Lindenbach BD. 2022. Reinventing positive-strand RNA virus reverse genetics. Adv Virus Res 112:1-29.
270. Walpita P, Flick R. 2005. Reverse genetics of negative-stranded RNA viruses: A global perspective. FEMS Microbiology Letters 244:9-18.
271. Aubry F, Nougairède A, Gould EA, de Lamballerie X. 2015. Flavivirus reverse genetic systems, construction techniques and applications: A historical perspective. Antiviral Research 114:67-85.
272. Yun S-I, Kim S-Y, Rice CM, Lee Y-M. 2003. Development and Application of a Reverse Genetics System for Japanese Encephalitis Virus. Journal of Virology 77:6450-6465.
273. Willemsen A, Zwart MP. 2019. On the stability of sequences inserted into viral genomes. Virus evolution 5:vez045-vez045.
274. Edmonds J, van Grinsven E, Prow N, Bosco-Lauth A, Brault AC, Bowen RA, Hall RA, Khromykh AA. 2013. A novel bacterium-free method for generation of flavivirus infectious DNA by circular polymerase extension reaction allows accurate recapitulation of viral heterogeneity. Journal of virology 87:2367-2372.
275. Nhu Thao TT, Labroussaa F, Ebert N, V'kovski P, Stalder H, Portmann J, Kelly J, Steiner S, Holwerda M, Kratzel A, Gultom M, Laloli L, Hüsser L, Wider M, Pfaender S, Hirt D, Cippà V, Crespo-Pomar S, Schröder S, Muth D, Niemeyer D, Müller MA, Drosten C, Dijkman R, Jores J, Thiel V. 2020. Rapid reconstruction of SARS-CoV-2 using a synthetic genomics platform. bioRxiv doi:10.1101/2020.02.21.959817:2020.02.21.959817.
276. Heather JM, Chain B. 2016. The sequence of sequencers: The history of sequencing DNA. Genomics 107:1-8.
277. Lee H, Gurtowski J, Yoo S, Nattestad M, Marcus S, Goodwin S, Richard McCombie W, Schatz MC. 2016. Third-generation sequencing and the future of genomics. bioRxiv doi:10.1101/048603:048603.
278. Eid J, Fehr A, Gray J, Luong K, Lyle J, Otto G, Peluso P, Rank D, Baybayan P, Bettman B. 2009. Real-time DNA sequencing from single polymerase molecules. Science 323:133-138.
279. Clarke J, Wu H-C, Jayasinghe L, Patel A, Reid S, Bayley H. 2009. Continuous base identification for single-molecule nanopore DNA sequencing. Nature Nanotechnology 4:265-270.

280. Bentley DR, Balasubramanian S, Swerdlow HP, Smith GP, Milton J, Brown CG, Hall KP, Evers DJ, Barnes CL, Bignell HR, Boutell JM, Bryant J, Carter RJ, Keira Cheetham R, Cox AJ, Ellis DJ, Flatbush MR, Gormley NA, Humphray SJ, Irving LJ, Karbelashvili MS, Kirk SM, Li H, Liu X, Maisinger KS, Murray LJ, Obradovic B, Ost T, Parkinson ML, Pratt MR, Rasolonjatovo IMJ, Reed MT, Rigatti R, Rodighiero C, Ross MT, Sabot A, Sankar SV, Scally A, Schroth GP, Smith ME, Smith VP, Spiridou A, Torrance PE, Tzonev SS, Vermaas EH, Walter K, Wu X, Zhang L, Alam MD, Anastasi C, et al. 2008. Accurate whole human genome sequencing using reversible terminator chemistry. Nature 456:53-59.
281. Wrenbeck EE, Faber MS, Whitehead TA. 2017. Deep sequencing methods for protein engineering and design. Current opinion in structural biology 45:36-44.
282. Hiatt JB, Patwardhan RP, Turner EH, Lee C, Shendure J. 2010. Parallel, tag-directed assembly of locally derived short sequence reads. Nat Methods 7:119-22.
283. Amarasinghe SL, Su S, Dong X, Zappia L, Ritchie ME, Gouil Q. 2020. Opportunities and challenges in long-read sequencing data analysis. Genome Biology 21:30.
284. Karst SM, Ziels RM, Kirkegaard RH, Sørensen EA, McDonald D, Zhu Q, Knight R, Albertsen M. 2021. High-accuracy long-read amplicon sequences using unique molecular identifiers with Nanopore or PacBio sequencing. Nature Methods 18:165-169.
285. Cirino PC, Mayer KM, Umeno D. 2003. Generating Mutant Libraries Using Error-Prone PCR, p 3-9. *In* Arnold FH, Georgiou G (ed), Directed Evolution Library Creation: Methods and Protocols doi:10.1385/1-59259-395-X:3. Humana Press, Totowa, NJ.
286. Cline J, Braman JC, Hogrefe HH. 1996. PCR fidelity of pfu DNA polymerase and other thermostable DNA polymerases. Nucleic Acids Res 24:3546-51.
287. Vanhercke T, Ampe C, Tirry L, Denolf P. 2005. Reducing mutational bias in random protein libraries. Analytical Biochemistry 339:9-14.
288. Miyazaki K, Arnold FH. 1999. Exploring Nonnatural Evolutionary Pathways by Saturation Mutagenesis: Rapid Improvement of Protein Function. Journal of Molecular Evolution 49:716-720.
289. Reetz MT, Carballeira JD. 2007. Iterative saturation mutagenesis (ISM) for rapid directed evolution of functional enzymes. Nature Protocols 2:891-903.
290. Hughes RA, Ellington AD. 2017. Synthetic DNA Synthesis and Assembly: Putting the Synthetic in Synthetic Biology. Cold Spring Harb Perspect Biol 9.
291. Cárcamo E, Roldán-Salgado A, Osuna J, Bello-Sanmartin I, Yáñez JA, Saab-Rincón G, Viadiu H, Gaytán P. 2017. Spiked Genes: A Method to Introduce Random Point Nucleotide Mutations Evenly throughout an Entire Gene Using a Complete Set of Spiked Oligonucleotides for the Assembly. ACS omega 2:3183-3191.
292. Green B, Bouchier C, Fairhead C, Craig NL, Cormack BP. 2012. Insertion site preference of Mu, Tn5, and Tn7 transposons. Mobile DNA 3:3.
293. Savilahti H, Rice PA, Mizuuchi K. 1995. The phage Mu transpososome core: DNA requirements for assembly and function. The EMBO journal 14:4893-4903.
294. Haapa S, Taira S, Heikkinen E, Savilahti H. 1999. An efficient and accurate integration of mini-Mu transposons in vitro: a general methodology for functional genetic analysis and molecular biology applications. Nucleic acids research 27:2777-2784.
295. Hoffmann M, Kleine-Weber H, Schroeder S, Krüger N, Herrler T, Erichsen S, Schiergens TS, Herrler G, Wu NH, Nitsche A, Müller MA, Drosten C, Pöhlmann S.

2020. SARS-CoV-2 Cell Entry Depends on ACE2 and TMPRSS2 and Is Blocked by a Clinically Proven Protease Inhibitor. Cell 181:271-280.e8.
296. Chan KK, Dorosky D, Sharma P, Abbasi SA, Dye JM, Kranz DM, Herbert AS, Procko E. 2020. Engineering human ACE2 to optimize binding to the spike protein of SARS coronavirus 2. Science 369:1261-1265.
297. Heinzelman P, Romero PA. 2020. Discovery of human ACE2 variants with altered recognition by the SARS-CoV-2 spike protein. bioRxiv doi:10.1101/2020.09.17.301861:2020.09.17.301861.
298. Cao L, Goreshnik I, Coventry B, Case JB, Miller L, Kozodoy L, Chen RE, Carter L, Walls AC, Park Y-J, Strauch E-M, Stewart L, Diamond MS, Veesler D, Baker D. 2020. De novo design of picomolar SARS-CoV-2 miniprotein inhibitors. Science (New York, NY) 370:426-431.
299. Linsky TW, Vergara R, Codina N, Nelson JW, Walker MJ, Su W, Barnes CO, Hsiang T-Y, Esser-Nobis K, Yu K, Reneer ZB, Hou YJ, Priya T, Mitsumoto M, Pong A, Lau UY, Mason ML, Chen J, Chen A, Berrocal T, Peng H, Clairmont NS, Castellanos J, Lin Y-R, Josephson-Day A, Baric RS, Fuller DH, Walkey CD, Ross TM, Swanson R, Bjorkman PJ, Gale M, Jr., Blancas-Mejia LM, Yen H-L, Silva D-A. 2020. De novo design of potent and resilient hACE2 decoys to neutralize SARS-CoV-2. Science (New York, NY) 370:1208-1214.
300. Whitehead TA, Chevalier A, Song Y, Dreyfus C, Fleishman SJ, De Mattos C, Myers CA, Kamisetty H, Blair P, Wilson IA, Baker D. 2012. Optimization of affinity, specificity and function of designed influenza inhibitors using deep sequencing. Nature biotechnology 30:543-548.
301. Fleishman SJ, Whitehead TA, Ekiert DC, Dreyfus C, Corn JE, Strauch E-M, Wilson IA, Baker D. 2011. Computational design of proteins targeting the conserved stem region of influenza hemagglutinin. Science (New York, NY) 332:816-821.
302. Bloom JD. 2015. Software for the analysis and visualization of deep mutational scanning data. BMC Bioinformatics 16:168.
303. Rubin AF, Gelman H, Lucas N, Bajjalieh SM, Papenfuss AT, Speed TP, Fowler DM. 2017. A statistical framework for analyzing deep mutational scanning data. Genome Biology 18:150.
304. Hilton SK, Huddleston J, Black A, North K, Dingens AS, Bedford T, Bloom JD. 2020. dms-view: Interactive visualization tool for deep mutational scanning data. bioRxiv doi:10.1101/2020.05.14.096842:2020.05.14.096842.
305. Remenyi R, Qi H, Su S-Y, Chen Z, Wu NC, Arumugaswami V, Truong S, Chu V, Stokelman T, Lo H-H, Olson CA, Wu T-T, Chen S-H, Lin C-Y, Sun R. 2014. A Comprehensive Functional Map of the Hepatitis C Virus Genome Provides a Resource for Probing Viral Proteins. mBio 5:e01469-14.
306. Alazard-Dany N, Denolly S, Boson B, Cosset FL. 2019. Overview of HCV Life Cycle with a Special Focus on Current and Possible Future Antiviral Targets. Viruses 11.
307. Qi H, Chu V, Wu NC, Chen Z, Truong S, Brar G, Su S-Y, Du Y, Arumugaswami V, Olson CA, Chen S-H, Lin C-Y, Wu T-T, Sun R. 2017. Systematic identification of anti-interferon function on hepatitis C virus genome reveals p7 as an immune evasion protein. Proceedings of the National Academy of Sciences of the United States of America 114:2018-2023.
308. Ross-Thriepland D, Harris M. 2015. Hepatitis C virus NS5A: enigmatic but still promiscuous 10 years on! Journal of General Virology 96:727-738.

309. Qi H, Olson CA, Wu NC, Ke R, Loverdo C, Chu V, Truong S, Remenyi R, Chen Z, Du Y, Su S-Y, Al-Mawsawi LQ, Wu T-T, Chen S-H, Lin C-Y, Zhong W, Lloyd-Smith JO, Sun R. 2014. A quantitative high-resolution genetic profile rapidly identifies sequence determinants of hepatitis C viral fitness and drug sensitivity. PLoS pathogens 10:e1004064-e1004064.
310. Gao M, Nettles RE, Belema M, Snyder LB, Nguyen VN, Fridell RA, Serrano-Wu MH, Langley DR, Sun JH, O'Boyle DR, 2nd, Lemm JA, Wang C, Knipe JO, Chien C, Colonno RJ, Grasela DM, Meanwell NA, Hamann LG. 2010. Chemical genetics strategy identifies an HCV NS5A inhibitor with a potent clinical effect. Nature 465:96-100.
311. Scheel TKH, Gottwein JM, Mikkelsen LS, Jensen TB, Bukh J. 2011. Recombinant HCV Variants With NS5A From Genotypes 1–7 Have Different Sensitivities to an NS5A Inhibitor but Not Interferon-α. Gastroenterology 140:1032-1042.e6.
312. Wyles DL, Luetkemeyer AF. 2017. Understanding Hepatitis C Virus Drug Resistance: Clinical Implications for Current and Future Regimens. Topics in antiviral medicine 25:103-109.
313. Fulton BO, Sachs D, Schwarz MC, Palese P, Evans MJ. 2017. Transposon Mutagenesis of the Zika Virus Genome Highlights Regions Essential for RNA Replication and Restricted for Immune Evasion. Journal of virology 91:e00698-17.
314. Ci Y, Liu Z-Y, Zhang N-N, Niu Y, Yang Y, Xu C, Yang W, Qin C-F, Shi L. 2020. Zika NS1-induced ER remodeling is essential for viral replication. The Journal of cell biology 219:e201903062.
315. Sourisseau M, Lawrence DJP, Schwarz MC, Storrs CH, Veit EC, Bloom JD, Evans MJ. 2019. Deep Mutational Scanning Comprehensively Maps How Zika Envelope Protein Mutations Affect Viral Growth and Antibody Escape. Journal of Virology 93:e01291-19.
316. Stettler K, Beltramello M, Espinosa DA, Graham V, Cassotta A, Bianchi S, Vanzetta F, Minola A, Jaconi S, Mele F, Foglierini M, Pedotti M, Simonelli L, Dowall S, Atkinson B, Percivalle E, Simmons CP, Varani L, Blum J, Baldanti F, Cameroni E, Hewson R, Harris E, Lanzavecchia A, Sallusto F, Corti D. 2016. Specificity, cross-reactivity, and function of antibodies elicited by Zika virus infection. Science 353:823.
317. Yang M, Dent M, Lai H, Sun H, Chen Q. 2017. Immunization of Zika virus envelope protein domain III induces specific and neutralizing immune responses against Zika virus. Vaccine 35:4287-4294.
318. Gong D, Zhang T-H, Zhao D, Du Y, Chapa TJ, Shi Y, Wang L, Contreras D, Zeng G, Shi P-Y, Wu T-T, Arumugaswami V, Sun R. 2018. High-Throughput Fitness Profiling of Zika Virus E Protein Reveals Different Roles for Glycosylation during Infection of Mammalian and Mosquito Cells. iScience 1:97-111.
319. Hamel R, Dejarnac O, Wichit S, Ekchariyawat P, Neyret A, Luplertlop N, Perera-Lecoin M, Surasombatpattana P, Talignani L, Thomas F, Cao-Lormeau V-M, Choumet V, Briant L, Desprès P, Amara A, Yssel H, Missé D. 2015. Biology of Zika Virus Infection in Human Skin Cells. Journal of Virology 89:8880.
320. Setoh YX, Amarilla AA, Peng NYG, Griffiths RE, Carrera J, Freney ME, Nakayama E, Ogawa S, Watterson D, Modhiran N, Nanyonga FE, Torres FJ, Slonchak A, Periasamy P, Prow NA, Tang B, Harrison J, Hobson-Peters J, Cuddihy T, Cooper-White J, Hall RA, Young PR, Mackenzie JM, Wolvetang E, Bloom JD, Suhrbier A, Khromykh AA. 2019. Determinants of Zika virus host tropism uncovered by deep mutational scanning. Nat Microbiol 4:876-887.

321. Wen Z, Song H, Ming G-L. 2017. How does Zika virus cause microcephaly? Genes & development 31:849-861.
322. Fan J, Liu Y, Yuan Z. 2014. Critical role of Dengue Virus NS1 protein in viral replication. Virol Sin 29:162-9.
323. Perry JW, Chen Y, Speliotes E, Tai AW. 2018. Functional Analysis of the Dengue Virus Genome Using an Insertional Mutagenesis Screen. Journal of virology 92:e02085-17.
324. Nemésio H, Palomares-Jerez F, Villalaín J. 2012. NS4A and NS4B proteins from dengue virus: Membranotropic regions. Biochimica et Biophysica Acta (BBA) - Biomembranes 1818:2818-2830.
325. Hassan NM, Alhossary AA, Mu Y, Kwoh C-K. 2017. Protein-Ligand Blind Docking Using QuickVina-W With Inter-Process Spatio-Temporal Integration. Scientific Reports 7:15451.
326. Abraham MJ, Murtola T, Schulz R, Páll S, Smith JC, Hess B, Lindahl E. 2015. GROMACS: High performance molecular simulations through multi-level parallelism from laptops to supercomputers. SoftwareX 1-2:19-25.
327. Alhossary A, Handoko SD, Mu Y, Kwoh C-K. 2015. Fast, accurate, and reliable molecular docking with QuickVina 2. Bioinformatics 31:2214-2216.
328. Ansarah-Sobrinho C, Nelson S, Jost CA, Whitehead SS, Pierson TC. 2008. Temperature-dependent production of pseudoinfectious dengue reporter virus particles by complementation. Virology 381:67-74.
329. Tian Y-S, Zhou Y, Takagi T, Kameoka M, Kawashita N. 2018. Dengue Virus and Its Inhibitors: A Brief Review. Chemical and Pharmaceutical Bulletin 66:191-206.
330. Biering SB, Akey DL, Wong MP, Brown WC, Lo NTN, Puerta-Guardo H, Tramontini Gomes de Sousa F, Wang C, Konwerski JR, Espinosa DA, Bockhaus NJ, Glasner DR, Li J, Blanc SF, Juan EY, Elledge SJ, Mina MJ, Beatty PR, Smith JL, Harris E. 2021. Structural basis for antibody inhibition of flavivirus NS1-triggered endothelial dysfunction. Science 371:194-200.
331. Orozco S, Schmid MA, Parameswaran P, Lachica R, Henn MR, Beatty R, Harris E. 2012. Characterization of a model of lethal dengue virus 2 infection in C57BL/6 mice deficient in the alpha/beta interferon receptor. Journal of General Virology 93:2152-2157.
332. Modhiran N, Gandhi NS, Wimmer N, Cheung S, Stacey K, Young PR, Ferro V, Watterson D. 2019. Dual targeting of dengue virus virions and NS1 protein with the heparan sulfate mimic PG545. Antiviral Research 168:121-127.
333. Songprakhon P, Thaingtamtanha T, Limjindaporn T, Puttikhunt C, Srisawat C, Luangaram P, Dechtawewat T, Uthaipibull C, Thongsima S, Yenchitsomanus PT, Malasit P, Noisakran S. 2020. Peptides targeting dengue viral nonstructural protein 1 inhibit dengue virus production. Sci Rep 10:12933.
334. Songprakhon P, Thaingtamtanha T, Limjindaporn T, Puttikhunt C, Srisawat C, Luangaram P, Dechtawewat T, Uthaipibull C, Thongsima S, Yenchitsomanus P-t, Malasit P, Noisakran S. 2020. Peptides targeting dengue viral nonstructural protein 1 inhibit dengue virus production. Scientific Reports 10:12933.
335. Falconar AK, Young PR. 1991. Production of dimer-specific and dengue virus group cross-reactive mouse monoclonal antibodies to the dengue 2 virus non-structural glycoprotein NS1. J Gen Virol 72 (Pt 4):961-5.
336. Rastogi M, Sharma N, Singh SK. 2016. Flavivirus NS1: a multifaceted enigmatic viral protein. Virol J 13:131.

337. Libraty DH, Young PR, Pickering D, Endy TP, Kalayanarooj S, Green S, Vaughn DW, Nisalak A, Ennis FA, Rothman AL. 2002. High circulating levels of the dengue virus nonstructural protein NS1 early in dengue illness correlate with the development of dengue hemorrhagic fever. J Infect Dis 186:1165-8.
338. Dixon AS, Schwinn MK, Hall MP, Zimmerman K, Otto P, Lubben TH, Butler BL, Binkowski BF, Machleidt T, Kirkland TA, Wood MG, Eggers CT, Encell LP, Wood KV. 2016. NanoLuc Complementation Reporter Optimized for Accurate Measurement of Protein Interactions in Cells. ACS Chem Biol 11:400-8.
339. Matulis D, Kranz JK, Salemme FR, Todd MJ. 2005. Thermodynamic stability of carbonic anhydrase: measurements of binding affinity and stoichiometry using ThermoFluor. Biochemistry 44:5258-66.
340. Dart ML, Machleidt T, Jost E, Schwinn MK, Robers MB, Shi C, Kirkland TA, Killoran MP, Wilkinson JM, Hartnett JR, Zimmerman K, Wood KV. 2018. Homogeneous Assay for Target Engagement Utilizing Bioluminescent Thermal Shift. ACS Medicinal Chemistry Letters 9:546-551.
341. Eyre NS, Johnson SM, Eltahla AA, Aloi M, Aloia AL, McDevitt CA, Bull RA, Beard MR. 2017. Genome-Wide Mutagenesis of Dengue Virus Reveals Plasticity of the NS1 Protein and Enables Generation of Infectious Tagged Reporter Viruses. J Virol 91.
342. Burton TD, Eyre NS. 2021. Applications of Deep Mutational Scanning in Virology. Viruses 13:1020.
343. Tan TY, Fibriansah G, Kostyuchenko VA, Ng T-S, Lim X-X, Zhang S, Lim X-N, Wang J, Shi J, Morais MC, Corti D, Lok S-M. 2020. Capsid protein structure in Zika virus reveals the flavivirus assembly process. Nature Communications 11:895.
344. Cimmperman P, Baranauskiene L, Jachimoviciūte S, Jachno J, Torresan J, Michailoviene V, Matuliene J, Sereikaite J, Bumelis V, Matulis D. 2008. A quantitative model of thermal stabilization and destabilization of proteins by ligands. Biophys J 95:3222-31.
345. Fujita T, Iwasa J, Hansch C. 1964. A New Substituent Constant, π, Derived from Partition Coefficients. Journal of the American Chemical Society 86:5175-5180.
346. Crill WD, Chang GJ. 2004. Localization and characterization of flavivirus envelope glycoprotein cross-reactive epitopes. J Virol 78:13975-86.
347. Labeau A, Simon-Loriere E, Hafirassou M-L, Bonnet-Madin L, Tessier S, Zamborlini A, Dupré T, Seta N, Schwartz O, Chaix M-L, Delaugerre C, Amara A, Meertens L. 2020. A Genome-Wide CRISPR-Cas9 Screen Identifies the Dolichol-Phosphate Mannose Synthase Complex as a Host Dependency Factor for Dengue Virus Infection. Journal of Virology 94:e01751-19.
348. Winkler G, Randolph VB, Cleaves GR, Ryan TE, Stollar V. 1988. Evidence that the mature form of the flavivirus nonstructural protein NS1 is a dimer. Virology 162:187-96.
349. Dixon AS, Schwinn MK, Hall MP, Zimmerman K, Otto P, Lubben TH, Butler BL, Binkowski BF, Machleidt T, Kirkland TA, Wood MG, Eggers CT, Encell LP, Wood KV. 2016. NanoLuc Complementation Reporter Optimized for Accurate Measurement of Protein Interactions in Cells. ACS Chemical Biology 11:400-408.
350. Falgout B, Chanock R, Lai CJ. 1989. Proper processing of dengue virus nonstructural glycoprotein NS1 requires the N-terminal hydrophobic signal sequence and the downstream nonstructural protein NS2a. J Virol 63:1852-60.

351. Brown LY, Dong W, Kantor B. 2020. An Improved Protocol for the Production of Lentiviral Vectors. STAR Protoc 1:100152.
352. Rampersad SN. 2012. Multiple applications of Alamar Blue as an indicator of metabolic function and cellular health in cell viability bioassays. Sensors (Basel, Switzerland) 12:12347-12360.
353. McDougal DP, Rajapaksha H, Pederick JL, Bruning JB. 2023. warpDOCK: Large-Scale Virtual Drug Discovery Using Cloud Infrastructure. ACS Omega 8:29143-29149.
354. Sadybekov AA, Sadybekov AV, Liu Y, Iliopoulos-Tsoutsouvas C, Huang X-P, Pickett J, Houser B, Patel N, Tran NK, Tong F, Zvonok N, Jain MK, Savych O, Radchenko DS, Nikas SP, Petasis NA, Moroz YS, Roth BL, Makriyannis A, Katritch V. 2022. Synthon-based ligand discovery in virtual libraries of over 11 billion compounds. Nature 601:452-459.
355. Cavasotto CN, Phatak SS. 2009. Homology modeling in drug discovery: current trends and applications. Drug Discovery Today 14:676-683.
356. Edeling MA, Diamond MS, Fremont DH. 2014. Structural basis of Flavivirus NS1 assembly and antibody recognition. Proceedings of the National Academy of Sciences 111:4285-4290.
357. Akey DL, Brown WC, Dutta S, Konwerski J, Jose J, Jurkiw TJ, DelProposto J, Ogata CM, Skiniotis G, Kuhn RJ, Smith JL. 2014. Flavivirus NS1 Structures Reveal Surfaces for Associations with Membranes and the Immune System. Science 343:881-885.
358. Winkler G, Maxwell SE, Ruemmler C, Stollar V. 1989. Newly synthesized dengue-2 virus nonstructural protein NS1 is a soluble protein but becomes partially hydrophobic and membrane-associated after dimerization. Virology 171:302-5.
359. Trott O, Olson AJ. 2010. AutoDock Vina: Improving the speed and accuracy of docking with a new scoring function, efficient optimization, and multithreading. Journal of Computational Chemistry 31:455-461.
360. Stank A, Kokh DB, Fuller JC, Wade RC. 2016. Protein Binding Pocket Dynamics. Acc Chem Res 49:809-15.
361. Shaker B, Ahmad S, Lee J, Jung C, Na D. 2021. In silico methods and tools for drug discovery. Comput Biol Med 137:104851.
362. Menchon G, Maveyraud L, Czaplicki G. 2018. Molecular Dynamics as a Tool for Virtual Ligand Screening. Methods Mol Biol 1762:145-178.
363. Irwin JJ, Tang KG, Young J, Dandarchuluun C, Wong BR, Khurelbaatar M, Moroz YS, Mayfield J, Sayle RA. 2020. ZINC20—A Free Ultralarge-Scale Chemical Database for Ligand Discovery. Journal of Chemical Information and Modeling 60:6065-6073.
364. Tan BEK, Beard MR, Eyre NS. 2023. Identification of Key Residues in Dengue Virus NS1 Protein That Are Essential for Its Secretion. Viruses 15:1102.
365. Pokidysheva E, Zhang Y, Battisti AJ, Bator-Kelly CM, Chipman PR, Xiao C, Gregorio GG, Hendrickson WA, Kuhn RJ, Rossmann MG. 2006. Cryo-EM Reconstruction of Dengue Virus in Complex with the Carbohydrate Recognition Domain of DC-SIGN. Cell 124:485-493.
366. Gandini R, Reichenbach T, Tan T-C, Divne C. 2017. Structural basis for dolichylphosphate mannose biosynthesis. Nature Communications 8:120.
367. Goyal U, Blackstone C. 2013. Untangling the web: mechanisms underlying ER network formation. Biochim Biophys Acta 1833:2492-8.
368. Rismanchi N, Soderblom C, Stadler J, Zhu PP, Blackstone C. 2008. Atlastin GTPases are required for Golgi apparatus and ER morphogenesis. Hum Mol Genet 17:1591-604.

369. Zhao G, Zhu P-P, Renvoisé B, Maldonado-Báez L, Park SH, Blackstone C. 2016. Mammalian knock out cells reveal prominent roles for atlastin GTPases in ER network morphology. Experimental Cell Research 349:32-44.
370. Neufeldt CJ, Cortese M, Scaturro P, Cerikan B, Wideman JG, Tabata K, Moraes T, Oleksiuk O, Pichlmair A, Bartenschlager R. 2019. ER-shaping atlastin proteins act as central hubs to promote flavivirus replication and virion assembly. Nat Microbiol 4:2416-2429.
371. Troost B, Smit JM. 2020. Recent advances in antiviral drug development towards dengue virus. Current Opinion in Virology 43:9-21.
372. Rawle DJ, Li D, Wu Z, Wang L, Choong M, Lor M, Reid RC, Fairlie DP, Harris J, Tachedjian G, Poulsen S-A, Harrich D, Silvestri G. 2019. Oxazole-Benzenesulfonamide Derivatives Inhibit HIV-1 Reverse Transcriptase Interaction with Cellular eEF1A and Reduce Viral Replication. Journal of Virology 93:e00239-19.
373. Li Z, Brecher M, Deng Y-Q, Zhang J, Sakamuru S, Liu B, Huang R, Koetzner CA, Allen CA, Jones SA, Chen H, Zhang N-N, Tian M, Gao F, Lin Q, Banavali N, Zhou J, Boles N, Xia M, Kramer LD, Qin C-F, Li H. 2017. Existing drugs as broad-spectrum and potent inhibitors for Zika virus by targeting NS2B-NS3 interaction. Cell research 27:1046-1064.
374. Pryor MJ, Wright PJ. 1994. Glycosylation mutants of dengue virus NS1 protein. J Gen Virol 75 (Pt 5):1183-7.
375. Utarini A, Indriani C, Ahmad RA, Tantowijoyo W, Arguni E, Ansari MR, Supriyati E, Wardana DS, Meitika Y, Ernesia I, Nurhayati I, Prabowo E, Andari B, Green BR, Hodgson L, Cutcher Z, Rancès E, Ryan PA, O'Neill SL, Dufault SM, Tanamas SK, Jewell NP, Anders KL, Simmons CP. 2021. Efficacy of Wolbachia-Infected Mosquito Deployments for the Control of Dengue. New England Journal of Medicine 384:2177-2186.
376. Ford SA, Allen SL, Ohm JR, Sigle LT, Sebastian A, Albert I, Chenoweth SF, McGraw EA. 2019. Selection on Aedes aegypti alters Wolbachia-mediated dengue virus blocking and fitness. Nat Microbiol 4:1832-1839.
377. Huang B, Yang Q, Hoffmann AA, Ritchie SA, van den Hurk AF, Warrilow D. 2020. Wolbachia Genome Stability and mtDNA Variants in Aedes aegypti Field Populations Eight Years after Release. iScience 23:101572.
378. Thi Hue Kien D, Edenborough K, da Silva Goncalves D, Thuy Vi T, Casagrande E, Thi Le Duyen H, Thi Long V, Thi Dui L, Thi Tuyet Nhu V, Thi Giang N, Thi Xuan Trang H, Lee E, Donovan-Banfield I, Thi Thuy Van H, Minh Nguyet N, Thanh Phong N, Van Vinh Chau N, Wills B, Yacoub S, Flores H, Simmons C. 2023. Genome evolution of dengue virus serotype 1 under selection by Wolbachia pipientis in Aedes aegypti mosquitoes. Virus Evol 9:vead016.
379. Kadkhodaei S, Memari HR, Abbasiliasi S, Rezaei MA, Movahedi A, Shun TJ, Ariff AB. 2016. Multiple overlap extension PCR (MOE-PCR): an effective technical shortcut to high throughput synthetic biology. RSC Advances 6:66682-66694.
380. Kadkhodaei S, Memari H, Abbasiliasi S, akhavan rezaei M, Movahedi A, Joo Shun T, Ariff A. 2016. Multiple overlap extension PCR (MOE-PCR): An effective technical shortcut to high throughput synthetic biology. RSC Advances 6.
381. Manual I. 2009. GeneMorph II Random Mutagenesis Kit. Stratagene.

382. Sriburi R, Keelapang P, Duangchinda T, Pruksakorn S, Maneekarn N, Malasit P, Sittisombut N. 2001. Construction of infectious dengue 2 virus cDNA clones using high copy number plasmid. Journal of Virological Methods 92:71-82.
383. Adikari TN, Riaz N, Sigera C, Leung P, Valencia BM, Barton K, Smith MA, Bull RA, Li H, Luciani F, Weeratunga P, Thein TL, Lim VWX, Leo YS, Rajapakse S, Fink K, Lloyd AR, Fernando D, Rodrigo C. 2020. Single molecule, near full-length genome sequencing of dengue virus. Sci Rep 10:18196.
384. Criscuolo A, Brisse S. 2013. AlienTrimmer: a tool to quickly and accurately trim off multiple short contaminant sequences from high-throughput sequencing reads. Genomics 102:500-6.
385. Grubaugh ND, Smith DR, Brackney DE, Bosco-Lauth AM, Fauver JR, Campbell CL, Felix TA, Romo H, Duggal NK, Dietrich EA, Eike T, Beane JE, Bowen RA, Black WC, Brault AC, Ebel GD. 2015. Experimental evolution of an RNA virus in wild birds: evidence for host-dependent impacts on population structure and competitive fitness. PLoS Pathog 11:e1004874.
386. Anders KL, Indriani C, Ahmad RA, Tantowijoyo W, Arguni E, Andari B, Jewell NP, Rances E, O'Neill SL, Simmons CP, Utarini A. 2018. The AWED trial (Applying Wolbachia to Eliminate Dengue) to assess the efficacy of Wolbachia-infected mosquito deployments to reduce dengue incidence in Yogyakarta, Indonesia: study protocol for a cluster randomised controlled trial. Trials 19:302.
387. Ong J, Ho SH, Soh SXH, Wong Y, Ng Y, Vasquez K, Lai YL, Setoh YX, Chong C-S, Lee V, Wong JCC, Tan CH, Sim S, Ng LC, Lim JT. 2022. Assessing the efficacy of male Wolbachia-infected mosquito deployments to reduce dengue incidence in Singapore: study protocol for a cluster-randomized controlled trial. Trials 23:1023.
388. Peleg J. 1968. Growth of arboviruses in primary tissue culture of Aedes aegypti embryos. Am J Trop Med Hyg 17:219-23.
389. Adikari TN, Riaz N, Sigera C, Leung P, Valencia BM, Barton K, Smith MA, Bull RA, Li H, Luciani F, Weeratunga P, Thein T-L, Lim VWX, Leo Y-S, Rajapakse S, Fink K, Lloyd AR, Fernando D, Rodrigo C. 2020. Single molecule, near full-length genome sequencing of dengue virus. Scientific Reports 10:18196.
390. Goethals O, Kaptein SJF, Kesteleyn B, Bonfanti J-F, Van Wesenbeeck L, Bardiot D, Verschoor EJ, Verstrepen BE, Fagrouch Z, Putnak JR, Kiemel D, Ackaert O, Straetemans R, Lachau-Durand S, Geluykens P, Crabbe M, Thys K, Stoops B, Lenz O, Tambuyzer L, De Meyer S, Dallmeier K, McCracken MK, Gromowski GD, Rutvisuttinunt W, Jarman RG, Karasavvas N, Touret F, Querat G, de Lamballerie X, Chatel-Chaix L, Milligan GN, Beasley DWC, Bourne N, Barrett ADT, Marchand A, Jonckers THM, Raboisson P, Simmen K, Chaltin P, Bartenschlager R, Bogers WM, Neyts J, Van Loock M. 2023. Blocking NS3–NS4B interaction inhibits dengue virus in non-human primates. Nature 615:678-686.
391. Labeau A, Simon-Loriere E, Hafirassou ML, Bonnet-Madin L, Tessier S, Zamborlini A, Dupré T, Seta N, Schwartz O, Chaix ML, Delaugerre C, Amara A, Meertens L. 2020. A Genome-Wide CRISPR-Cas9 Screen Identifies the Dolichol-Phosphate Mannose Synthase Complex as a Host Dependency Factor for Dengue Virus Infection. J Virol 94.
392. Fox T, Sguassero Y, Chaplin M, Rose W, Doum D, Arevalo-Rodriguez I, Villanueva G. 2024. Wolbachia-carrying Aedes mosquitoes for preventing dengue infection. Cochrane Database Syst Rev 4:Cd015636.

393. Zabalou S, Riegler M, Theodorakopoulou M, Stauffer C, Savakis C, Bourtzis K. 2004. Wolbachia-induced cytoplasmic incompatibility as a means for insect pest population control. Proceedings of the National Academy of Sciences 101:15042-15045.
394. Gwee SXW, St John AL, Gray GC, Pang J. 2021. Animals as potential reservoirs for dengue transmission: A systematic review. One Health 12:100216.
395. Dolan PT, Taguwa S, Rangel MA, Acevedo A, Hagai T, Andino R, Frydman J. 2021. Principles of dengue virus evolvability derived from genotype-fitness maps in human and mosquito cells. eLife 10:e61921.